# TRANSIENT FLOW OF WATER IN SATURATED-UNSATURATED SOIL PROFILES

by

WAYNE STUART KETTERINGHAM

A half thesis submitted to the University of Cape Town
in partial fulfilment of the requirements for the degree of
Master of Science in Engineering.
Course work completed by the candidate for the above degree
is listed in Appendix A.

Department of Civil Engineering
University of Cape Town

January 1990

## DECLARATION BY CANDIDATE

I, Wayne Stuart Ketteringham, hereby declare that this thesis represents my own work and has not been submitted for a degree at another university.

Signed by candidate

W.S. KETTERINGHAM

JANUARY 1990

## SYNOPSIS

In this thesis the transient flow of water, during the drainage process in saturated-unsaturated soil profiles, was studied. Drainage experiments were performed on two different soil profiles. The first experiment undertaken was the drainage of a vertical column of sand. This experiment was performed on two sands of differing grain size and grading. The second experiment undertaken was the drainage towards a well from a wedge of sand (cake slice) using yet a different coarse sand.

A numerical model, using the finite element method for formulating the flow equation and a finite difference based method for handling the time derivative, was used to simulate the above drainage experiments. The model was also used to simulate a third experiment performed by another investigator.

A one-dimensional approximation of the column drainage experiment was made while a two-dimensional axisymmetric approximation could be made of the drainage experiment performed on the wedge of sand. This could be done due to its radial symmetry. A two-dimensional plane approximation was made of the third experiment.

The above-mentioned model, which contained features to avoid time consuming numerical integration, was coded for use on a personal computer. A comparison between the experimental and numerical drainage results could then be made. For the drainage experiments simulated, good comparisons between the results were obtained. Certain features in the code and the model could, however, be improved to provide closer comparisons.

Also included in this thesis is certain background theory pertaining to interaction of soil and water in both the saturated and unsaturated zones of the soil profile. Furthermore, the soil and soil-moisture characteristics necessary to the code, for simulating the drainage problems, were determined experimentally.

## ACKNOWLEDGEMENTS

I would like to express my sincere thanks and appreciation to :

Professor A.D.W. Sparks for supervising this thesis.

Foundation of Research Development for their financial assistance.

Mr J.J. Williams for his assistance in the laboratory.

Cheryl Wright for her time and patience in typing this thesis.

# TABLE OF CONTENTS

## LIST OF SYMBOLS

| Symbol | Description | Dimension |
|---|---|---|
| a | constant | |
| $A^e_{ij}, \underset{\approx}{A}^e$ | element matrix for the Pichard iterative scheme | |
| A | cross-sectional | $L^2$ |
| b | constant | |
| $B^e_{ij}, \underset{\approx}{B}^e$ | element matrix for the Pichard iterative scheme | |
| B | solution boundary | |
| $B_1$ | prescribed head boundary | |
| $B_2$ | prescribed flux boundary | |
| $B_3$ | seepage face | |
| $C(\theta/Sr)$ | specific moisture capacity | 1/L |
| $D_{10}$ | a soil parameter | L |
| $D(\theta)$ | moisture diffusivity | $L^2/T$ |
| $d_{d,b}$ | diameters | L |
| $e_1$ | unit normal vector | |
| e | void ratio | |
| $F^e_i, \underset{\sim}{F}^e$ | right-hand-side vector in the Pichard iterative scheme | |
| g | gravitational acceleration | $L/T^2$ |
| h | total hydraulic head | L |
| $h_c$ | height of capillary rise | L |
| i | hydraulic gradient | |
| i,j | coordinate or nodal subscripts | |
| $k_{sat}$ | saturated coefficient of permeability | L/T |
| $k(\theta/Sr)$ | unsaturated coefficient of permeability | L/T |
| $k_r$ | relative permeability | |
| k,k+1 | time level indices | |
| $k_{ij}, \underset{\approx}{k}$ | the tensor of $k_{sat}$ | L/T |
| $\ell^e$ | length of a finite element | L |
| $\ell_s$ | length of a soil sample | L |

| | | |
|---|---|---|
| $\Delta\ell$ | a distance increment | L |
| m | number of finite elements in the solution domain | |
| $M_s, s_{i,d,t}$ | mass of object | M |
| n | porosity | |
| $N_i$ | interpolation functions | |
| $p_o$ | atmospheric pressure | $MLT^{-2}/L^2$ |
| $p_c$ | capillary pressure | $MLT^{-2}/L^2$ |
| q | flux vector | L/T |
| $Q_i$ | normal nodal flux vector | L/T |
| Q | volume of water | $L^3$ |
| r | cylindrical coordinate | L |
| $r_1, r_2$ | radii determining the capillary pressure | L |
| r, r+1 | iteration level indices | |
| R | solution domain | |
| $R^e$ | element subdomain | |
| Sr | degree of saturation | |
| $S_s$ | specific storage | 1/L |
| $S_g$ | specific gravity/relative density | |
| $S_{ro}$ | residual saturation | |
| t | time elapsed | T |
| $\Delta t$ | a time increment | T |
| $V_{i,n}$ | normal nodal fluxes | L/T |
| v | Darcian velocity | L/T |
| $V_t$ | total volume occupied by sand | $L^3$ |
| $V_s$ | volume of sand | $L^3$ |
| $V_v$ | volume of voids | $L^3$ |
| $V_w$ | volume of water | $L^3$ |
| $V_f$ | volume of filters | $L^3$ |
| w | time weighting factor | |
| x,y,z | cartesian coordinates | |
| z | elevation/gravitational head | L |
| $\alpha$ | contact angle | |
| $\beta$ | constant | |
| $\gamma$ | surface tension force | $ML/T^2$ |
| $\delta$ | relaxation factor | |

| | | |
|---|---|---|
| $\zeta$ | isoparametric coordinate | |
| $\xi$ | isoparametric coordinate | |
| $\eta$ | total compressibility coefficient of the soil | 1/L |
| $\theta$ | volumetric moisture content | |
| $\mu_a$ | viscosity of air | M/LT |
| $\mu_w$ | viscosity of water | M/LT |
| $\pi$ | pi | |
| $\rho$ | density | $M/L^3$ |
| $\rho_b$ | dry bulk density of sand | $M/L^3$ |
| $\tau$ | a time factor | |
| $\phi_t$ | total potential | $M/LT^2$ |
| $\phi_g$ | gravitational potential | $M/L^2$ |
| $\phi_p$ | pressure potential | $M/LT^2$ |
| $\Psi$ | pressure head | L |
| $\underset{\sim}{\Psi}, \Psi_j$ | pressure head vector | L |
| $\dot{\underset{\sim}{\Psi}}$ | time derivative of $\underset{\sim}{\Psi}$ | L/T |
| $\approx$ | tensor representation | |
| $\sim$ | vector representation | |
| $\cdot$ | scalar product | |
| $\nabla$ | gradient | |
| $\partial$ | partial derivative | |

# CHAPTER ONE

## INTRODUCTION

Water is a substance vital to the existence of all living organisms. Not all the rain water finds its way into dams where it can be utilized by man. A large percentage of the water infiltrates into the ground, under the action of gravity, to form part of the ground water system. It can, therefore, be seen that ground water represents a large potential source of water. If the movement of ground water is not fully understood then this water source may be permanently damaged.

When water infiltrates into the ground, under the action of gravity, it moves downwards towards the saturated zone. In this zone, below the water table, gases are seldom present in the pore spaces between the soil particles. Methane might occur in decomposing vegetative water while acid waters can give rise to other gases. However, in the zone connecting the ground surface to the water table, both air and water are present in the pore spaces. The soil in this unsaturated zone has an affinity to the wetting phase (i.e. water) and hence retards the gravity flow of water. The affinity of the soil to the water gives rise to different flow characteristics in this zone when compared with those in the saturated zone. The slower movement of the water in the unsaturated zone gives rise to longer time delays during seepage in this zone.

Although ground water movement consists of both saturated and unsaturated flow, flow in the unsaturated zone has generally been ignored in the past. When dealing with aquifer discharge and recharge the amount of water obtained from the unsaturated zone is generally small when compared with the amount of water obtained from the saturated zone. Due to this fact and the time delays involved, unsaturated flow has generally been ignored.

Lately, however, with the need to produce agricultural crops more efficiently, scientists and farmers have become more interested in the flow in the unsaturated zone. Since plants obtain their water from the unsaturated zone and

since there is a particular moisture content at which optimum yield is obtained, unsaturated flow needs to be understood for improved irrigation and drainage of farmlands.

Perhaps the most important reason why interest in the unsaturated zone has grown in the past decade, is due to the increased dumping of toxic, nuclear and industrial wastes in the ground. These wastes migrate through the unsaturated zone to find their way into the ground water system. Due to the hazardous effects these wastes have on life, it is essential that the direction of movement and concentration of the wastes can be determined. Hence the need to include the unsaturated zone in ground water flow.

In this thesis I have presented a finite element model which simulates ground water movement, considering combined saturated-unsaturated flow. This model was then coded in order that the numerical results, obtained from this programme, be compared against the equivalent experimental results obtained from three different experiments. In this manner the accuracy of the model in simulating the experiments could be tested. Different numerical variables were used in the simulations to determine the effect they had on the solution procedure. All the soil and soil-water characteristics required as input in the programme were determined experimentally by the author.

Background information pertaining to the interaction of soil and water, in both the saturated and unsaturated zones, is also presented in this thesis.

# CHAPTER 2

# BACKGROUND THEORY PERTAINING TO SOIL AND SOIL-WATER

## 2.1 THE PROPERTIES OF SOIL

### 2.1.1 General

In order to understand processes such as aquifer discharge and recharge, irrigation, drainage and the migration of toxins and other pollutants, which may find their way into the soil-water system, we first have to be able to understand and quantify the properties of both soil and water.

This thesis deals primarily with the drainage process of the water in the soil. Soil is the outer layer of the earth's surface formed by the decomposition and disintegration of rock via mechanical, chemical and biological processes.

Soil is a porous system; the soil particles being of such shape and packing that they form voids (pores), of varying size, between the soil particles. These voids may be connected to form a maze of passages. It is through these tortuous passages that the water flows. If these pores are entirely filled with water then we define the flow as saturated flow. If, however, air is also present in these voids then we define the flow as unsaturated flow.

The soil particles, constituting a solid matrix, vary greatly in shape, size and size distribution. This gives rise to a complex geometry which is impossible to describe mathematically. Hence all the properties are determined at a macroscopic level and represent averaged rather than exact values.

The soils dealt with in this study are assumed to be isotropic and homogeneous (properties uniform throughout). Under field

conditions, however, soils are anisotropic (properties vary with direction), and may be non-homogeneous (e.g. layered into different types).

### 2.1.2 Mass and volume relations

In order to define the soil properties, a soil sample is idealized into its three phases (solid, liquid and gas), as shown in Figure 2.1 below :

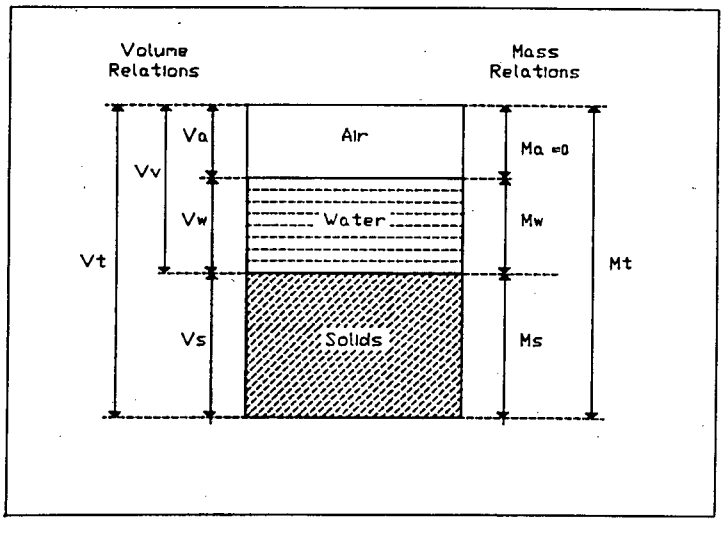


Figure 2.1 - Schematic diagram of the soil in its three phases

Using the above diagram we can now define the soil properties used to compare different soils.

1. Density

$$\rho = \frac{M}{V} \tag{2.1}$$

2. Dry Bulk Density

$$\rho_b = \frac{M_s}{V_t} \tag{2.2}$$

3. Porosity

$$n = \frac{V_v}{V_t} = \frac{V_t - V_s}{V_t} \tag{2.3}$$

4. Void Ratio

$$e = \frac{V_v}{V_s} = \frac{V_t - V_s}{V_s} \qquad (2.4)$$

5. Volumetric Moisture Content

$$\theta = \frac{V_w}{V_t} \qquad (2.5)$$

6. Degree of Saturation

$$Sr = \frac{V_w}{V_v} = \frac{V_w}{V_t - V_s} \qquad (2.6)$$

7. Interrelations

7.1 $$e = \frac{n}{1 - n} \qquad (2.7)$$

7.2 $$n = \frac{e}{1 + e} \qquad (2.8)$$

7.3 $$\theta = nSr \qquad (2.9)$$

Sparks suggested a water ratio $\theta$ for Soil Mechanics (1961) but this has been used considerably by irrigation scientists in many recent publications.

Although the above relations greatly assist in the description of a soil, they are not necessarily complete. Other factors such as soil texture (the predominant particle size and range of particle sizes) and soil structure (particle size distribution and organisation) are also necessary to fully describe the soil.

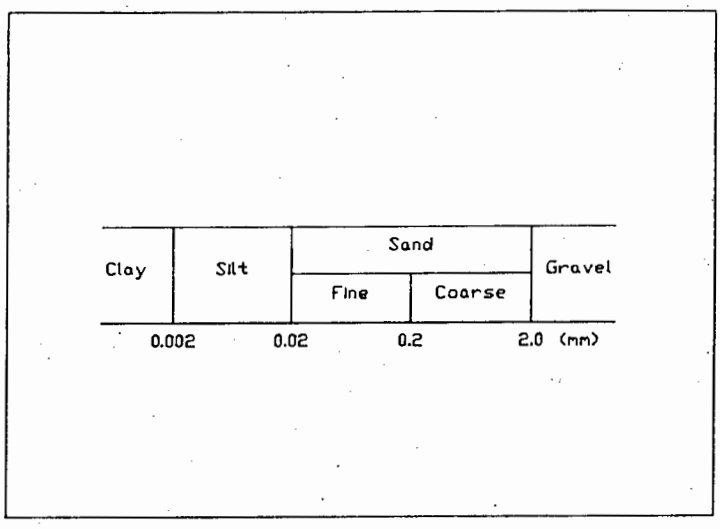


Figure 2.2 - Textural classification of soil according to particle diameter

## 2.2 THE PROPERTIES OF WATER

### 2.2.1 General

Water is one of the most common substances on the earth's surface. Even in dry climates water is present; normally in a vapour form. Knowledge of the properties of water is essential to understand its interactions within the soil system.

### 2.2.2 Molecular structure

A water molecule consists of two hydrogen atoms and one oxygen atom. The hydrogen atoms are asymmetrically arranged so as to cause an imbalance or electrostatic charges within the molecule.

The oxygen side of the molecule has an excess negative charge while the hydrogen sides have excess positive charges. This distribution of electrical charges gives rise to electrical polarity. Hence a water molecule is known as a dipole. The oxygen atom of one molecule may also form a secondary link (hydrogen bond) with a hydrogen atom of another water molecule. It is this bonding which gives water its unusually high values of specific heat, viscosity,

surface tension and boiling and melting points when compared with other liquids.

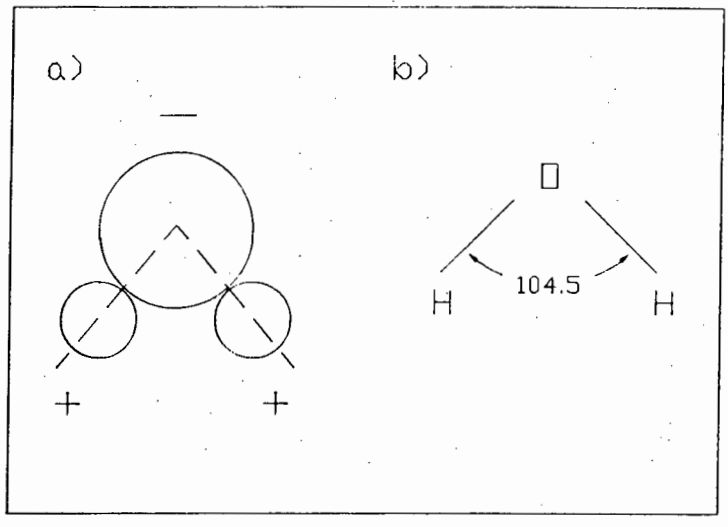


Figure 2.3 - A schematic representation of a water molecule showing
a) the dipole nature of the molecule and
b) the non-linear arrangement of the atoms

2.2.3 Density and compressibility

The density of water is defined as its mass per unit volume. The open packing of the water molecules accounts for its relatively low density. Water has its maximum density at 4°C. Below this temperature a lattice structure forms causing the phase to expand. At higher temperatures the motion of the molecules prevents a dense packing. The thermal coefficient of expansion of water is low. In a temperature range from 4°C to 50°C the density only decreases from 1.000 g/cm$^3$ to 0.988 g/cm$^3$. In this study the density is assumed to be constant at 0.9982 g/cm$^3$.

The compressibility of water is defined as the relative change in density with pressure. In the soil-water-air context, water can be considered to be incompressible as the pressures present are generally small.

### 2.2.4 Viscosity

The viscosity of a liquid is a measure of its resistance to motion. Viscous forces are shear forces. When water is made to move (adjacent layers made to slide over each other), these viscous forces first need to be overcome. Viscosity is temperature dependent; decreasing with increasing temperature.

### 2.2.5 Surface tension

Surface tension, as the name suggests, is a surface phenomenon. The molecules on the surface of the liquid are attracted, to a greater extent, by the cohesive forces of the molecules in the body of the liquid phase, than by the molecules in the gaseous phase. This force imbalance causes the surface to be in a constant state of tension and hence have the tendency to contract. By contracting, the surface attempts to reach the lowest possible energy state. In doing this it behaves as if it were covered by an elastic membrane. Surface tension decreases with increasing temperature.

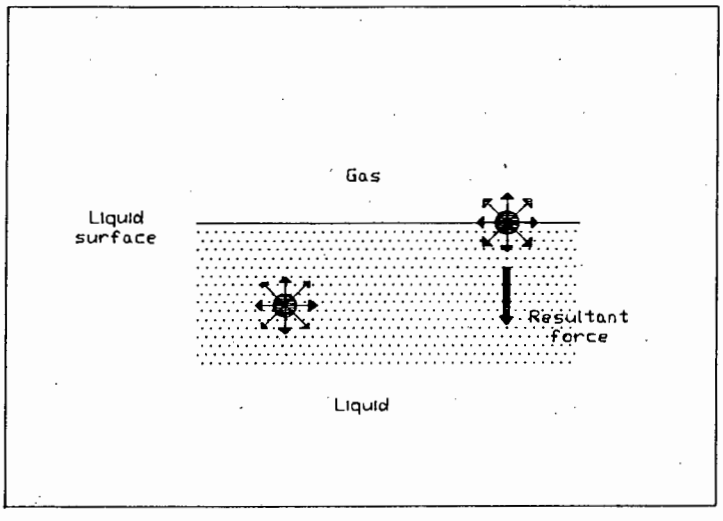


Figure 2.4 - The cohesive forces of attraction acting on
a) a water molecule in the body of the liquid
b) a water molecule on the surface of the liquid

Surface tension is closely associated with the capillarity phenomenon which we will discuss later in this chapter.

### 2.2.6 Contact angles and wettability

If a drop of liquid is placed on a clean, dry solid surface it will displace the gaseous phase and spread over the solid surface to some extent. Where the spreading ceases, the edge of the drop will interface with the gas and the solid at some typical angle $\alpha$ ; known as the contact angle.

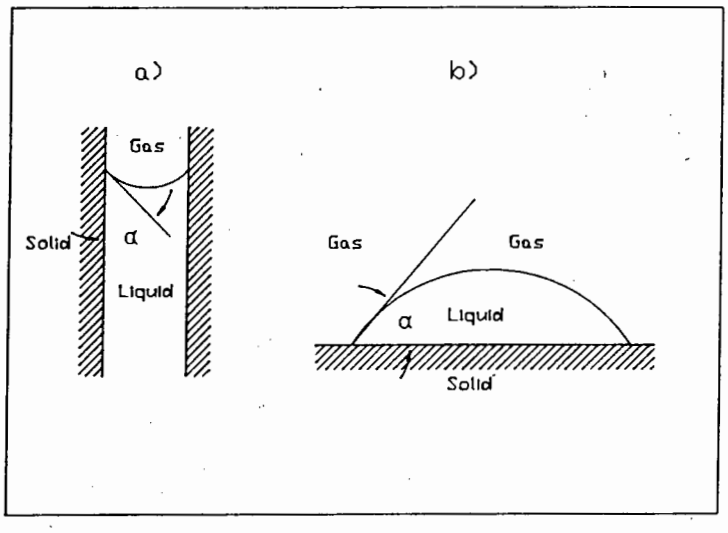


Figure 2.5 - Contact angles of :

a) A meniscus in a capillary tube

b) A drop resting on a solid plane surface

If the adhesive forces between the solid and the liquid are greater than the cohesive forces of attraction between the gas and the solid, then the contact angle (liquid-solid) will be acute ($\alpha < 90°$) and the liquid will wet the solid. If $\alpha = 0°$ then we would have complete wetting of the solid. If $\alpha = 180°$ (if it were possible) then we would have complete non-wetting of the solid by the liquid.

The contact angle of a liquid on a solid is generally constant for given physical conditions. This angle may, however, change if the liquid is advancing or receding on the solid surface. This phenomenon of lag in the adjustment of the contact angle is known as hysteresis.

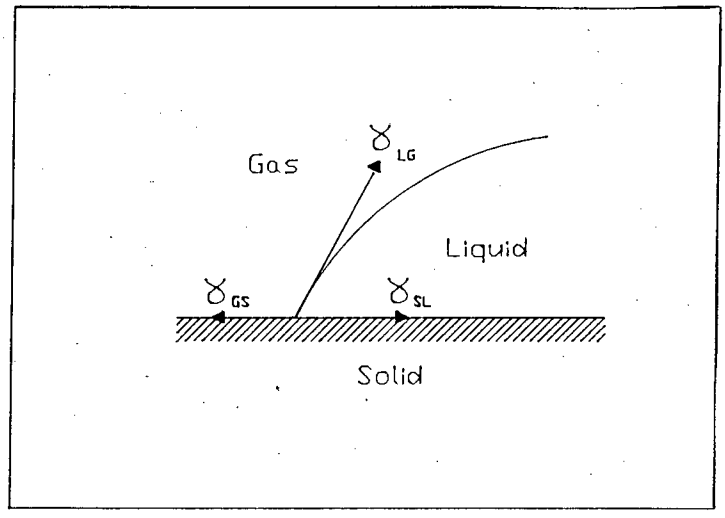


Figure 2.6 - Equilibrium of surface-tension forces on the edge of a drop

Considering the equilibrium situation shown in Figure 2.6 above, we may show that :

$$\gamma_{GS} = \gamma_{SL} + \gamma_{LG} \cos \alpha \qquad (2.10)$$

and hence the contact angle may be determined by :

$$\cos \alpha = \frac{\gamma_{GS} - \gamma_{SL}}{\gamma_{LG}} \qquad (2.11)$$

where $\gamma$ represents the surface tension forces.

2.2.7 Capillarity

When a thin tube is dipped into a body of water a curved liquid-gas interface (meniscus) forms. This is due to the surface tension forces and the contact angle. A pressure difference (capillary pressure) arises, across this interface, due to its curvature. The magnitude of this pressure difference is given by :

$$\Delta p_c = p_o - p_1 = \frac{2\gamma}{r} \qquad (2.12)$$

where $r$ is the mean radius of curvature of the meniscus
$p_o$ is atmospheric pressure ($p_o = 0$)
$p_1$ is the pressure in the water adjacent to the meniscus.

If the meniscus is concave towards the air (acute contact angle) then the water just below the interface is at a sub-atmospheric pressure. Water will, therefore, be driven up the tube. The water will rise to a height such that the weight of the water column is balanced by the surface tension forces.

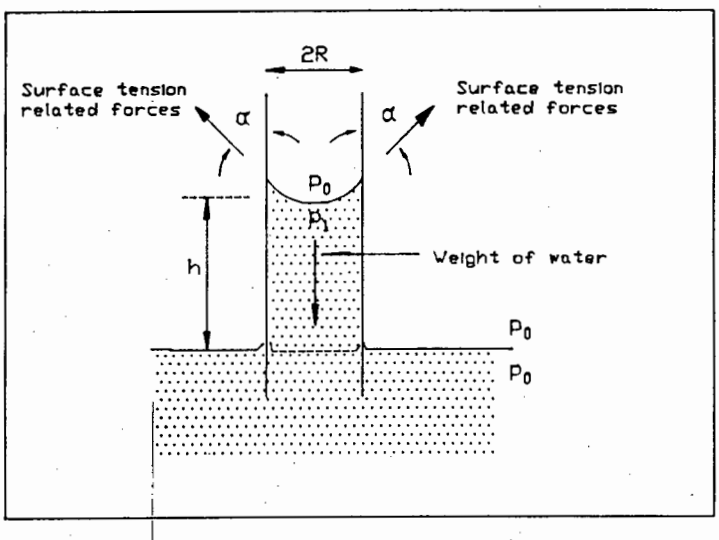


Figure 2.7 - Forces and geometry involved in capillary rise

By balancing the forces shown in Figure 2.7 we get:

$$h\pi R^2 \rho g = 2\pi R \gamma \cos \alpha \qquad (2.13)$$

where $h$ is the height of the capillary rise
$R$ is the radius of the tube
$\rho$ is the density of the liquid
$g$ is the acceleration due to gravity
$\gamma$ is the surface tension forces (liquid-air)
$\alpha$ is the contact angle.

The height to which the water will rise in the tube can then be determined from (2.13) by :

$$h = \frac{2\gamma \cos \alpha}{\rho g R} \qquad (2.14)$$

From (2.14) it can be seen that the narrower the tube the higher the capillary rise.

The phenomenon of capillarity is of particular importance in the unsaturated flow case. Capillary pressure is a measure of the tendency of the unsaturated soil to suck in the water and is, therefore, often called a suction or a tension.

The water pressure in the capillaries in an unsaturated soil is given by :

$$p_c = -\gamma \left(\frac{1}{r_1} + \frac{1}{r_2}\right) + \left( \begin{array}{l}\text{the air pressure in the} \\ \text{continuous air void}\end{array} \right) \qquad (2.15)$$

where $r_1$ and $r_2$ are the two radii determining the curvature of the air-water interface. Sign conventions are applied to $r_1$ and $r_2$

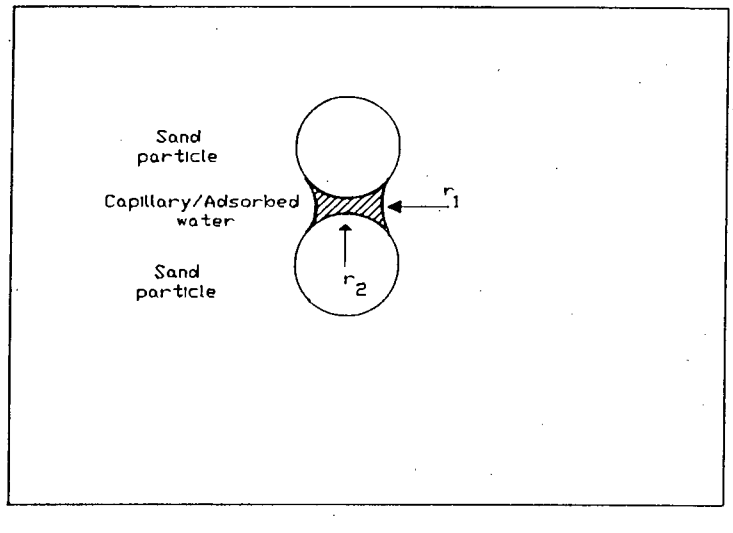


Figure 2.8 - The two radii determining the curvature of the the interface of the capillary water

2.2.8 Adsorption

Due to the dipole nature of the water molecule it is attracted to charged soil particles. These electrostatical forces (Coulomb forces) act in the contact zones and may cause the water in these zones to exhibit different properties from ordinary water at the same temperature. The density and viscosity are two such properties which may exhibit differences.

Adsorbed water can be removed from a soil sample by placing the sample in an oven, heated to between 105°C and 110°C. Higher temperatures would cause a breakdown in the chemical composition of the soil. In this study the term oven dried soil is often used. This refers to a soil where the adsorbed water has been removed.

2.2.9 Vapour pressure

Water molecules in a liquid are in a constant state of motion and hence collide with each other. When they collide, a molecule may absorb sufficient kinetic energy to leave the liquid and join the atmosphere.

This kinetic energy would be used by such a molecule to overcome the intermolecular forces of attraction (surface tension forces) of the molecules in the liquid phase. Molecules in the gaseous phase are also in motion and may re-join the liquid phase when they collide with the liquid surface.

At equilibrium the water molecules re-join and leave the liquid phase at the same rate. The relative pressure of the vapour in the atmosphere at equilibrium is known as saturation vapour pressure.

Vapour pressure is dependent on the temperature, pressure and chemical conditions of the water. It is particularly sensitive to temperature changes, increasing with an increase in temperature.

The movement of moisture in soils at low moisture contents (arid areas) is primarily in a vapour form. The water vapour moves due to the existence of a vapour pressure gradient in the soil.

## 2.3 THE INTERACTION OF SOIL AND WATER

### 2.3.1 Classification of soil-water

A)

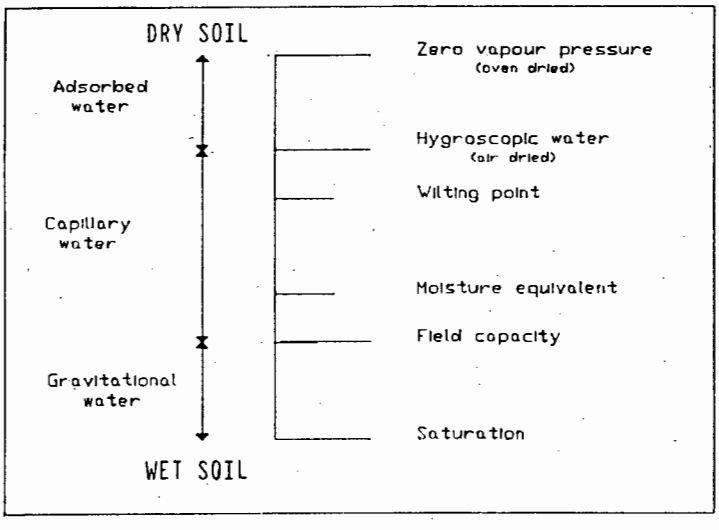


B)

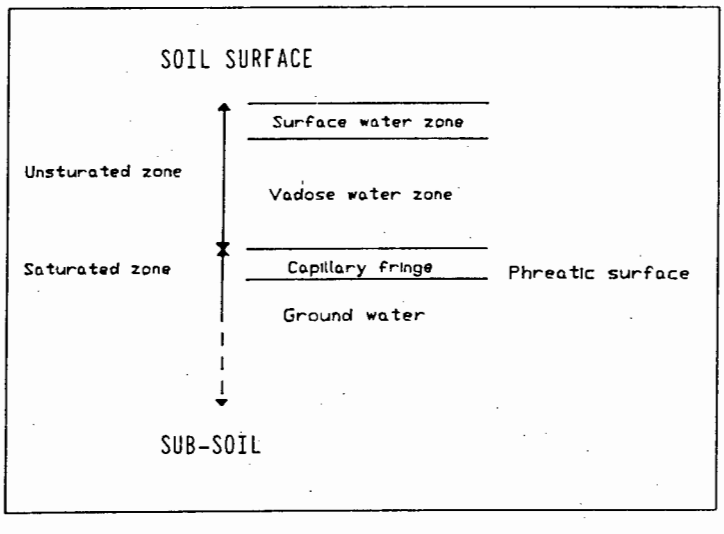


Figure 2.9 - Terms used to describe levels of water in a saturated-unsaturated soil profile
A) From Bear (1972)
B) From Hillel (1971)

### 2.3.2 Soil moisture energies

All bodies in nature possess energy in one form or another. Although other forms do exist, kinetic and potential energies are the most common forms.

The kinetic energy of soil-water during seepage is proportional to its velocity squared and is negligible since the flow rate of soil-water is generally very slow. The potential energy of the soil-water, which is due to its position and condition, is the main form of energy determining soil moisture movement.

Soil-water obeys the universal laws of motion by moving from areas of high potential energy to areas of low potential energy in order to achieve equilibrium. The rate at which potential energy decreases with distance is the force or pressure gradient causing flow. If the potential energy of the soil-water is known at certain points, then we can determine the local directions and fluxes of the soil-water in its attempts to reach equilibrium.

It should be noted that it is only the relative potential energies that are of importance. A datum is, therefore, normally used from which potential energies are compared. This gives rise to the concept of soil-water potential. The datum used is a body of water at the same pressure and temperature as the soil-water and of constant elevation.

The total potential of the soil-water can be considered as a sum of the contributing potentials [Hillel (1971)].

$$\phi_t = \phi_g + \phi_p + \ldots \qquad (2.16)$$

where $\phi_t$ is the total potential
$\phi_g$ is the gravitational potential
$\phi_p$ is the pressure potential
... are all the other contributing potentials.

It will be assumed, for this study, that the only potentials causing flow are gravitational and pressure potentials.

2.3.3 Gravitational potential

Soil-water, due to its mass, is pulled towards the centre of the earth. The magnitude of this gravitational force is dependent on the position of the body of water in the gravitational field relative to some datum, and may be determined by :

$$\phi_g = \rho g z \qquad (2.17)$$

where $\rho$ is the density of the water
$g$ is the acceleration due to gravity
$z$ is the elevation of the body above the datum
$\phi_g$ is the gravitational potential per unit volume.

Hence it can be seen that gravitational potential is dependent purely on elevation relative to some fixed datum.

2.3.4 Pressure potential

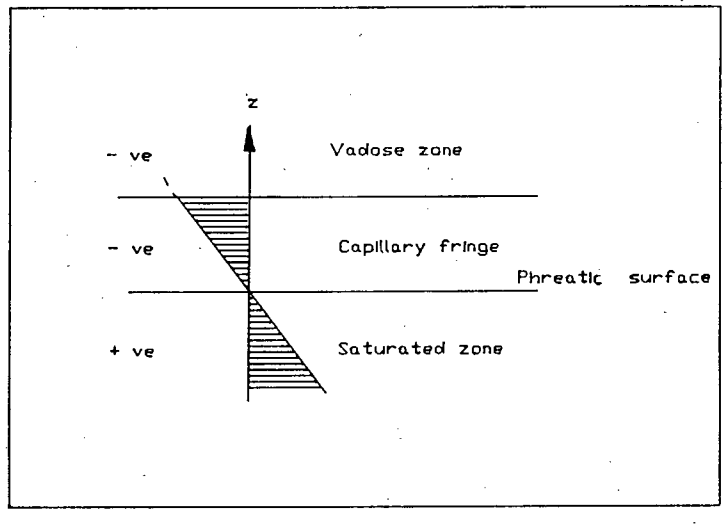


Figure 2.10 - Diagram showing the pressure potential distribution above and below the phreatic surface

Water below the phreatic surface (saturated soils) has a positive pressure potential while the water above the phreatic surface (unsaturated soils) has a negative pressure potential, known as capillary or matric potential. These pressure potentials are measured relative to yet another datum. This datum is normally the location, of the particular body of water of interest, within the gravitation field. In the above diagram (Figure 2.10) the phreatic surface was taken as this datum.

The pressure potential of the body of water may be determined as follows :

$$\phi_p = \rho g \Psi \qquad (2.18)$$

where $\Psi$ is a distance from a datum

$\phi_p$ is the pressure potential per unit volume.

This potential is the result of the capillary and adsorbtive forces which bind the water to the soil particles. It is difficult to distinguish between the capillary water and adsorbed water since they are in equilibrium with each other.

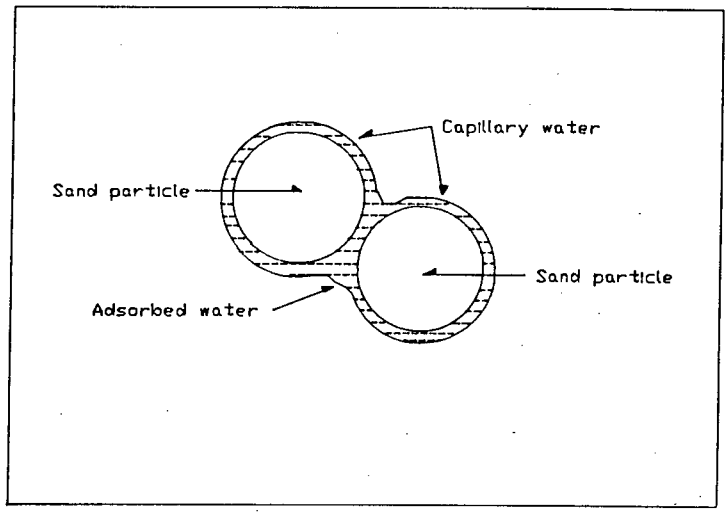


Figure 2.11 - Capillary and adsorbed water in unsaturated soil

It is often more convenient to represent the energy state of the soil-water in head terms as opposed to potential terms. The total head is then defined as :

$$h = z + \psi \qquad (2.19)$$

where $\psi$ is the pressure head

$z$ is the gravitational/elevation head.

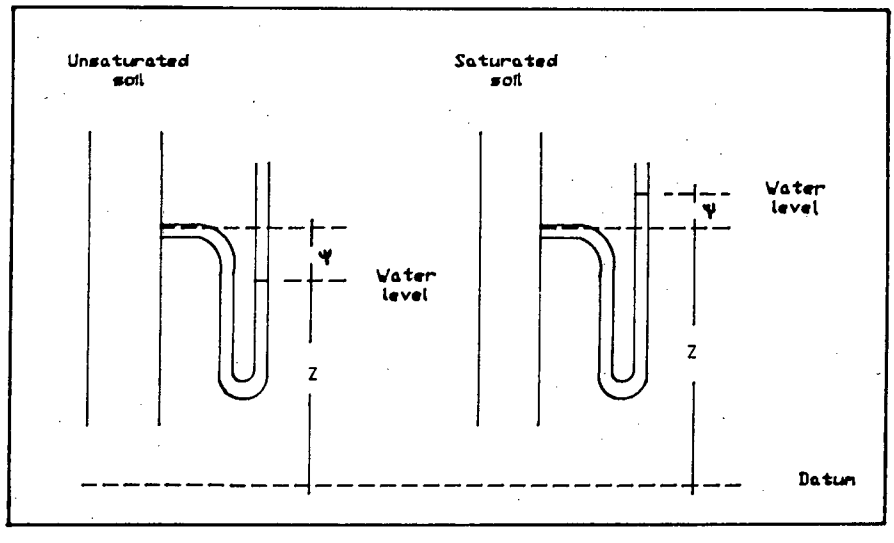


Figure 2.12 - Diagram showing the relation between total, pressure and gravitational heads in a manometer tube

## 2.4 SATURATED FLOW

### 2.4.1 Darcy's Law

Water flows through tortuous passages in the soil. These passages, comprising of interconnected pore spaces, have numerous 'dead ends' and 'necks' causing the velocity to vary greatly, even from one point to another in the same passage. Due to this complex nature of the soil, water flow is described at a macroscopic level. Hence the macroscopic water velocity is an average of all the microscopic water velocities.

The French engineer Henri Darcy found the following relation :

$$Q = kA \frac{\Delta h}{\ell} \tag{2.20}$$

$Q$ , the volume flow rate per unit time, is proportional to the cross-sectional area $A$ and the hydraulic head drop $\Delta h$ and is inversely proportional to the length of the column of soil $\ell$ . The head drop per unit distance $\frac{\Delta h}{\ell}$ is known as the hydraulic gradient and is the factor causing flow. The proportionality factor $k$ , is known as the coefficient of permeability.

The flux density $q$ (volume of water flowing through the cross-sectional area per unit time) is proportional to the hydraulic gradient.

$$q = - k \frac{\Delta h}{\ell} \tag{2.21}$$

This is known as Darcy's Law and is applicable to one-dimensional flow. The negative sign accounts for the fact that flow is in the direction of decreasing head. Darcy's Law may, however, be expanded to the three dimensional case and can account for anisotropy in a medium.

$$\underset{\sim}{q} = - \underset{\approx}{k} \nabla h \tag{2.22}$$

where $\underset{\approx}{k}$ is the symmetrical permeability tensor

$\nabla h$ is the gradient of the hydraulic head

$\underset{\sim}{q}$ is the flux vector.

It should be noted that the average velocity differs from the flux as defined above. Flow does not take place through the entire cross-section $A$ , but rather only through the porous fraction of the soil. The real area through which flow takes place is smaller than $A$ and hence the average real velocity must be greater than the flux $q$ .

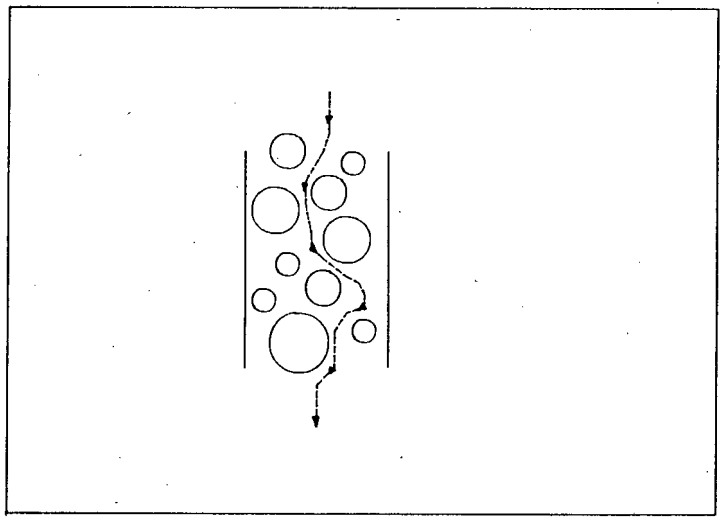

Figure 2.13 - Diagram showing the tortuous path water takes when flowing through a soil

Darcy's Law is only valid for laminar flow; once turbulence occurs Darcy's Law is no longer valid. It has been found for porous media that the flux remains laminar for Reynolds numbers less than unity. At very low hydraulic gradients the adsorptive forces, in fine grained soils, cause a threshold gradient below which the flux is zero or less than predicted by Darcy's Law. The fluid then shows Bingham liquid properties.

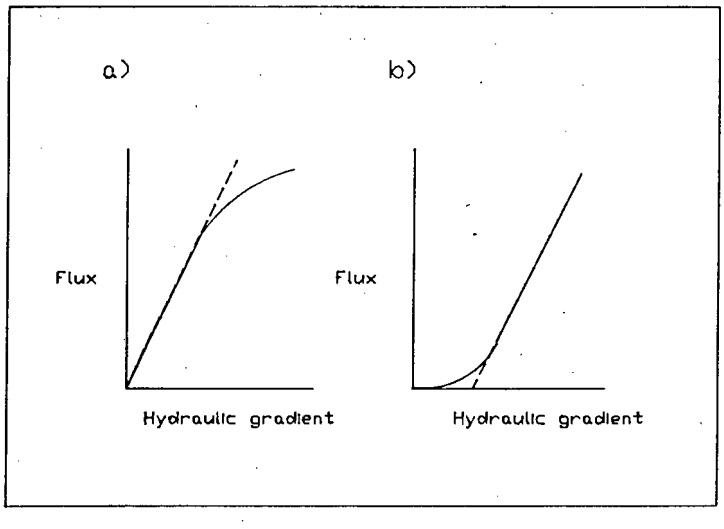


Figure 2.14 - Deviations from Darcy's Law

a) When flow becomes turbulent

b) At low hydraulic gradients

### 2.4.2 Steady-state saturated flow equations

Using Darcy's Law :

$$\underset{\sim}{q} = - \underset{\approx}{k} \nabla h \tag{2.23}$$

and the continuity equation:

$$\frac{\partial \theta}{\partial t} = - \nabla . \underset{\sim}{q} \tag{2.24}$$

we obtain the general equation for saturated flow.

$$\frac{\partial \theta}{\partial t} = \nabla . \underset{\approx}{k} \nabla h \tag{2.25}$$

but for steady-state saturated flow $\frac{\partial \theta}{\partial t} = 0$ and $k$ is constant, hence the above (2.25) reduces to :

$$\nabla . \nabla h = 0 \tag{2.26}$$

which is the Laplace equation.

## 2.5 UNSATURATED FLOW

### 2.5.1 General

Under most field conditions the soil is in the unsaturated condition. This means that both air and water are present in the pore spaces. The varying water content in a soil affects its properties such as the matric suction and the coefficient of permeability. They are both, in turn, affected by hysteresis.

### 2.5.2 Comparison between saturated and unsaturated flow

The air that is present in the pore spaces, in an unsaturated soil, also moves from pore to pore. If water drains from a soil column then the air takes its place. Unsaturated flow is, therefore, a two-phase flow situation with the air, present in the voids, assumed

to be at atmospheric pressure. Saturated flow, on the other hand, is a one-phase flow situation.

It was stated earlier that moisture flow in soils is caused by a potential gradient (comprised of both gravitational and pressure potentials), with the flux being proportional to this gradient. It was also noted that flow was from an area of high potential to an area of low potential.

In saturated soils the pressure potential is positive, while in unsaturated soils there is a negative pressure potential (suction is a driving force). Water in an unsaturated soil tends to be drawn from areas where the water surrounding the soil particles is thick (menisci are less curved/low suction areas) to areas where the water surrounding the soil particles is thinner (menisci are more curved/high suction area).

The coefficient of permeability in saturated soils is constant while it varies in unsaturated soils. The coefficient of permeability in unsaturated soils is a function of moisture content or matric suction and decreases with decreasing moisture content or increasing matric suction.

Coarse grained soils conduct water more readily than fine grained soils in the saturated state. The opposite is, however, true for soils in the unsaturated state. This is due to the large number of big pores in the coarse grained soils. These big pores (most conductive) drain first, leaving the water to flow in the smaller pores (less conductive).

| Saturated Flow | | Unsaturated Flow | |
|---|---|---|---|
| 1. | $\Psi > 0$ | 1. | $\Psi < 0$ |
| 2. | $Sr = 1$ | 2. | $Sr(\Psi)$ |
| 3. | $k(Sr) = k_{sat} = \text{constant}$ | 3. | $k(Sr)$ $Sro < Sr < 1$ |
| | | | $k = 0$ $0 < Sr < Sro$ |

Table 2.1 - The essential differences between flow in saturated and unsaturated soils

2.5.3 The soil-moisture characteristic curve

This curve relates the matric suction of the soil to its moisture content. The matric suction increases with decreasing moisture content. Since this curve shows how the soil retains the water, by capillary forces, against gravity, it is also known as the retention curve. There are separate curves for the drainage process (desorption curve) and for the wetting process (sorption curve). This phenomenon is known as hysteresis. There are also curves (scanning curves) to describe the transitions from one process to the other.

A critical suction first needs to be applied to a saturated soil sample before the air starts to displace the water from the soil. This critical suction is known as the air entry suction and is dependent on the soil texture and structure.

As the suction increases the water first starts to drain from the larger pores. This is due to the capillary forces not being as strong in the larger pores as they are in the smaller pores. As the suction increases, the smaller the pores are that start to drain. A stage is reached when the retained water only remains in pendular rings (hydration envelopes) around the soil particles. At this point the water's presence is independent of the suction and will not be removed by increasing the suction. The saturation at which this occurs is known as the residual saturation.

At high moisture contents the matric suction is primarily due to the capillary effect of the water while at low moisture contents, however, the matric solution is primarily due to the adsorption of water.

The retention curves may be repeatedly traced provided the soil does not compact or consolidate. Upon rewetting air may become entrapped in the soil. This also prevents the curves from being repeatedly traced.

As yet there are no empirical formulae to describe the retention curves from basic soil properties. Visser in Hillel (1966) proposed :

$$\psi = \frac{a\ (n-\theta)^b}{\theta^c} \qquad (2.27)$$

while Gardener in Hillel (1970) proposed :

$$\psi = a\ \theta^{-b} \qquad (2.28)$$

where $\theta$ is the volumetric moisture content
n is the porosity
a,b,c are constants.

The use of these formulae are, however, restricted to certain matric suction ranges. The determination of the constants and the hysteresis phenomenon further hampers the use of these formulae.

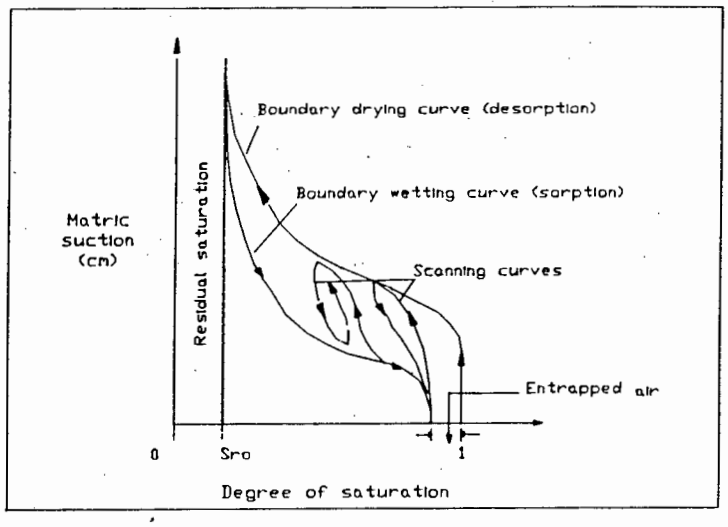


Figure 2.15 - A soil-moisture characteristic curve showing the hysteresis phenomenon

It should be noted that the shape of this retention curve is dependent on the soil texture and structure (e.g. compaction).

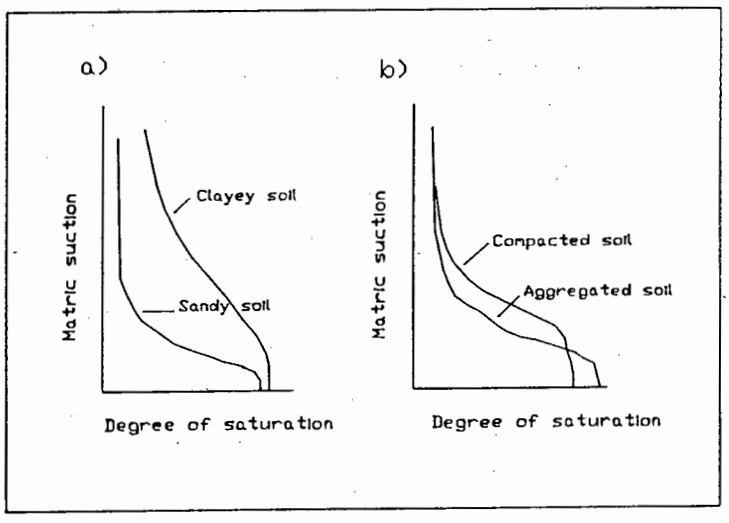


Figure 2.16 - Typical retention curves showing the effect of
a) soil texture and
b) soil structure

2.5.4 The relative permeability curve

As was stated earlier, the permeability of an unsaturated soil is not constant, but decreases with decreasing moisture content.

As the moisture content decreases, the larger pores (most conductive) drain first leaving the water to flow in the smaller pores (less conductive). As the pores drain the tortuosity of the flow paths also increases (cross-sectional area available to flow decreases and the lengths of the flow paths increase). These factors cause a rapid decrease in permeability with decreasing moisture content.

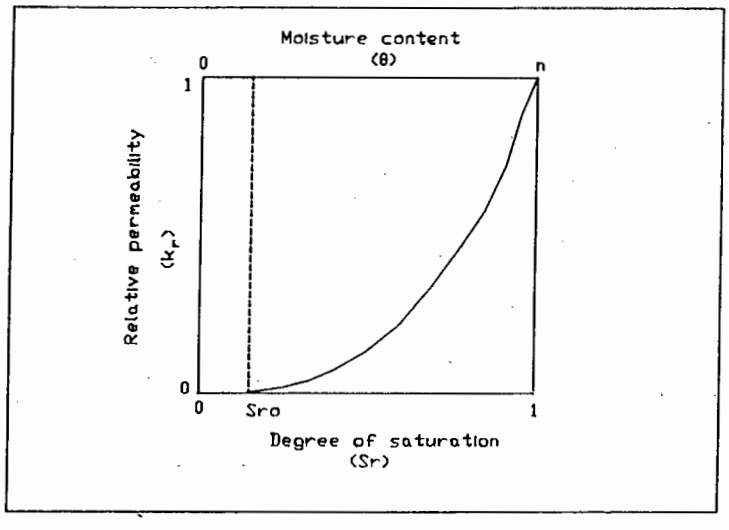


Figure 2.17 - A typical relative permeability curve

When the water is no longer in a continuous phase but rather in pendular rings (hydration envelopes) around the soil particles, it ceases to flow. This occurs at the residual saturation.

The relative permeability of a soil is also subjected hysteresis. The function $k(\Psi)$ is, however, subjected to a larger hysteresis effect than the functions $k(Sr)$ or $k(\theta)$.

Bear et al (1987) recommends that the relative permeability concept not be applied to anisotropic media. They found the function

k(Sr) not to be a unique function of the degree of saturation, but also to be dependent on the direction of flow.

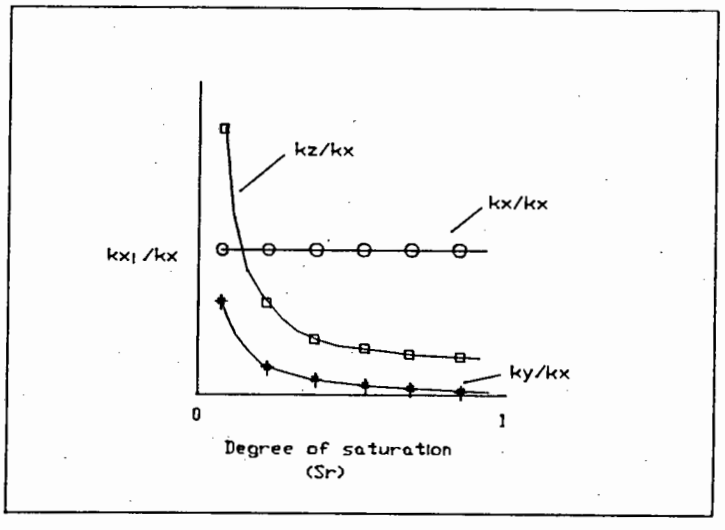


Figure 2.18 - Graph showing the effect of anisotropy on the permeability of a soil at varying degrees of saturation. From Bear et al (1987)

($k_{xi}$ in the term $\frac{k_{xi}}{k_x}$ represents k for any specific direction).

2.5.5 The hysteresis effect

The matric suction-moisture content function is not a single valued function. As was seen in Figure 2.15, the soil-moisture characteristic curve has two separate continuous retention curves: the desorption curve and the sorption curve.

At equilibrium, the soil-moisture content at any given suction is greater for the desorption curve than for the sorption curve. See Figure 2.15. This path dependency is known as hysteresis.

Hysteresis is the result of two main phenomena: the first is the ink bottle effect. This is a result of the pore geometry. Pores consist of a narrow neck and a wide void space, with the capillary effect being greater in the neck than in the void.

When the soil is drained a suction, greater than the capillary drainage suction for the neck of the pore, needs to be applied before the pore drains. The pore then drains abruptly.

The water suction, upon rewetting, needs to be lowered to a suction less than the capillary drainage suction in the void space of the pore. The pore then fills abruptly.

The second effect is called **the raindrop effect**. This effect is the result of an advancing interface having a different contact angle to a receding interface. The curvature of the interface determines the magnitude of the suction.

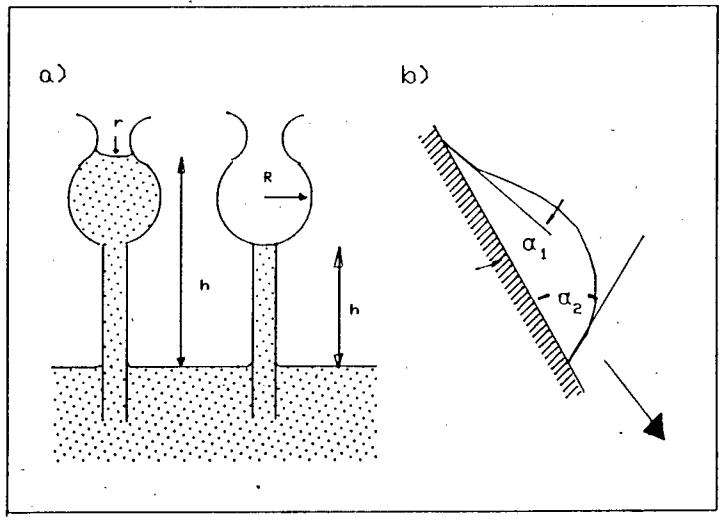


Figure 2.19 - Factors causing hysteresis :
a) Ink bottle effect
b) Raindrop effect

Entrapped air, upon rewetting, and possible consolidation (or swelling) of the soil also gives rise to hysteresis effects.

2.5.6 Equations for unsaturated flow

Darcy's Law for saturated flow may be extended to unsaturated flow with the provision that the coefficient of permeability is now a function of the moisture content or of the matric suction.

$$\underset{\sim}{q} = - \underset{\approx}{k}\,(\theta)\ \nabla h \qquad (2.29)$$

If we now introduce the continuity equation :

$$\frac{\partial \theta}{\partial t} = - \nabla . \underset{\sim}{q} \qquad (2.30)$$

and combine it with Darcy's Law we get the general equation for unsaturated flow.

$$\frac{\partial \theta}{\partial t} = \nabla . \underset{\approx}{k}\,(\theta)\ \nabla h \qquad (2.31)$$

Re-writing this equation and remembering from 2.19 that $h = z + \Psi$ we get :

$$\frac{\partial \theta}{\partial \Psi}\,(\theta)\ \frac{\partial \Psi}{\partial t} = \frac{\partial}{\partial x_i}\left[ k_{ij}\,(\theta)\ \left(\frac{\partial \Psi}{\partial x_j} + e_j\right) \right] \qquad (2.32)$$

where $x_i$ $(i = 1,2,3)$ are the Cartesian coordinates
with $x_3 = z$ (vertical coordinate)
$e_j$ is the unit gravitational vector in the vertical direction.

Equation (2.32) above is $\Psi$-based and is known as the Richards equation. It should be noted that the above equation reduces to the equation for saturated flow when $k(\theta)$ is taken to be constant and $\frac{\partial \theta}{\partial \Psi} = 0$. The derivations of the above equation may be found in works presented by Bear (1979), De Wiest (1969) and Freeze (1969). Most of the publications read by the author did contain background information relating to the governing flow equation in the unsaturated zone.

The term $\frac{\partial \theta}{\partial \Psi}$ is known as the specific moisture capacity and may be represented by $C(\theta)$. This term is defined as the inverse of the slope of the soil-moisture characteristic curve (see Figure 2.15) and is hence also subjected to hysteresis.

The Richards equation may be modified to become $\theta$-based. This is done using the diffusity concept [Freeze (1969)]. The Richards equation then becomes :

$$\frac{\partial \theta}{\partial t} = \frac{\partial}{\partial x_i}\left[ D_{ij}(\theta) \frac{\partial \theta}{\partial x_j} \right] + \frac{\partial k(\theta)}{\partial x_3} \qquad (2.33)$$

where

$$D(\theta) = k(\theta) \frac{\partial \Psi}{\partial \theta} \qquad (2.34)$$

and is known as the coefficient of moisture diffusivity [Bear (1979)].

The following difficulties arise when attempting to solve the unsaturated flow equation :

1. The highly non-linear nature of the functions $k(\theta)$ and $C(\theta)$ virtually preclude exact analytical solutions.

2. The above functions can only be determined experimentally and are subject to hysteresis.

3. Possible difficulties due to irregular boundary conditions and/or inhomogeneity of the medium.

## 2.6 VAPOUR FLOW

### 2.6.1 General

At all times the pores in the soil contain a certain amount of water. As mentioned earlier, water molecules leave and re-join the liquid phase. The molecules that leave the liquid phase and join the gaseous (vapour) phase are free to move from pore to pore in the soil. Vapour movement is a diffusion process while water flow is a mass flow process.

Water vapour movement is due to a vapour pressure gradient. Vapour moves from areas of higher vapour pressure to areas of lower vapour pressure.

2.6.2 Vapour movement

Under normal field conditions soil air can be considered to be nearly vapour saturated. At constant temperature conditions only small vapour pressure changes result from a change in the matric suction.

A change in temperature, however, causes considerable differences in vapour pressure. A 1°C change in temperature has about the same effect on the vapour pressure as a 100 bar change in the matric suction.

An increase in temperature causes an increase in vapour pressure and hence vapour tends to move from warmer to cooler areas. Since the earth's surface is warmer than the lower layers, during the day, water vapour tends to move downwards during this period. The opposite, however, occurs at night. Temperature gradients may also cause seasonal migration of water vapour.

Vapour movement does not constitute a major portion of moisture movement under normal field conditions. It can, however, be the main contributor in soils which have low moisture contents. This is the case in arid areas.

Vapour movement is also dependent on the compaction of the soil; occurring less readily in compacted soils than in loose soils with the same moisture content.

# CHAPTER 3

## EXPERIMENTAL APPARATUS AND THE PROCEDURES

(used to determine the soil-water characteristics)

### 3.1 INTRODUCTION

In this study three drainage problems were modelled using a finite element based model, presented in Chapter 4, which had been coded for application on a personal computer (a description of the programme is presented in Chapter 5).

The drainage problems modelled were a 1-D, 2-D plane and an axisymmetrical drainage problem. Only the 1-D and axisymmetrical problems were performed experimentally by the author. The experimental results for the 2-D plane problem were obtained from the work done by Wardle (1986) in equipment designed and constructed by Sparks (1966).

The first problem was a one-dimensional column drainage problem. A column of soil was first saturated and then allowed to drain: the drainage being due to a sudden drop in the water table. Experimental results of the outflow velocity, cumulated outflow and the remaining mass of the system versus time were compared against those obtained from the finite element programme.

The second problem was a three-dimensional (2-D plane problem). A block of saturated sand was drained by instantaneously lowering the water level at the one end of the block. Soil-moisture profiles and flow rates were used as the basis by which the experimental and numerical results were compared.

The third problem was a three-dimensional (axisymmetrical) problem. The experiment simulated radial flow to a well: the flow being caused by a rapid drop of the water level in the well. Soil-moisture profiles and flow rates were again used as the basis for the comparison.

However, before any attempts can be made to model a flow situation, the relevant soil properties and soil-water characteristics, particular to the soil, first need to be determined. They are the following :

1. The soil-moisture characteristic curve

2. The saturated coefficient of permeability as a function of the void ratio

3. The relative permeability curve as a function of $\theta$ or Sr

4. The particle size distribution

5. The relative mass density (i.e. specific gravity) of the sand

6. The void ratio of the sand in the model.

The above properties/characteristics were determined experimentally for two sands; sand A and sand B. These sands were used in the 1-D column drainage experiment. A third sand was used for the 2-D plane and axisymmetrical experiments. The properties/characteristics for this sand, sand C, were obtained from the work done by Wardle (1986).

See Appendix B for all the above mentioned soil properties/characteristics of the three sands.

## 3.2 DESCRIPTIONS OF THE SANDS

### 3.2.1 Sand A

Sand A is a sand commonly found on the Cape flats. This Cape flats sand was a uniformly graded, medium grained sand with a $D_{10}$ = 0,27 mm. There was a high percentage of organic material in this sand. An attempt was made to remove as much as possible of this material since it does affect the 'permeability characteristics' of the sand.

3.2.2 Sand B

Sand B was a gap-graded coarse grained sand with a $D_{10}$ = 0,62 mm. This whitish-grey sand is specified in the Concrete Technology Hand Book, for mortar testing.

3.2.3 Sand C

This sand was also a gap-graded, coarse grained sand with well rounded particles and had a $D_{10}$ = 0,74 mm. This whitish-yellow sand is a rare coarse sand obtained by Professor Sparks and a previous student. Further supplies of this sand have not been obtainable. Wardle (1986) performed his drainage experiments using this sand.

The $D_{10}$ rating of a soil is determined from a sieve analysis test and corresponds to the sieve mesh size permitting 10% (by mass), of the soil, to pass through it.

For all the calculations performed in this chapter the following units were used :

| | | |
|---|---|---|
| 1. | dimensions | cm |
| 2. | volumes | $cm^3$ |
| 3. | masses | g |
| 4. | velocities | cm/min |
| 5. | flow rates | $cm^3$/min |
| 6. | coefficients of permeability | cm/min |
| 7. | $\rho_w$ or $S_g$ | $g/cm^3$. |

## 3.3 THE EXPERIMENT TO DETERMINE THE SOIL-MOISTURE CHARACTERISTIC CURVE

The matric suction-moisture content relation is a characteristic of the soil which governs the flow of water in unsaturated soils. It is, therefore, required as input in the finite element programme. Since this function is subject to hysteresis, only the desorption curve (drying portion) was obtained from this experiment. It was, however, also possible to obtain the sorption curve and the intermediate scanning curves from this apparatus.

### 3.3.1 Apparatus

The apparatus used for this experiment was a circular plastic dish. Uniformly arranged in the dish, were four unglazed glass filters. Plastic tubes connected these filters to a burette.


Figure 3.1 - Apparatus used to determine the soil-moisture characteristic curve

### 3.3.2 Experimental procedure

The volume of the filters, in the dish, were first determined via water displacement. De-aired water was then placed in the dish and allowed to be drawn, by capillary action, into the filters through the connecting tubes and into the burette. Once equilibrium had been reached, the water in the dish was removed and the mass of the system and the water level in the burette recorded.

Unglazed glass filters were used as they have a high air-entry value and would prevent air from being drawn into the system at high suctions.

An oven dried sand sample, of known mass, was placed into the dish and 'saturated'. This was achieved by placing the sand into the dish, already containing a measure of de-aired water. The sand was then lightly stirred to remove entrapped air. The above method ensures a high degree of saturation. The system was then left for 24 hours to reach equilibrium. The mass of the system and the water level in the burette were then recorded at 24 hour intervals. The experiment was stopped when the mass of the whole system remained constant while the water level in the burette continued to drop. At this point the 'residual saturation' had been reached.

The water in the glass filters was in equilibrium with the water in the sand. As the soil moisture was evaporated from the sand, the water in the burette was sucked into the soil by capillary forces; the flow being as a result of the menisci in the sand being more curved (higher capillary pressure) than the menisci in the glass filters (lower capillary pressure). The drop in the water level in the burette was, therefore, a measure of the matric suction. The moisture content of the sand was then determined by mass.

The system was first saturated and then the soil was allowed to dry to obtain the desorption curve. If equilibrium readings had been taken as the soil was re-saturated, the sorption curve would have been obtained.

3.3.3 Readings

1. $M_d$ mass of empty dish (with water to equilibrium level in the burette)
2. $M_s$ mass of oven dried sand
3. $M_{si}$ subsequent mass readings of the system (dish, sand and water)
4. $h_o$ initial equilibrium water level in the burette

5. $h_i$ subsequent burette readings
6. $d_d$ diameter of the dish
7. $d_b$ diameter of the burette
8. $\ell_s$ length/thickness of the sand column.

3.3.4 Calculations

(a) The pressure head (matric suction) was determined from :

$$\psi = h_i - h_o \tag{3.1}$$

(b) The degree of saturation was determined from :

$$Sr = \frac{V_w}{V_v} \tag{3.2}$$

where $$V_w = [M_{si} - (M_s + M_d)]/\rho_w + \frac{\pi(d_b)^2}{4}(h_o - h_i) \tag{3.3}$$

$$V_v = V_t - V_s - V_f \tag{3.4}$$

where $$V_t = \frac{\pi(d_d)^2}{4}\ell_s \tag{3.5}$$

$$V_s = \frac{M_s}{S_g} \tag{3.6}$$

$V_f$ = volume of the filters
$S_g$ = relative mass density of the sand solids.

3.3.5 Comments

1. The above method used to determine the soil-moisture characteristic curve is a very lengthy procedure. It may take up to two weeks to obtain the full range of the curve.

A faster, less accurate method, could have been used. After the equilibrium water level is recorded, the burette may be lowered, to some predetermined height. The relevant readings are then recorded once the water stops flowing out

of the burette. It is assumed that at this stage equilibrium has been reached. It may, however, be difficult to determine this point as the flow may be very slow.

2. Maulem (1976) proposed a method for extrapolating parts of the soil-moisture characteristic curve. If a portion of the curve, above the air entry value, is available then the remaining parts may be extrapolated. It was found that this method yields good results. The initial parts of the curve may, therefore, be determined using the slow experimental method while the remaining parts could be extrapolated, using the method proposed by Maulem. This would be a faster way of determining the full range of the retention curve.

3. Some soils (clays) exhibit extremely high matric suctions at low moisture contents. A log scale is, therefore, sometimes used to express the large variation in matric suction. The scale used is known as the pF scale [$pF = \log_{10} \Psi(cm)$].

4. The results of this experiment for Sand A and Sand B may be found in Appendix B.

## 3.4 THE SATURATED PERMEABILITY TEST

The saturated coefficient of permeability of the soil is also an important input for the finite element programme. It can be obtained by either using a constant head or a falling head permeameter. For the sands used in this study it was possible to use a constant head permeameter. Falling head permeameters are normally used for soils which have low permeabilities, e.g. clays.

The saturated coefficient of permeability is dependent on the void ratio of the soil and can, therefore, be found as a function of the void ratio.

### 3.4.1 Apparatus

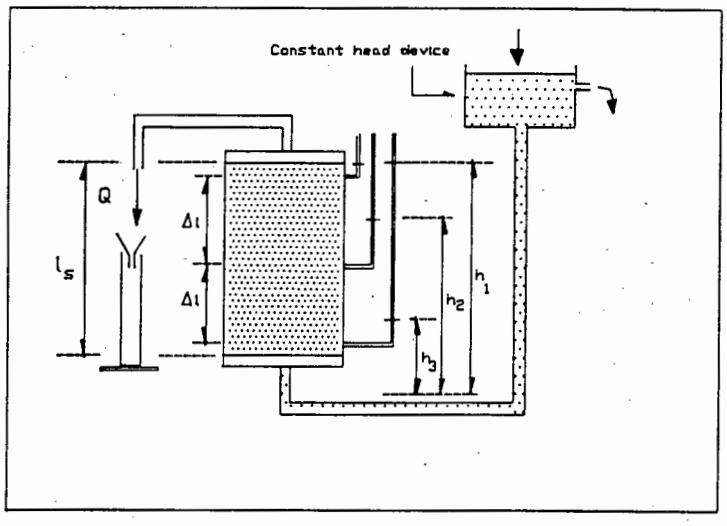


Figure 3.2 - Diagram of a constant head permeameter

### 3.4.2 Test procedure

An oven dried sand sample, of known mass, was placed in the permeameter which already contained a measure of water. A slight 'quick sand' condition was then induced to 'boil off' the entrapped air. The above procedure ensures a 'saturated state' (near saturated).

Quick sand conditions are brought about by feeding water through the bottom of the soil column at a high flow rate. The upward movement of the water, through the sand, causes the sand to boil. This occurs when the hydraulic gradient is in the vicinity of one.

The inflow was then stopped and the sand sample tamped, from the bottom up, with a thin wooden ramrod which had its end rounded. The length and diameter of the sand sample were then recorded.

Water was then allowed to flow into the soil at a constant rate. The quantity of water flowing out of the sample, in a given time, was recorded. The hydraulic gradient was determined from the piezometer readings. The coefficient of permeability could then be obtained by applying Darcy's Law.

This procedure was repeated, with increased inflow rates, until quicksand conditions occurred. Thereafter the procedures were repeated with decreasing inflow rates.

The length of the soil column remained constant and then increased as the hydraulic gradient approached unity. After quicksand conditions had occurred the flow rate was decreased, causing the length of the soil column to first shorten and then to remain constant. Where the length of the soil column remained constant, plots of seepage velocity versus the hydraulic gradient were made. The coefficient of permeability is represented by the slope of these straight line plots.

As the final length of the column was longer than the original length, the coefficient of permeability could be obtained for a dense (low void ratio) and a loose (high void ratio) packing in one run.

The experiment was repeated a number of times so that the coefficient of permeability could be written as a function of the void ratio. This was achieved by plotting the coefficient of permeability against $e^3/1+e$ and then doing a linear regression on this plot to obtain a linear function. The saturated coefficient of permeability could then be predicted for the same sand at any void ratio.

3.4.3 Readings

1. $M_s$ mass of oven dried sand
2. $d$ internal diameter of the permeameter
3. $\ell_s$ length of the sand column
4. $Q$ volume of water flowing out the permeameter
5. $\Delta t$ time interval in which $Q$ was recorded
6. $h_i$ piezometer readings ($i = 1,2,3$)
7. $\Delta \ell$ distance between piezometers.

### 3.4.4 Calculations

(a) The saturated coefficient of permeability was determined from :

$$k = \frac{v}{i} \tag{3.7}$$

where $$v = \frac{Q}{\Delta t A} \tag{3.8}$$

$$i = \frac{(h_1-h_2) + (h_2-h_3)}{2\Delta\ell} = \frac{h_1-h_3}{2\Delta\ell} \tag{3.9}$$

(b) The void ratio was determined from :

$$e = \frac{V_t-V_s}{V_s} \tag{3.10}$$

where $$V_t = \frac{\pi d^2}{4} \ell_s \tag{3.11}$$

$$V_s = \frac{M_s}{S_g} \tag{3.12}$$

### 3.4.5 Comments

1. The above method worked well for the coarse grained, gap-graded sand (sand B). It was, however, found for the uniformly grained sand, sand A, that the quick sand conditions caused a separation of the fines. For this reason only the initial readings were considered. A linear regression was then performed with these readings.

2. There are alternative methods to determine the saturated coefficient of permeability. One method uses the $D_{10}$ value of the sand, and is known as **Hazen's formula**. The formula is as follows :

$$k = c\,(D_{10})^2 \quad \text{cm/s} \tag{3.13}$$

where c is a constant dependent on the soil texture and structure.

c lies in a range from 45 (for clayey soils) to 140 (for pure sands). A value of 100 is, however, normally used.

the $D_{10}$ value is given in cm.

3. The results of all permeameter tests and linear regressions performed on Sand A and Sand B may be found in Appendix B.

## 3.5 THE EXPERIMENT TO DETERMINE THE RELATIVE PERMEABILITY CURVE

The relative permeability curve is also required as input for the programme. As the permeability-moisture content relation is subject to hysteresis, only that portion of the curve required for monotonic drainage calculations was obtained.

This curve is independent of the void ratio and is obtained by determining the permeability of the soil, at some moisture content, relative to the saturated permeability. The saturated permeability of the sand having been determined from the previous experiment. The ratio of the unsaturated permeability to the saturated permeability is known as the relative permeability of the soil.

### 3.5.1 Apparatus

The apparatus for this experiment comprised of a long perspex tube, with tensiometers positioned at determined lengths along the tube. The tube was suspended from a mass balance.

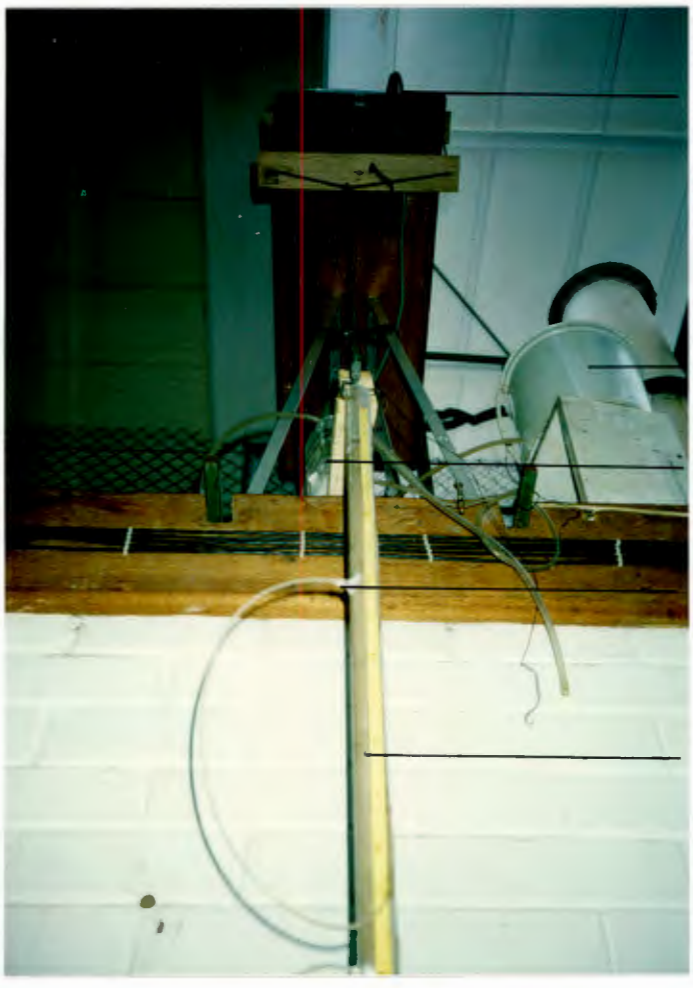


Figure 3.3 - Experimental apparatus

3.5.2 Experimental procedure

An oven dried sand sample, of known mass, was placed in the tube and its length recorded. De-aired water was then fed in through the top of the sample. The sample was nearly saturated (ponding did not occur) in this manner.

Once equilibrium was reached (inflow rate equal to the outflow rate), the mass of the system as well as the volume of water leaving the system in a given time was recorded. The hydraulic gradient was obtained from the tensiometers. The piezometric levels $h_1$, ... $h_5$ were recorded relative to the same base level (e.g. the outlet level). The unsaturated coefficient of permeability was then calculated using Darcy's Law and the full cross-sectional area while the moisture content was determined by mass.

The inflow rate was then reduced, and after equilibrium had been re-obtained, the above readings were again recorded. By repeatedly reducing the inflow rate the full range of the curve could be obtained.

The unsaturated coefficient of permeability was divided by the saturated coefficient of permeability to obtain the relative permeability. The relative permeability was then plotted against the degree of saturation of the unsaturated soil to obtain the relative permeability curve.

3.5.3 Readings

1. $M_t$ mass of the empty tube
2. $M_s$ mass of the oven dried sand
3. $M_{si}$ mass of the whole system (tube, sand and water)
4. d diameter of the tube
5. $\ell_s$ length of the sand column
6. Q outflow volume of water
7. $\Delta t$ time interval in which the outflow volume was recorded
8. $h_i$ piezometric level readings (i = 1,2,3,4,5)
9. $\Delta\ell$ distance between the tensiometers.

3.5.4 Calculations

(a) The unsaturated permeability was determined from :

$$k(\theta) = \frac{v}{i} \tag{3.14}$$

where $$v = \frac{Q}{A\Delta t} \tag{3.15}$$

$$i = \frac{(h_1-h_2) + (h_2-h_3) + \ldots (h_4-h_5)}{4\ \Delta\ell} \tag{3.16}$$

(b) The relative permeability was determined from :

$$kr = \frac{k(\theta)}{k_{sat}} \tag{3.17}$$

(c) The degree of saturation was determined from :

$$Sr = \frac{V_w}{V_v} \tag{3.18}$$

$$\text{where } V_w = [M_{si} - (M_t + M_s)]/\rho_w \tag{3.19}$$

$$\text{and } V_v = V_t - V_s \tag{3.20}$$

($V_t$ and $V_s$ calculated as before).

3.5.5 Comments

1. For this experiment it was hoped that the moisture content would be uniform down the length of the tube. A phenomenon known as the end-effect does, however, cause there to be a build-up of moisture just above the outflow face. The end-effect is a result of the soil, just above the outflow face, having to be of a certain moisture content before water will leave the sand column. Water leaves the outflow face when the water pressure, in this region, is equal to atmospheric pressure, and the degree of saturation approaches unity.

   Due to the end-effect, it is essential that a long tube be used for this experiment, the length of the tube used is dependent on the soil structure and texture. The finer grained the soil the more pronounced the end-effect and hence the longer the tube required.

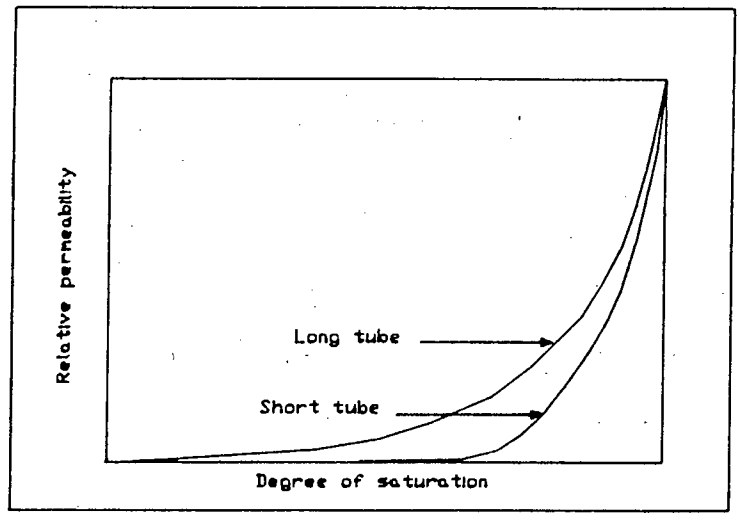


Figure 3.4 - Diagram showing the affect the end-effect may have on the relative permeability curve

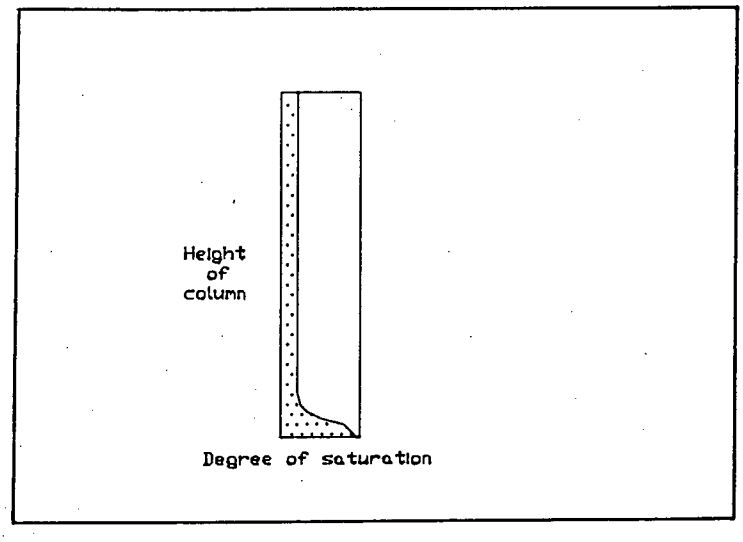


Figure 3.5 - The affect of the end-effect on the moisture distribution in the column

2. Maulem (1976) proposed a method for predicting the relative permeability curve from the soil-moisture characteristic curve. The formula used to predict the curve is :

$$kr = \left( \frac{Sr - S_{ro}}{1 - S_{ro}} \right)^{\beta} \qquad (3.21)$$

where $\beta$ is a constant in the range 3 - 4.

It was found, by the author, for the sands tested that $\beta = 3{,}75$ compared favourably with the experimental data.

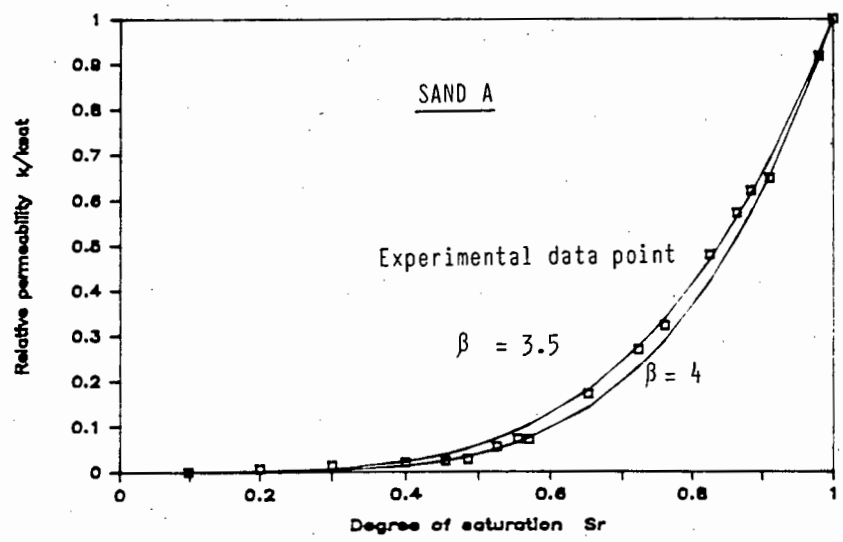


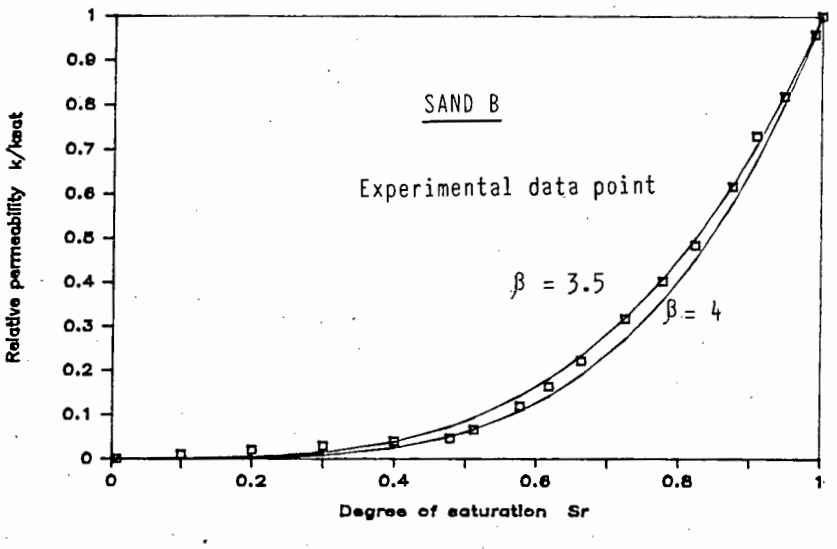


Figure 3.6 - Relative permeability curves obtained using Maulem's formula

Inherent in Maulem's method for extrapolating the retention curve was a way to determine the residual saturation. This is important as the choice of $S_{ro}$ directly affects the accuracy of the predicted relative permeability curve.

## 3.6 SIEVE ANALYSIS

A sieve analysis was performed on the sands to obtain their particle size distribution curves (grading curves). Although these curves are not used in the programme they are, however, needed to fully describe the soil. The grading curve may even vary for different samples of the same sand. Since the 'permeability characteristics' of the soil are dependent on the particle size distribution, it is important to keep a batch of sand. Sand from this batch should be used for all the experiments and should even be 'quartered' regularly to prevent separation of the fines.

In order to obtain meaningful results, when running tests, undisturbed soil samples should be used. This is, however, almost impossible to achieve. The affect of the grading on the permeability of the soil should, never the less, not be forgotten.

### 3.6.1 Test procedure

Standard dry sieving procedures were used.

See Appendix B for the grading curves of sand A, sand B and sand C.

## 3.7 THE RELATIVE MASS DENSITY TEST (i.e. Specific Gravity)

The relative mass density of most sands is about 2,65 ; the density of the sand being relative to the density of water at standard temperature and pressure. The relative mass density of a sand was required in order that the volume of the sand could be determined from its mass.

### 3.7.1 Test Procedures

Standard procedures were used to obtain the relative mass density of the sands.

See Appendix B for the results of the tests performed on Sand A and Sand B.

# CHAPTER 4

## THE MODEL FOR SIMULATING SATURATED-UNSATURATED FLOW

### 4.1 INTRODUCTION

The programme used to simulate the transient flow of water in a variably saturated soil profile, was based on a numerical model using both finite element and finite difference procedures. The Galerkin finite element method was used to approximate the governing flow equation, over the discretized flow domain, while a Pichard iterative scheme, using the finite difference approach of the time derivative, was used for time marching.

The programme was based primarily on the models presented by Huyakorn et al (1984) and Huyakorn et al (1986). Other models were, however, looked at and parts of them were incorporated into the programme. The other models which were looked at were models presented by Cooley (1983), Dagan (1979), Freeze (1969), Frind et al (1978), Khaleel et al (1988), Narasimhan et al (1978), Neuman (1973) and Tracy et al (1987).

All these models were based on the following assumptions :

1. The soil air was assumed to be stagnant and at atmospheric pressure, i.e. one-phased flow.

2. The matric suction and the relative permeability relationships of the soil are single valued continuous functions of the moisture content.

3. Darcy's law was applicable to flow in both the saturated and the unsaturated zones.

Wipplinger (1986) wrote a finite difference programme to simulate the two-phase flow situation in variably saturated soils. This was done by taking the viscosities of both the air and the water into account.

The water exerts a force on the air, in the pore space, as a result of the difference in their respective viscosities. Due to this transfer of viscous forces, the $\frac{\mu_w}{\mu_a}$ ratio affects the specific discharge. In order to extend Darcy's law to the two-phase flow situation the relative permeability must be written as a function of both the moisture content and the viscosity ratio.

The concept that the relative permeability is a function of the moisture content only is, however, a good approximation of the two-phase flow situation.

The model presented by Huyakorn was chosen as a basis for the programme as it contained certain features which enhanced the efficiency of the solution process. This model was also capable of handling complex seepage faces and boundary conditions associated with infiltration and evaporation.

The features inherent in the model are :

1. A method for evaluating the element matrices

   Due to the large number of iterations required to model a transient flow process, a method which avoids timely numerical integration is used.

   When modelling a one-dimensional flow situation, such as the column drainage experiment, for 10 minutes, using 20 elements, a 0,25 minute time increment with 10 iterations per time step, requires the calculation of 24 000 element matrices. This number increases the greater the accuracy required (more elements and smaller time steps) and the more complex the problem becomes (2-D, 3-D problems).

   An "influence coefficient" matrix technique is used to bypass numerical integration.

2. A solution algorithm capable of treating highly nonlinear flow conditions

The retention and relative permeability curves, which are determined experimentally, are highly nonlinear relationships which govern the flow of water in unsaturated soils.

The specific moisture capacity $\frac{\partial \theta}{\partial \Psi}$ ($n \frac{\partial Sr}{\partial \Psi}$) , is determined using a chord slope approximation. This is preferred to finding the tangent of the slope of the retention curve, as it leads to improved convergence (reduces oscillations about the solution).

3. A technique for matrix assembly and solution

This technique is essential when dealing with three-dimensional problems. Conventional procedures lead to a system of algebraic equations with large bandwidths. Since such systems are time consuming to solve a more economical technique is used.

It is essential, even in one-dimensional cases, to utilize the banded nature and symmetrical properties of the matrices.

4. An empirical method for updating the nodal pressure values, after each iteration

This, under relaxation technique developed by Cooley (1983), enhances convergence by dampening oscillations, in the pressure head values, from iteration to iteration.

## 4.2 THE GOVERNING FLOW EQUATION

### 4.2.1 General

The equation governing the isothermal flow of water in a variably saturated, three-dimensional soil, is the equation derived in Chapter 2 for unsaturated flow. Since this equation has the saturated flow case as a special case and since there is sufficient continuity across the phreatic surface, it can be used to model a saturated-unsaturated flow situation. The equation is :

$$\frac{\partial}{\partial X_i}\left[ kr\, k_{ij} \left(\frac{\partial \Psi}{\partial X_j} + e_3\right) \right] = \eta \frac{\partial \Psi}{\partial t} - q \qquad (4.1)$$

where $X_i$ $(i = 1,2,3)$ are the Cartesian coordinates
$e_3$ is the unit vector in the vertical direction
$k_{ij}$ is the saturated permeability tensor
$q$ is the volumetric flow rate via sources and sinks
$\eta$ is the overall storage coefficient
$kr\, k_{ij} = k_{ij}(\theta)$

Equation (4.1) may be written in a simplified form for 2-D plane and axisymmetrical problems. See Appendix C for these equations.

If the compressibility of the soil matrix is taken into account then :

$$\eta = \frac{\partial \theta}{\partial \Psi} + Sr\, S_s \qquad (4.2)$$

where $S_s$ is the specific storage and relates the change in the storage capacity of the soil with a change in its volume.

Neuman (1973) and Chung et al (1987) represent the overall storage coefficient as :

$$\eta = \frac{\partial \theta}{\partial \Psi} + \beta\, S_s \qquad (4.3)$$

where $\beta = 1$ for saturated flow
$\beta = 0$ for unsaturated flow.

The specific storage may be neglected for unsaturated flow ($\beta = 0$) as the effect of the compressibility of the soil matrix, on the overall storage of water, is small when compared with the effect of the changes in the moisture content.

If the compressibility of the soil matrix is neglected, as it is in this study, the overall storage coefficient reduces to the specific moisture capacity.

The flow equation has now been written with the pressure head $\psi$ as the primary variable. The pressure head is related to the soil moisture content by a highly nonlinear constitutive relationship dependent on the soil texture and structure. The relative permeability kr is also a nonlinear function which may be written in terms of the moisture content or the pressure head (matric suction).

4.2.2 Boundary and initial conditions

Equation (4.1) is solved subject to initial and boundary conditions, which may take the following form :

1. Initial pressure head conditions

$$\psi (X_i,0) = \psi_o (X_i) \qquad t = 0 \tag{4.4}$$

2. A prescribed pressure head boundary condition (Dirichet)

$$\psi (X_i,t) = \tilde{\psi} \text{ on } B_1 \qquad t > 0 \tag{4.5}$$

3. A prescribed flux boundary condition (Neuman)

$$V_i\, e_i = - V_n \text{ on } B_2 \qquad t > 0 \tag{4.6}$$

4. A moving boundary condition particular to seepage problems (associated with a falling water table/phreatic surface)

$$h = z \text{ on } B_s \qquad t \geq 0 \tag{4.7}$$
$$(\psi = 0)$$

where $e_i$ is the outward unit vector normal to the boundary. The negative sign represents flow out of the system.

The union of $B_1$ and $B_2$ forms the exterior boundary of the solution domain.

$B_s$ is the seepage face which is part of $B_2$.

Tracy et al (1987) incorporates in his model a method for simulating the interaction of ponded surface water with the water in the variably saturated soil. Where most authors prescribed a constant pressure head boundary condition along the water surface boundary of the soil, Tracy expresses this pressure head as a function of the soil-water flux. This aspect was, however, not looked into in this study.

Neuman (1973) presents a procedure for simulating seepage-face boundary conditions. This will be discussed in greater depth later in this chapter.

## 4.3 FORMULATION OF THE GOVERNING FLOW EQUATION USING THE GALERKIN FINITE ELEMENT METHOD

### 4.3.1 General

The finite element method of analysis is a numerical procedure whereby the flow domain, no matter how complex, is divided into discrete sub-domains known as elements. The primary variable $\Psi$ is approximated over each of these elements by a trial function such that the governing flow equation can be approximated over each of the elements using the Galerkin method. The flow equations for each element, over the whole domain, are then connected using the continuity of the primary variable between elements. After the initial and boundary conditions have been imposed the connected set of equations are then solved to determine the primary variable.

A finite element is a line (1-D), area (2-D) or a volume (3-D) with points (nodes) located along the elements boundary or at some intermediate points within the element.

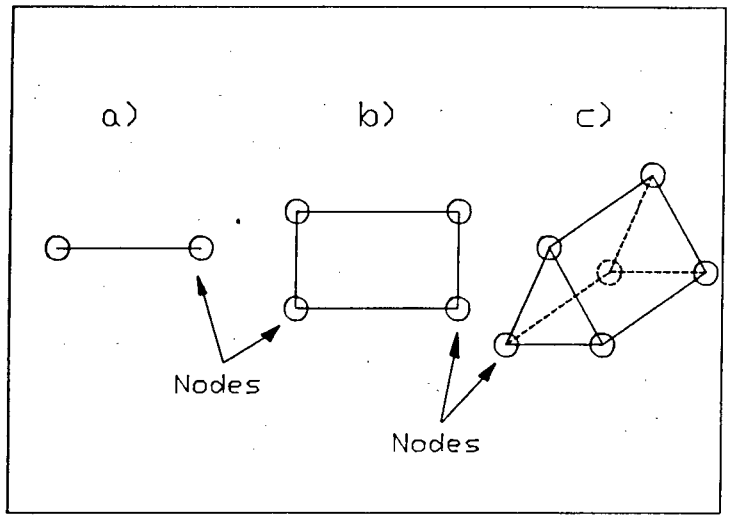


Figure 4.1 - Some typical finite elements
a) a two-noded linear element (1-D)
b) a four-noded square element (2-D)
c) a six-noded traingular prism element (3-D).

The primary variable is determined at these nodes and approximated within the element using the trial functions. The initial and boundary conditions are also specified at these nodes.

The shape, size and number of elements depends on the nature of the domain and the accuracy of the solution required.

### 4.3.2 Interpolation functions

The primary variable is approximated by the following trial function

$$\Psi(X_i,t) \approx \tilde{\Psi}(X_i,t) = \sum_{j=1}^{m} N_j(X_i)\,\Psi_j(t) \qquad (4.8)$$

where $N_j(X_i)$ are interpolation functions
$\Psi_j(t)$ are the nodal pressure head values at time $t$
$m$ is the number of elements comprising the domain.

The interpolation functions are not dependent on the problem itself but only on the type of element chosen (geometry and number of nodes per element). Since these functions are also used to define the geometry and the solution field, the efficiency of any particular element type, will depend on how capable it is of representing both the geometry and the solution field of the problem. See Appendix C for the interpolation functions used.

The interpolation functions have the following properties :

$$1. \qquad N_i^e(X_j) = \left\{ \begin{array}{l} 0 \quad \text{if} \quad i \neq j \\ 1 \quad \text{if} \quad i = j \end{array} \right\} \tag{4.9a}$$

$$2. \qquad \Sigma N_i^e (X_j) = 1 \tag{4.9b}$$

Condition one ensures that $N_i$ are linearly independent and that the primary variable is continuous between elements. Condition two permits problems, in which the primary variable is constant over an interval, to be modelled.

4.3.3 <u>The formulation of the flow equation</u>

The Galerkin method gives rise to a finite set of equations describing the state of the flow domain in terms of the approximated primary variable $\tilde{\Psi}$ . The value of $\tilde{\Psi}$ is determined at the nodes which define the geometry of the flow domain.

Applying the Galerkin procedure to (4.1) leads to the following set of equations :

$$\underset{\approx}{A}\,\underset{\sim}{\Psi} + \underset{\approx}{B}\,\dot{\underset{\sim}{\Psi}} = \underset{\sim}{F} \tag{4.10}$$

where $\underset{\approx}{A}$ is the conductance matrix

$\underset{\approx}{B}$ is the capacity matrix

$\underset{\sim}{F}$ is a vector including source and sink terms

$\dot{\underset{\sim}{\Psi}}$ is the time derivative of $\underset{\sim}{\Psi}$

The coefficient matrices are defined as :

$$\underset{\approx}{A} = \Sigma A_{ij}^{e} = \Sigma \int_{R^e} k_{ij}\, kr\, \frac{\partial N_j}{\partial X_j}\, dR \qquad (4.11)$$

$$\underset{\approx}{B} = \Sigma \int_{R^e} \eta\, N_i N_j\, dR \qquad (4.12)$$

and the right-hand-side vector as :

$$\begin{aligned} \underset{\sim}{F} = \Sigma F_i^e = \Sigma \Big( & \int_{R^e} - k_{ij}\, kr\, \frac{\partial N_i}{\partial X_i}\, e_j\, dR \Big) \\ & + \int_{R^e} N_i\, q\, dR \\ & + \Sigma \Big( \int_{B^e} V_n\, N_i\, dB \Big) \end{aligned} \qquad (4.13)$$

where $R^e$ is the element sub-domain with boundary $B^e$ and the summation is performed over the total number of elements.

q represents source and sink terms and will from now on be neglected as they are not considered in this study.

## 4.4 THE PICHARD ITERATIVE SCHEME

### 4.4.1 General

Equation (4.9) assumes that $k_{ij}$ , $S_s$ and n are constant over each element while kr and $\frac{\partial \theta}{\partial \Psi}$ vary within the element. It should also be noted that (4.10) is only valid at a particular instant in time. This is where the Pichard iterative scheme comes in. In this

scheme the time derivatives of the pressure heads $\dot{\underset{\sim}{\psi}}$ are replaced by finite differences.

$$\frac{\partial \psi}{\partial t} = \frac{\psi^{k+1} - \psi^{k}}{\Delta t} \tag{4.14}$$

where $\psi^{k+1}$ and $\psi^{k}$ represent pressure heads at the current and previous time levels respectively.

Equation (4.10) now reduces to :

$$\left\{ w\, A_{ij}^{k+w} + \frac{B_{ij}^{k+w}}{\Delta t_k} \right\} \psi_j^{k+1} = F_i^{k+w}$$

$$+ (w-1)\, A_{ij}^{k+w}\, \psi_j^{k} + \frac{B_{ij}^{k+w}}{\Delta t_k}\, \psi_j^{k} \tag{4.15}$$

where $w$ is a time weighting factor

$k$ and $k+1$ denote previous and current time levels respectively

$\Delta t_k$ is the kth time increment ($\Delta t_k = t_{k+1} - t_k$)

It should be noted that (4.15) represents a nonlinear set of equations as $A_{ij}$, $B_{ij}$ and $F_j$ are functions of the nodal unknowns $\psi_j^{k+1}$.

4.4.2 The solution procedure

Given the initial conditions $\psi_j^1$ (and the boundary conditions), equation (4.15) is solved to determine $\psi_j^2$. However, since (4.15) is a nonlinear set of equations the results may be improved using an iterative process. After satisfactory convergence of $\psi_j^2$ is achieved, it is then used to determine $\psi_j^3$. Time marching is achieved in this manner.

Since $A_{ij}$ , $B_{ij}$ and $F_i$ are functions of the nodal unknowns $\psi_j^{k+1}$ the values of $\psi_j$ at $t^{k+w}$ need to be determined to calculate $A_{ij}$ , $B_{ij}$ and $F_i$ . This is done using :

$$\psi_j^{k+w} = (1 - w)\, \psi_j^k + w\, \psi_j^{k+1} \qquad (4.16)$$

The most recent nodal values of $\psi_j^{k+1}$ are used to compute the matrices and the right-hand-side vector, after each iteration.

As can be seen from (4.16) $\psi_j^{k+1}$ needs to be approximated for the first iteration of each time step. The approximations are made using the following formulae :

$$\psi_j^{k+1} = \psi_j^k \qquad k = 1 \qquad (4.17a)$$

$$\psi_j^{k+1} = \psi_j^k + (\psi_j^k - \psi_j^{k+1}) \frac{\Delta t_k}{2\Delta t_{k-1}} \qquad k = 2 \qquad (4.17b)$$

$$\psi_j^{k+1} = \psi_j^k + (\psi_j^k - \psi_j^{k+1}) \frac{\log (\frac{t_{k+1}}{t_k})}{\log (\frac{t_k}{t_{k-1}})} \qquad k > 2 \qquad (4.17c)$$

4.4.3 The under-relaxation technique for dampening oscillations

The values of the pressure heads $\psi_j^{k+1}$ may oscillate from iteration to iteration. Cooley (1983) developed an under-relaxation technique to dampen these oscillations. This technique involves updating the nodal pressure head values, after each iteration, using the following empirical formula :

$$\psi_j^{r+1} = (1 - \delta^{r+1})\, \psi_j^r + \delta\, \psi_j^{r+1} \qquad (4.18)$$

where $r$ and $r+1$ denote previous and current iterations of time step $t_{k+1}$

$\delta$ is an iteration-dependent relaxation factor $(0 < \delta < 1)$

$\Psi_j^{r+1}$ is the current approximation of $\Psi_j^{k+1}$.

The relaxation factor is determined from :

$$\delta^{r+1} = \frac{3 + \xi}{3 + |\xi|} \qquad \xi \geq -1 \tag{4.19a}$$

$$\delta^{r+1} = \frac{0.5}{|\xi|} \qquad \xi < -1 \tag{4.19b}$$

where $\xi$ is an iteration parameter defined as follows :

$$\xi = 1 \qquad r = 0 \tag{4.20a}$$

$$\xi = \frac{\epsilon_{r+1}}{\delta^r \epsilon_r} \qquad r > 0 \tag{4.20b}$$

If the value of $\delta^{r+1}$ is :

$$\delta^{r+1} |\epsilon_{r+1}| > \epsilon_{max} \tag{4.21}$$

then $$\delta^{r+1} = \frac{\epsilon_{max}}{|\epsilon_{r+1}|} \tag{4.22}$$

where $r$ is the previous iteration level

$\epsilon_{r+1}$ is the largest absolute pressure head difference between iterations $r$ and $r+1$

$\epsilon_{max}$ is the maximum prescribed change in head per iteration.

It was, however, found by the author that by ignoring (4.19b) and not allowing $\delta^{r+1}$ to be below 0,5, convergence was improved.

In order to save on computational time and to further reduce the effect of the oscillations Huyakorn et al (1986) recommended that the number of nonlinear iterations per time step be limited to between 5 and 10.

4.4.4 The technique for handling the specific moisture capacity term

The specific moisture capacity term $\frac{\partial \theta}{\partial \Psi}$ is evaluated using a chord-slope formula. This method is preferred to finding the tangent of the slope of the retention curve as it enhances convergence.

Remembering that :

$$\frac{\partial \theta}{\partial \Psi} = n \frac{\partial S_r}{\partial \Psi} \tag{4.23}$$

the specific moisture capacity is evaluated using :

$$\frac{\partial Sr}{\partial \Psi} = \frac{Sr^{r+1} - Sr^{r}}{\Psi^{r+1} - \Psi^{r}} \qquad r > 1 \tag{4.24a}$$

where the absolute value of the denominator is not less than some small prescribed tolerance $\Delta\Psi$ min.

For the first iteration in each time step the specific moisture capacity needs to be determined from :

$$\frac{\partial Sr}{\partial \Psi} = \frac{Sr\ (\Psi^{k} + \Delta\Psi \text{ min}) - Sr\ (\Psi^{k})}{\Delta\Psi \text{ min}} \tag{4.24b}$$

This chord-slope approximation of the specific moisture capacity term can not be used when a fully explicit forward difference time stepping scheme is employed. This is due to the fact that there are no iterations involved in this scheme as (4.15) is no longer a non-linear equation.

Time stepping schemes will be discussed later in this chapter.

4.4.5 The influence coefficient matrix technique

In the Pichard iterative scheme the element matrices $A_{ij}$ and $B_{ij}$ and the right-hand-side vector $F_i$ need to be evaluated for each iteration of each time step. As was mentioned earlier kr and $\frac{\partial Sr}{\partial \Psi}$ vary within each element. If these values, within the element, were approximated using the interpolation functions.

$$\hat{kr} = \sum_{j=1}^{\ell} N_j (X_i) \hat{kr}_j (t) \tag{4.25}$$

$$\frac{\hat{\partial Sr}}{\partial \Psi} = \sum_{j=1}^{\ell} N_j (X_i) \frac{\hat{\partial Sr}}{\partial \Psi} (t) \tag{4.26}$$

where $\ell$ is the number of nodes per finite element

then it can be seen that the solution process would be extremely time-consuming due to the numerical integration involved.

If, instead, the centroidal values of kr and $\frac{\partial Sr}{\partial \Psi}$ are used in the evaluation of $A^e_{ij}$, $B^e_{ij}$ and $F^e_i$ then the numerical integration can be avoided. This leads to a great time saving and is adequate when used in conjunction with a sufficiently refined element mesh.

For a two-noded line element $A^e_{ij}$, $B^e_{ij}$ and $F^e_i$ are evaluated from :

$$A^e_{ij} = \frac{k_{sat}\ kr}{\ell^e} A^x_{ij} \tag{4.27}$$

$$B^e_{ij} = \frac{\eta\ \ell^e}{6} B^x_{ij} \tag{4.28}$$

$$F^e_i = - k_{sat}\ kr\ F^x_i \tag{4.29}$$

where $\ell^e$ is the element length

$X$ is the spatial coordinate

$A^x_{ij}, B^x_{ij}$ are the "influence coefficient" matrices

$F^x_i$ is the "influence coefficient" vector

$kr$ the centroidal value of the relative permeability

$\eta$ the centroidal value of the storage coefficient.

The term "influence coefficient" is used as the matrices and vector are independent of the geometry of the element.

See Appendix C for all influence coefficient matrices and vectors employed in the finite element programme.

4.4.6 The time increment

The value of the time increment, used in the analysis, determines how far into the future we predict the new pressure head values $\psi_j^{k+1}$, for each time step. The choice of the time increment may directly affect the accuracy and stability of the analysis. The choice of the time increment is, therefore, not arbitrary.

The size of the time increment is critical especially during the initial stages of the analysis. Gradients are large during the initial stages of the analysis but reduce with time. It is, therefore, possible to increase the value of the time increment logarithmically, from some small starting value to some predetermined maximum during the solution process. Once the maximum value has been reached the time increment remains constant at this value. Huyakorn recommends that the following formula be used to determine the initial value of the time increment.

$$\Delta t = \frac{\tau\, n\, (\Delta z)^2}{k_{sat}} \qquad (4.30)$$

where $\tau$ is a dimensionless time factor $0.01 < \tau < 0.1$

$n$ is the porosity

$\Delta z$ is the length on a finite element.

Subsequent time increments may then be determined from :

$$\Delta t_k = \beta \Delta t_{k-1} \qquad (4.31)$$

where $\beta$ lies in the range $1.2 < \beta < 1.4$.

The time increment may also be held constant throughout the entire analysis although this does increase the computational time required. Constant time increments were used when modelling the drainage problems, as they allowed for easier comparison between experimental and numerical results. Vermeer et al (1981) proved that when constant time increments are used, all time stepping schemes with $w > 0.5$ remain unconditionally stable.

The capacity matrix $B_{ij}$ is a nondiagonal matrix (non-zero off-diagonal terms). This fact gives rise to numerical difficulties, [Narasimhan et al (1978)]. The time increment may, therefore, not be too big or too small as it would not preserve the maximum principle. The maximum principle states that in the absence of a source $q$ the maximum value of the pressure head must occur at the initial time or at the boundary.

Vermeer et al (1981) found there to be oscillations, in the pore pressure, when using too small an initial time increment when modelling consolidation problems. Oscillations caused by too small a time increment are also apparent in other applications (e.g. soil seepage).

### 4.4.7 The time weighting factor

The choice of the time weighting factor ($0 < w < 1$) determines which time stepping scheme is employed. Some of the well known schemes are :

| | | | |
|---|---|---|---|
| 1. | $w = 0$ | Euler forward difference scheme | (fully explicit) |
| 2. | $w = ½$ | Crank-Nicholson time-centered scheme | (explicit-implicit) |
| 3. | $w = 2/3$ | Galerkin scheme | (explicit-implicit) |
| 4. | $w = 1$ | backward difference scheme | (fully implicit) |

The backward difference time stepping scheme is numerically unconditionally stable. That is to say that it will remain numerically stable irrespective of the time increment chosen. This does not mean, however, that the results will be accurate. More accurate results are achieved using a smaller time increment. All other schemes are numerically conditionally stable (time increment must be within some prescribed range).

Edwards in Narasimhan et al (1978) found empirically that $w = 0,57$ tends to eliminate persistent oscillations. He also found that the forward difference and time-centered schemes approach equilibrium too rapidly and, therefore, proposed a solution scheme where $w$ is a variable. This mixed explicit-implicit scheme uses $w = 0,57$ during the initial stages of the analysis and then allows $w$ gradually to tend towards 1 as equilibrium is approached. This prevents the loss of accuracy which results when $w$ is kept constant.

If a fully explicit or an explicit-implicit (Galerkin, Crank-Nicolson) scheme is used to model a soil where $S_s = 0$ then it may have a shortfall. This occurs when modelling the elements in the saturated zone. Since $S_s = 0$ and $\frac{\partial \theta}{\partial \Psi} = 0$ (saturated soil) the capacity matrix $B_{ij}$ falls away. The governing equation then becomes elliptical, [Neuman (1973)]. If a sudden change in boundary conditions, around the saturated zone, now occurs (the element de-saturates) it will have an instantaneous effect on $\Psi$ throughout the saturated zone and $\Psi_j^k$ will then become unknown.

Huyakorn et al (1984) and Neuman (1973) recommend that the fully implicit backward difference scheme be used to overcome this problem. When using the backward difference scheme in the saturated

zone with $S_s = 0$, it is not necessary to know $\psi_j^k$ to determine $\psi_j^{k+1}$. If the element de-saturates during the time step $B_{ij}$ becomes non-zero and hence $\psi_j^k$ is needed for the evaluation of $\psi_j^{k+1}$. It is, therefore, justifiable to set $\psi_j^k = 0$ if the values of $\psi_j^k$ become unknown due to a sudden change in boundary conditions, during a time step.

Neuman recommends that the coefficient matrices $A_{ij}$ and $B_{ij}$ and the right-hand-side vector $F_i$ still be evaluated at the half-time step. This dampens the tendency for $\psi$ to oscillate around its limit.

4.4.8 Seepage faces

The treatment of seepage faces was based on Neuman (1973).

A seepage face is an external boundary condition of the saturated zone. Water leaves the system (drains to the atmoshphere) along this face and hence $\psi = 0$. (Tail-end water levels are not considered). The face may not, however, be treated as a prescribed pressure head boundary as this would lead to a seepage face of constant length which is contrary to the physics of transient flow.

The seepage face may neither be treated as a prescribed flux boundary as:

$$Q_i = \Sigma \int_{B_e} V_n N_i \, dB \qquad (4.32)$$

is generally not known.

It should be noted that $Q_i$ is part of the right-hand-side vector $F_i$ and has a negative sign for flow out of the system.

A seepage face is, therefore, handled in the following way. (This section only refers to those nodes on the outflow face which may, at some stage during the analysis, become part of the seepage face).

The distinction between the outflow face and the seepage face should be made clear at this stage. The outflow face is the entire vertical boundary where water could possibly leave the flow domain (i.e. includes both the saturated and unsaturated portions of this boundary). Water, however, only leaves the domain from the saturated portion of the outflow face. It is this portion of the outflow face (whose length varies with time) that is known as the seepage face.

1. It is assumed that the position of the seepage is known at $t_k$ and needs to be predicted at $t_{k+1}$.

2. For the first iteration set $\psi = 0$ at all nodes along the seepage face. The seepage face is now treated as a prescribed pressure head boundary.

3. Also for the first iteration set $Q = 0$ for all nodes with $\psi < 0$ (unsaturated zone). This boundary is treated as a prescribed flux boundary.

4. The solution should yield $Q < 0$ where $\psi = 0$ was prescribed and $\psi < 0$ where $Q = 0$ was prescribed.

5. If $Q > 0$ is encountered where $\psi = 0$ was prescribed then set $Q = 0$ for the next iteration.

6. If $\psi > 0$ is encountered where $Q = 0$ was prescribed then set $\psi = 0$ for the next iteration.

7. If we set $Q = 0$ at a node for one iteration, then $Q = 0$ must remain for subsequent iterations.

8. The modification of the boundary conditions should proceed sequentially from node to node, starting at the saturated end of the outflow face. This enhances convergence.

# CHAPTER 5

# THE PROGRAMME FOR SIMULATING SATURATED-UNSATURATED FLOW

## 5.1 INTRODUCTION

The programme used for the simulations of the three drainage problems was written in True Basic for use on a personal computer. The programme was based on the theory presented in Chapter 4.

A dual floppy disk drive personal computer was adequate when simulating the one-dimensional drainage problem. It was, however, necessary to use a hard disk drive personal computer when simulating the two-dimensional drainage problems. This was due to the increased memory requirements for the more complex problems. A hard disk drive personal computer was adequate provided that the finite element mesh was not overly refined. It, nevertheless, took an exceedingly long time to complete the simulation of the two-dimensional drainage problems, even when an AT hard drive personal computer was used. It can, therefore, be seen that the main frame computer should have been used for efficient simulations of complex saturated-unsaturated flow problems.

## 5.2 DESCRIPTION OF THE PROGRAMME

The programme for simulating the saturated-unsaturated flow problems utilizes a constant, as opposed to an increasing, time increment and consists of a main driver programme and nine subroutines which are called to from the driver programme.

### 5.2.1 The driver programme

This section of the programme constitutes the main body of the programme where all the decisions are made. The theory presented in Chapter 4 is coded into this portion of the programme.

The driver programme consists essentially of two sections. The first section deals with the first iteration in a time level while the other section deals with all the remaining iterations in the time level. There are a maximum of 10 iterations per time level as

recommended by Huyakorn et al (1984). If, however, the largest absolute value of the difference in the pressure heads, between iterations, is less than 0,1 cm, then convergence is assumed and the programme moves to the next time level. If the finite element mesh is sufficiently refined then convergence will be achieved within the prescribed number of iterations.

In the first section of the driver programme $\Psi_j^{k+1}$, for the first iteration of the first time level, is approximated using (4.17a). Thereafter (4.17b) is used. (4.17c) was, however, not used in this programme as constant time increments were utilized. The moisture capacity term is calculated using (4.24b), and (4.19a) and (4.20a) are used when applying the under-relaxation formula.

In the second section (4.24a) is used to determine the moisture capacity term, while (4.19a) and (4.20b) are used when applying the under-relaxation formula. It was found that convergence was enhanced by not allowing $\delta^{r+1}$ to be below 0,5. For this reason (4.19b) was not incorporated into the programme.

All the relevant input data is fed into this programme in this section. The input data being the following :

1. The dimensions of the flow domain

2. The number of elements into which the domain is divided

3. The porosity of the sand

4. The saturated coefficient of permeability

5. The value of the time increment to be used in the analysis

6. The length of time for the simulation

7. The initial nodal pressure head values.

5.2.2 Sub Matdat

This subroutine is called to only once from the driver programme and contains the element matrices utilized in the programme.

Two noded linear elements were used for the one-dimensional flow problem while four noded rectangular elements were used for the two-dimensional flow problems. See Appendix C for the element matrices used in the programme.

5.2.3 Sub Moist

This subroutine basically represents the soil-moisture characteristic curve.

When using the influence coefficient matrix technique the centroidal value of the moisture capacity term is used to determine the relevant matrix coefficient. The centroidal value of the moisture capacity term is determined using the degree of saturation at the centroid of the element in either equation (4.24a) or (4.24b), depending on the iteration level.

The degree of saturation is determined in this subroutine from the soil-moisture characteristic curve, given the pressure head at the centroid of the element, which are approximated by :

$$\bar{\Psi}_j = \frac{\Psi_i + \Psi_{i+1}}{2} \quad \text{for 1-D problems} \tag{5.1}$$

and

$$\bar{\Psi}_j = \frac{\Psi_i + \Psi_{i+1} + \Psi_{znode+i} + \Psi_{znode+i+1}}{4} \quad \text{for 2-D problems} \tag{5.2}$$

where znode is the number of nodes in the vertical direction.

Equation (5.2) is applicable due to the way in which the finite element mesh was numbered for the two-dimensional problems. The node numbering will be described later in this chapter.

Due to the difficulty in describing the entire range of the retention curve with one equation, a series of polynomials were

used. This could give rise to discontinuities in the curve and hence cause severe oscillations when determining $\psi_j^{k+1}$. Caution should, therefore, be exercised when determining these best fit polynomials. See Appendix B for the polynomials used to describe the retention curves of the sands used in the drainage experiments.

5.2.4 Sub Perm

This subroutine basically represents the relative permeability curve. The curve is approximated using the formula given by Maulen (1976). See Appendix B for the formulae used to describe the relative permeability curves of the sands used in the drainage experiments.

The centroidal relative permeability value is also used to determine the relevant matrix coefficients. This is achieved by using the degree of saturation, determined in "sub moist" above, in Maulem's formula (3.21).

Both "sub perm" and "sub moist" are called to, for each iteration in each time level, from the driver programme.

5.2.5 Sub Elemat

In this subroutine the coefficients for the element matrices given in "sub matdat" are evaluated using the values determined in "sub moist" and "sub perm".

The equations for determining the matrix coefficients for all three flow problems can be found in Appendix C.

The moisture capacity term, used when evaluating matrix coefficients, is determined from either (4.24a) or (4.24b) depending on the iteration level.

5.2.6 Sub Globalmat

In this subroutine the element matrices are combined, according to the node numbering of the finite element mesh, to form the global

matrices. This can be done due to the continuity of the primary variable (the pressure head) between elements.

The global matrices are assembled using the symmetrical and banded properties of the element matrices. This cuts down on the amount of memory storage space required and on the number of repetitive calculations that need to be performed. By making use of the banded and symmetrical properties of the matrices, the run time is greatly reduced.

The way in which symmetrical matrices can be stored in banded form will now be shown using three 2x2 matrices.

If the element matrix is :

$$\begin{bmatrix} 2 & 1 \\ 1 & 2 \end{bmatrix}$$

then the global matrix consisting of three such elements would be :

$$\begin{bmatrix} 2 & 1 & 0 & 0 \\ 1 & 4 & 1 & 0 \\ 0 & 1 & 4 & 1 \\ 0 & 0 & 1 & 2 \end{bmatrix}$$

This matrix could, however, be stored as :

$$\begin{bmatrix} 2 & 1 \\ 4 & 1 \\ 4 & 1 \\ 2 & 0 \end{bmatrix}$$

in the programme, where the bandwidth of the above matrix is two. It can now be seen how the storage space required can be greatly reduced when storing a symmetrical matrix in its banded form.

Since all the zero terms, which are off the bandwidth, are neglected the computational time is greatly reduced, by avoiding repetitive calculations involving these zero terms.

For the one-dimensional finite element mesh the node numbering is not important with regard the way it effects the bandwidth of the global matrices. For the two-dimensional problems, however, the node numbering of the mesh can have a great affect on the bandwidth and hence the storage space and computational time required.

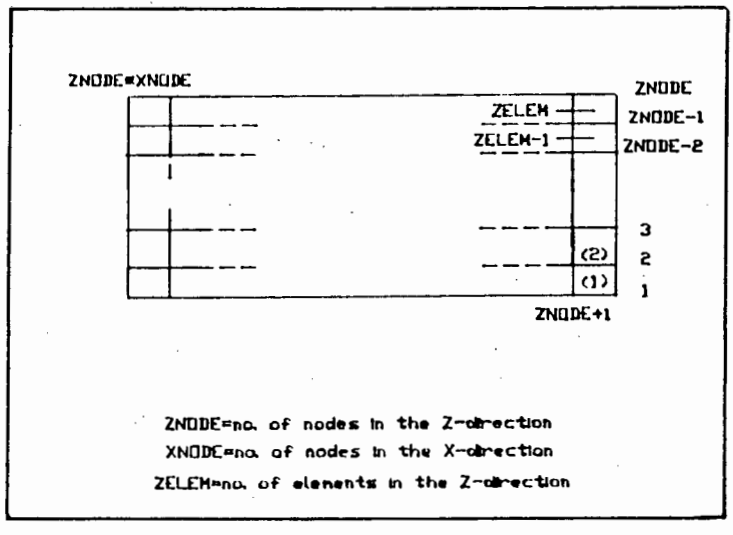


Figure 5.1 - The node numbering of the mesh used in the two-dimensional problems

The above node numbering gives the narrowest possible bandwidth for a domain where there are more elements in the x-direction than in the z-direction.

5.2.7 Sub Equatmat

In this subroutine the global conductance matrix $\underset{\approx}{A}$, the capacity matrix $\underset{\approx}{B}$ and the right-hand-side vector $\underset{\sim}{F}$ are assembled according to the flow equation (4.15) to obtain the final matrices to be used in the calculations.

These final matrices, from which $\Psi_j^{k+1}$ is determined, are also assembled in banded form. It is on these final matrices that the matrix calculations are performed.

5.2.8 Sub Matsolve

The final matrices assembled according to equation (4.15) in "sub equatmat" are now solved to determine $\Psi_j^{k+1}$ in this subroutine, subject to the boundary conditions.

The matrix solver used in this programme is adapted to handle the matrices in their banded form. It is this portion of the solution process which is so time consuming and hence the importance of reducing the number of calculations required by storing matrices in their banded form.

5.2.9 Sub Backsub

In this subroutine the normal nodal fluxes for the nodes on the seepage face are determined by back substituting $\Psi_j^{k+1}$ into (4.15).

The outflow face is treated partly as a prescribed pressure head boundary condition (saturated portion) and partly as a prescribed flux boundary condition (unsaturated portion). The nodal fluxes on the saturated portion are, therefore, unknowns and can only be determined by back substituting $\Psi_j^{k+1}$ into (4.15).

5.2.10 Sub Output

The results of the simulation may be written either to the screen, printer or a file in this subroutine. The results are only given at predetermined time intervals in order to facilitate the comparison between experimental and numerical output.

It is possible to achieve the following output from the programme :

1. Pressure and total heads at the nodes of each element

2. The permeability and degree of saturation at the centroid of each element

3. The Darcian velocity at the centroid of each element

4. The normal nodal fluxes at those nodes on the seepage face.

From the above data it is then possible to determine the following :

1. soil-moisture profiles

2. velocity profiles

3. total and pressure head profiles

4. the location of the water table/phreatic surface

5. the outflow velocities/fluxes

at various time intervals during the drainage process. In this way the drainage process can be monitored.

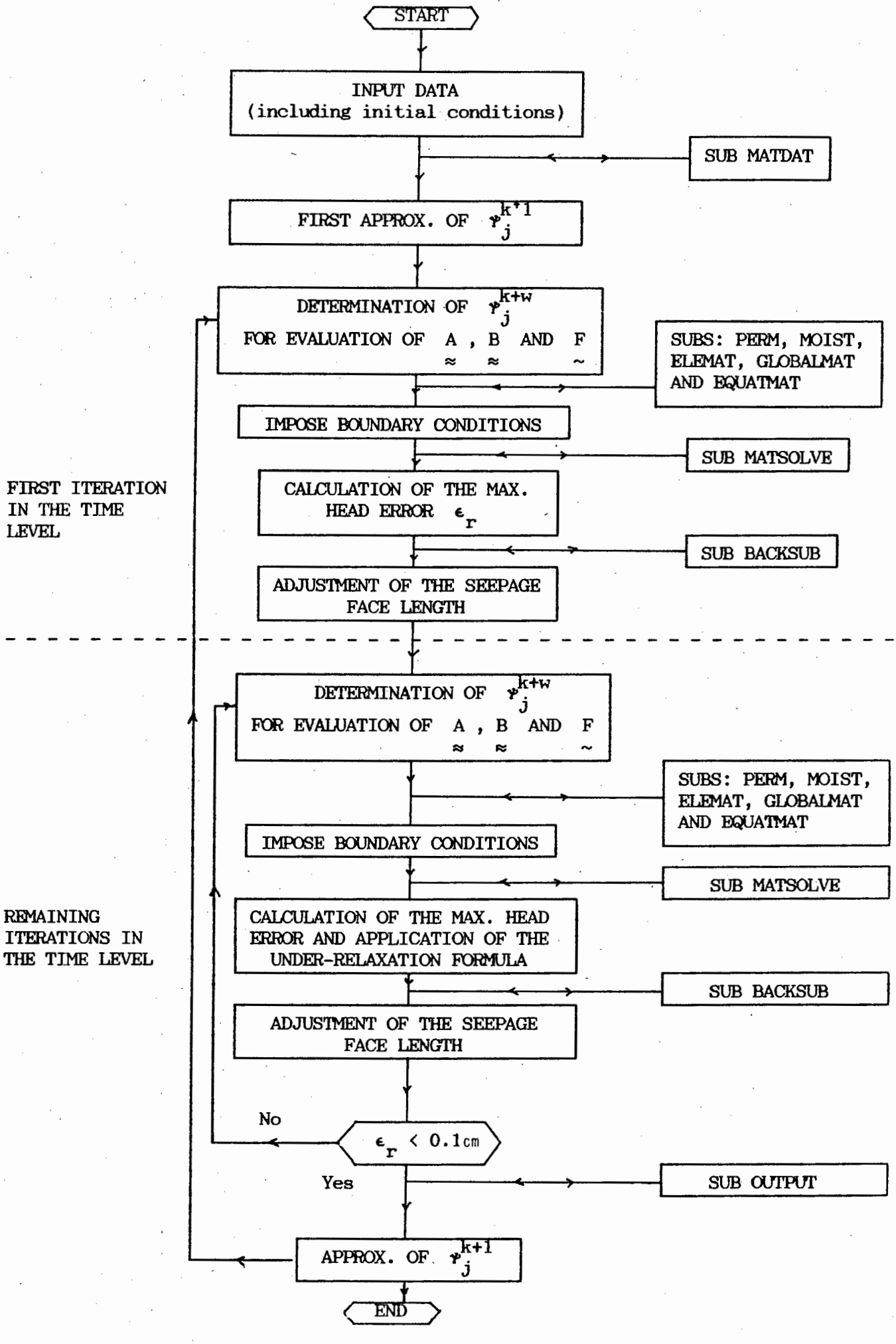
START
INPUT DATA
(including initial conditions)
SUB MATDAT
FIRST APPROX. OF $\psi_j^{k+1}$
DETERMINATION OF $\psi_j^{k+w}$
FOR EVALUATION OF $\approx A$ , $\approx B$ AND $\sim F$
SUBS: PERM, MOIST, ELEMAT, GLOBALMAT AND EQUATMAT
IMPOSE BOUNDARY CONDITIONS
SUB MATSOLVE
FIRST ITERATION IN THE TIME LEVEL
CALCULATION OF THE MAX. HEAD ERROR $\epsilon_r$
SUB BACKSUB
ADJUSTMENT OF THE SEEPAGE FACE LENGTH
DETERMINATION OF $\psi_j^{k+w}$
FOR EVALUATION OF $\approx A$ , $\approx B$ AND $\sim F$
SUBS: PERM, MOIST, ELEMAT, GLOBALMAT AND EQUATMAT
IMPOSE BOUNDARY CONDITIONS
SUB MATSOLVE
REMAINING ITERATIONS IN THE TIME LEVEL
CALCULATION OF THE MAX. HEAD ERROR AND APPLICATION OF THE UNDER-RELAXATION FORMULA
SUB BACKSUB
ADJUSTMENT OF THE SEEPAGE FACE LENGTH
No
$\epsilon_r$ < 0.1cm
Yes
SUB OUTPUT
APPROX. OF $\psi_j^{k+1}$
END

## 5.4 COMMENTS

All the subroutines, except "sub matdat", are called from the driver programme, for each iteration in every time level.

Since the seepage face length and the position of the water table (phreatic surface) are constantly changing, the boundary conditions have to be updated at the end of every iteration. The boundary conditions are updated and imposed within the driver section of the programme.

The under-relaxation formula, which is also applied at the end of every iteration, is first applied before determining the nodal fluxes on the seepage face and updating the boundary conditions.

The fault with this programme is that it is not sufficiently flexible when dealing with 2-D problems. It was coded for 4 noded rectangular elements with the mesh numbered in a particular way. No other element type or node numbering is permissible. The flow domain may also only be subdivided into elements in a particular way, thus giving rise to finite elements of the same size. This is possibly the greatest fault of the programme.

Smaller elements are needed near the outflow face, where the gradients are larger, while larger sized elements may be utilized further from this face. The size of the mesh used, when simulating the two-dimensional drainage problems, was limited by the memory capacity of the computers used. The larger than required number of elements in the upstream portion of the flow domain increased the computational time required.

This programme could be improved by making it more flexible. The ability to handle elements of varying size and possibly other element types, would greatly improve on the performance of this programme.

Finally, it should be noted that the finite elements used in this programme are constant in both shape and position and do not change as the phreatic surface falls. The water content, matric suction and permeability merely change in the element with time.

# CHAPTER 6

# THE ONE-DIMENSIONAL COLUMN DRAINAGE PROBLEM

## 6.1 INTRODUCTION

The first drainage problem which was modelled using the finite element programme, described in Chapter 5, was the drainage of an initially 'saturated' (nearly saturated) vertical column of sand. The results from this drainage experiment, which was performed using both sand A and sand B, were compared against the equivalent results obtained from the finite element programme.

The drainage of the sand column was as a result of a sudden drop in the water table. The water did not, however, drain to a new table, but rather drained from the bottom of the column to waste. The mass of the column, the outflow velocity and the cumulative outflow were the parameters by which this transient process was monitored.

The drainage of the column was modelled using two different theories. The first theory assumed that only saturated flow took place (unsaturated flow was entirely ignored). The second theory was the combined saturated-unsaturated theory. By doing this the importance of considering the unsaturated zone, in the flow of moisture, was revealed. Different numerical variables were also used in the analysis to determine the effect they had on the accuracy of the simulation.

Graphs showing the comparisons between experimental and numerical results may be found at the end of this chapter.

## 6.2 THE EXPERIMENT

### 6.2.1 Experimental apparatus

A long perspex tube suspended from a mass balance was the basis of the apparatus used in this experiment. A wire mesh with supports was fixed to one end of the tube. This mesh retained the sand in the column and formed the outflow face. A rubber-lined perspex

stopper, through which de-aired water was fed into the column, could be attached to the bottom end of the perspex tube. Apart from being used to saturate the sand, the stopper could be instantaneously removed to simulate a sudden drop of the water table.


Figure 6.1 - The apparatus used in the column drainage experiment

6.2.2 Experimental procedure

The mass balance was first zeroed before an oven dried sand sample was placed in the suspended tube. The length and the mass of the sand column were then recorded in order that the void ratio of the sand be determined. From the void ratio and the results of the permeability tests described in Chapter 3 the saturated coefficient of permeability of the sand could be estimated. Both the void ratio

(porosity) and the coefficient of permeability were required as input in the programme.

The perspex stopper was then fixed to the bottom of the tube and the sand column saturated. High degrees of saturation were achieved by feeding de-aired water in through the bottom of the column. The column could have been saturated by feeding the de-aired water in through the top of the column. Although this method does not initially yield high degrees of saturation, the entrapped air can be removed with continuous flow of water through the column. The entrapped air is removed by the viscous forces imposed on it by the flowing water. When using this method, suitable degrees of saturation may, however, only be achieved after some time.

When saturating the column, the water was allowed to rise above the level of the sand in the column. The stopper was then released and the column allowed to drain. The drainage process was monitored, at various time intervals, over a one hour period, from when the falling water table reached the top of the sand column. The water table was allowed to rise above the sand column before drainage commenced as this gave the system time to stop oscillating after the stopper had been removed. Oscillations of the system hampered the mass being recorded.

By determining the mass of the system at various time intervals both the cumulative outflow and the outflow velocity could be determined. These values were used for the comparison with the equivalent values obtained from the computer programme. Due to the slow response time of the tube tensiometers, on the side of the perspex column, soil moisture profiles could not be used as a means of comparison.

An alternative method of inclining the tube, for a short time during the drainage process, was attempted. By inclining the tube and using a rough iterative method, both a pressure head and an approximate soil moisture profile could be obtained.

During the drainage process the mass of the system was recorded in both the vertical and inclined positions. At various time intervals the tube was inclined, to some pre-determined position, and the mass recorded. The tube was inclined in such a manner that the end support reactions remained vertical. By inclining the tube, the contributions of the sand and the water to the total mass of the system could be separated. Since the mass and centre of mass of the sand was known and constant during the drainage process, the mass and centre of mass of the water remaining in the column could be determined.

See Appendix D for an explanation of the analysis of the "inclined tube" procedure.

Since the tube was moved so often, a scale accurate to 5 g's was used to record the mass of the system. This dampened the oscillations of the mass reading displayed on the mass balance. It was, however, discovered that the scale was not sensitive enough to determine the outflow velocities accurately enough. It was also felt that the drainage pattern was disturbed when the tube was inclined, even though the tube was inclined for only a short time.

It was, therefore, decided to use a scale accurate to 0,1 g's to record the mass of the column and to keep the tube vertical during the entire drainage process. It was hoped by doing this that more accurate and realistic results could be achieved for comparison with the numerical ones.

6.2.3 Readings

1. $M_s$ mass of the oven dried sand
2. $M_{so}$ initial mass of the system (water table at the top of the sand column)
3. $M_{si}$ subsequent masses of the system
4. $t_o$ time when the initial mass of the system was recorded

5. $t_i$ times when the subsequent masses of the system were recorded
6. d internal diameter of the tube
7. $\ell_s$ length of the sand column.

6.2.4 Calculations

For the calculations performed in this chapter the following units were used :

| | | |
|---|---|---|
| 1. | dimensions | cm |
| 2. | volumes | $cm^3$ |
| 3. | masses | g |
| 4. | velocities | cm/min |
| 5. | $\rho_w$ and $S_g$ | $g/cm^3$ |

(a) The void ratio was determined from :

$$e = V_v/V_s \tag{6.1}$$

where $$V_v = V_t - V_s \tag{6.2}$$

$$V_t = \frac{\pi d^2}{\Psi} \ell_s \tag{6.3}$$

$$V_s = \frac{M_s}{S_g} \tag{6.4}$$

(b) The initial degree of saturation was determined from :

$$S_r = \frac{V_v}{V_s} \tag{6.5}$$

where $$V_w = \frac{M_{so} - M_s}{\rho_w} \tag{6.6}$$

$V_v$ as above.

(c) The cumulative outflow was determined from :

$$Q_i = [M_{so} - M_{si}]/\rho_w \tag{6.7}$$

(d) The outflow velocity was determined from :

$$v_i = \frac{(M_{s(i-1)} - M_{s(i)})/\rho_w}{(\frac{\pi d^2}{4})(t_{i-1} - t_i)} \tag{6.8}$$

## 6.3 MODELLING THE PROBLEM

The relevant soil and soil-moisture characteristics, initial and boundary conditions first had to be fed into the finite element programme before it could be used to simulate the drainage problem.

It was found, during the simulations, that certain numerical variables, such as the time weighting factor and the time increment could greatly affect the accuracy of the results achieved and, therefore, could not be chosen arbitrarily. This applied more to the time increment than the time weighting factor.

### 6.3.1 Input data

Relevant input data first had to be fed into the programme before the simulation could be made. Apart from the retention and relative permeability curves, which had to be determined experimentally, the following input data was also fed into the programme :

Sand A

Length of sand column = 184,5 cm
Porosity of the sand = 0,399
Saturated coefficient of permeability = 2,53 cm/min
The number of finite elements comprising the domain = 20
The time weighting factor = 1
The pressure head at the top node = -6 cm
The pressure head at the bottom node = -0,5 cm
(pressure heads at the intermediate nodes were determined using linear pressure distribution).

Sand B

Length of the sand column = 185,4 cm
Porosity of the sand = 0,361
Saturated coefficient of permeability = 10,68 cm/min
The number of finite elements comprising the domain = 20
The time weighting factor = 1
The pressure head at the top node = -1,27 cm
The pressure head at the bottom node = -0,75 cm
(pressure heads at the intermediate nodes were determined using a linear pressure distribution).

### 6.3.2 Discretization of the column

The column of sand (the flow domain) was divided into a number of two noded linear finite elements. These elements, connected at their nodes, constituted the finite element mesh.

For the one-dimensional simulation of the column drainage problems a 20 element mesh was used. Although more refined meshes could have been used, it was found for both sand A and sand B, that a 40 element mesh gave no significant improvement of the results. See Figures 6.12 and 6.13 for a comparison of the results obtained from a 20 element and a 40 element mesh for sand A and Figures 6.26 and 6.27 for sand B.

The more refined a mesh the more accurate the results but the greater computational time required. One, therefore, has to find some suitable compromise. The author decided to use a 20 element mesh for all the simulations, due to the shorter computational time required.

The finite element mesh was numbered as follows :

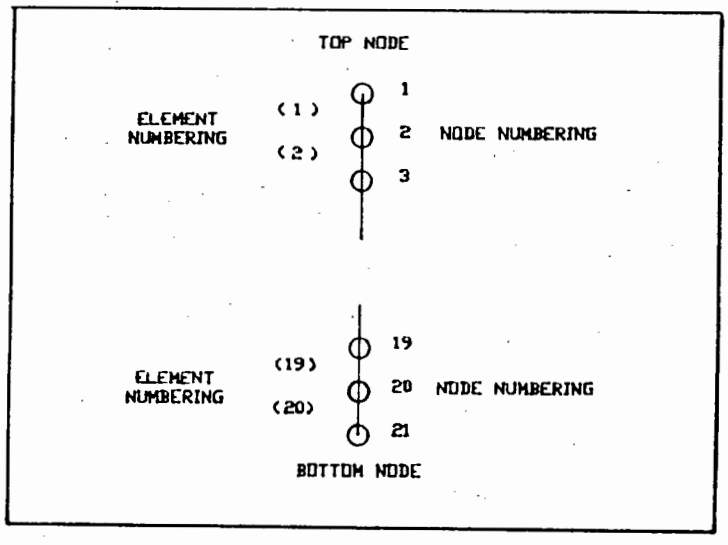


Figure 6.2 - The node and element numbering of the flow domain

The way in which the mesh is numbered may affect the bandwidth of the global matrices and the accuracy of the results achieved. This effect is, however, not significant for one-dimensional problems.

6.3.3 Initial and boundary conditions

Boundary conditions imposed on the flow domain were a Dirichet boundary condition at the bottom node and a Neuman boundary condition at the top node. A zero pressure head boundary condition was imposed at the bottom node, as the water drained from the column to the atmosphere at this node. After the initial free water above the upper soil surface vanished downwards into the soil, no further water was added to the column. As there was no inflow into the column during the drainage process the top node was treated as a zero flux boundary condition.

Initial conditions imposed on the flow domain were in the form of prescribed pressure heads down the length of the sand column. These pressure heads were prescribed at the nodes of the elements.

Difficulties arose when trying to determine the initial conditions. Due to the slow response time of the tube tensiometers, fixed to the side of the column, it was difficult to determine the pressure heads as the water table fell from its initial position to the top of the sand column.

The prescribed pressure heads were therefore approximated using the initial degree of saturation of the column and the retention curve. Since the column was saturated from the bottom up, it was felt that lower portions of the tube would be more saturated than the upper portions. Pressure heads were, therefore, prescribed at the top and bottom nodes with the pressure heads at the intermediate node evaluated using a linear distribution. The distribution was such that the overall degree of saturation was maintained.

This may seem a very crude method, but since the column was nearly saturated, only a small pressure gradient existed between the top and bottom nodes of the column. Using these pressure heads the moisture contents of each element was determined via the retention curve. Using these moisture contents the initial total mass of the column could be evaluated (mass of sand was known). For both sands the initial mass was calculated to within 0,2% of the experimental value. The author, therefore, felt it adequate that the pressure heads could be determined in this manner.

### 6.3.4 The time weighting factor and the time increment

As was mentioned in Chapter 4, different time marching schemes may be employed in the analysis, simply by choosing a value for $w$ (time weighting factor) in the range $0 \leq w \leq 1$. The governing flow equation (4.15) is a nonlinear equation since $A_{ij}$, $B_{ij}$ and $F_i$ are functions of the nodal unknowns $\Psi_j^{k+1}$. The choice of $w$ determines the percentage of the unknowns $\Psi_j^{k+1}$ used to evaluate these matrices.

Two of the classical schemes, the backward difference scheme and the central difference scheme, were used in the analysis of these problems. The central difference scheme is numerically stable provided a sufficiently small time increment is utilized. Although the backward difference scheme is unconditionally stable the time increment must be small enough to obtain accurate results.

Vermeer et al (1981), however, found that if the time increment was too small, oscillations occurred which affected the accuracy of the results. This is especially true during the initial stages of the analysis when gradients are large.

Huyakorn et al (1986) recommended that equation (4.30), presented in Chapter 4, be used as a guideline when determining the magnitude of the time increment to be utilized.

A range of time increments were employed in conjunction with both time marching schemes, in order that the effect they have on the analysis be revealed. In this manner equation (4.30) could be validated. The numerical results obtained using the different time marching schemes and time increments may be found at the end of this chapter.

Constant, as opposed to variable, time increments were used for the analyses. Although this increased the computational time required it did, however, facilitate the comparison of the experimental and numerical results. Vermeer et al (1981), also proved that all time marching schemes with $w > 0,5$ were unconditionally stable when constant time increments were employed.

## 6.4 DISCUSSION OF THE RESULTS

When one looks at the results of the analyses of the drainage experiments performed on the two sands, one can see that the same general trends occur for both sands. A direct comparison between the two sands can, however, not be made as at any instant sand B had drained to a larger extent than sand A. This is due to the larger grain size and lack of fine particles in sand B.

6.4.1 Saturated versus combined saturated-unsaturated theory

The two theories were used to show the effect the unsaturated zone has on the overall drainage pattern. Admittedly the flow in this experiment was essentially unsaturated flow, but the experiment did, nevertheless, reveal that unsaturated flow can not be approximated using saturated flow theory. Figures 6.4 and 6.5 show the results of the analyses performed, using both theories, on sand A while figures 6.18 and 6.19 are applicable to sand B. It can be seen from these figures that the unsaturated zone retards flow and hence causes a time delay in the drainage of water. It can also be seen that the difference between the two theories is more pronounced for the coarser grained of the two sands, sand B.

6.4.2 The numerical variables

A series of simulations were performed on both sands using a 20 element mesh while varying the numerical variables. The objective of this was to determine the time marching scheme and value of the time increment best suited to modelling these problems. The results of the simulation, best suited to modelling the problem, were then used to discuss the general trends.

The time increment, as calculated using the formula recommended by Huyakorn et al (1986), should lie in the range $0{,}133 < \Delta t < 1{,}33$ min for sand A and $0{,}029 < \Delta t < 0{,}29$ min for sand B. Time increments of 1 min, 0,5 min and 0,05 min where used in conjunction with the backward difference scheme when simulating the drainage of sand A; the results of which may be seen in Figures 6.14 and 6.15. For sand B, time increments of 0,5 min, 0,25 min and 0,05 min were used. See Figures 6.28 and 6.29 for these results.

It can be seen from these figures that the time increments which lay in the range specified by Huyakorn's formula did yield the best results. The time increments closer to the upper limit of the range did, however, appear to yield the best results. The time increments of 1 min for sand A and 0,25 min for sand B were, therefore, used for all subsequent simulations.

Using these time increments, it appeared from Figures 6.16 and 6.17 (sand A) and 6.30 and 6.31 (sand B) that the backward difference scheme yielded better results than the central difference scheme. As expected the central difference method yielded better results with smaller time increments.

The simulations using the backward difference scheme and the time increments decided upon above, are now used as the basis from which the comparison between the numerical and experimental results will be discussed.

6.4.3 The outflow velocity

The comparisons between the experimental and numerical results were at first based primarily on the outflow velocity. It can be seen from Figure 6.7 (sand A) and Figure 6.21 (sand B) that the outflow velocity could not always be predicted to within 10% of the experimental value.

This may give the impression that the numerical results are not that accurate. It was, however, felt that the wire mesh and the supports supporting the sand in the column were restricting the outflow by reducing the area available to flow. Since sand B is a coarser grained sand than sand A, the effect of the mesh, on the drainage of sand B, would be more noticeable. This can, in fact, be seen from the above-mentioned figures.

If the mesh did restrict the outflow it would explain why, during the initial stages of the drainage process, the experimental results are lower than numerically predicted. This can be seen from Figures 6.8 (sand A) and Figure 6.20 (sand B). This reasoning would also explain why the experimental results were subsequently larger than numerically predicted. The moisture content of the sand would, during this period, be higher than numerically predicted. This can be seen from the cumulative outflow graphs Figures 6.8 (sand A) and 6.22 (sand B). The higher moisture content results in a higher coefficient of permeability and hence a higher outflow velocity.

An attempt was made to model the effect of the mesh and the supports. This was done by reducing the area of the bottom element and refining the mesh. When doing this, small positive pressures arose at the nodes near the bottom of the column. This gave rise to an unlikely pressure distribution as the bottom node was still treated as a zero prescribed pressure head boundary condition.

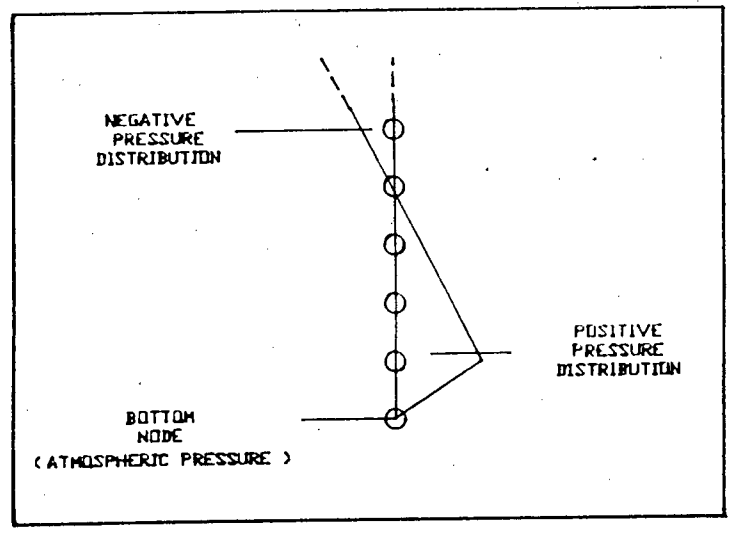


Figure 6.3 - The pressure distribution at the bottom end of the column

From the pressure distribution shown above it would appear that the pressure head at the bottom node was, in fact, non-zero. Since the outflow velocity is calculated from the nodal pressure heads of the bottom element, any discrepancies in these pressure heads would greatly affect the outflow velocity.

When looking at Figure 6.20 one sees a kink in the numerical curve at about $t = 25$ min. It was, at first, felt that this was a result of a discontinuity in the retention curve, but this kink persisted after attempts had been made to smooth the curve. It was then felt that a small negative pressure could possibly exist at the bottom node during the latter stages of the drainage process.

6.4.4 The cumulative outflow and the mass of the system

Owing to the uncertainty of the pressure head at the bottom node of the column, the cumulative outflow and the mass of the system (sand and water) were also used as parameters by which comparisons could be made. It was hoped that these parameters would be less sensitive to the possible existence of pressure heads, at the bottom node, as they represent more globalised results.

As can be seen from Figures 6.10 (sand A) and 6.23 (sand B) the cumulative outflow could, at every instance, be predicted to within 10% of the experimental values.

The mass of the system could, however, be predicted to within 1% of the experimental value. One must, however, remember that the mass of sand (a large constant mass) would make this parameter less sensitive. See Figures 6.12 (sand A) and 6.25 (sand B) for these results.

6.4.5 General

Two noded linear finite elements give rise to constant pressure gradients across the elements. This results in a discontinuity (a jump) in the pressure gradient across the node. Higher order elements, e.g. 3 noded elements, would improve the accuracy of the numerical results as they give rise to linear pressure gradients across the elements, thus avoiding jumps in the pressure gradients between elements.

The porosity of the sands from which the retention curves were determined differed from the porosity of the sands on which the drainage experiments were performed. Although the differences in the porosities were not large, it is not possible to determine the extent to which these differences affected the drainage results.

For the numerical simulations it was assumed that the porosity was constant down the length of the tube. Considering the way in which the sand was poured into the tube, this would be unlikely. It was, however, felt that this would not affect the results significantly.

## 6.5 CONCLUSIONS AND RECOMMENDATIONS

From the above it can be seen that the difference in the results could be either of a numerical or an experimental nature. Bugs, in the code itself, may also have caused some discrepancies. Therefore, in the absence of an analytical solution it is difficult to assess the accuracy with which the programme simulated the column drainage experiment.

Since the cumulative outflow and the mass of the system could, at any stage, be predicted to within 10% of the experimental value, the author feels that the model and the programme are suitably accurate. The dependency of the model (programme) on the experimentally determined retention and relative permeability curves should not be forgotten. The author, however, feels that the main reason for the discrepancies lies in the fact that the wire mesh, at the bottom of the column, was not suitably taken into account.

For any future work on this particular experiment the author feels that instantaneous or null-flow devices be used to record the pressure heads. They would assist greatly in the following :

1. Accurate determination of the initial conditions

2. Reveal the possible existance of pressure heads at the outflow face (bottom node of the column).

On the numerical side the author feels that use of higher order finite elements (3 or 4 noded elements) would improve the accuracy of the numerical results and hence lead to greater compatibility between the experimental and the numerical results.

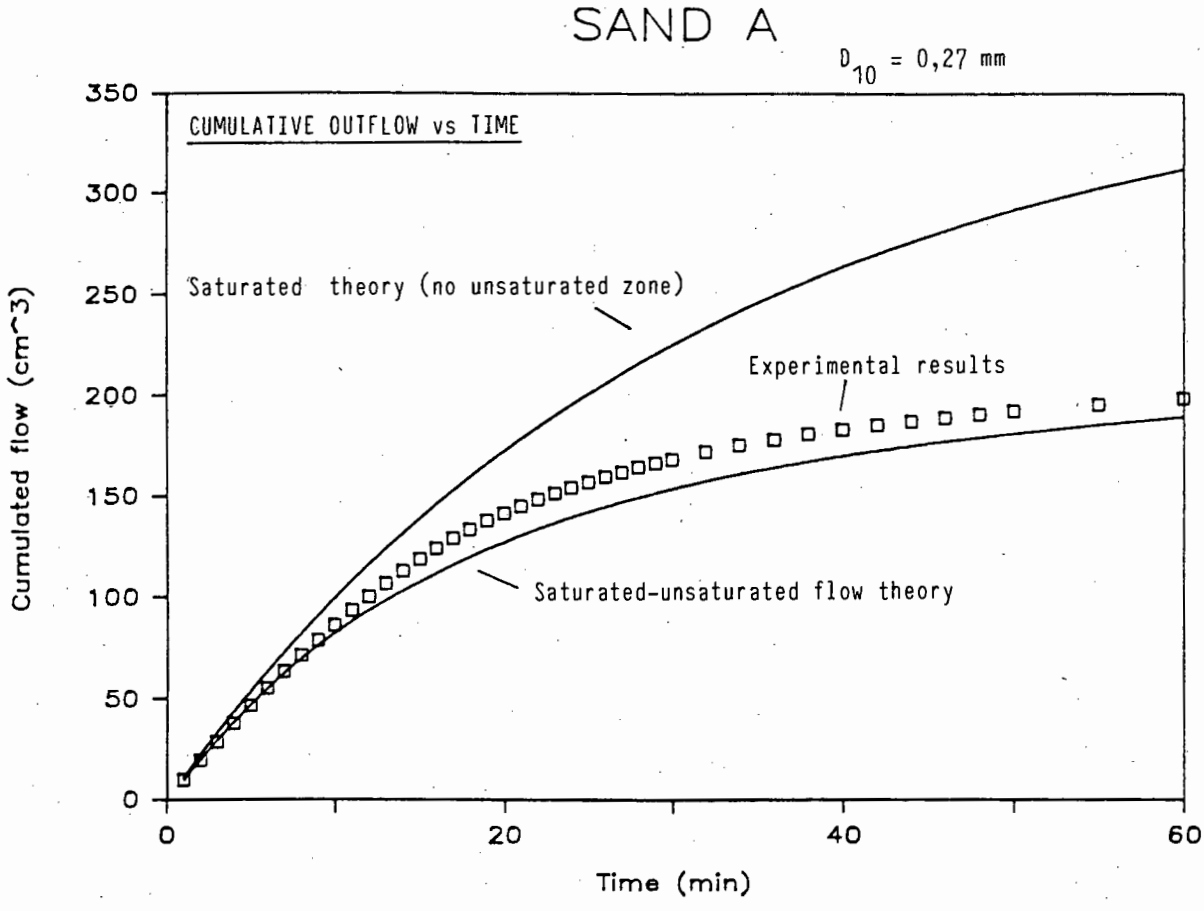


FIGURE 6.4. The difference between saturated and combined saturated-unsaturated flow theories

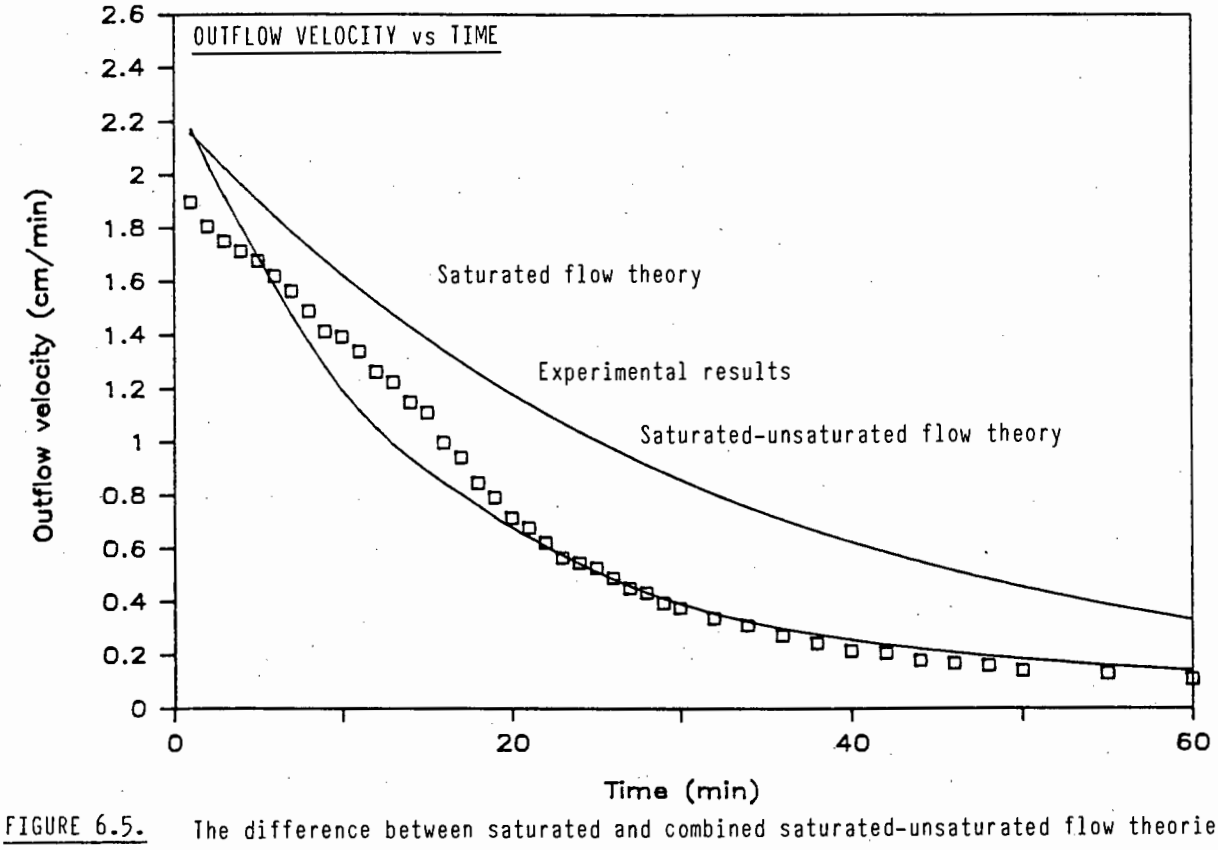


FIGURE 6.5. The difference between saturated and combined saturated-unsaturated flow theories

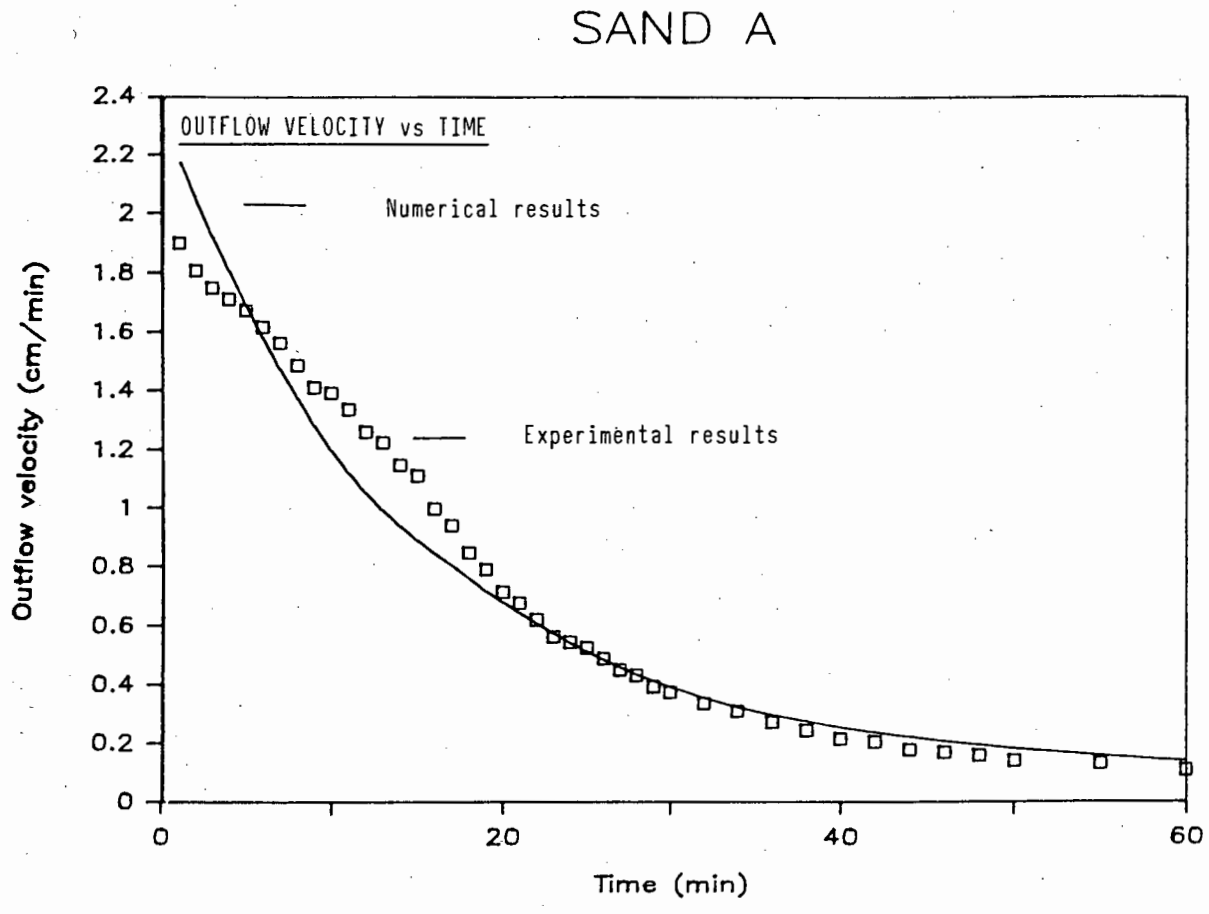


FIGURE 6.6. Backward difference scheme (20 elements and $\Delta t$ = 1.0 min)

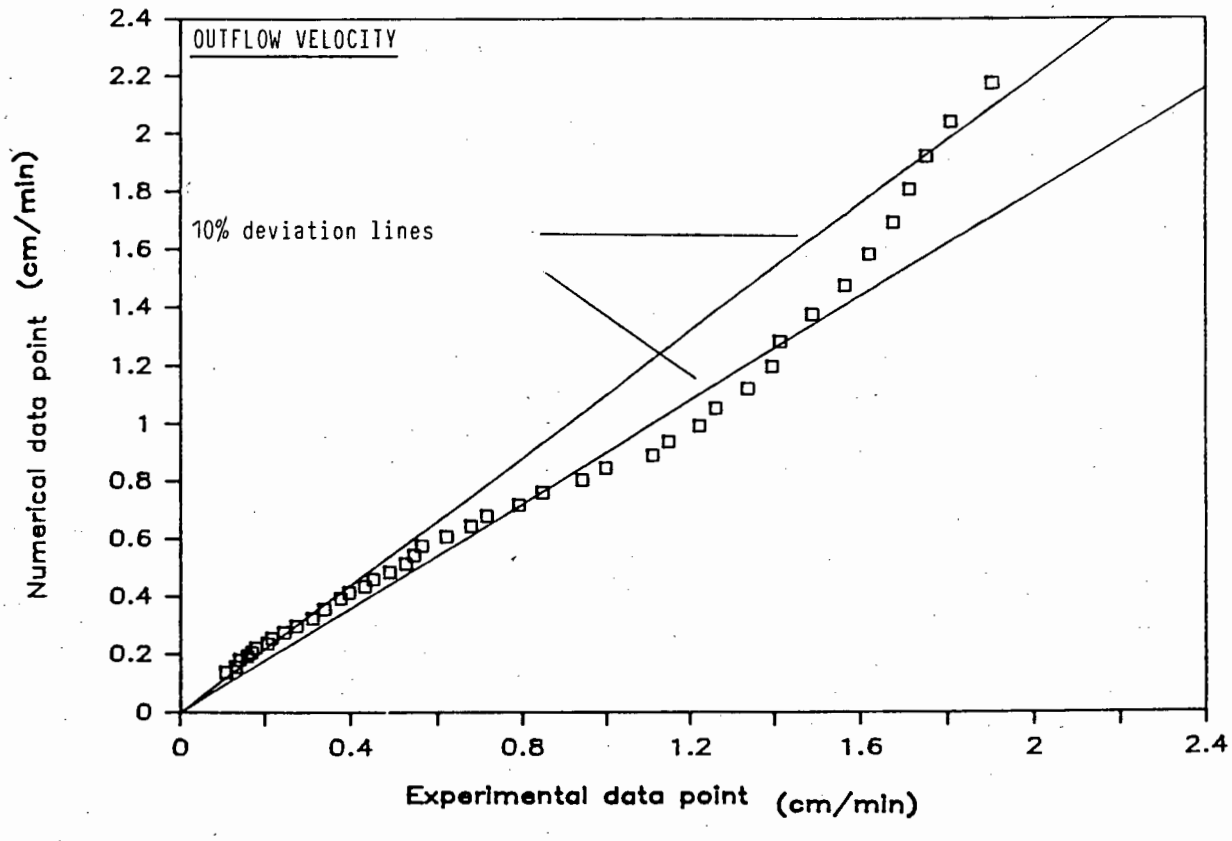


FIGURE 6.7. Backward difference scheme (20 elements and $\Delta t$ = 1.0 min)

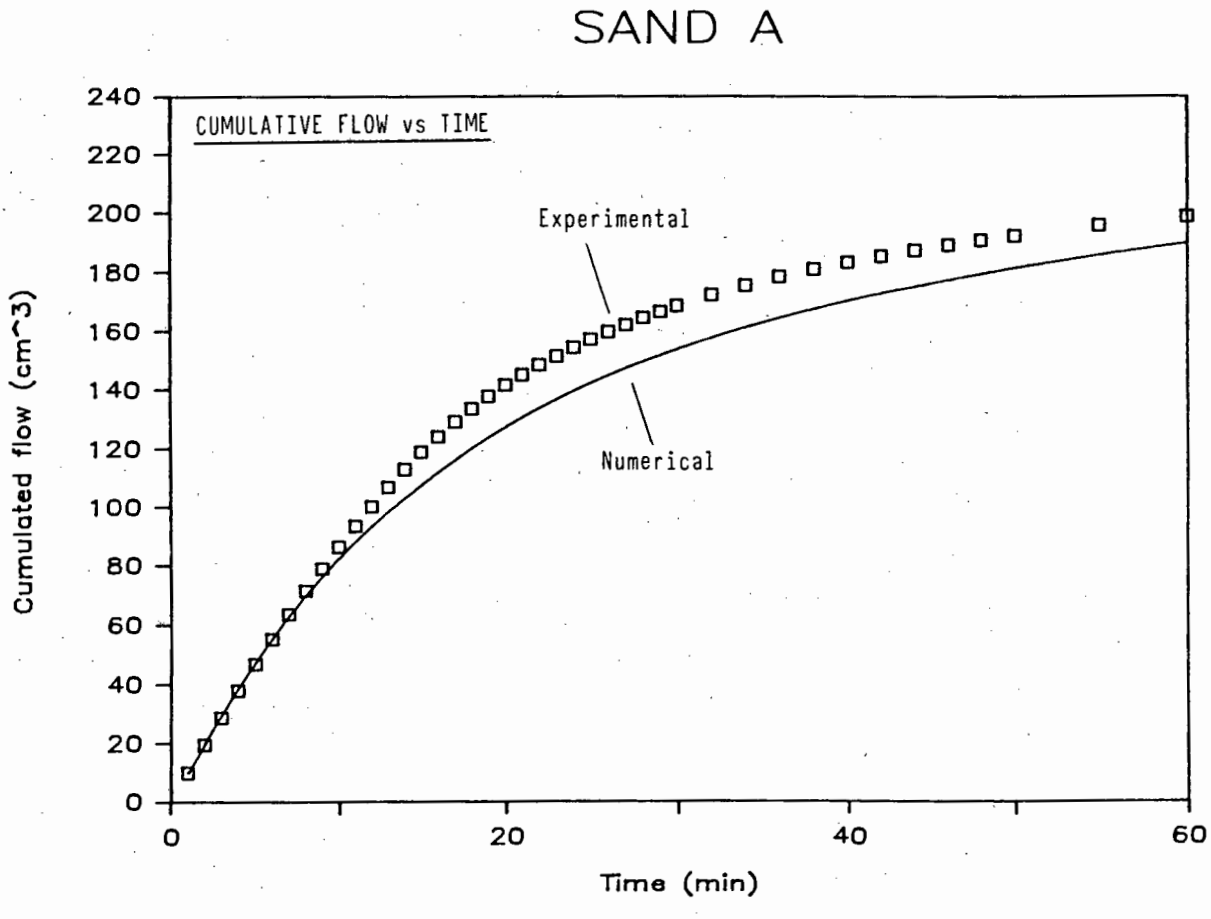


FIGURE 6.8. Backward difference scheme (20 elements and $\Delta t$ = 1.0 min)

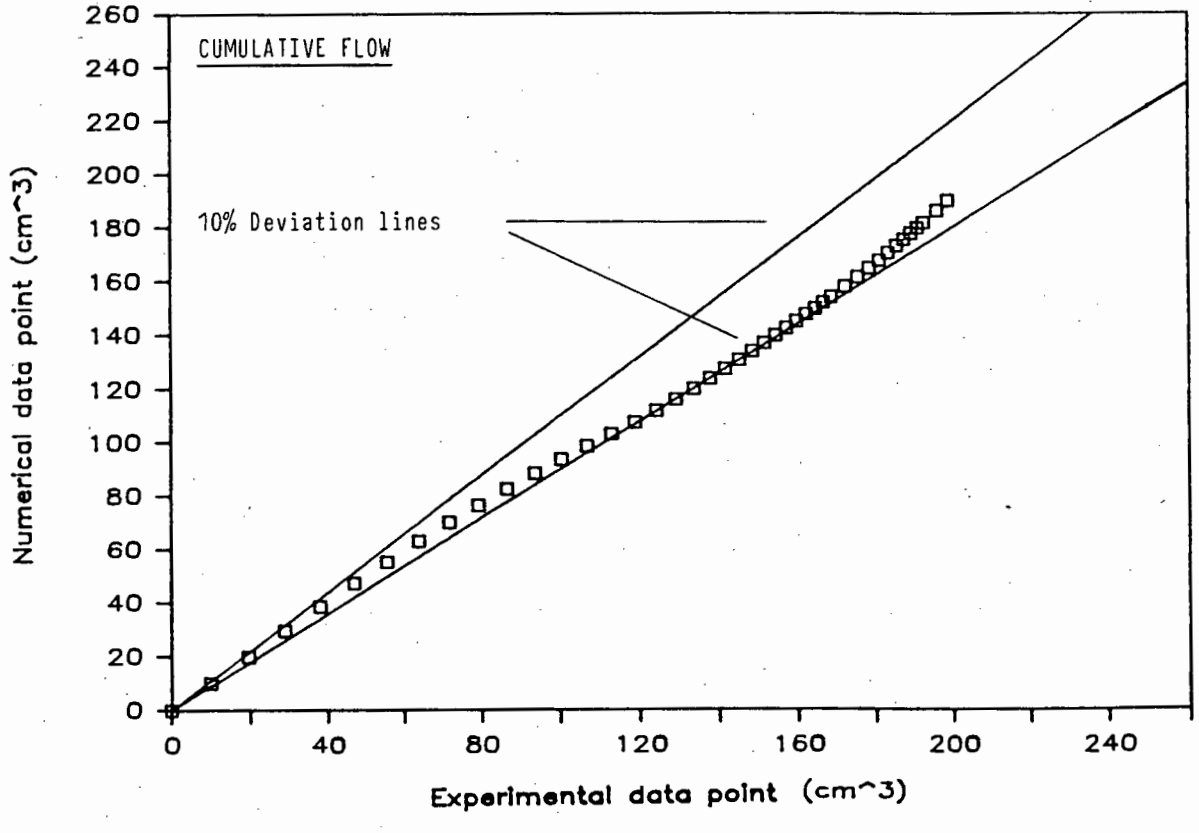


FIGURE 6.9. Backward difference scheme (20 elements and $\Delta t$ = 1.0 min)

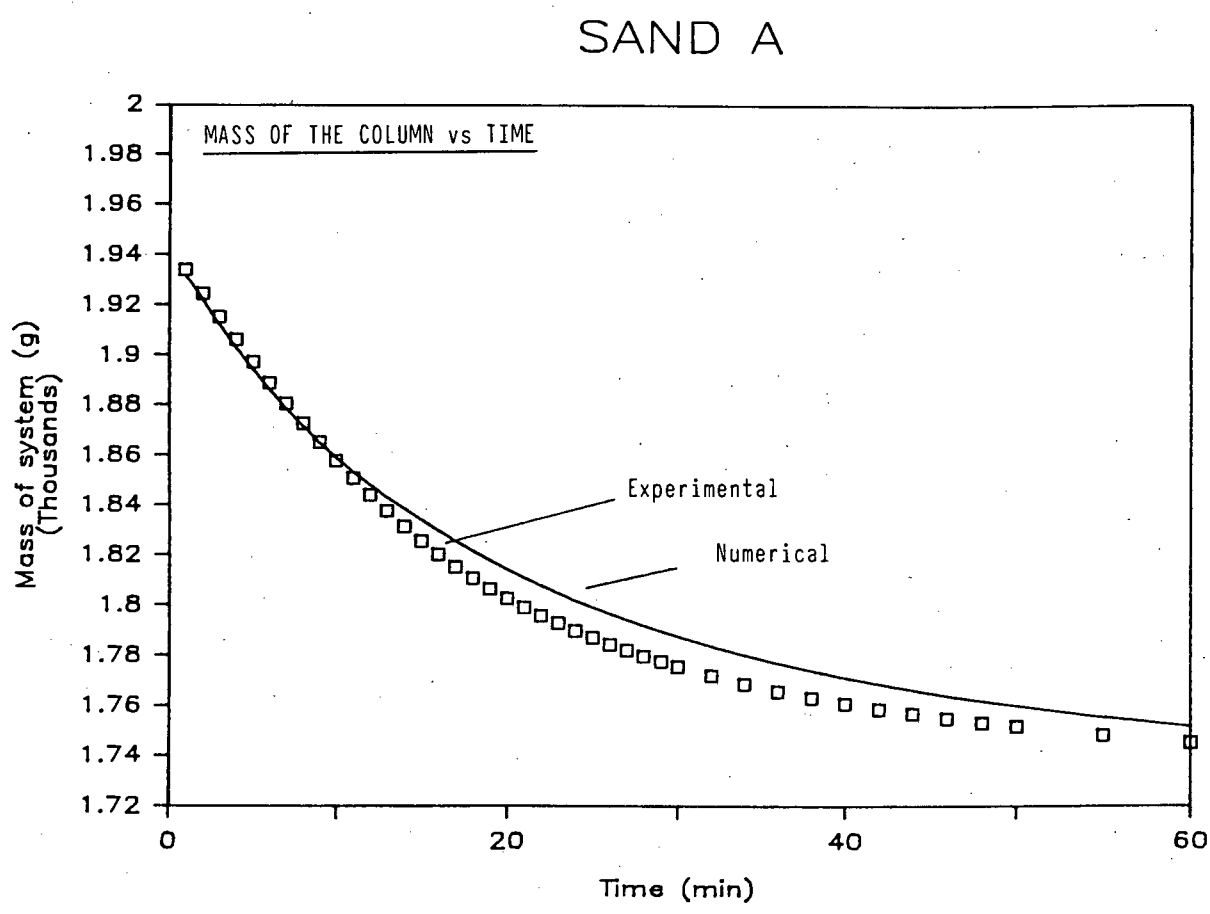


FIGURE 6.10. Backward difference scheme (20 elements and $\triangle t$ = 1.0 min)

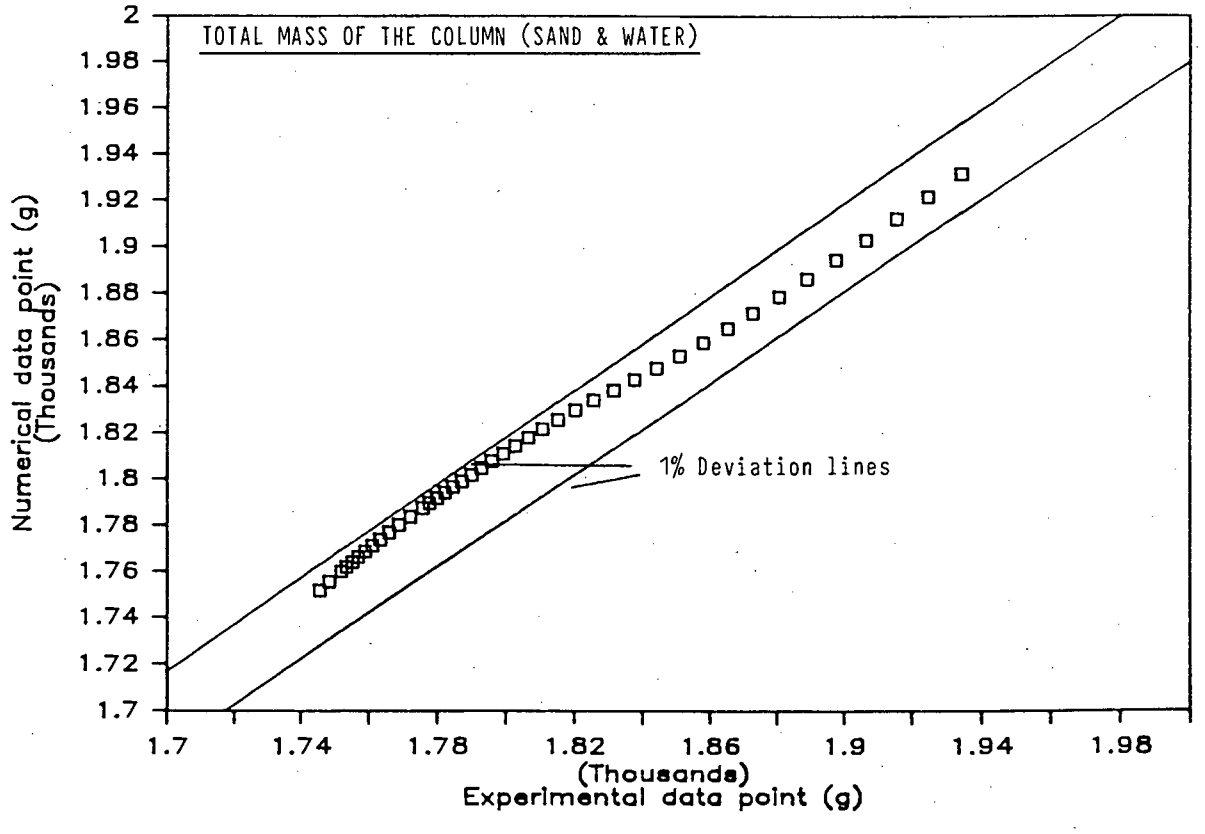


FIGURE 6.11. Backward difference scheme (20 elements and $\triangle t$ = 1.0 min)

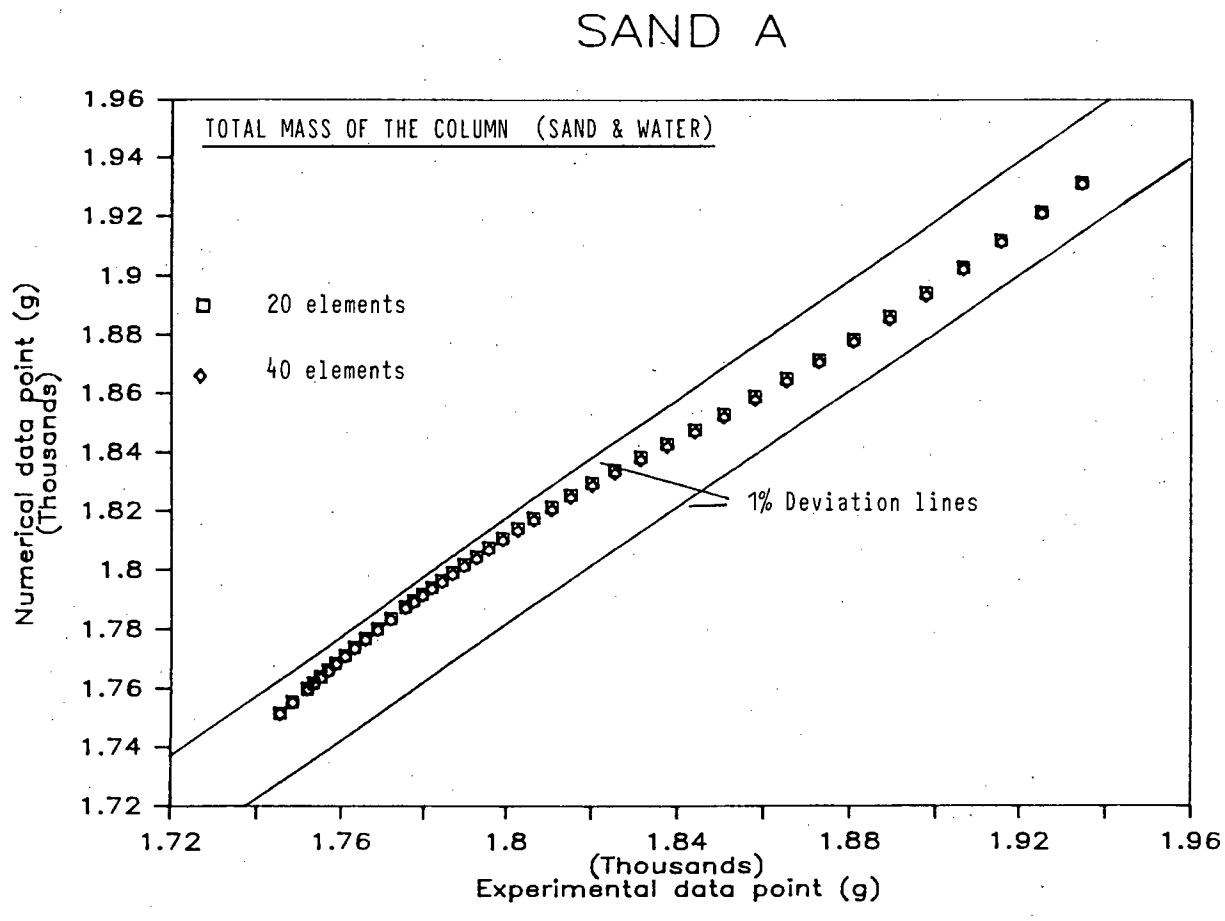


FIGURE 6.12. Backward difference scheme ( $\triangle t$ = 1.0 min)

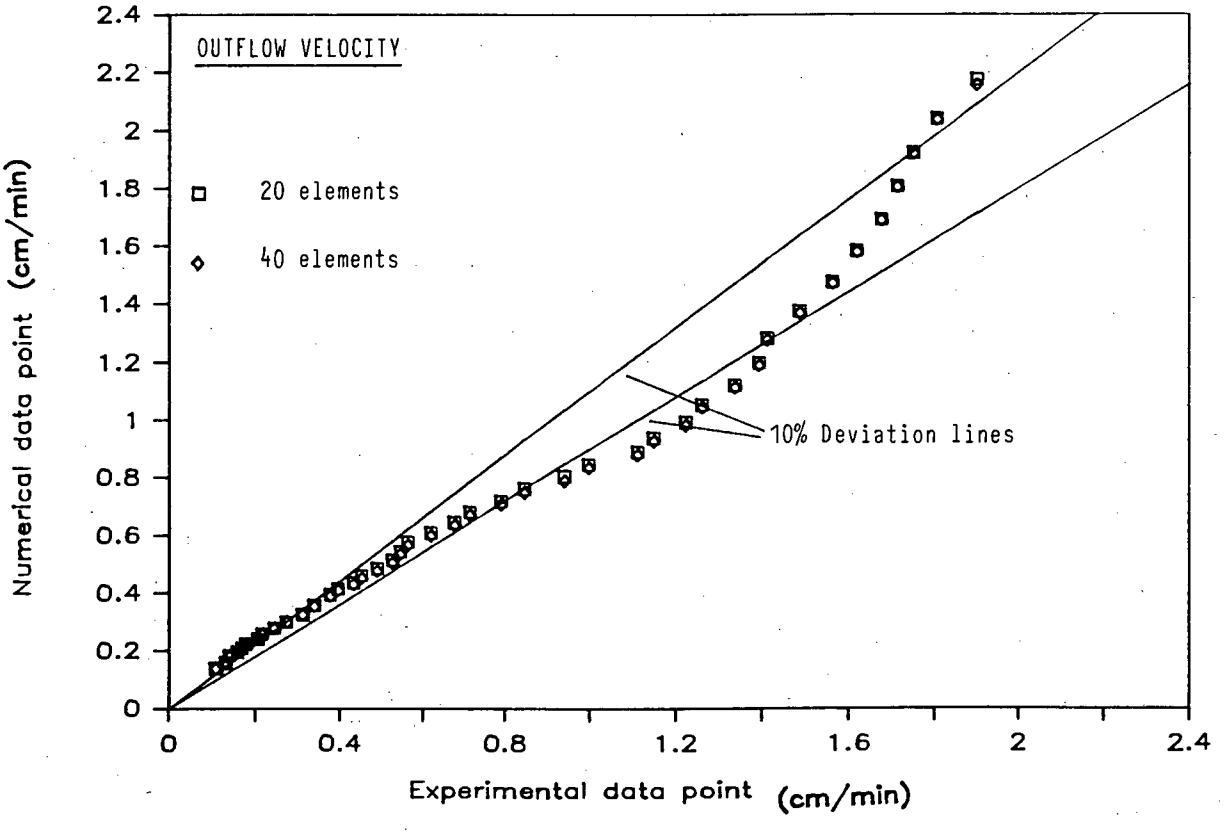


FIGURE 6.13. Backward difference scheme ( $\triangle t$ = 1.0 min)

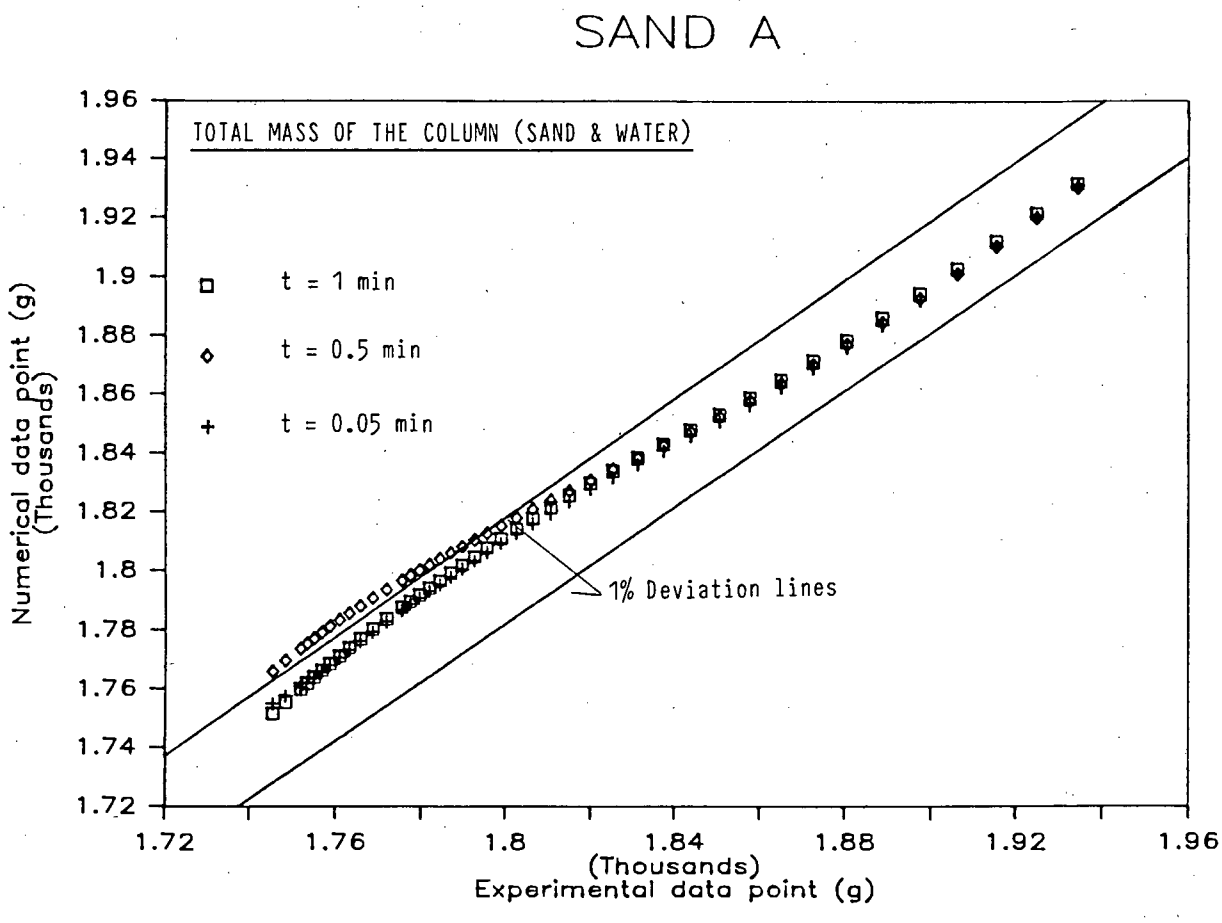


FIGURE 6.14 Backward difference scheme (20 elements)

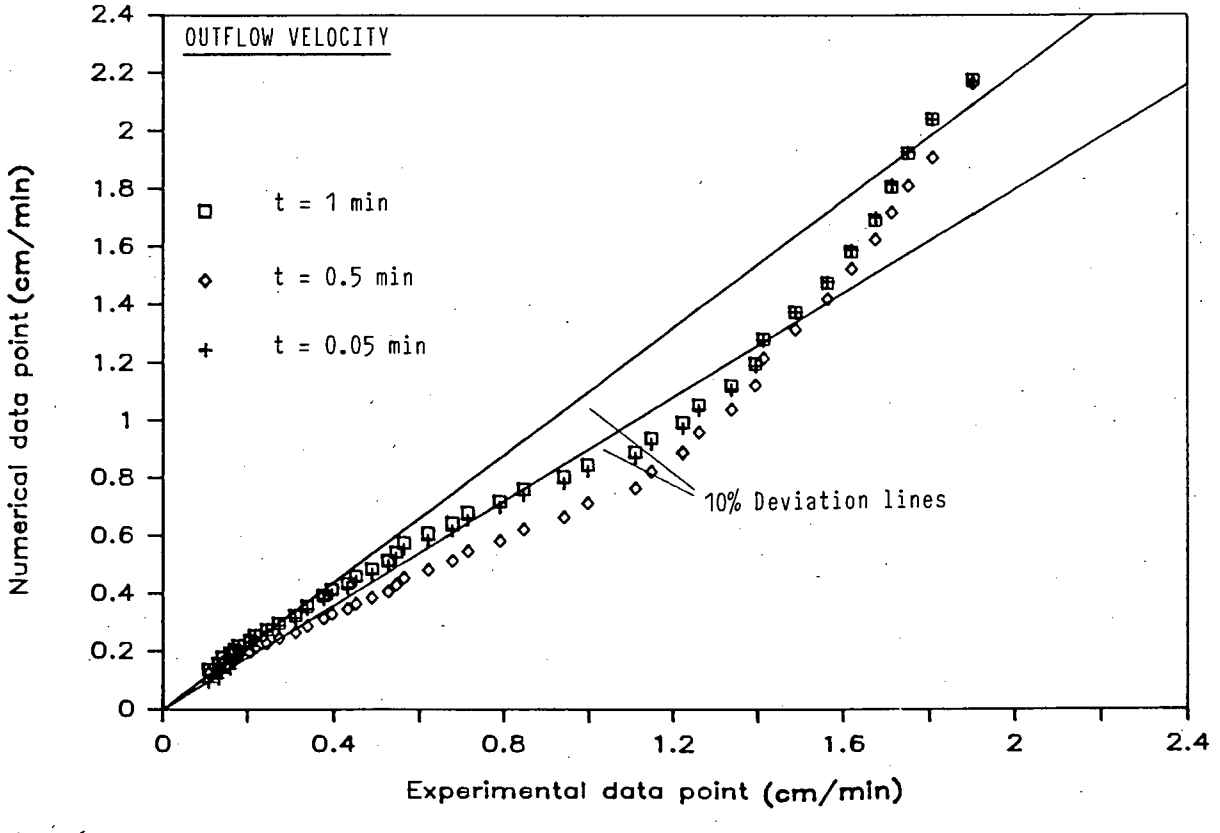


FIGURE 6.15. Backward difference scheme (20 elements)

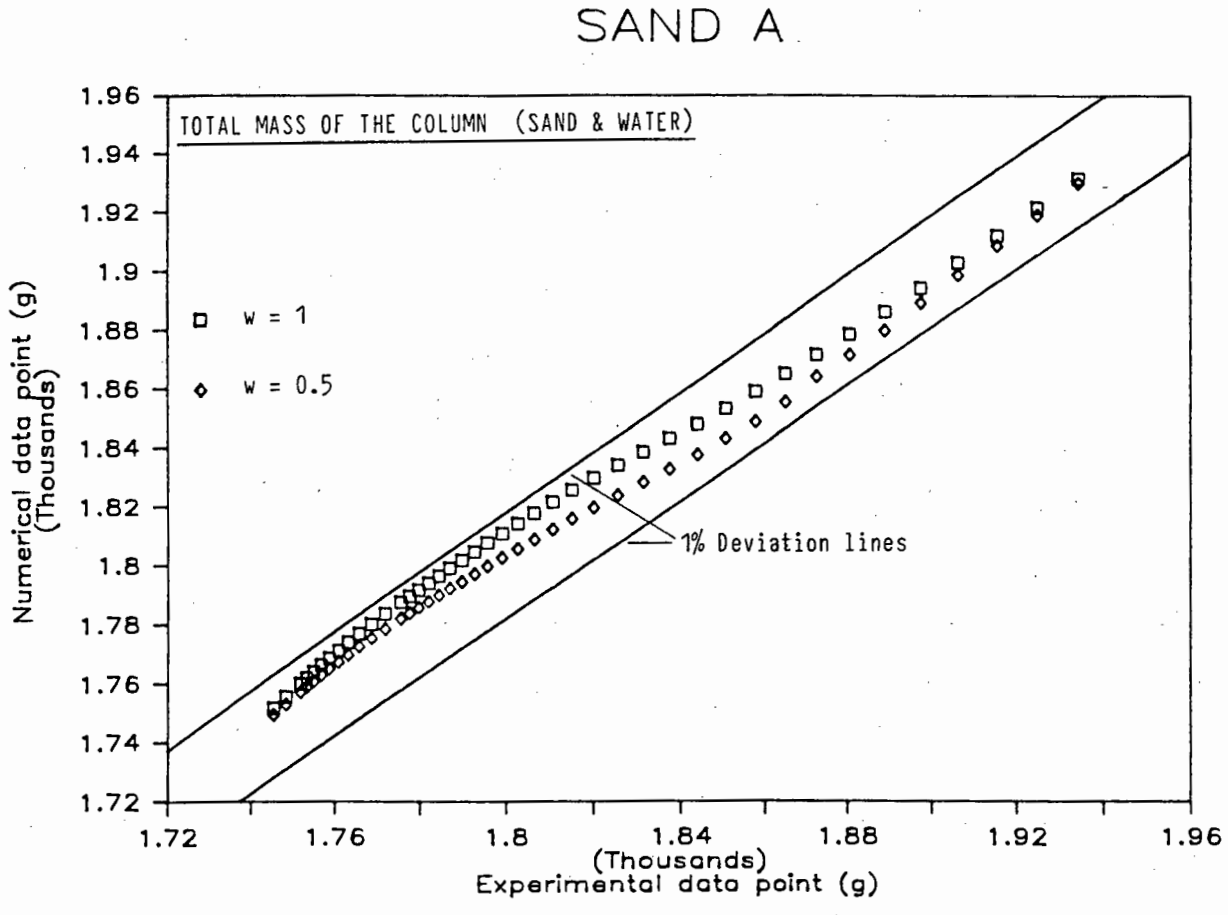


FIGURE 6.16. 20 Elements and $\triangle t$ = 1.0 min

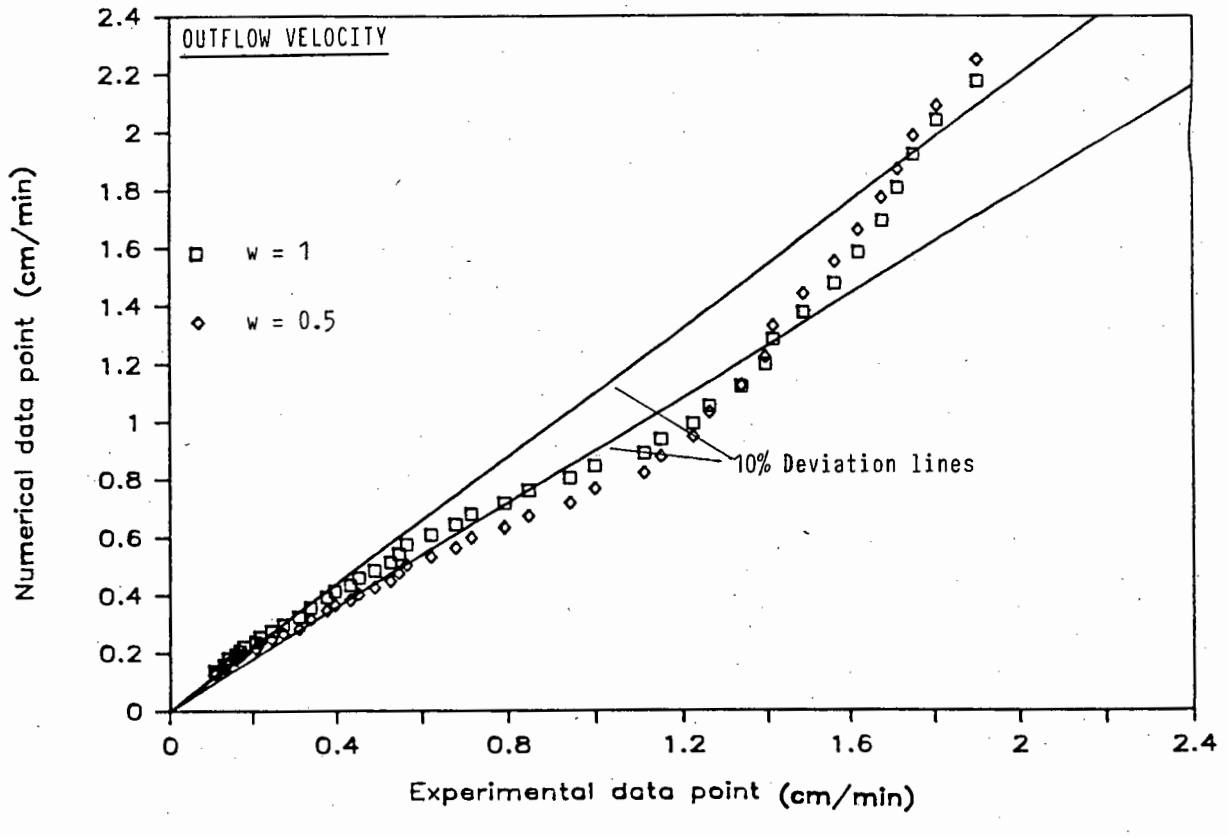


FIGURE 6.17. 20 Elements and $\triangle t$ = 1.0 min

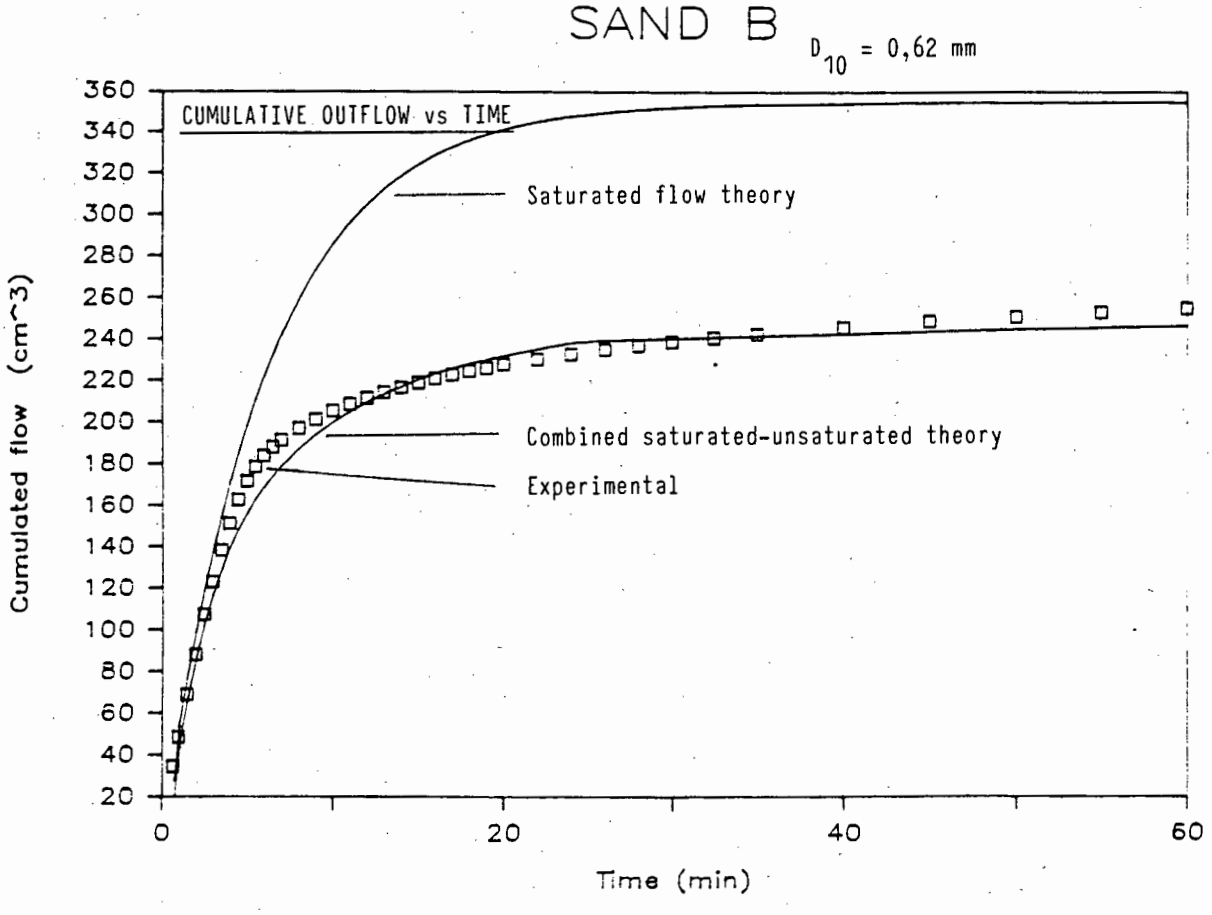


FIGURE 6.18. Difference between saturated and combined saturated-unsaturated theories

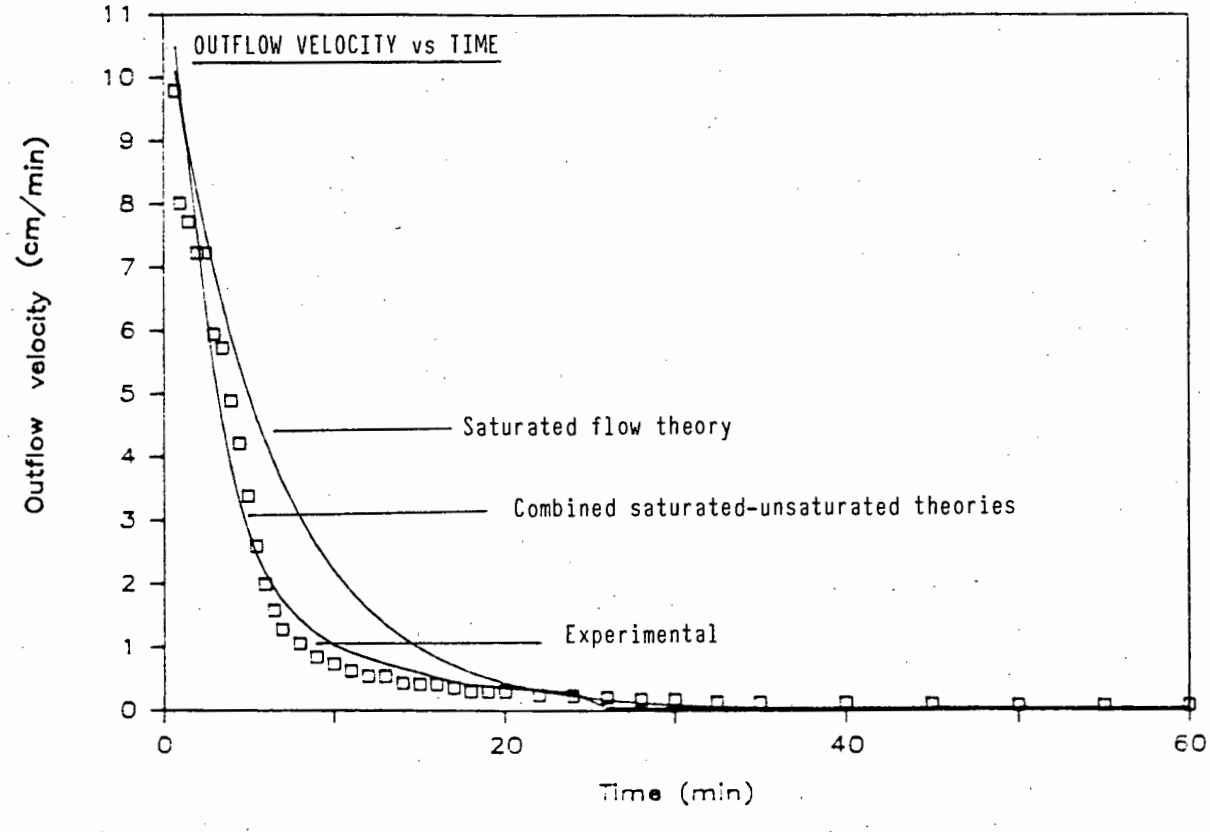


FIGURE 6.19. Difference between saturated and combined saturated-unsaturated theories

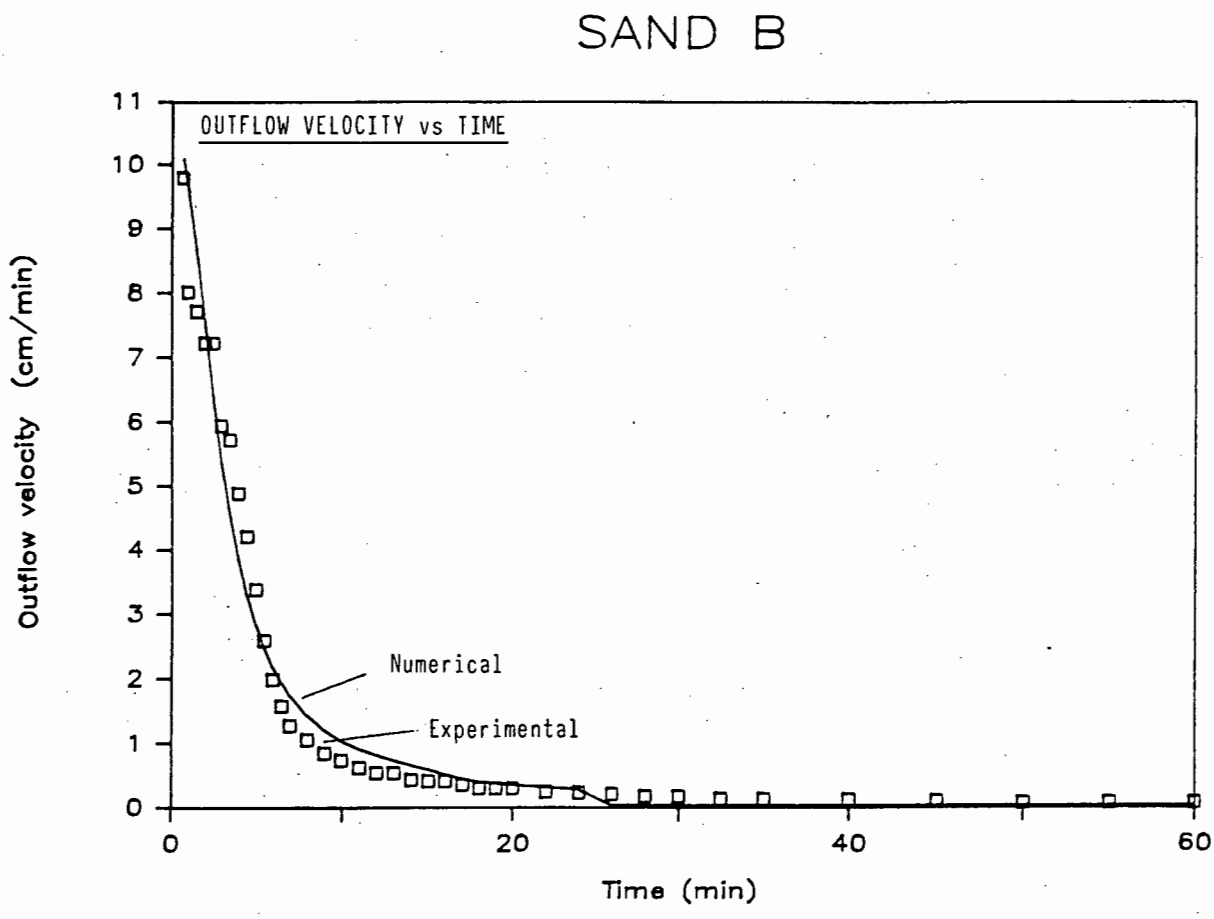


FIGURE 6.20. Backward difference scheme (20 elements and $\Delta t$ = 0.25 min)

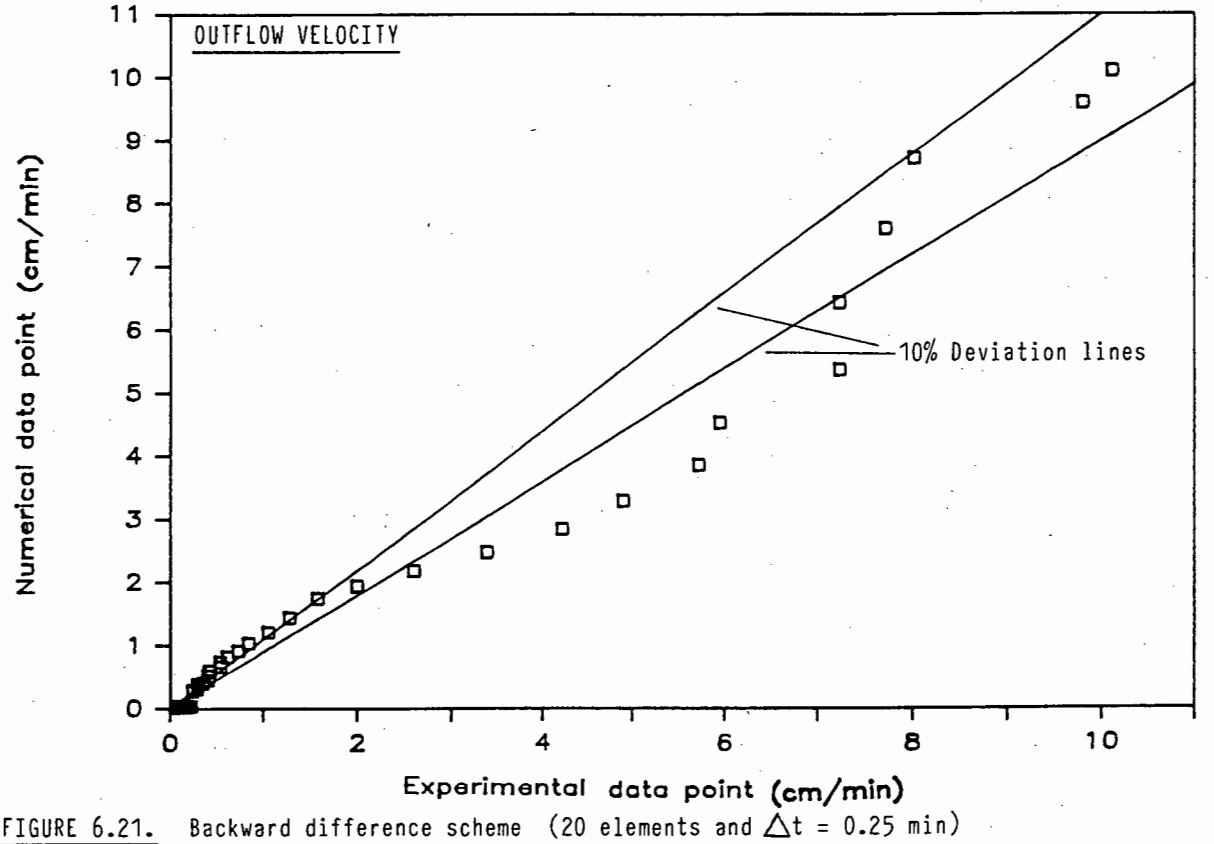


FIGURE 6.21. Backward difference scheme (20 elements and $\Delta t$ = 0.25 min)

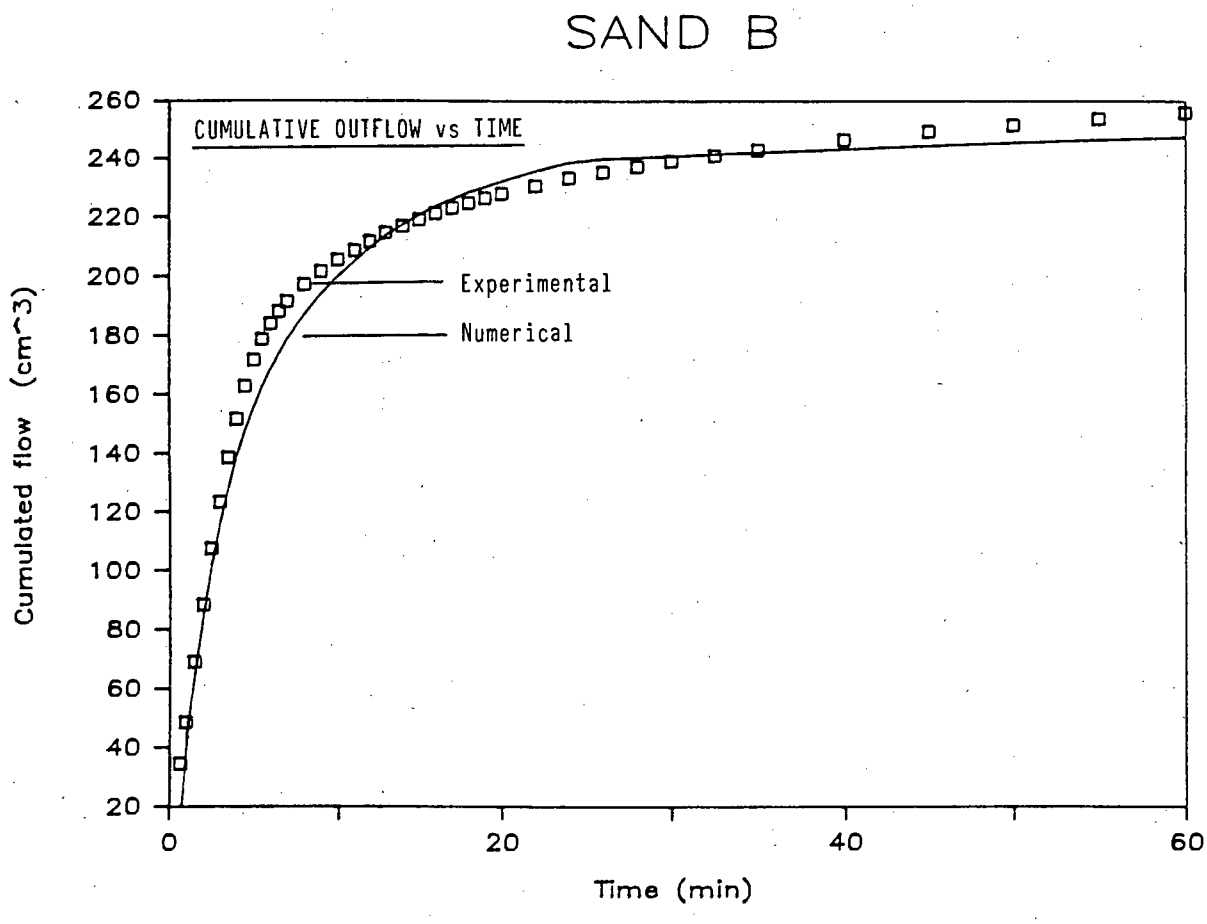


FIGURE 6.22. Backward difference scheme (20 elements and $\Delta t$ = 0.25 min)

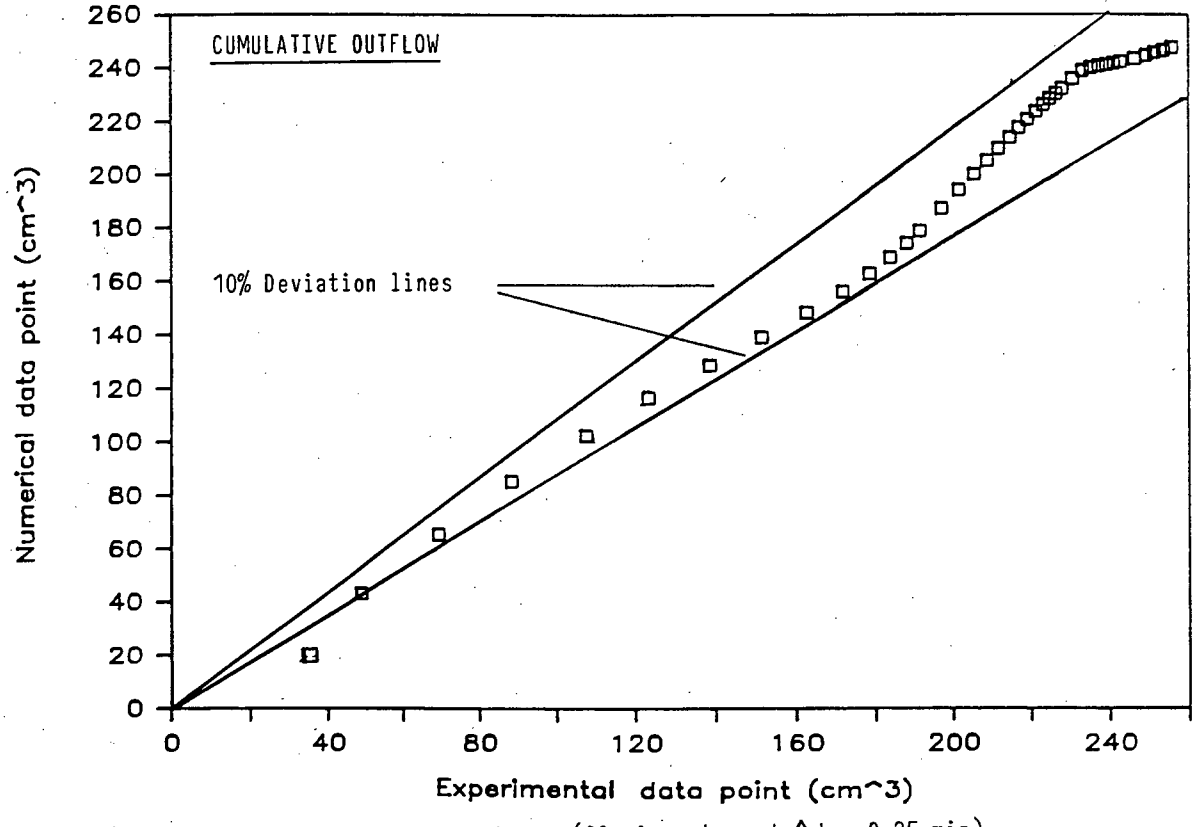


FIGURE 6.23. Backward difference scheme (20 elements and $\Delta t$ = 0.25 min)

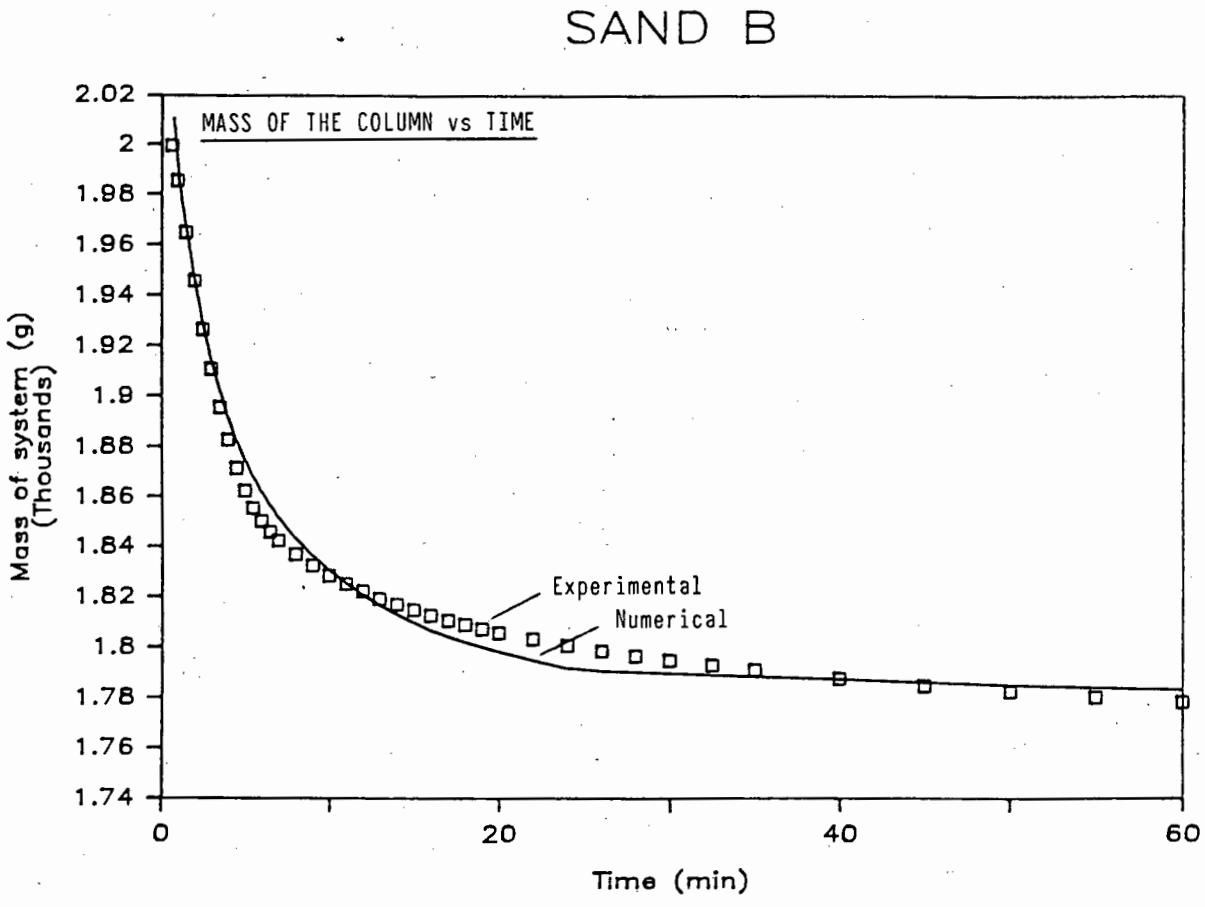


FIGURE 6.24. Backward difference scheme (20 elements and $\Delta t$ = 0.25 min)

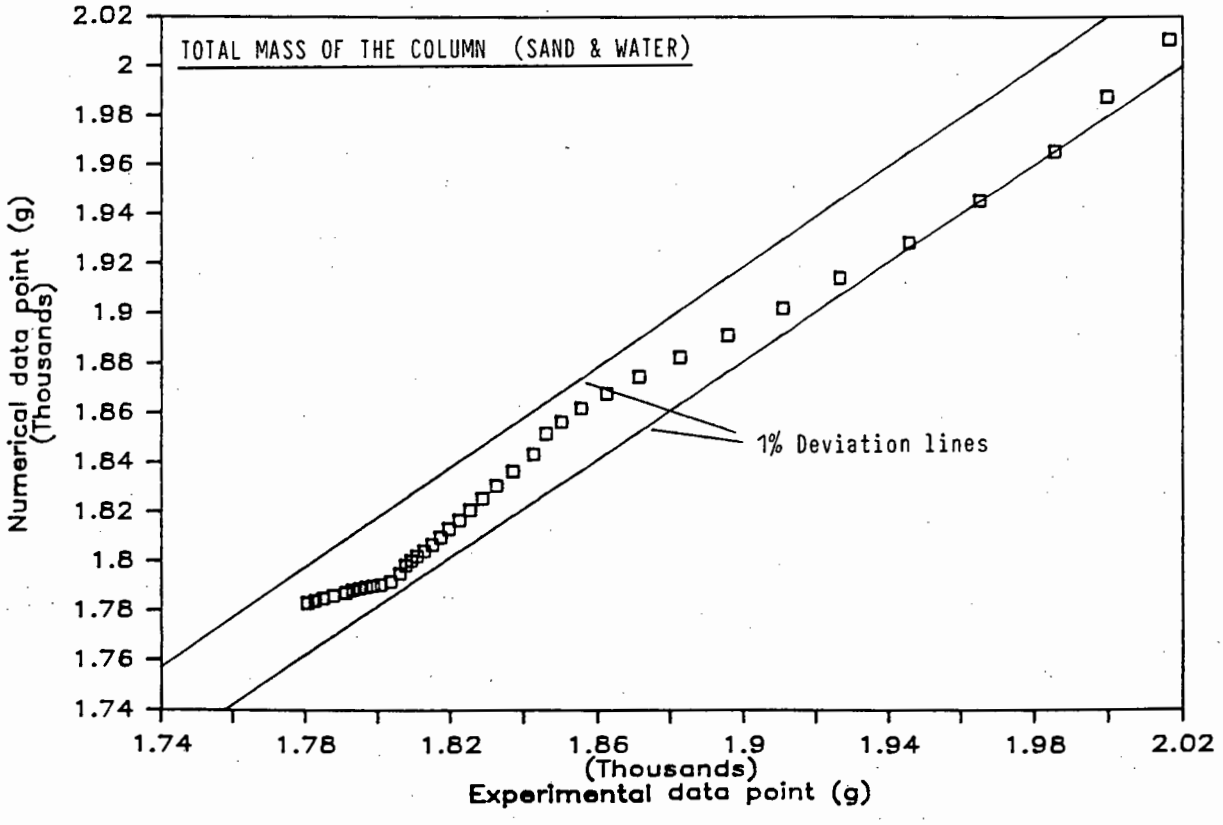


FIGURE 6.25. Backward difference scheme (20 elements and $\Delta t$ = 0.25 min)

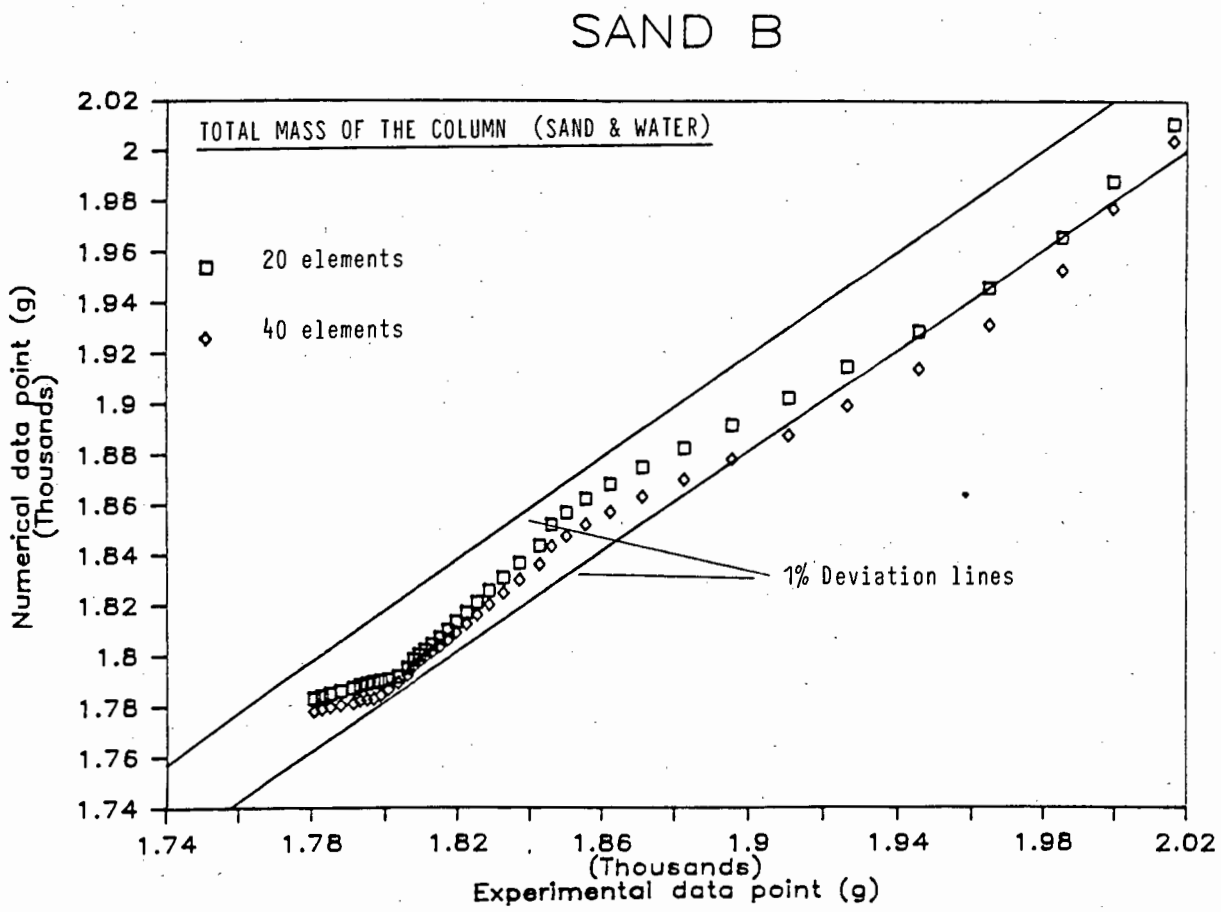


FIGURE 6.26. Backward difference scheme ( $\Delta t$ = 0.25 min)

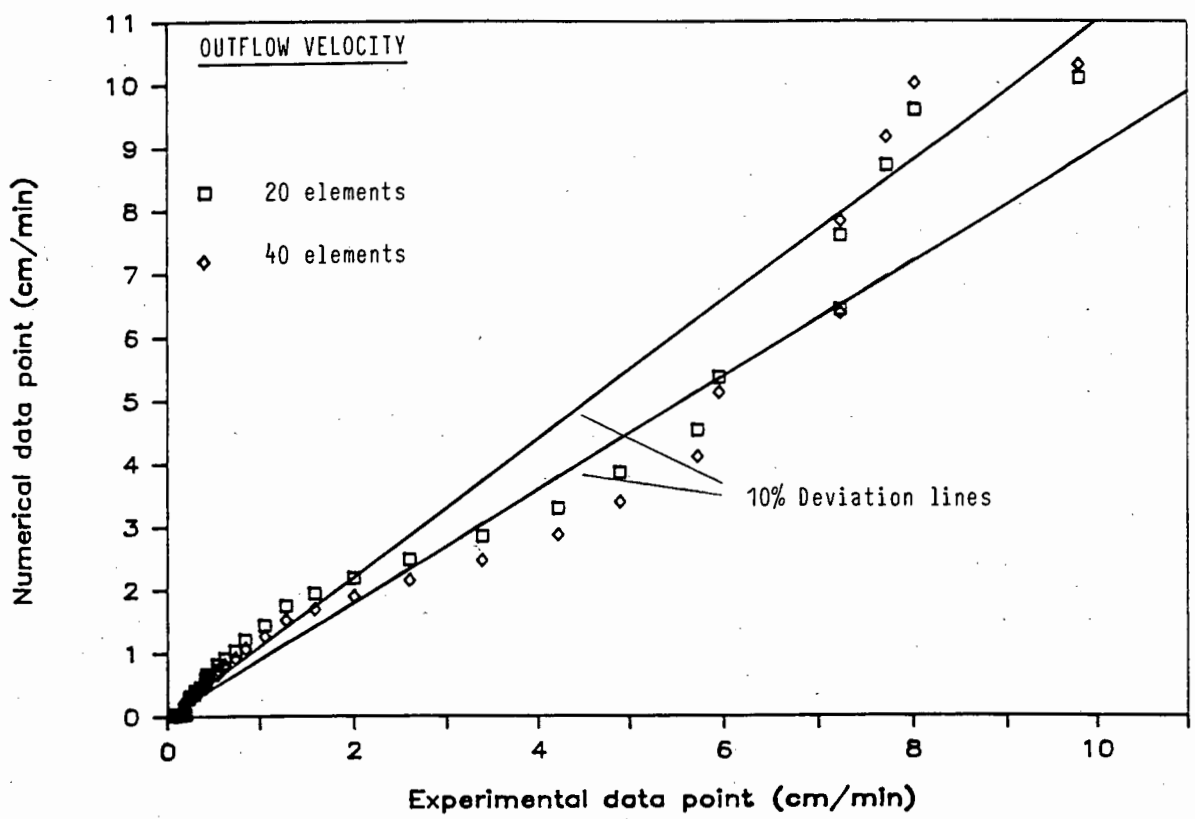


FIGURE 6.27. Backward difference scheme ( $\Delta t$ = 0.25 min)

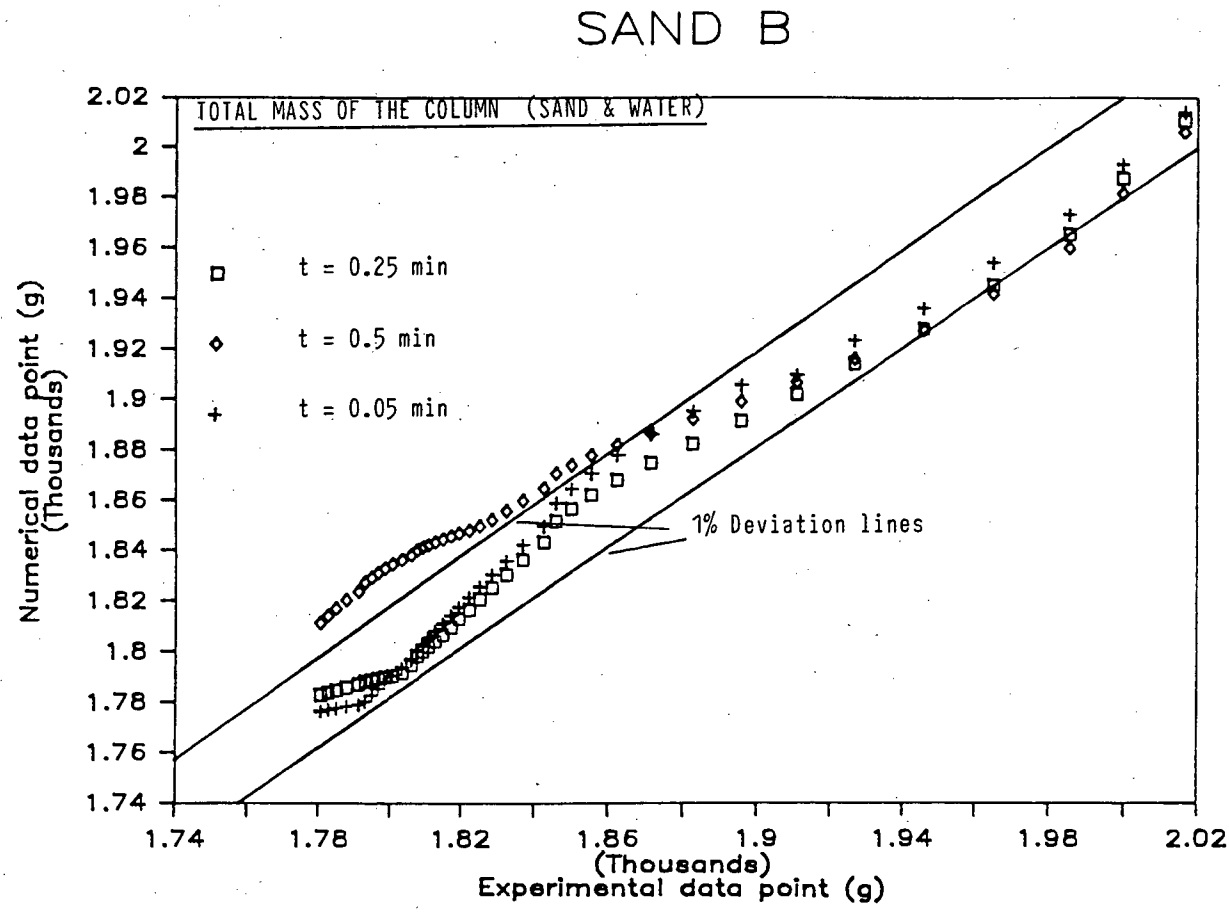


FIGURE 6.28. Backward difference scheme (20 elements)

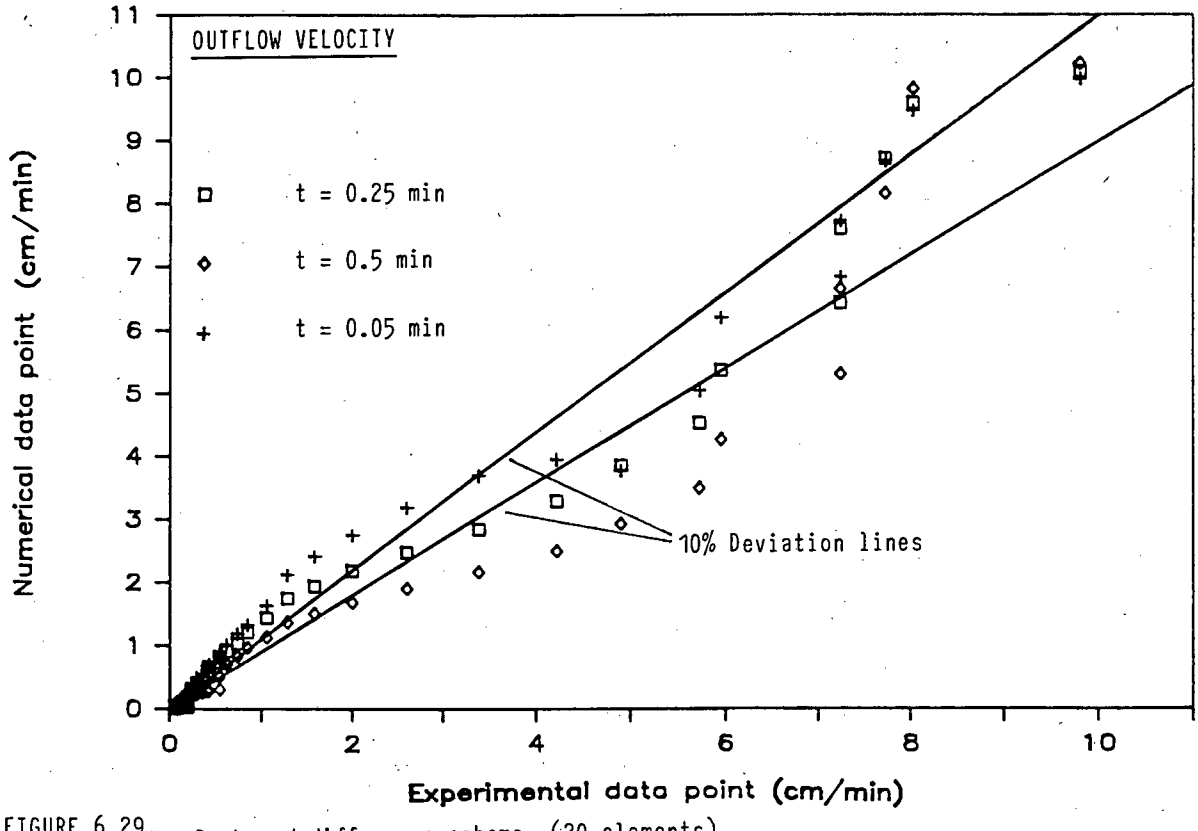


FIGURE 6.29. Backward difference scheme (20 elements)

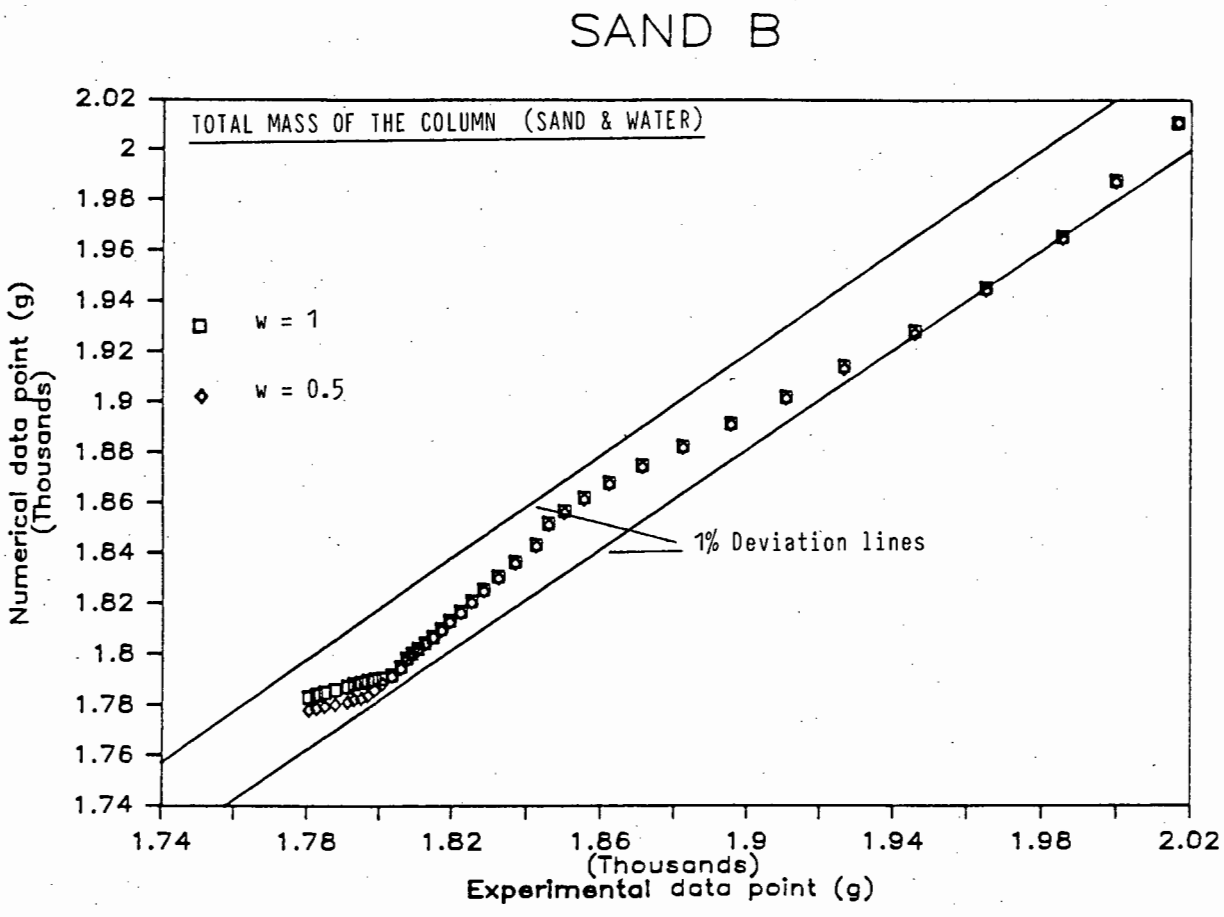


FIGURE 6.30. 20 Elements and $\triangle t$ = 0.25 min

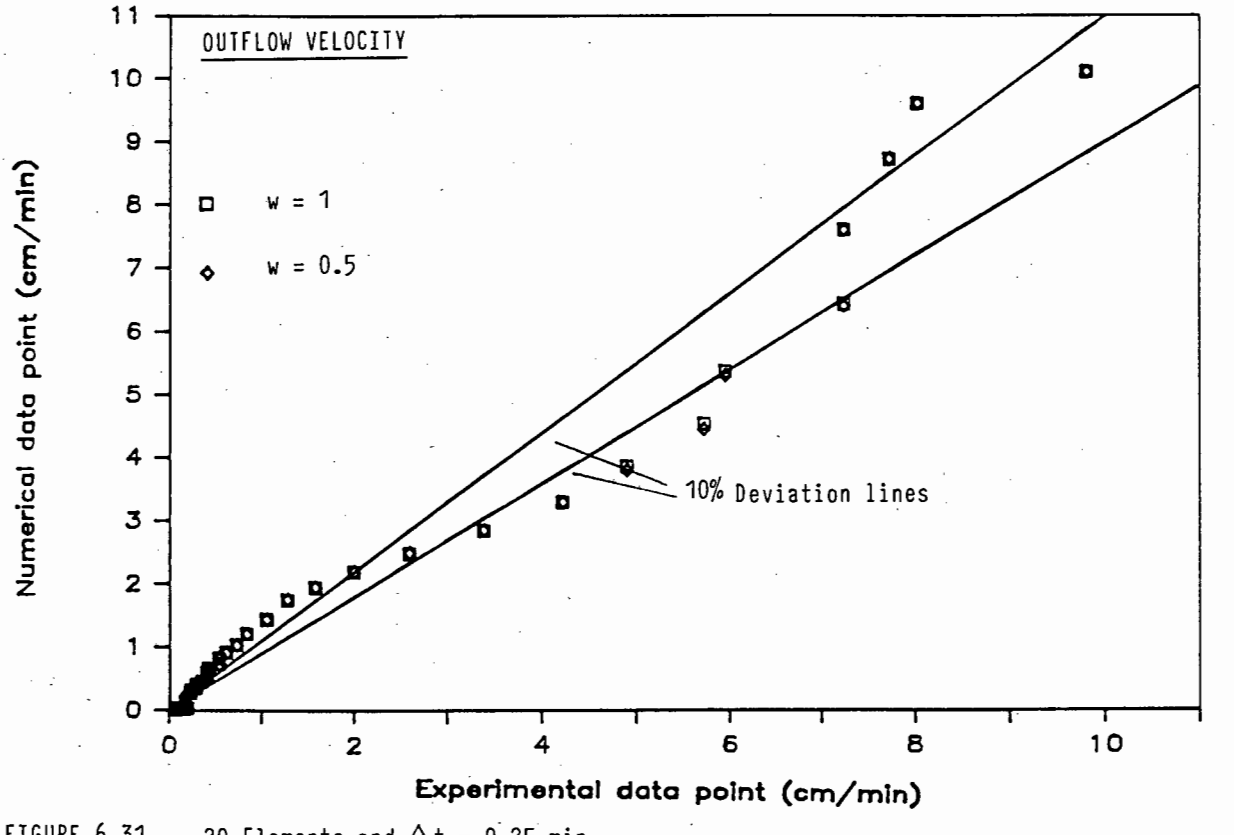


FIGURE 6.31. 20 Elements and $\triangle t$ = 0.25 min

# CHAPTER 7

# THE TWO-DIMENSIONAL DRAINAGE PROBLEMS

## 7.1 INTRODUCTION

The finite element programme used to model the one-dimensional column drainage experiment was updated to model two, two-dimensional drainage problems. The problems were, in fact, three-dimensional situations but owing to their geometry two-dimensional approximations of the real situations could be made.

The first problem modelled was the drainage of a rectangular block of sand which was performed experimentally by Wardle (1986) under the supervision of Professor Sparks. Owing to the symmetry of the flow domain a two-dimensional plane approximation could be made of this problem.

The second problem modelled was the drainage of a wedge or 'cake slice' of sand. This problem was performed experimentally by the author, in the same seepage tank using the same sand sample as Wardle. The two problems were essentially the same (initial and boundary conditions were of the same form) except for their geometry. The soil and soil-moisture characteristics of this sand, sand C, may be found in Appendix B.

Apart from the geometry of the flow domain, the significant difference between the two drainage experiments was the apparatus used to record the pressure heads, as they varied with time. The author used four null-flow devices, apart from the piezometer tubes located in the side wall of the seepage tank. Wardle, however, used pressure transducers linked to a computer for rapid acquisition and recording of data.

The relevant input data, including the dimensions of the flow domain and the numerical results of the simulation of the experiment performed by Wardle, may be found in Appendix E.

## 7.2 THE EXPERIMENT

### 7.2.1 Experimental apparatus

Both the plane and axisymmetrical drainage experiments were carried out in the same seepage tank. This seepage tank was 290 cm long, 50 cm high and 31,5 cm wide and comprised of two perspex side walls (length of the tank), two vertical metal faces (ends of the tank) and an impervious metal base. An outlet was positioned, in the base, at one end of the tank. It was through this outlet that the draining water left the seepage tank.

Wooden shuttering (vertical wall with supports) was placed diagonally down the tank to form the wedge or 'cake slice' for the axisymmetrical drainage experiment. This shuttering did, however, stop short of the length of the tank, thereby forming a well into which the water drained. The wooden shuttering was placed so that the outlet, in the base of the tank, was positioned inside the well. The vertical outflow face comprised of wire mesh attached to the shuttering and one of the sidewalls of the seepage tank. Wire mesh, extending the entire height and width of the tank was also placed 14 cm from the upstream face. This zone, which was filled with ¼ inch stone chips, was used when saturating the wedge. De-aired water could be fed into the tank, via this zone, without disturbing the packing (void ratio) of the sand wedge.

A wooden stopper, which nearly occupied the entire volume of the well, formed an integral part of the apparatus. This stopper could be rapidly removed, thereby causing an 'instantaneous' (nearly so) drop in the water level in the well. It was this drop in water level which caused the wedge to drain.


Figure 7.1 - Photograph of the seepage tank in which the drainage experiments were performed.

The wedge, therefore, consisted of four impervious faces (the two side walls, the upstream face and the base of the seepage tank). Although both the top face of the wedge and the seepage face were pervious, no flow occurred across the top of the sand wedge.

7.2.1.1 The sidewall piezometers

The sidewall of the seepage tank was made of perspex and had an inch grid etched onto it. Piezometer tubes, which were located uniformly over the grid, were drilled into this perspex sidewall. These sidewall piezometers were used to locate the position of the

phreatic surface with respect to time. The water in these sidewall piezometers was connected via sponge filters to the water in the sand wedge. As the wedge drained, water flowed from the piezometer tubes into the wedge and hence they took some time to respond to a change in the level of the phreatic surface. Piezometers are, therefore, known as flow devices. This response time causes the water level in the piezometers to lag behind the falling phreatic surface. Piezometers may, therefore, not be that accurate in locating the phreatic surface, especially near the outflow face where the phreatic surface drops rapidly.

7.2.1.2 The null-flow devices

Due to the slow response time of the sidewall piezometers four null-flow devices, designed by Professor Sparks, were used in conjunction with the sidewall piezometers to locate the position of the phreatic surface near the seepage face. Due to the fact that these devices were null-flow devices, it was hoped that their response time would be faster than those of the side wall piezometer's and hence the phreatic surface could be located more accurately. The null-flow devices actually consisted of flow and non-flow portions. The non-flow portion was used to transmit the soil-water pressure head to the device while the flow portion of the device was used to display this pressure head.

These null-flow devices consisted of two 8 cm x 8 cm perspex plates 1 cm thick which had grooves machined into one of their sides. These grooves were machined in a pattern similar to that of a dartboard. The two plates were then bolted together (grooves facing each other) with a rubber membrane separating them. The spaces between the membrane and the plates, caused by the grooves, comprised the flow and non-flow portions of the device.

The non-flow portion of the device was connected via a thin nylon tube to the sand wedge. The free end of the nylon tube had a cotton wool filter attached to it and was held in a predetermined position in the wedge by a wooden dial attached to the shuttering. This

portion of the device (nylon tube and space between and grooves and membrane) had to be primed with de-aired water before the apparatus could be used.

The perspex plate on the flow side of the device had a 2 mm diameter outlet hole drilled through the centre of the plate while two tubes were connected to the grooves in the plate. One tube, which was fixed to the side of the seepage tank, was used to display the pressure head. The other tube was attached to a constant head device which supplied tap water to the device. Water flowed from the constant head supply tank into the flow side of the device and up the pressure display tube while the excess water left the apparatus via the outlet hole.

The soil pressures transmitted via the de-aired water in the nylon pipe caused the rubber membrane to arch and thereby regulate the amount of water flowing through the opposite side of the device. This, in turn, determined the height of water in the pressure display tube. The device was calibrated by regulating the flow from the constant head supply tank. The flow of water from the constant head supply tank enables both increasing and decreasing pressure heads to be recorded. As no infiltration took place during the drainage of the wedge, the devices were not used to record increasing pressure heads. It should be noted that the diameter of the outlet hole largely determined the response time of this device.

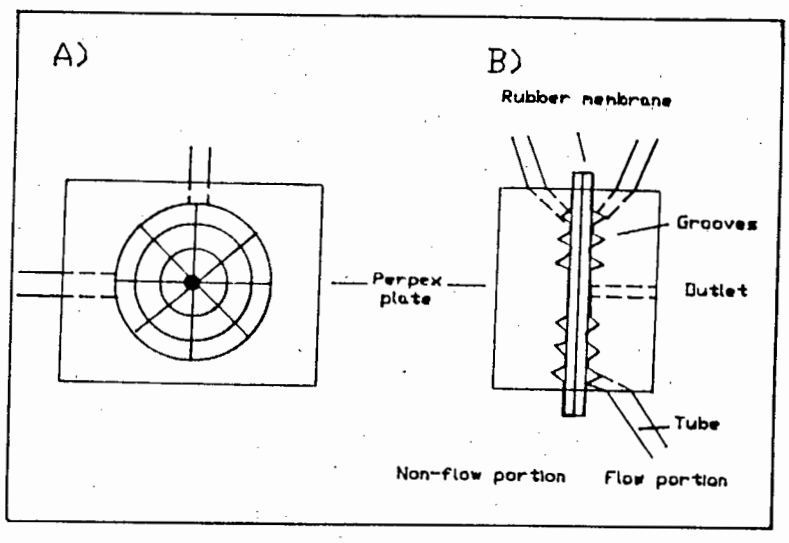


Figure 7.2 - Diagrams of the 'null-flow' device used to measure small pressure heads

a) The perspex plate on the flow side of the device showing the pattern of the grooves

b) A side view of the 'null flow' device showing both the flow and non-flow sections of the device

7.2.2 Experimental procedures

A transient and a steady-state flow experiment were performed on the sand wedge. The transient flow experiment was simulated using the finite element programme while the steady-state flow experiment was performed to determine the coefficient of permeability of the sand comprising the wedge. This coefficient, which was needed as input in the programme, was used as a check against the coefficient determined from the permeability tests.

7.2.2.1 Transient flow procedures

The outlet, in the well portion of the seepage tank, was closed and the wooden stopper fitted into the well. The seepage tank was then filled to about one third of its height with de-aired water before air dried sand of known mass was carefully placed into the tank. The tank was first filled with de-aired water to facilitate the priming of the null-flow devices and to reduce the amount of air

becoming entrapped in the sand wedge. After the sand in the seepage tank had been levelled off, more de-aired water was fed into the tank by running it over the ¼ stone chips. By saturating the wedge in this manner the packing of the sand was not disturbed. It was essential that the void ratio be as uniform as possible throughout the wedge, as an isotropic approximation of the flow domain had been made.

The water level in the tank was allowed to rise above the level of the sand, before it was again lowered by opening the outlet in the well. The system was then left for one day in order that equilibrium conditions be achieved. Once equilibrium conditions had been achieved, the null-flow devices were calibrated. This was achieved by regulating the flow rate from the constant head supply tank, so that the water level in the pressure display tube coincided with the level of the water in the wedge. The initial height of the water table was recorded using the side wall piezometer tubes. Green dye had been placed in these tubes in order that the water levels in them be more detectable.

The wooden stopper was then removed from the well while the outlet was opened simultaneously. In this way the water level in the well was rapidly lowered to the base of the tank. The water leaving the wedge via the outlet was tapped into pre-weighed buckets. The cumulative outflow and flow rates could be determined in this manner, provided the time it took to fill a bucket was recorded.

As the wedge drained, the water level in the piezometer tubes were marked directly onto the perspex sidewall using a wax pencil. Due to the large number of sidewall piezometers their levels could not all be recorded instantaneously. They were, therefore, recorded at various time levels. A contouring method was then used to determine the location of the phreatic surface at particular time levels.

The drainage of the sand wedge was, in this manner, monitored for nearly four hours. After that time there was no significant outflow nor drop in the water level in the side wall piezometers.

7.2.2.2 Steady-state flow procedures

A steady-state flow experiment was undertaken on the same sand wedge used in the transient flow experiment. The aim of this experiment was to determine the coefficient of permeability of the sand for input in the programme.

The wedge was resaturated by feeding the de-aired water over the stone chips. Once the wedge had been saturated the outlet in the well was opened and the wedge allowed to drain. It should be noted that the wooden stopper was not used for this experiment. The water was at first allowed to drain to waste before being tapped into pre-weighed buckets and returned to the system via the stone chips. This method was repeated until the amount of water draining from the wedge (determined by mass) was constant.

Once steady-state conditions had been achieved the location of the phreatic surface was recorded with the aid of the sidewall piezometers. The coefficient of permeability could then be determined using the following formula:

$$k = \frac{Q}{\pi (h_2^2 - h_1^2)} \log_e \frac{r_2}{r_1} \qquad (7.1)$$

where $k$ is the coefficient of permeability

$Q$ is the constant flow rate from the well

$h_{1,2}$ are heights of the phreatic surface above the base of the seepage tank

$r_{1,2}$ are the distances from the centre of the well to the respective phreatic surface heights.

The above formula is applicable to the cone of depression, of the phreatic surface, caused by constant pumping of a well in an unconfined aquifer. Since this wedge represents a portion of an

aquifer, the flow rate determined from the experiment needed to be multiplied by a factor before it could be used in equation (7.1). The flow rate used in equation (7.1) represents flow from the entire aquifer and not from just a portion (wedge) of it.

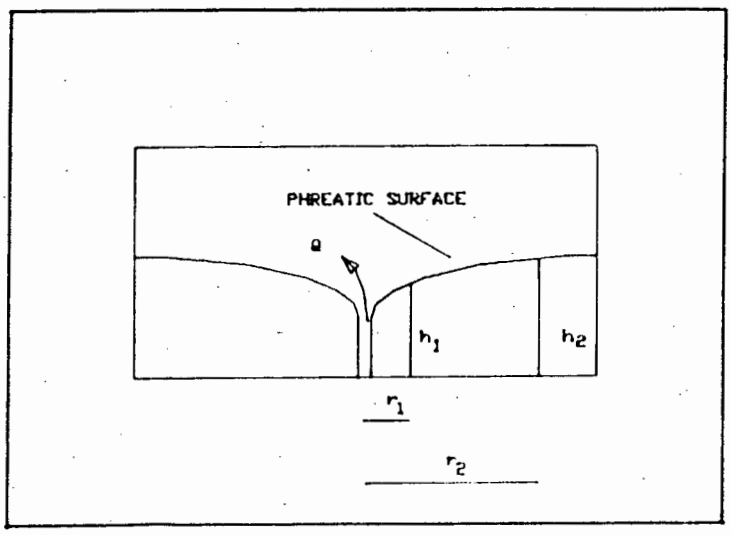


Figure 7.2 - The cone of depression caused by constant rate pumping of an unconfined aquifer

The results of the steady-state flow experiment may be found in Appendix F.

The coefficient of permeability calculated using the above formula was $k = 39,97$ cm/min. $Q$ having been determined from the average of the last 20 readings (amount of water collected in a bucket per minute). $k$ was also determined from an average of a few piezometer height readings. The value of $k$ determined from the void ratio and the permeability tests was $k = 42,78$ cm/min. Since these two values are within 7% of each other it was decided that an average of the two ($k = 41,375$ cm/min) be used as the input in the programme.

The lower coefficient of permeability, determined from the steady-state flow experiment, could be as a result of air becoming entrapped in the sand upon rewetting. The coefficient would, however, also include the flow occurring in the unsaturated zone.

It was, therefore, felt than an average of the two coefficients would be suitable as the input value in the programme.

7.2.3 Readings

Apart from the heights of the water level in the side wall piezometers, which were used to determine the initial conditions and the position of the phreatic surface with respect to time, the following readings were also recorded.

$M_s$ = mass of the air-dried sand used to construct the wedge
$M_{wi}$ = mass of water drained from the wedge in a time interval
$t_i$ = time at the start of the time interval
$t_f$ = time at the end of the time interval
$h_s$ = height of the sand wedge
$\ell_s$ = length of the sand wedge
$w_{us}$ = width of the sand wedge at the upstream face
$w_{ds}$ = width of the sand wedge at the outflow face

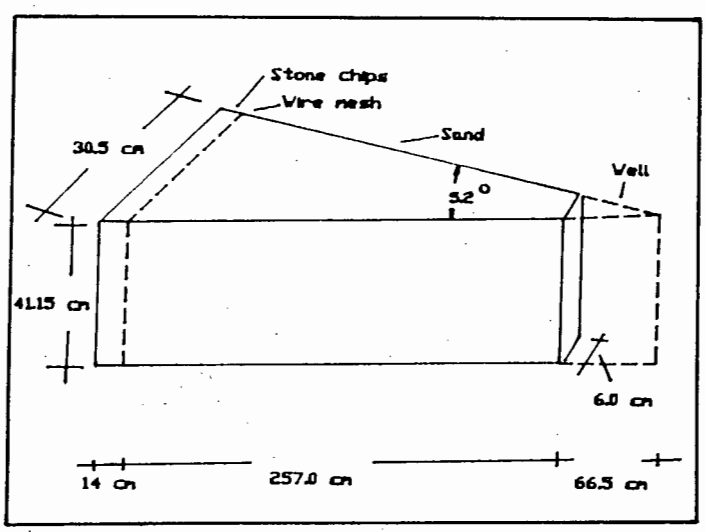


Figure 7.3 - Dimensions of the wedge

7.2.4 Calculations

For the calculations performed in this chapter the following units were used :

| | | |
|---|---|---|
| 1. | dimensions | cm |
| 2. | volumes | $cm^3$ |
| 3. | masses | g |
| 4. | $\rho_w$ and $S_g$ | $g/cm^3$ |

(a) The void ratio was determined from :

$$e = \frac{V_v}{V_s} \tag{7.2}$$

where $$V_v = V_t - V_s \tag{7.3}$$

$$V_t = (w_{us} + w_{ds}) \times \ell_s \times h_s \tag{7.4}$$

$$V_s = \frac{M_s}{S_g} \tag{7.5}$$

(b) The flow rate was determined from :

$$Q_i = \frac{[M_{w(i-1)} - M_{w(i)}] / \rho_w}{t_{(i-1)} - t_{(i)}} \tag{7.6}$$

## 7.3 MODELLING THE PROBLEM

All the relevant soil and soil-moisture characteristics, initial and boundary conditions first had to be fed into the programme before it could be used to simulate the respective drainage problems.

### 7.3.1 Input data

The input data used to model the two-dimensional plane problem may be found in Appendix G while the following input data was used when simulating the axisymmetrical drainage problem.

| | | | |
|---|---|---|---|
| 1. | length of the flow domain | = | 271 cm |
| 2. | height of the flow domain | = | 41,15 cm |
| 3. | porosity of the sand | = | 0,395 |
| 4. | saturated coefficient of permeability | = | 41,375 cm/min |
| 5. | number of elements in the r-direction | = | 40 |

| | | | |
|---|---|---|---|
| 6. | number of elements in the z-direction | = | 10 |
| 7. | time weighting factor | = | 1 |
| 8. | time increment | = | 0,125 min |
| 9. | length of time for programme to run | = | 60 min |
| 10. | initial height of the water table above the base of the seepage tank | = | 39,1 cm. |

7.3.2 Discretization of the flow domain

When simulating the drainage of the sand wedge a 40 x 10 finite element mesh was used. The length of the flow domain was divided into 40 elements while the height of the flow domain was divided into 10 elements. The above discretization gave rise to mesh comprised of 400 equisized finite elements.

As was mentioned in Chapter 5, it would have been preferable to use smaller elements near the outflow face and larger elements towards the upstream face. This was due to the larger gradients existing near the outflow face. It was found, when simulating the two two-dimensional drainage problems, that a 40 x 15 finite element mesh was about the largest mesh possible on the personal computers used. It can, therefore, be seen that computers with larger RAM capacities should be used when simulating large or complex flow problems. The length of time it took to simulate the problems also made the use of personal computers unfeasible.

The element and node numbering of the mesh, shown in Chapter 5, gave rise to the final global matrices having the smallest possible bandwidths. The smaller the matrix bandwidths are, the shorter the computational run time. The element numbering also ensured that the direction of analysis was from the saturated to the unsaturated zones. Neuman (1976) recommends this, for improved convergence, when treating the seepage face.

7.3.3 Initial and boundary conditions

The initial and boundary conditions imposed on both the plane and axisymmetrical drainage problems were of the same nature. This was

since the problems, excepting for their geometry, were essentially the same.

The initial conditions imposed on the flow domain were in the form of pressure heads prescribed at the nodes of the mesh. The position of the phreatic surface was first determined with the aid of the sidewall piezometers. The pressure heads prescribed for those nodes, below the phreatic surface (saturated zone), were determined using a hydrostatic pressure distribution. For both problems simulated, the distance between the phreatic surface and the top of the flow domain was less than the air entry head of the sand comprising the flow domain. The negative pressure heads assigned to the nodes above the phreatic surface were, therefore, also determined using a linear pressure distribution.

All the boundaries of the flow domain, excepting the outflow face, were treated as zero flux boundary conditions, i.e. no flow took place across these boundaries. The outflow face was treated as described in Chapter 4.

The boundary conditions were imposed, before solving the final flow equations, by deleting the relevant rows and columns from the final global matrices. The elements pertaining to the seepage face were, however, stored and later used to determine the normal nodal fluxes on this face, by back substitution.

7.3.4 The outflow face

As was mentioned in Chapter 4 the outflow face was treated partly as a prescribed pressure head boundary condition (i.e. atmospheric pressure for those nodes below the phreatic surface) and partly as a zero flux boundary condition (for those nodes above the phreatic surface).

The length of the seepage face was adjusted at the end of every iteration after the normal nodal fluxes on this face had been determined. Once the seepage face length had been shortened after

an iteration, it could not be increased in subsequent iterations as this would be contrary to transient drainage theory.

Due to the large gradients existing during the initial stages of the drainage process, inaccuracies could creep into the numerical analysis. Since the seepage face length could not be increased after it had been shortened, and the possible existence of numerical errors, the author felt it desirable not to reduce the seepage face length too drastically after the first iteration in the first time step. The length of the seepage face was, therefore, increased by two finite element lengths after it had been determined. This was, however, only applicable for the first iteration in the first time level. Thereafter, the seepage face length was calculated as described in Chapter 4.

7.3.5 The element matrices

The element matrices used when simulating both the plane and axisymmetrical problems may be found in Appendix C.

It should be noted that the element matrices, used when modelling these problems, are essentially the same. The only difference is the $2\pi r$ term found in the coefficients of the element matrices used to simulate the axisymmetrical problem. The $r$ term represents the radial distance from the axis of symmetry to the integration points on the element.

Time-consuming numerical integration was, however, avoided in the model presented by Huyakorn et al (1984). The relevant values, previously calculated at the integration points, were approximated at the centroid of the element. This approximation is adequate provided the finite element mesh is suitably refined. Allaire (1985) states that $r$, for the axisymmetrical problem, may also be approximated to the centroid of the element, as opposed to the integration points, provided the finite element is of sufficient distance from the axis of symmetry of the flow domain. This condition was met for the axisymmetrical problem modelled in this thesis.

In Chapter 4 it was mentioned that $\Psi_j^k$ could become unknown at the beginning of a time step when modelling the saturated zone of a sand whose specific storativity was zero [Neuman (1976)]. This problem arose when a change in boundary conditions occurred, around the saturated zone, during a time interval. The capacity matrix $B_{ij}$ is zero for a saturated sand whose specific storativity ($S_s$) is zero. This is since the specific moisture capacity $n \frac{dS_r}{d\Psi}$ is zero for a saturated sand. The coefficient of the capacity matrix, as given in Chapter 4, is :

$$\eta = S_s S_r + n \frac{dS_r}{d\Psi} \qquad (7.7)$$

When an element becomes desaturated during an iteration the capacity matrix becomes non-zero causing an instantaneous change in the pressure heads throughout the saturated zone.

To overcome this problem a specific storativity value of $1 \times 10^{-6}$ was assigned to the sand. Furthermore, the backward difference time marching scheme, as recommended by Neuman (1976), was employed. This value of the specific storativity was small enough not to affect the overall results but yet prevented the above-mentioned problem from arising.

7.3.6 The time weighting factor and the time increment

When simulating the two-dimensional drainage problems only the backward difference time marching scheme was employed. The backward difference scheme was employed for the above-mentioned reasons and as it yielded the best results when simulating the one-dimensional column drainage experiment. The scheme was also employed as it remained stable irrespective of the time increment employed.

Equation (4.30) presented by Huyakorn et al (1984), for determining the value of the time increment to be employed, was only applicable for one-dimensional problems. The value of the time increment for

the two-dimensional problems, therefore, had to be chosen intuitively. Hence the backward difference scheme was employed for time marching.

Constant, as opposed to variable, time increments were again employed in the simulations. Although the use of variable time increments would have reduced the computational run time, constant time increments facilitated the comparison between numerical and experimental results and were hence employed.

## 7.4 DISCUSSION OF THE RESULTS

Two parameters; the flow rate and the location of the phreatic surface with respect to time, were the two parameters by which the experimental and numerical drainage results were compared. The results of the comparison for the two-dimensional plane problem may be found in Appendix E while those for the axisymmetrical problem may be found at the end of this chapter.

It should again be noted that the discrepancies could be of an experimental or numerical nature. Discrepancies could also have arisen due to the way this model was coded.

Although the discrepancies for the drainage problems simulated were not large, the author still feels that an analytical solution be obtained. With this data, or the data obtained from another model, more certainty as to the exact cause of the discrepancies may be achieved.

### 7.4.1 The location of the phreatic surface

As can be seen from both the two-dimensional drainage problems modelled, the location of the phreatic surface predicted numerically was always lower than experimentally determined. The only exception to this was with the axisymmetrical problem in the vicinity of the outflow face.

At first one might feel that the above discrepancy was due to the slow response time of the side wall piezometers. The water level in these tubes did tend to lag behind the phreatic surface. Since the

same problem arose when modelling the two-dimensional plane problem (transducers used to record pressure heads) this may not be the main cause of the discrepancy.

A possible cause of the discrepancy could lie in the way in which the flow domain was modelled. The volume of water in the zone containing the stone chips (used when saturating the wedge) also participated in the flow and hence had to be considered in the drainage of the wedge. The length of the flow domain was, therefore, lengthened to include this zone. In doing this it was assumed that the stone chips had the same porosity and soil-moisture characteristics as the sand comprising the wedge. These approximations were made for the lack of a better way in which to incorporate that volume of water into the overall flow pattern. The discrepancies could easily have arisen as a result of these approximations.

The contouring method used to determine the location of the phreatic surface (at a particular time level) from the side wall piezometer readings (at various time intervals) could be another possible source of error. Since the response time of certain piezometers seemed to be slower than others, judgement was needed during the contouring process. The vulnerability of the side wall piezometers becoming blocked was another shortfall of this apparatus.

Finally, it can be seen that the largest discrepancies arose in the vicinity of the outflow face. Larger discrepancies were apparent when modelling the plane problem than when the axisymmetrical problem was modelled. For the axisymmetrical problem, it can be seen that location of the phreatic surface (numerically predicted) was higher than experimentally determined. This was a strange feature as one would have expected the piezometer water levels to have lagged significantly behind the phreatic surface in this region.

One must, however, be reminded that the null-flow devices were also used to determine the location of the phreatic surface near the outflow face. Towards the latter stages of the drainage process, however, large air bubbles were present in these devices, thereby rendering them inaccurate.

Apart from the contouring method, the numerical model may also give rise to discrepancies in this area. When modelling the seepage face, its length is adjusted by finite jumps. No feature exists in the model whereby the length of the seepage face may be adjusted smoothly. Hence the possible cause for the discrepancies in the area.

It was noted when modelling both the drainage problems that convergence was not achieved, within the specified number of iterations, for the first two time steps. This was the case even when very small time increments were employed. This could possibly be overcome with a more refined finite element mesh. This was, however, not possible on the computers used. The programme continues, even if convergence is not achieved within a time step, using the results from the time step for future predictions. Possible errors could, therefore, arise due to the lack of convergence in these iterations.

### 7.4.2 The outflow rate

The rate at which water drained from the wedge was another parameter used to compare the experimental and numerical drainage results. Although the programme did determine the normal nodal fluxes on the seepage face they were not used to determine the outflow rates. Instead the Darcian velocities, calculated at the centroids of those saturated elements bounding on the outflow face, were used to determine the outflow rate.

The velocities at the centroids of the elements on the outflow face were determined from

$$V = k\,(S_r)\,(h_1 + h_4 - h_3 - h_2) \,/\, 2\,\ell \qquad (7.8)$$

where $k$ is the coefficient of permeability

$h_{1,2,3,4}$ are the total head values at the nodes of the element

$\ell$ is the length of the element

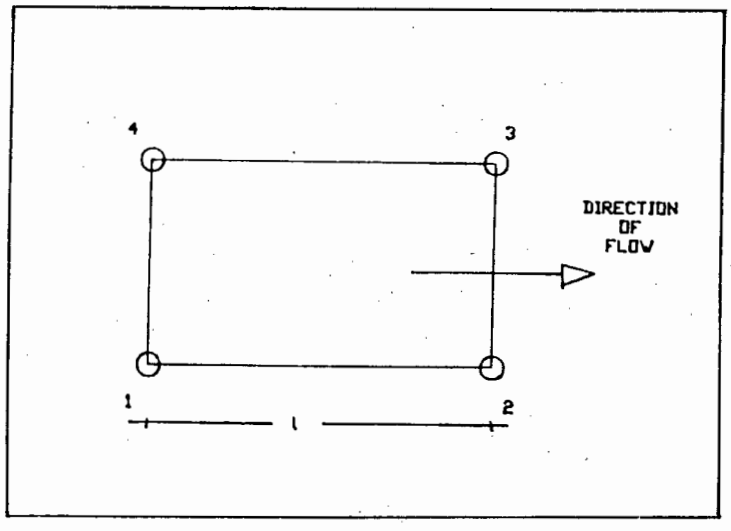


Figure 7.5 - Diagram of a typical element bounding on the seepage face
(segment 2-3 forms part of the seepage face)

The approximated flow rate through the element was then determined by multiplying the outflow velocity by the element height and by $2\pi r$ , where $r$ is the radial distance from the axis of symmetry to the outflow face. The sum of all the flow rates through all the elements, comprising saturated portion of the outflow face, equalled the total outflow rate from the whole aquifer. This flow rate was, therefore, altered to represent the flow rate from the wedge (portion of the aquifer).

The flow rate as a parameter for comparison between experimental and numerical (determined as described above) drainage results had varying success. The flow rate could be predicted to within 10% of the experimental value in the case of the plane problem. For the axisymmetrical problem, however, the flow rate at certain instances could only be predicted to within 20% of the experimental value.

Since smooth flow rate and cumulative outflow versus time curves were obtained from the axisymmetrical experiment (see Appendix F) it is unlikely that the experimental results were inaccurate. It should be noted that in all cases the outflow rate calculated from the numerical results was lower than experimentally determined.

## 7.5 CONCLUSIONS AND RECOMMENDATIONS

The numerically determined flow rates and locations of the phreatic surface were at all instances lower than the equivalent experimental values. The author, therefore, feels that the flow problem was not correctly modelled. The approximations concerning the 'stone chips' were the most possible cause for this discrepancy.

Although its not certain that this problem could be overcome, besides possibly finding an alternative method to saturate the wedge, its effect could definitely be reduced. It is recommended for future experiments that the length of this zone be significantly reduced. The wedge could still be saturated in the same manner but the volume of water in this zone would be significantly reduced.

The author also feels that the lack of convergence after the first two time steps was also a major contributor to the discrepancies. It is, therefore, recommended that main frame computers be used for future modelling. Not only would the use of these computers enable a more refined mesh to be used but the run time would also be significantly reduced.

Finally, the author recommends than an alternative method for determining the location of the phreatic surface, with respect to time, be found. If one could determine all the sidewall piezometer heights at one particular instance, it would be possible to see which piezometer tubes were blocked (water level always above phreatic surface). The problem does not lie so much in the instruments themselves (including the null-flow devices) but rather the rapid acquisition of their data. Alternatively, more people could be used to record the piezometer water heights (especially in the null-flow devices).

## Phreatic surface at 2 min.

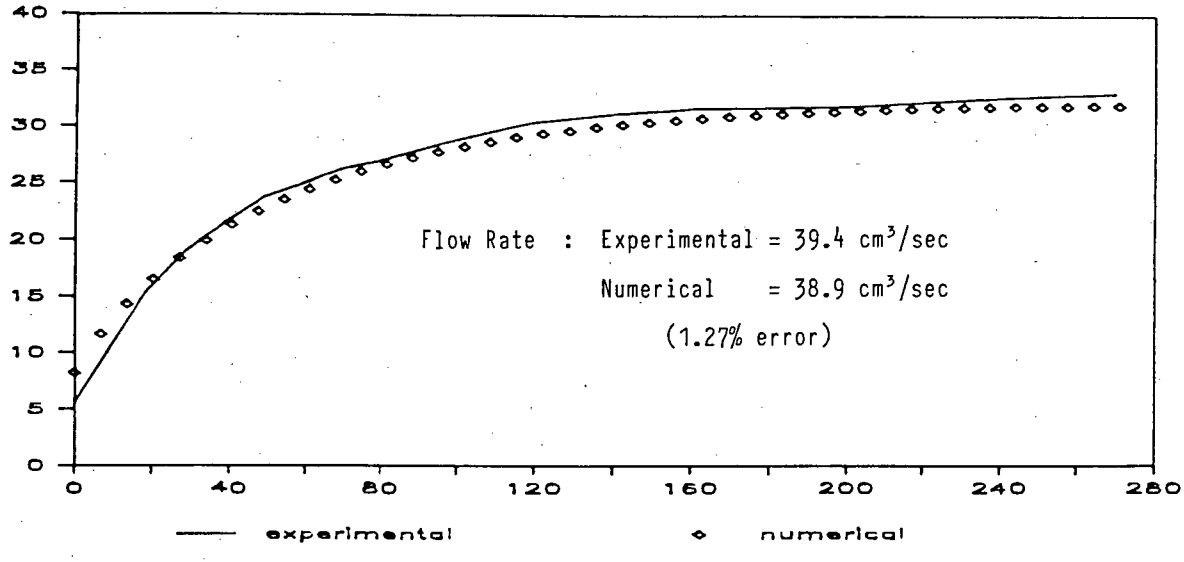


## Phreatic surface at 5 min.

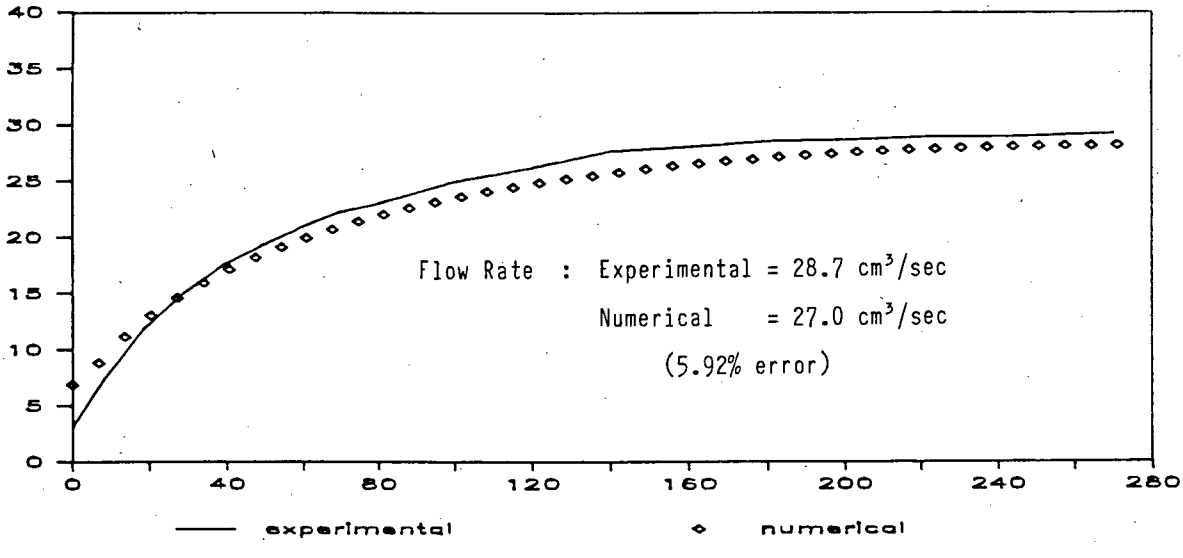


## Phreatic surface at 10 min.

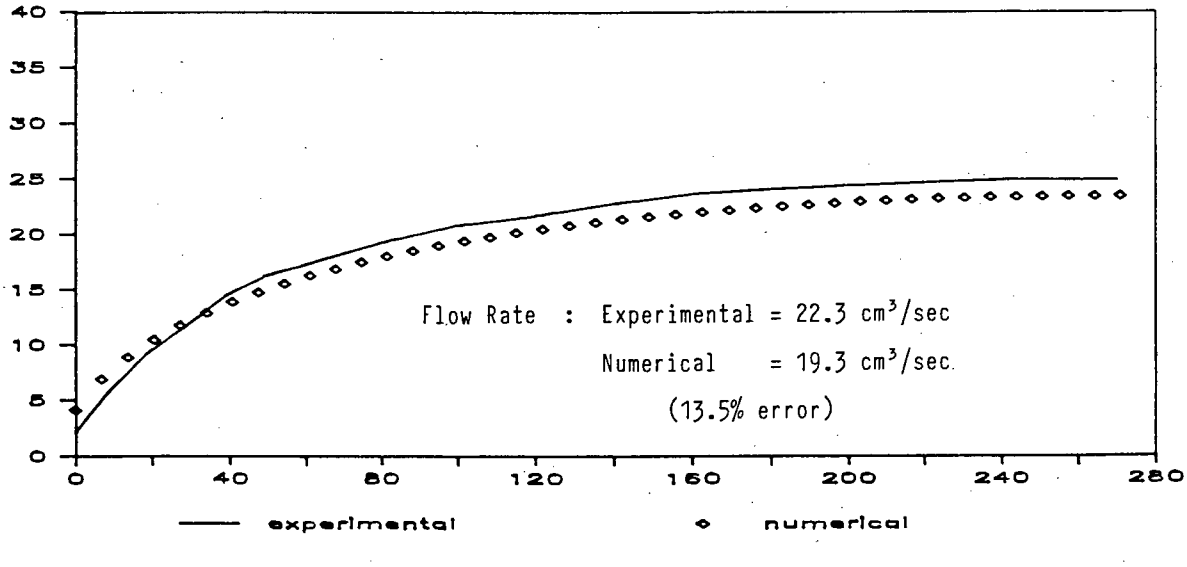

## Phreatic surface at 15 min.

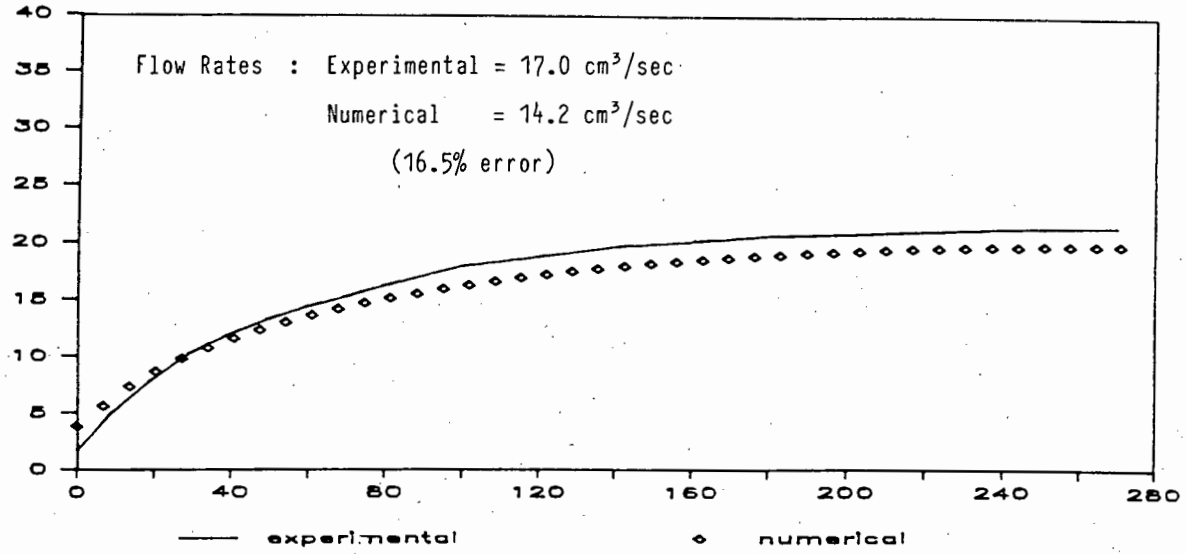


## Phreatic surface at 30 min.

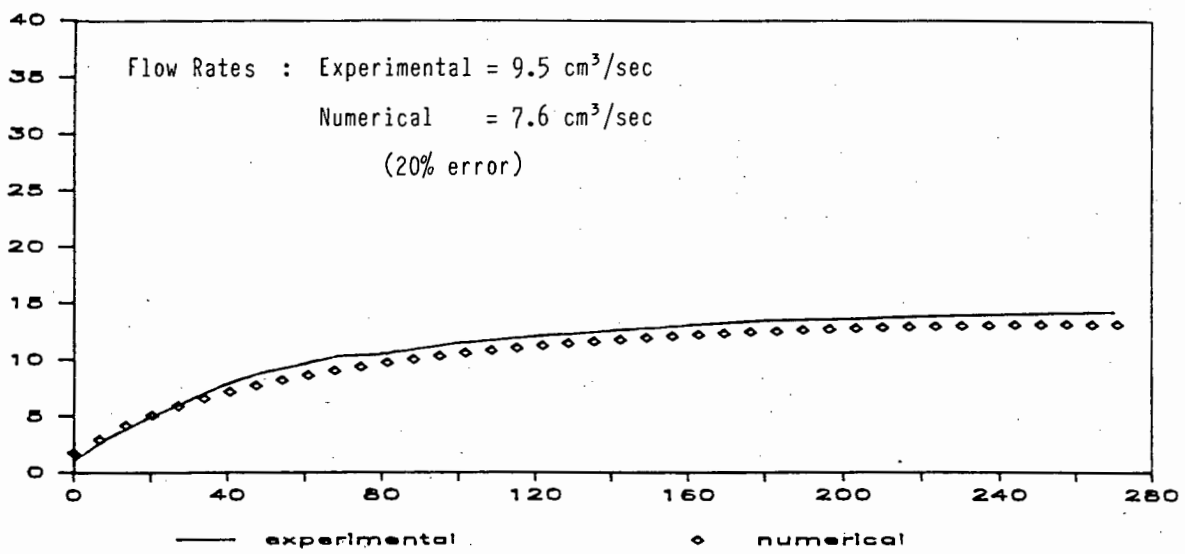


## Phreatic surface at 60 min.

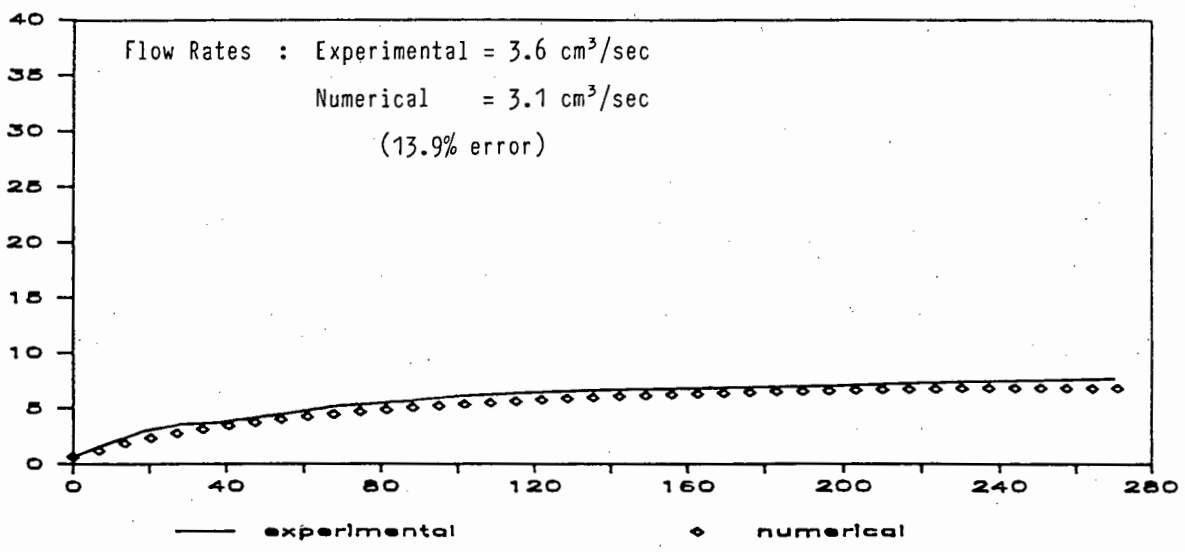

# CHAPTER 8

## CONCLUDING REMARKS

In this thesis the transient drainage process of water in saturated-unsaturated soil profiles was studied. The main emphasis was placed on using the finite element method of analysis as a tool for simulating flow problems. Of particular importance was the capability of this numerical method to include the unsaturated flow, which occurs above the phreatic surface, in the flow problems.

A literature review was undertaken in order that the factors influencing the flow of water through saturated and unsaturated soil profiles were understood and could be taken into account in either the experimental or numerical portions of this thesis.

Two drainage experiments were performed by the author on sands of varying grain size and grading. The results of a third drainage experiment, performed by another investigator, were also obtained by the author. These experiments were then simulated using a finite element based model.

The model presented in this thesis is based on models presented by a number of other authors. Certain features from these models were incorporated into the model presented in this work, while modifications were made by the author to improve the accuracy and efficiency of the computational model when simulating the above experiments.

The model was then coded in True Basic by the author for use on a personal computer so that the above-mentioned experiments could then be simulated using this programme. In this manner the accuracy with which this numerical method simulated these saturated-unsaturated flow problems could be determined.

In general, good comparisons were achieved between the experimental and the numerical results. There were, however, various numerical and experimental shortfalls which hampered the use of this programme and could be the cause for the discrepancies in certain areas. These shortfalls were :

1. Certain features of the experimental apparatus, essential to the experiment, could not be accurately accounted for in the numerical model.

2. The constitutive curves governing the flow of water through the soil profiles needed to be determined experimentally before they could be incorporated in the programme. Furthermore, it was not possible to determine these curves from basic soil properties.

3. The numerical treatment of the seepage face seemed coarse. A more refined method needs to be found as the largest discrepancies occurred in this vicinity.

4. The numerical programme was not sufficiently flexible. It should be modified to handle finite elements of varying size or possibly even varying element types. The finite element meshes used when simulating the drainage problems were possibly not refined to a large enough extent. The meshes (two-dimensional cases) could not be further refined owing to the limited memory capacity of the computer used. Furthermore, the run time on the personal computer made it uneconomical to use. Main frame computers should, therefore, be used to overcome the above-mentioned problems.

5. Finally, the experimental apparatus used to determine the pressure heads in the soil should be improved. When monitoring the drainage process it is preferable to obtain a large number of pressure head readings (various locations in the soil) at one particular instance. This was not possible with the instrumentation used. Furthermore, the ability to determine in-situ soil moisture contents (as they vary with time) would greatly facilitate further research in this area.

This thesis illustrates the usefulness of comparing the results from theoretical and experimental models. This thesis was made possible because of the available specialized seepage tank in the geotechnical laboratory, and the microcomputers in the Engineering Faculty at the University of Cape Town.

The author, on concluding this thesis, regards the finite element method of analysis as a powerful tool for analysing saturated-unsaturated flow problems.

Its ability to handle unsaturated flow, whose importance has been revealed, makes it a useful tool for analysing certain flow problems which are primarily unsaturated flow based. There are, however, certain facets of the model which need to be improved to make this method more viable. Finally, all future analysis should be done on main frame computers to keep this method of analysis economically viable.

## REFERENCES


ALEXANDER, L. AND SKAGGS, R.W.: "Predicting unsaturated hydraulic conductivity from soil texture", *J. Irrig. Drain. Div. Am. Soc. Civ. Eng.*, 113(2), 184-197, 1987.

ALLAIRE, P.E.: *Basics of the finite element method*, W.C. Brown, 1985.

BATHE, K.J.: *Finite element procedures in engineering analysis*, Mc-Graw-Hill, 1971.

BAVER, L.D., GARDENER, W.H. AND GARDENER, W.R.: *Soil Physics*, 4th edit., John Wiley, 1972.

BEAR, J.: *Dynamics of fluids in porous media*, Elsevier, 1972.

BEAR, J.: *Hydraulics of groundwater*, McGraw-Hill, 1979.

BEAR, J. AND BRAESTER, C.: "Comments on 'A three-dimensional finite element model for simulating water in variably saturated porous media' by P.S. Huyakorn et al", *Water Resour. Res.*, 23(8), 1705-1706, 1987.

CHUNG, S-O AND AUSTIN, T.A.: "Modelling saturated-unsaturated water flow in soils", *J. Irrig. Drain. Div. Am. Soc. Civ. Eng.*, 113(2), 233-250, 1987.

COOLEY, R.L.: "Some new procedures for numerical solution of variably saturated flow problems", *Water Resour. Res.*, 19(5), 1271-1285, 1983.

DAGAN, G. AND KRONSZYNSKI, U.: "Drainage of a vertical column", in *Biological studies: Physical aspects of soil water and salts in ecosystems*, vol. 4, edited by A. Hadas, D. Swartzendruber, P.E. Rijtman, M. Fuchs and B. Yaron, Chap. 2, Springer-Verlag, 1973.

DAGAN, G.: "Models of groundwater flow in statistically homogeneous porous formations", *Water Resour. Res.*, 15(1), 47-63, 1979.

DESAI, C.S.: "Finite element method for flow in porous media", in *Finite elements in fluids*, Vol. 1, edited by R.H. Gallagher, J.T. Oden, C. Taylor and O.C. Zienkiewicz, Chap. 8, John Wiley, 1975.

DE WIEST, R.J.M., *Flow through porous media*, Academic Press, 1969.

FREEZE, R.A.: "The mechanism of natural ground-water recharge and discharge 1. One-dimensional, vertical, unsteady, unsaturated flow above a recharging or discharging groundwater flow system", *Water Resour. Res.*, 5(1), 153-171, 1969.

FRIND, E.O. AND VERGE, M.J.: "Three-dimensional modelling of groundwater flow systems", *Water Resour. Res.*, 14(5), 844-856, 1978.

GREAT BRITAIN ROAD RESEARCH LABORATORY, *Soil mechanics for road engineers*, H.M.S.O., 1954.

HILLEL, D.: *Soil and water: physical principles and processes*, Academic Press, 1971.

HILLEL, D.: *Introduction to soil physics*, Academic Press, 1982.

HUYAKORN, P.S., THOMAS, S.D. AND THOMPSON, B.M.: "Techniques for making finite elements competitive in modelling flow in variably saturated porous media", *Water Resour. Res.*, 20(8), 1099-1115, 1984.

HUYAKORN, P.S., MERCER, J.W. AND WARD, D.S.: "Finite element matrix and mass balance computational schemes for transport in variably saturated porous media", *Water Resour. Res.*, 22(3), 346-358, 1985.

HUYAKORN, P.S., SPRINGER, E.P., GUVANASEN, V. AND WADSWORTH, T.D.: "A three-dimensional finite element model for simulating water flow in variably saturated porous media", *Wate Resour. Res.*, 22(13), 1790-1808, 1986.

IRONS, B. AND ALIDAD, S.: *Techniques of finite elements*, John Wiley, 1980.

KHALEEL, R. AND YEH, T-C.: "A Galerkin finite element program for simulating unsaturated in porous media", *Ground water*, 23(1), 90-96, 1985.

MARSHALL, T.J. AND HOLMES, J.W.: *Soil physics*, Cambridge University Press, 1979.

MAULEM, Y.: "A new model for predicting the hydraulic conductivity of unsaturated porous media", *Water Resour. Res.*, 12(3), 513-522, 1976.

MAULEM, Y.: "Extension of the similarity hypothesis used for modelling the soil water characteristics", *Water Resour. Res.*, 13(4), 773-780, 1977.

NARASIMHAN, T.N., NEUMAN, S.P. AND WITHERSPOON, P.A., "Finite element method for subsurface hydrology using a mixed explicit-implicit scheme", *Water Resour. Res.*, 14(2), 863-877, 1978.

NEUMAN, S.P.: Saturated-unsaturated seepage by finite elements", *J. Hydraul. Div. Amer. Soc. Civ. Eng.*, 99(HY12), 2233-2250, 1973.

NEUMAN, S.P.: "Galerkin method of analyzing nonsteady flow in saturated-unsaturated porous media", in *Finite elements in fluids*, Vol. 1, edited by R.H. Gallagher, J.T. Oden, C. Taylor and O.C. Zienkiewicz, Chap. 10, John Wiley, 1975.

RAO, S.S.: *The finite element method in engineering*, Pergamon Press, 1982.

SPARKS, A.D.W. AND OTHER STUDENTS: Experimental apparatus, 1961-1986.

SWARTZENDRUBER, D. AND HILLEL, D.: "The physics of infiltration", in *Ecological studies*: *Physical aspects of soil water and salts in ecosystems*, Vol. 4, edited by A. Hadas, D. Swartzendruber, P.E. Rijtman, M. Fuchs and B. Yaron, Chap. 1, Springer-Verlag, 1973.

TRACY, J.C. AND MARINO, M.A.: "Seepage into variably saturated porous medium", *J. Irrig. Drain. Div. Am. Soc. Civ. Eng.*, 113(2), 198-212, 1967.

VERMEER, P.A. AND VERRUIJT, A.: "An accuracy condition for consolidation by finite elements", *Int. J. Num. Analy. Meth. Geom.*, 5, 1-14, 1981.

WARDLE, G.R.: "Aspects of the drainage process in soils", *MSc thesis*, University of Cape Town, 1986.

WIPPLINGER, O.: "Two phase analysis of unit flow in irrigation and aquifer recharge", *PhD thesis*, University of Stellenbosch, 1986.

YEH, G-T.: "On the computation of Darcian velocity and mass balance in the finite element modelling of groundwater flow", *Water Resour. Res.*, 17(5), 1529-1534, 1981.

ZIENKIEWICZ, O.C.: "*The finite element method*", 3rd edit., McGraw-Hill, 1977.

# APPENDIX A

COURSE WORK UNDERTAKEN BY CANDIDATE
FOR THE PARTIAL FULFILMENT FOR THE DEGREE OF
MASTER OF SCIENCE IN ENGINEERING

| Course Code | Description of Course | Credit Rating | Symbol Achieved |
|---|---|---|---|
| CIV 516F | Coastal Hydraulics | 5 | 2+ |
| CIV 540F | Finite Element Analysis | 4 | 2+ |
| CIV 588F | Applied Mechanics I | 3 | 2- |
| CIV 592F | Project Management | 3 | 2+ |
| CIV 543S | Airport Design | 3 | 2- |
| CIV 504S | Structural Dynamics | 3 | 1 |
| CIV 539S | Applied Mechanics II | 3 | 1 |
| | Total | 24 | |

Course work credit requirement : 20

Half thesis credit rating : 20

Total credits required for the degree MSc (Eng) : 40

# APPENDIX B

## EXPERIMENTAL RESULTS FROM THE EXPERIMENTS USED TO DETERMINE THE SOIL AND SOIL MOISTURE CHARACTERISTICS

# DRY SIEVE ANALYSIS RESULT SHEET

## SAND A

Initial mass of sand (Mi) = 1976.9 g
Final mass of sand (Mf) = 1976.6 g

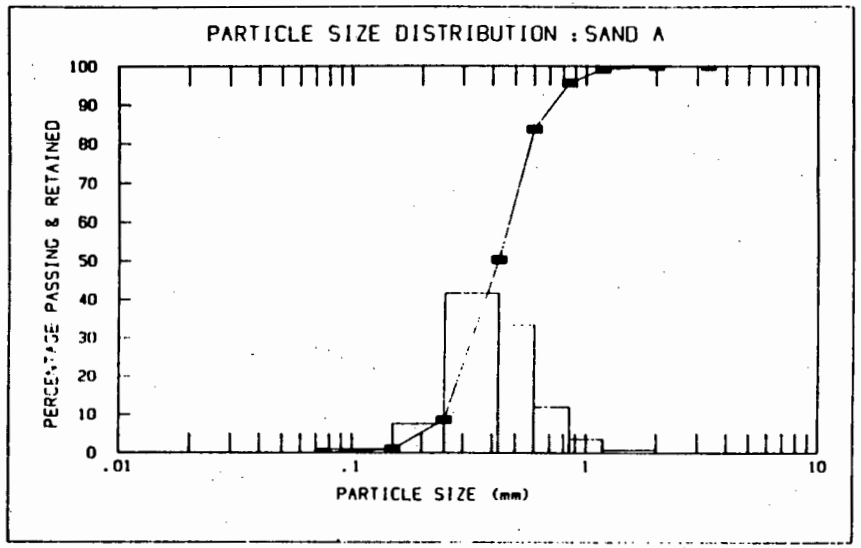


| Sieve size (mm) | Mass retained N (g) | Percentage retained R (%) | Cummulative % passing S (%) | Percentage passing P (%) |
|---|---|---|---|---|
| 3.350 | 0.1 | 0.005 | 0.005 | 99.995 |
| 2.000 | 0.1 | 0.005 | 0.010 | 99.990 |
| 1.180 | 14.8 | 0.749 | 0.759 | 99.241 |
| 0.850 | 71.3 | 3.607 | 4.366 | 95.634 |
| 0.600 | 236.6 | 11.970 | 16.336 | 83.664 |
| 0.425 | 659.7 | 33.375 | 49.712 | 50.288 |
| 0.250 | 823.6 | 41.668 | 91.379 | 8.621 |
| 0.150 | 150.4 | 7.609 | 98.988 | 1.012 |
| 0.075 | 18.4 | 0.931 | 99.919 | 0.081 |
| pan | 1.6 | 0.081 | 100.000 | .000 |

Calculations

R=(N/MF)*100
P=100-S

# SPECIFIC GRAVITY / RELATIVE DENSITY TEST

## SAND A

| | | |
|---|---|---|
| Density of water | | = 0.9982 g/cm^3 |
| Mass of dry bottle | | = 35.215 g |
| Mass of sand and bottle | | = 55.552 g |
| Mass of water, sand and bottle | | = 97.720 g |
| Mass of water and bottle | | = 84.980 g |
| Mass of dry sand | = (55.552-35.215) | = 20.337 g |
| Mass of water added | = (97.720-55.552) | = 42.168 g |
| Mass of water displaced by sand | = (84.980-35.215)-42.168 | = 7.597 cm^3 |
| Volume of water added | = (42.168/0.9982) | = 42.244 cm^3 |
| Volume of water displaced by sand | = 7.597/0.9982 | = 2.601 cm^3 |
| Density of sand | = (20.337/7.601) | = 2.676 g/cm^3 |
| Relative density of sand | = (2.676/0.9982) | = 2.680 |

## PERMEABILITY TEST : SAND A

Dry mass of sand = 1601.8 g
Sg of sand = 2.68

Diameter of permeameter = 7 cm
Distance between tappings = 20 cm

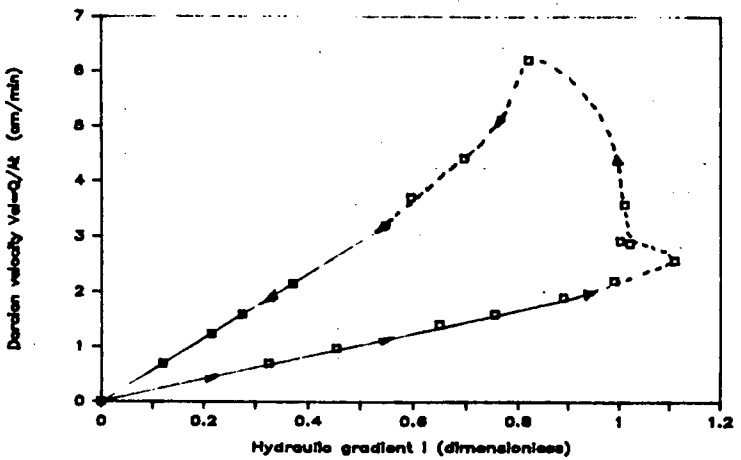


| Height of sand (cm) | h1 (cm) | h2 (cm) | h3 (cm) | Q (cm^3) | time (sec) | vel (cm/min) | i ( ) | e ( ) | k (cm/min) |
|---|---|---|---|---|---|---|---|---|---|
| 25.1 | 45.2 | 42.0 | 38.7 | 163 | 360 | 0.7060 | 0.325 | 0.616 | 2.1723 |
| 25.1 | 48.2 | 43.4 | 39.1 | 229 | 360 | 0.9919 | 0.455 | 0.616 | 2.1799 |
| 25.1 | 52.5 | 45.7 | 39.5 | 247 | 270 | 1.4264 | 0.650 | 0.616 | 2.1945 |
| 25.1 | 54.7 | 46.9 | 39.6 | 279 | 270 | 1.6112 | 0.755 | 0.616 | 2.1341 |
| 25.1 | 57.7 | 48.6 | 39.9 | 258 | 210 | 1.9157 | 0.890 | 0.616 | 2.1524 |
| 25.2 | 59.9 | 50.0 | 40.1 | 213 | 150 | 2.2141 | 0.990 | 0.622 | 2.2365 |
| 25.7 | 61.8 | 50.5 | 39.6 | 199 | 120 | 2.5858 | 1.110 | 0.655 | 2.3295 |
| 25.8 | 59.6 | 49.4 | 39.2 | 167 | 90 | 2.0933 | 1.020 | 0.661 | 2.8365 |
| 25.8 | 58.9 | 48.9 | 38.9 | 179 | 95 | 2.9380 | 1.000 | 0.661 | 2.9380 |
| 26.6 | 59.3 | 48.9 | 39.1 | 161 | 70 | 3.5863 | 1.010 | 0.713 | 3.5508 |
| 29.0 | 48.1 | | 31.7 | 199 | 50 | 6.2058 | 0.820 | 0.867 | 7.5681 |
| 28.5 | 44.5 | | 30.6 | 170 | 60 | 4.4179 | 0.695 | 0.835 | 6.3567 |
| 28.2 | 42.0 | 36.6 | 30.1 | 190 | 80 | 3.7032 | 0.595 | 0.816 | 6.2239 |
| 28.1 | 47.3 | 43.5 | 39.9 | 166 | 120 | 2.1570 | 0.370 | 0.809 | 5.8296 |
| 28.1 | 44.9 | 42.3 | 39.4 | 154 | 150 | 1.6008 | 0.275 | 0.809 | 5.8212 |
| 28.1 | 43.3 | 41.5 | 39.0 | 240 | 300 | 1.2474 | 0.215 | 0.809 | 5.8019 |
| 28.1 | 40.8 | 39.7 | 38.4 | 134 | 300 | 0.6965 | 0.120 | 0.809 | 5.8039 |

## PERMEABILITY TEST : SAND A

Dry mass of sand = 1603.4 g
Sg of sand = 2.68

Diameter of permeameter = 7 cm
Distance between tappings = 20 cm

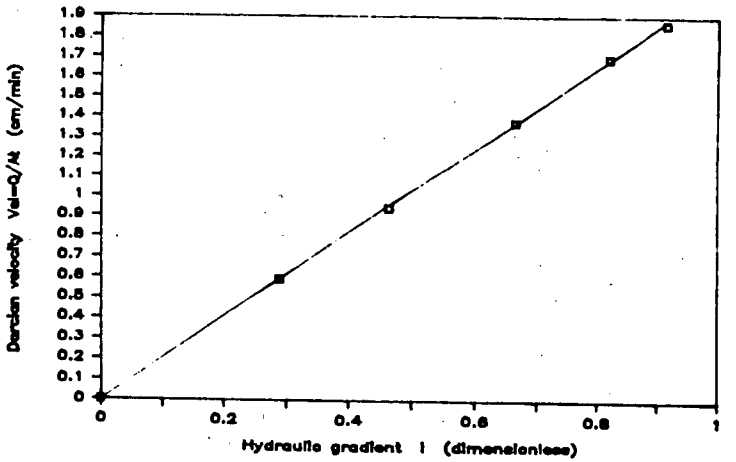


| Height of sand (cm) | h1 (cm) | h2 (cm) | h3 (cm) | Q (cm^3) | time (min) | vel (cm/min) | i ( ) | e ( ) | k (cm/min) |
|---|---|---|---|---|---|---|---|---|---|
| 24.9 | 44.3 | | 38.5 | 114 | 5 | 0.5925 | 0.290 | 0.602 | 2.0432 |
| 24.9 | 48.6 | | 39.3 | 163 | 4.5 | 0.9413 | 0.465 | 0.602 | 2.0244 |
| 24.9 | 53 | | 39.7 | 145 | 2.75 | 1.3703 | 0.665 | 0.602 | 2.0605 |
| 24.9 | 56.5 | | 40.1 | 179 | 2.75 | 1.6916 | 0.820 | 0.602 | 2.0629 |
| 24.9 | 58.6 | | 40.3 | 215 | 3 | 1.0824 | 0.915 | 0.602 | 2.0355 |

## PERMEABILITY TEST : SAND A

Dry mass of sand = 1601.8 g
Sg of sand = 2.68

Diameter of permeameter = 7 cm
Distance between tappings = 20 cm

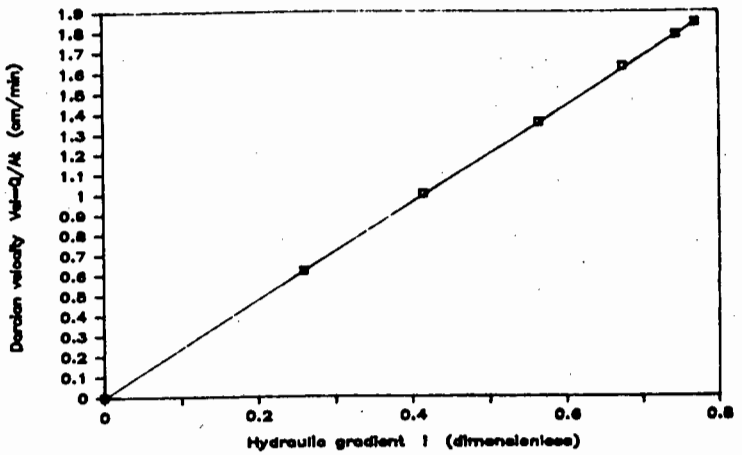


| Height of sand (cm) | h1 (cm) | h2 (cm) | h3 (cm) | Q (cm^3) | time (sec) | vel (cm/min) | i ( ) | e ( ) | k (cm/min) |
|---|---|---|---|---|---|---|---|---|---|
| 28.1 | 44.3 | | 39.1 | 174 | 7.25 | 0.6237 | 0.260 | 0.640 | 2.39884 |
| 28.1 | 48.2 | | 39.9 | 202 | 5.25 | 0.9999 | 0.415 | 0.640 | 2.40939 |
| 28.1 | 51.8 | | 40.5 | 235 | 4.5 | 1.3571 | 0.565 | 0.640 | 2.40199 |
| 28.1 | 54.6 | | 41.1 | 282 | 4.5 | 1.6286 | 0.675 | 0.640 | 2.41266 |
| 28.1 | 56.6 | | 41.7 | 223 | 3.25 | 1.7831 | 0.745 | 0.640 | 2.39348 |
| 28.1 | 57.4 | | 42 | 195 | 2.75 | 1.8428 | 0.770 | 0.640 | 2.39318 |

## PERMEABILITY TEST : SAND A

Dry mass of sand = 1601.8 g
Sg of sand = 2.68

X-sectional area = 38.48 cm*cm
Distance between tappings = 20 cm

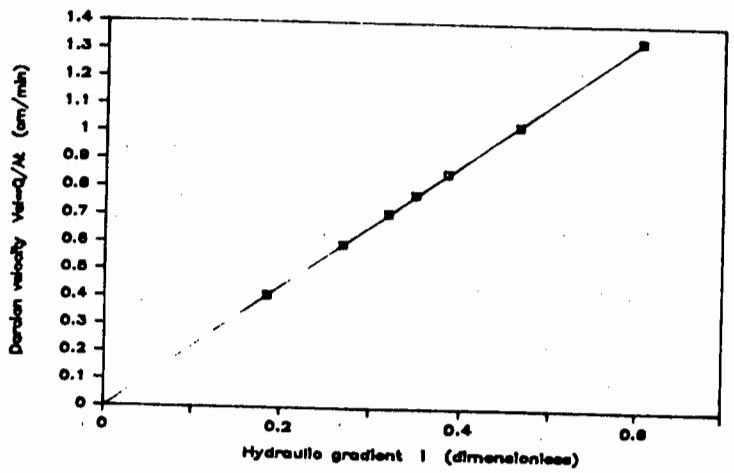


| Height of sand (cm) | h1 (cm) | h2 (cm) | h3 (cm) | Q (cm^3) | time (sec) | vel (cm/min) | i ( ) | e ( ) | k (cm/min) |
|---|---|---|---|---|---|---|---|---|---|
| 25.2 | 42.0 | | 38.3 | 79 | 15.00 | 0.411 | 0.185 | 0.622 | 2.21947 |
| 25.2 | 43.8 | | 38.4 | 115 | 15.00 | 0.598 | 0.270 | 0.622 | 2.21375 |
| 25.2 | 44.9 | | 38.5 | 137 | 15.00 | 0.712 | 0.320 | 0.622 | 2.22518 |
| 25.2 | 45.5 | | 38.5 | 150 | 15.00 | 0.780 | 0.350 | 0.622 | 2.22750 |
| 25.2 | 46.3 | | 38.6 | 165 | 15.00 | 0.858 | 0.385 | 0.622 | 2.22750 |
| 25.2 | 48.0 | | 38.7 | 198 | 15.00 | 1.029 | 0.465 | 0.622 | 2.21313 |
| 25.2 | 51.2 | | 39.1 | 258 | 15.00 | 1.341 | 0.605 | 0.622 | 2.21645 |

## PERMEABILITY TEST : SAND A

Dry mass of sand = 1603.4 g
Sg of sand = 2.68

Diameter of permeater = 7 cm
Distance between tappings = 20 cm

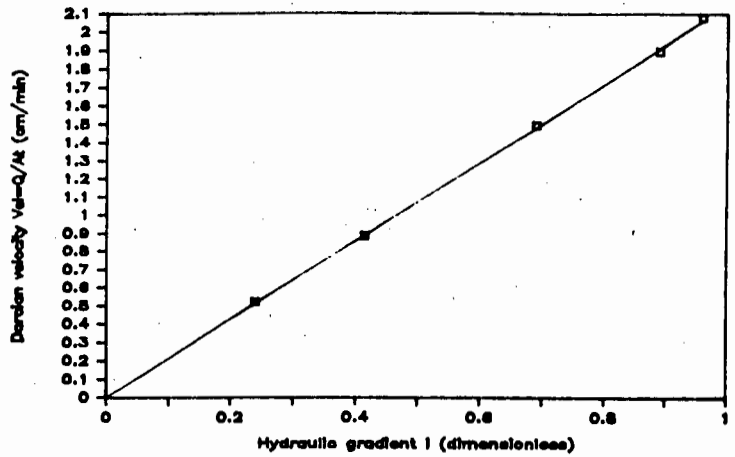


| Height of sand (cm) | h1 (cm) | h2 (cm) | h3 (cm) | Q (cm^3) | time (min) | vel (cm/min) | i ( ) | e ( ) | k (cm/min) |
|---|---|---|---|---|---|---|---|---|---|
| 24.7 | 43.1 | | 38.3 | 121 | 6 | 0.5241 | 0.240 | 0.589 | 2.18367 |
| 24.7 | 47 | | 38.7 | 154 | 4.5 | 0.8894 | 0.415 | 0.589 | 2.14301 |
| 24.7 | 53.3 | | 39.5 | 115 | 2 | 1.4943 | 0.690 | 0.589 | 2.16562 |
| 24.7 | 57.6 | | 39.8 | 146 | 2 | 1.8971 | 0.890 | 0.589 | 2.13156 |
| 24.7 | 59.2 | | 40 | 160 | 2 | 2.0790 | 0.960 | 0.589 | 2.16562 |

## LINEAR REGRESSION RESULTS
(permeability Sand A)

e=void ratio
k=saturated permeability

k(e)=experimental result
k(lin)=predicted result

all=all readings
[k=23.527*(e^3/1+e)-.924]

first= first reading of permeameter test
[k=10.25*(e^3/1+e)+.75]

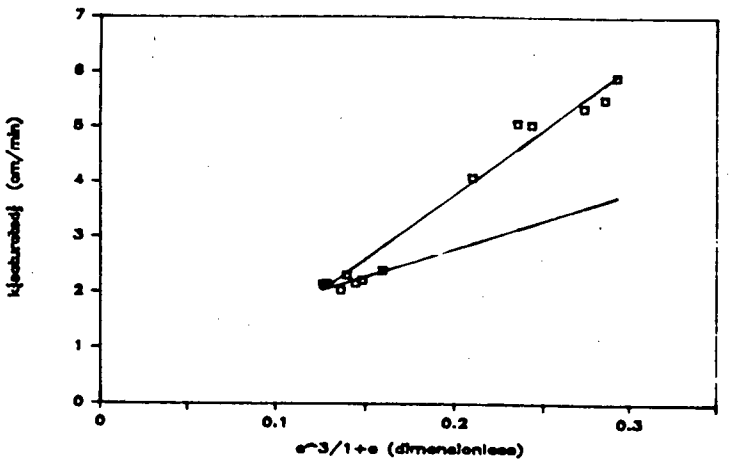


| e | e^3/1+e | k(e) (cm/min) | k(lin) all (cm/min) | k(lin) first (cm/min) |
|---|---|---|---|---|
| 0.585 | 0.1269 | 2.1464 | 2.0477 | 2.0447 |
| 0.589 | 0.1286 | 2.1579 | 2.1014 | 2.0681 |
| 0.602 | 0.1362 | 2.0452 | 2.2800 | 2.1459 |
| 0.608 | 0.1398 | 2.3159 | 2.3645 | 2.1827 |
| 0.616 | 0.1446 | 2.1666 | 2.4790 | 2.2326 |
| 0.622 | 0.1484 | 2.2204 | 2.5665 | 2.2707 |
| 0.640 | 0.1598 | 2.4015 | 2.8366 | 2.3884 |
| 0.711 | 0.2101 | 4.0935 | 4.0183 | 2.9032 |
| 0.753 | 0.2436 | 5.0484 | 4.8062 | 3.2465 |
| 0.749 | 0.2358 | 5.0730 | 4.6125 | 3.1621 |
| 0.788 | 0.2737 | 5.3467 | 5.5144 | 3.5550 |
| 0.801 | 0.2854 | 5.5103 | 5.7895 | 3.6749 |
| 0.809 | 0.2927 | 5.9167 | 5.9621 | 3.7501 |

RELATIVE PERMEABILITY CURVE DATA: SAND A

Mass of sand and tube = 2207.1 g
Mass of tube = 508.6 g
Dry mass of sand = 1698.5 g
Sg of sand = 2.68

Saturated permeability = 2.108 cm/min

Length of sand column = 190.5 cm
Diameter of column = 2.6 cm

Distance between tappings = 40 cm

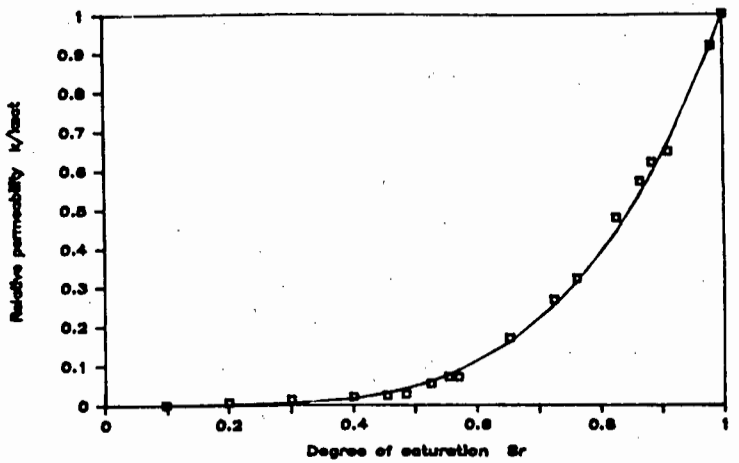


| Mass of system (g) | Q (cm^3) | TIME (min) | h1 (cm) | h2 (cm) | h3 (cm) | h4 (cm) | h5 (cm) | vel (cm/min) | i ( ) | k (cm/min) | k/ksat ( ) | Sr ( ) |
|---|---|---|---|---|---|---|---|---|---|---|---|---|
| 2577.2 | 55.3 | 6.00 | 4.525 | 4.243 | 3.901 | 3.446 | 3.089 | 1.736 | 0.898 | 1.934 | 0.917 | 0.980 |
| 2550.6 | 38.5 | 5.50 | 4.615 | 4.320 | 3.882 | 3.472 | 3.071 | 1.319 | 0.965 | 1.366 | 0.648 | 0.910 |
| 2540.7 | 92.4 | 15.00 | 4.490 | 4.165 | 3.830 | 3.418 | 3.070 | 1.160 | 0.888 | 1.307 | 0.620 | 0.883 |
| 2533.3 | 84.9 | 15.00 | 4.485 | 4.084 | 3.805 | 3.390 | 3.069 | 1.066 | 0.885 | 1.205 | 0.571 | 0.864 |
| 2518.4 | 72.0 | 15.25 | 4.475 | 4.035 | 3.789 | 3.330 | 3.066 | 0.889 | 0.881 | 1.010 | 0.479 | 0.824 |
| 2494.3 | 48.5 | 15.00 | 4.487 | 4.053 | 3.790 | 3.260 | 3.052 | 0.609 | 0.897 | 0.679 | 0.322 | 0.761 |
| 2480.3 | 39.9 | 15.00 | 4.464 | 4.035 | 3.792 | 3.233 | 3.048 | 0.501 | 0.885 | 0.566 | 0.268 | 0.724 |
| 2453.1 | 41.9 | 25.00 | 4.440 | 4.016 | 3.792 | 3.205 | 3.039 | 0.316 | 0.876 | 0.361 | 0.171 | 0.652 |
| 2422.3 | 28.6 | 40.50 | 4.455 | 4.041 | 3.719 | 3.193 | 3.031 | 0.133 | 0.890 | 0.149 | 0.071 | 0.570 |
| 2416.3 | 33.1 | 47.50 | 4.425 | 4.014 | 3.719 | 3.189 | 3.030 | 0.131 | 0.872 | 0.151 | 0.071 | 0.554 |
| 2405.3 | 40.9 | 77.50 | 4.406 | 3.993 | 3.612 | 3.170 | 3.025 | 0.099 | 0.863 | 0.115 | 0.055 | 0.525 |
| 2390.3 | 20.3 | 73.00 | 4.458 | 3.966 | 3.613 | 3.141 | 3.025 | 0.052 | 0.896 | 0.058 | 0.028 | 0.485 |
| 2378.7 | 13.6 | 82.00 | 3.998 | 3.972 | 3.757 | 3.157 | 3.025 | 0.031 | 0.608 | 0.051 | 0.024 | 0.454 |

RENTENTION CURVE DATA: SAND A

Mass of (dish +water) = 580.4
Mass of (dish+water+sand) = 1092.9
Mass of sand (dry) = 512.5

Diameter of dish = 15 cm
Height of sand in dish = 1.9 cm
Equilbrium height of water = 99.9 c

Volume of filters = 28.3 c

| Mass of isystem (g) | Height of water (cm) | Suction head (cm) | Sr ( ) |
|---|---|---|---|
| | 99.9 | 0.0 | 1.000 |
| 1202.2 | 97.4 | 2.5 | 0.944 |
| 1199.3 | 96.3 | 3.6 | 0.921 |
| 1196.0 | 95.1 | 4.8 | 0.895 |
| 1188.6 | 92.7 | 7.2 | 0.835 |
| 1187.1 | 92.1 | 7.8 | 0.823 |
| 1179.4 | 89.2 | 10.7 | 0.762 |
| 1178.3 | 88.7 | 11.2 | 0.754 |
| 1175.6 | 87.8 | 12.1 | 0.732 |
| 1165.8 | 86.4 | 13.5 | 0.650 |
| 1162.3 | 85.7 | 14.2 | 0.621 |
| 1152.4 | 84.4 | 15.5 | 0.538 |
| 1150.4 | 84.0 | 15.9 | 0.522 |
| 1145.0 | 83.4 | 16.5 | 0.476 |
| 1138.0 | 82.3 | 17.6 | 0.418 |
| 1133.5 | 81.6 | 18.3 | 0.381 |
| 1129.2 | 80.4 | 19.5 | 0.294 |
| 1120.2 | 79.9 | 20.0 | 0.269 |
| 1112.3 | 78.5 | 21.4 | 0.204 |
| 1109.5 | 78.1 | 21.8 | 0.180 |
| 1105.3 | 77.7 | 22.2 | 0.145 |
| 1101.9 | 76.9 | 23.0 | 0.117 |
| 1101.1 | 75.8 | 24.1 | 0.112 |
| 1099.0 | 73.4 | 26.5 | 0.098 |
| 1098.8 | 72.3 | 27.6 | 0.098 |

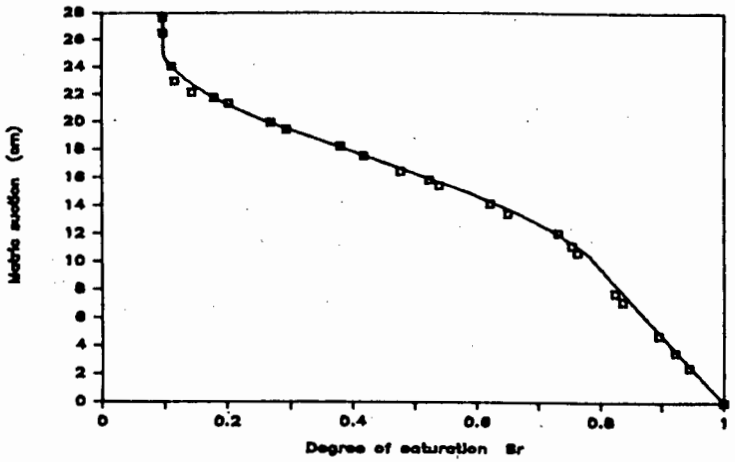

# DRY SIEVE ANALYSIS RESULT SHEET

SAND B

Initial mass of sand (Mi) = 1359.8 g
Final mass of sand (Mf) = 1359.9 g

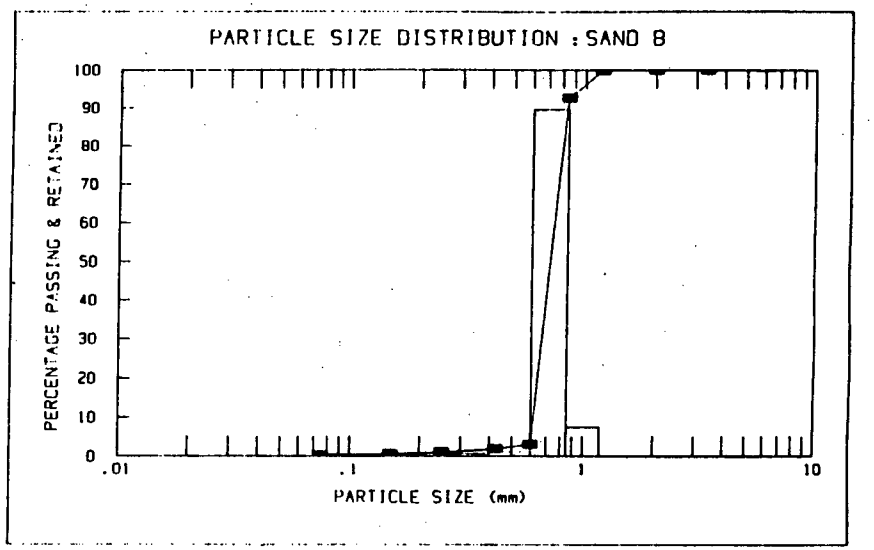


| Sieve size (mm) | Mass retained N (g) | Percentage retained R (%) | Cummulative % passing S (%) | Percentage passing P (%) |
|---|---|---|---|---|
| 3.350 | 0.0 | 0.000 | 0.000 | 100.000 |
| 2.000 | 0.0 | 0.000 | 0.000 | 100.000 |
| 1.180 | 0.1 | 0.007 | 0.007 | 99.993 |
| 0.850 | 102.0 | 7.501 | 7.508 | 92.492 |
| 0.600 | 1216.2 | 89.433 | 96.941 | 3.059 |
| 0.425 | 16.3 | 1.199 | 98.140 | 1.860 |
| 0.250 | 11.1 | 0.816 | 98.956 | 1.044 |
| 0.150 | 6.2 | 0.456 | 99.412 | 0.588 |
| 0.075 | 5.5 | 0.404 | 99.816 | 0.184 |
| pan | 2.5 | 0.184 | 100.000 | 0.000 |

Calculations

R=(N/Mf)*100
P=100-S

## SPECIFIC GRAVITY / RELATIVE DENSITY TEST

### SAND B

| | | | |
|---|---|---|---|
| Density of water | | | = 0.9982 g/cm^3 |
| Mass of dry bottle | | | = 35.212 g |
| Mass of sand and bottle | | | = 58.507 g |
| Mass of water, sand and bottle | | | = 99.534 g |
| Mass of water and bottle | | | = 84.980 g |
| Mass of dry sand | = | (58.507-35.212) | = 23.295 g |
| Mass of water added | = | (99.534-58.507) | = 41.027 g |
| Mass of water displaced by sand | = | (84.980-35.212)-41.027 | = 8.741 cm^3 |
| Volume of water added | = | (41.027/0.9982) | = 41.101 cm^3 |
| Volume of water displaced by sand | = | 8.741/0.9982 | = 7.757 cm^3 |
| Density of sand | = | (23.295/8.757) | = 2.660 g/cm^3 |
| Relative density of sand | = | (2.660/0.9982) | = 2.665 |

## PERMEABILITY TEST : SAND B

Dry mass of sand = 1682.5 g
Sg of sand = 2.67

Diameter of permeameter = 38.48 cm^2
Distance between tappings = 20 cm

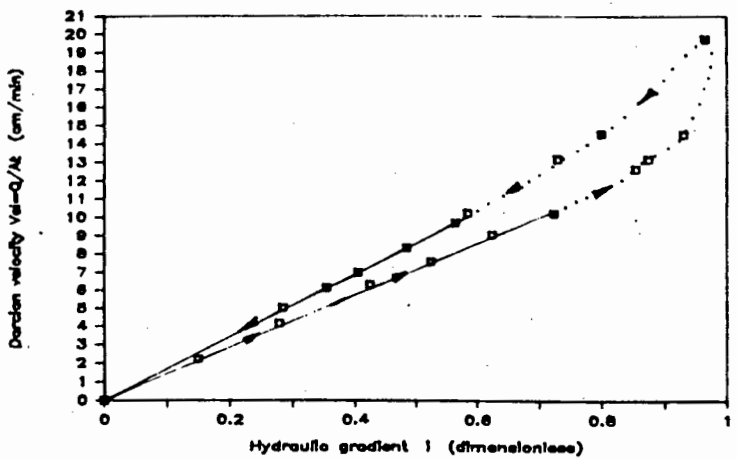


| Height of sand (cm) | h1 (cm) | h3 (cm) | Q (cm^3) | time (sec) | vel (cm/min) | i ( ) | e ( ) | k (cm/min) |
|---|---|---|---|---|---|---|---|---|
| 26.7 | 42.1 | 39.1 | 129 | 90 | 2.235 | 0.150 | 0.630 | 14.900 |
| 26.7 | 28.9 | 23.3 | 242 | 90 | 4.193 | 0.280 | 0.630 | 14.974 |
| 26.7 | 32.8 | 24.3 | 365 | 90 | 6.324 | 0.425 | 0.630 | 14.879 |
| 26.7 | 35.4 | 24.9 | 292 | 60 | 7.588 | 0.525 | 0.630 | 14.454 |
| 26.7 | 37.7 | 25.2 | 349 | 60 | 9.070 | 0.625 | 0.630 | 14.511 |
| 26.8 | 39.8 | 25.3 | 263 | 40 | 10.252 | 0.725 | 0.637 | 14.141 |
| 27.1 | 42.9 | 25.8 | 244 | 30 | 12.682 | 0.855 | 0.655 | 14.833 |
| 27.2 | 43.4 | 25.9 | 254 | 30 | 13.202 | 0.875 | 0.661 | 15.088 |
| 27.3 | 44.8 | 26.2 | 233 | 25 | 14.532 | 0.930 | 0.667 | 15.626 |
| 28.3 | 47.2 | 27.9 | 316 | 25 | 19.709 | 0.965 | 0.728 | 20.424 |
| 27.9 | 41.8 | 25.8 | 280 | 30 | 14.553 | 0.800 | 0.704 | 18.191 |
| 27.9 | 40.0 | 25.4 | 254 | 30 | 13.202 | 0.730 | 0.704 | 18.084 |
| 27.7 | 35.8 | 24.1 | 296 | 45 | 10.256 | 0.585 | 0.691 | 17.532 |
| 27.7 | 35.2 | 23.9 | 280 | 45 | 9.702 | 0.565 | 0.691 | 17.172 |
| 27.7 | 33.2 | 23.5 | 240 | 45 | 8.316 | 0.485 | 0.691 | 17.146 |
| 27.7 | 30.9 | 22.8 | 251 | 56 | 6.989 | 0.405 | 0.691 | 17.256 |
| 27.7 | 29.7 | 22.6 | 235 | 60 | 6.107 | 0.355 | 0.691 | 17.203 |
| 27.7 | 27.6 | 21.9 | 225 | 70 | 5.012 | 0.285 | 0.691 | 17.586 |

## PERMEABILITY TEST :Sand B

Dry mass of sand = 1611.8 g
Sg of sand = 2.67

Diameter of permeameter = 7 cm
Distance between tappings = 20 cm

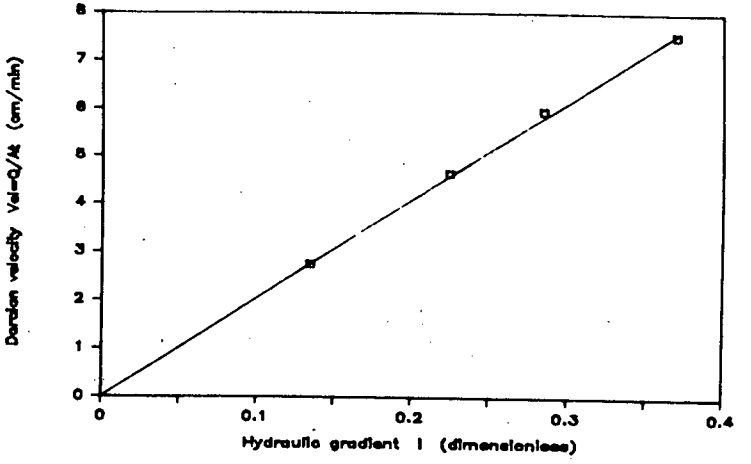


| Height of sand (cm) | h1 (cm) | h3 (cm) | Q (cm^3) | time (min) | Vel (cm/min) | i ( ) | e ( ) | k (cm/min) |
|---|---|---|---|---|---|---|---|---|
| 27.2 | 23.9 | 21.2 | 159 | 1.50 | 2.7547 | 0.135 | 0.734 | 20.4050 |
| 27.2 | 26.5 | 22 | 179 | 1.00 | 4.6518 | 0.225 | 0.734 | 20.6745 |
| 27.2 | 28.1 | 22.4 | 230 | 1.00 | 5.9771 | 0.285 | 0.734 | 20.9723 |
| 27.2 | 30.5 | 23.1 | 290 | 1.00 | 7.5364 | 0.370 | 0.734 | 20.3686 |

## PERMEABILITY TEST :Sand B

Dry mass of sand = 1611.8 g
Sg of sand = 2.67

Diameter of permeameter = 7 cm
Distance between tappings = 20 cm

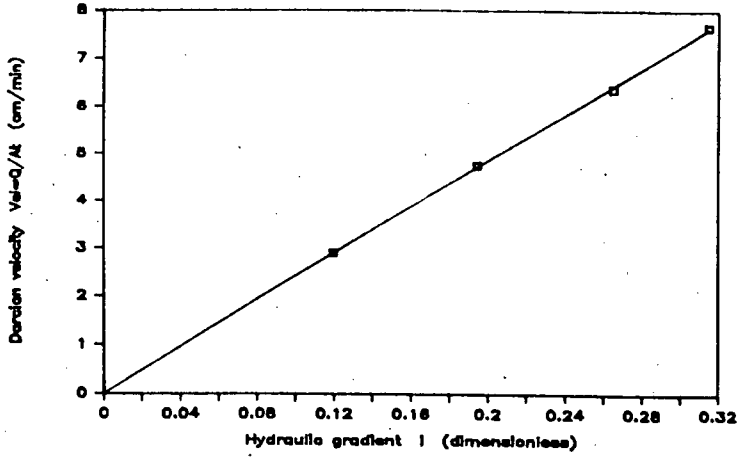


| Height of sand (cm) | h1 (cm) | h3 (cm) | Q (cm^3) | time (min) | Vel (cm/min) | i ( ) | e ( ) | k (cm/min) |
|---|---|---|---|---|---|---|---|---|
| 27.8 | 23.7 | 21.3 | 140 | 1.25 | 2.9106 | 0.120 | 0.772 | 24.2550 |
| 27.8 | 25.9 | 22 | 183 | 1.00 | 4.7557 | 0.195 | 0.772 | 24.3882 |
| 27.8 | 27.9 | 22.6 | 245 | 1.00 | 6.3669 | 0.265 | 0.772 | 24.0262 |
| 27.8 | 29.5 | 23.2 | 295 | 1.00 | 7.6663 | 0.315 | 0.772 | 24.3375 |

## PERMEABILITY TEST :Sand B

Dry mass of sand = 1600.5 g
Sg of sand = 2.67

Diameter of permeameter = 7 cm
Distance between tappings = 20 cm

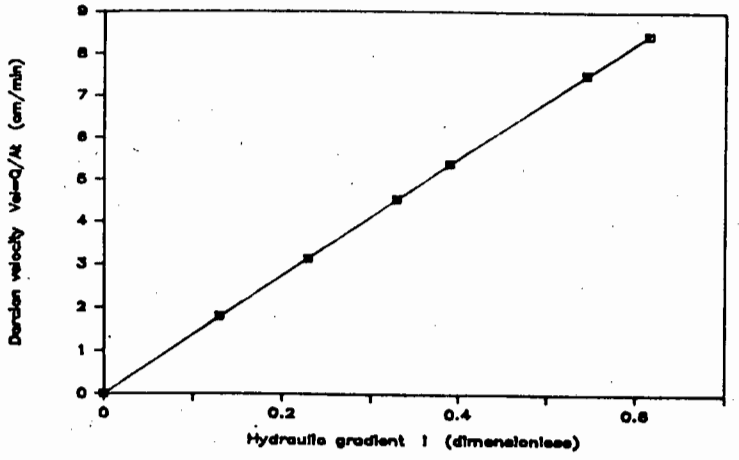


| Height of sand (cm) | h1 (cm) | h3 (cm) | Q (cm^3) | time (min) | Vel (cm/min) | i ( ) | e ( ) | k (cm/min) |
|---|---|---|---|---|---|---|---|---|
| 26.2 | 41.1 | 38.5 | 139 | 2.00 | 1.8061 | 0.130 | 0.600 | 13.893 |
| 26.2 | 43.1 | 38.5 | 242 | 2.00 | 3.1445 | 0.230 | 0.600 | 13.672 |
| 26.2 | 45.1 | 38.5 | 175 | 1.00 | 4.5478 | 0.330 | 0.600 | 13.781 |
| 26.2 | 46.3 | 38.5 | 207 | 1.00 | 5.3794 | 0.390 | 0.600 | 13.793 |
| 26.2 | 35.3 | 24.4 | 289 | 1.00 | 7.5104 | 0.545 | 0.600 | 13.781 |
| 26.2 | 37.1 | 24.8 | 325 | 1.00 | 8.4459 | 0.615 | 0.600 | 13.793 |

## PERMEABILITY TEST :Sand B

Dry mass of sand = 1682.5 g
Sg of sand = 2.67

Diameter of permeameter = 7 cm
Distance between tappings = 20 cm

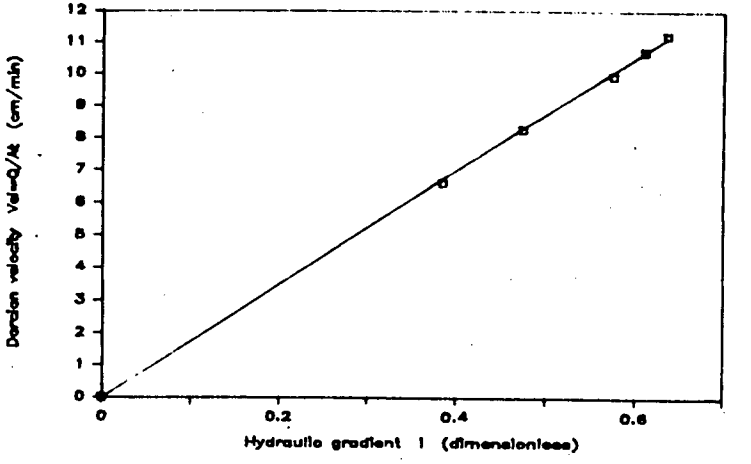


| Height of sand (cm) | h1 (cm) | h3 (cm) | Q (cm^3) | time (min) | Vel (cm/min) | i ( ) | e ( ) | k (cm/min) |
|---|---|---|---|---|---|---|---|---|
| 27.5 | 36.3 | 23.6 | 324 | 0.75 | 11.2266 | 0.635 | 0.679 | 17.6797 |
| 27.5 | 35.6 | 23.4 | 309 | 0.75 | 10.7069 | 0.610 | 0.679 | 17.5522 |
| 27.5 | 34.6 | 23.1 | 287 | 0.75 | 9.9446 | 0.575 | 0.679 | 17.2948 |
| 27.5 | 32 | 22.5 | 239 | 0.75 | 8.2814 | 0.475 | 0.679 | 17.4344 |
| 27.5 | 29.5 | 21.8 | 191 | 0.75 | 6.6182 | 0.385 | 0.679 | 17.1900 |

LINEAR REGREESSION RESULTS
(permeability Sand 8)

e=void ratio
k=saturated permeability

k(e)=experimental result
k(lin)=predicted result

k(lin)=96.824*(e^3/1+e)-.476

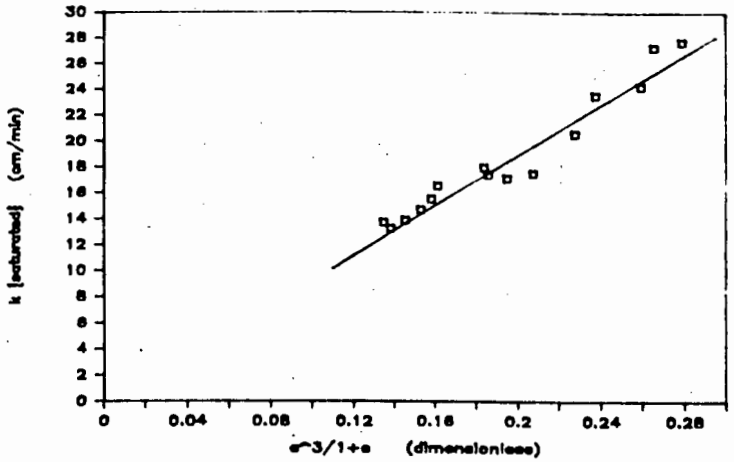


| e ( ) | e^3/1+e ( ) | k(e) (cm/min) | k(lin) (cm/min) |
|---|---|---|---|
| 0.6 | 0.1350 | 13.7756 | 12.5952 |
| 0.606 | 0.1386 | 13.2790 | 12.9410 |
| 0.618 | 0.1459 | 13.9305 | 13.6484 |
| 0.63 | 0.1534 | 14.7436 | 14.3771 |
| 0.638 | 0.1585 | 15.5585 | 14.8748 |
| 0.643 | 0.1618 | 16.5601 | 15.1907 |
| 0.676 | 0.1843 | 17.9980 | 17.3703 |
| 0.679 | 0.1864 | 17.4303 | 17.5767 |
| 0.691 | 0.1951 | 17.1510 | 18.4158 |
| 0.708 | 0.2078 | 17.5531 | 19.6425 |
| 0.734 | 0.2281 | 20.6051 | 21.6052 |
| 0.746 | 0.2378 | 23.5499 | 22.5466 |
| 0.772 | 0.2596 | 24.2518 | 24.6643 |
| 0.779 | 0.2657 | 27.2776 | 25.2528 |
| 0.794 | 0.2790 | 27.7086 | 26.5401 |

RELATIVE PERMEABILITY CURVE DATA: SAND B

Mass of sand and tube = 2236.5 g
Dry mass of sand = 1726.9 g
Sg of sand = 2.67

Saturated permeability = 11.104 cm/min

Length of sand column = 191.0 cm
Diameter of column = 2.6 cm

Distance between tappings = 40 cm

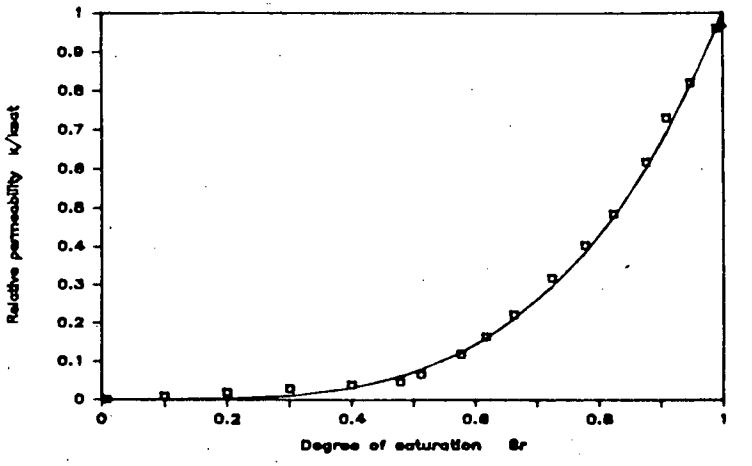


| Mass of System (g) | Q (cm^3) | Time (min) | h1 (m) | h2 (m) | h3 (m) | h4 (m) | h5 (m) | vel (cm/min) | | k (cm/min) | k/ksat ( ) | Sr ( ) |
|---|---|---|---|---|---|---|---|---|---|---|---|---|
| 2600.0 | 149.8 | 2.75 | 4.649 | 4.324 | | 3.500 | 3.107 | 10.260 | 0.964 | 10.646 | 0.959 | 0.990 |
| 2584.4 | 175.6 | 3.75 | 4.656 | 4.197 | 3.818 | 3.450 | 3.107 | 8.820 | 0.968 | 9.111 | 0.820 | 0.947 |
| 2570.1 | 144.8 | 3.50 | 4.642 | 4.203 | 3.804 | 3.339 | 3.107 | 7.793 | 0.959 | 8.123 | 0.732 | 0.908 |
| 2557.7 | 160.4 | 4.50 | 4.647 | 4.221 | 3.865 | 3.460 | 3.081 | 6.714 | 0.979 | 6.860 | 0.618 | 0.875 |
| 2538.5 | 127.2 | 4.50 | 4.650 | 4.230 | 3.857 | 3.425 | 3.068 | 5.324 | 0.989 | 5.385 | 0.485 | 0.822 |
| 2521.8 | 105.3 | 4.50 | 4.637 | 4.217 | 3.811 | 3.394 | 3.062 | 4.408 | 0.984 | 4.478 | 0.403 | 0.777 |
| 2502.5 | 91.5 | 5.00 | 4.620 | 4.189 | 3.797 | 3.394 | 3.054 | 3.447 | 0.979 | 3.522 | 0.317 | 0.724 |
| 2480.0 | 76.8 | 6.00 | 4.611 | 4.189 | 3.790 | 3.385 | 3.044 | 2.411 | 0.979 | 2.462 | 0.222 | 0.663 |
| 2463.2 | 66.5 | 7.00 | 4.609 | 4.188 | 3.785 | 3.380 | 3.039 | 1.789 | 0.981 | 1.824 | 0.164 | 0.617 |
| 2448.4 | 61.9 | 9.00 | 4.607 | 4.186 | 3.783 | 3.380 | 3.043 | 1.295 | 0.978 | 1.325 | 0.119 | 0.577 |
| 2424.4 | 62.8 | 16.50 | 4.603 | 4.184 | 3.778 | 3.375 | 3.031 | 0.717 | 0.982 | 0.730 | 0.066 | 0.512 |
| 2412.0 | 53.9 | 20.00 | 4.601 | 4.184 | 3.776 | 3.375 | 3.029 | 0.508 | 0.983 | 0.517 | 0.047 | 0.478 |

RETENTION CURVE DATA: SAND B

Mass of (dish+water) = 550.0 g
Mass of (dish+water+sand) = 1137.6 g
Mass of (sand) = 587.6 g
Sg of sand = 2.67

Diameter of dish = 15 cm
Height of sand in dish = 2.15 cm
Equilibrium height of water = 97.4 cm

Volume of filters = 29.8 cm^3

| Mass of System (g) | Height of Water (cm) | Suction Head (cm) | Sr ( ) |
|---|---|---|---|
| | | 0.0 | 1 |
| 1259.1 | 96.1 | 3.2 | 0.940 |
| 1254.7 | 95.5 | 3.8 | 0.907 |
| 1252.6 | 94.7 | 4.6 | 0.892 |
| 1244.0 | 93.8 | 5.5 | 0.827 |
| 1242.9 | 93.6 | 5.7 | 0.819 |
| 1228.8 | 92.1 | 7.2 | 0.713 |
| 1227.5 | 91.8 | 7.5 | 0.703 |
| 1222.7 | 91.4 | 7.9 | 0.667 |
| 1215.9 | 90.7 | 8.6 | 0.616 |
| 1210.4 | 90.4 | 8.9 | 0.574 |
| 1203.6 | 89.9 | 9.4 | 0.522 |
| 1200.5 | 89.7 | 9.6 | 0.499 |
| 1195.4 | 89.6 | 9.7 | 0.460 |
| 1188.2 | 89.1 | 10.2 | 0.405 |
| 1186.6 | 88.8 | 10.5 | 0.393 |
| 1170.8 | 88.3 | 11.0 | 0.272 |
| 1167.4 | 88.1 | 11.2 | 0.246 |
| 1154.7 | 87.4 | 11.9 | 0.150 |
| 1149.6 | 87.1 | 12.2 | 0.111 |
| 1142.2 | 86.6 | 12.7 | 0.055 |
| 1137.8 | 85.9 | 13.4 | 0.022 |
| 1135.9 | 85.3 | 14.0 | 0.008 |
| 1135.5 | 83.8 | 15.5 | 0.008 |

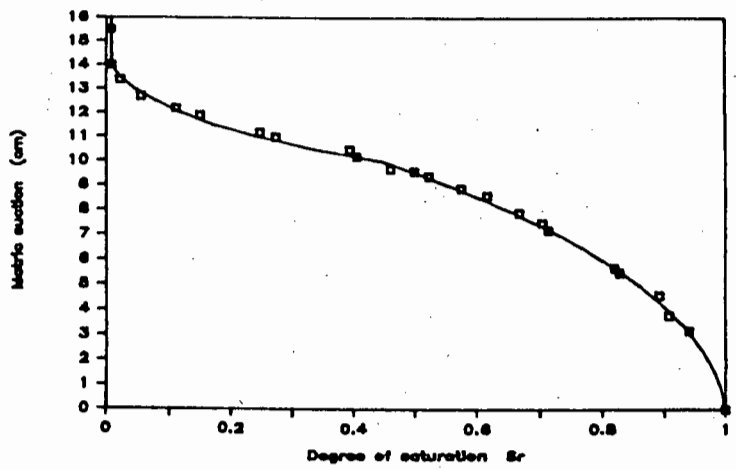

## DRY SIEVE ANALYSIS RESULT SHEET

SAND C

Initial mass of sand (Mi) = 1093.3 g
Final mass of sand (Mf) = 1093.2 g

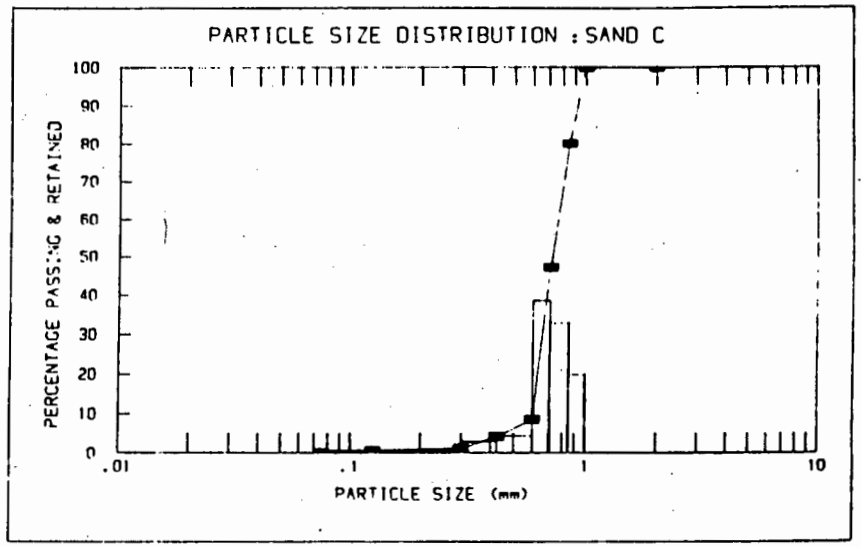


| Sieve size (mm) | Mass retained N (g) | Percentage retained P (%) | Cummulative % passing S (%) | Percentage passing p (%) |
|---|---|---|---|---|
| 2.000 | 1.2 | 0.110 | 0.110 | 99.890 |
| 1.000 | 220.8 | 20.198 | 20.307 | 79.693 |
| 0.850 | 376.3 | 34.422 | 54.729 | 45.271 |
| 0.710 | 424.2 | 38.804 | 93.533 | 6.467 |
| 0.600 | 44.5 | 4.071 | 97.603 | 2.397 |
| 0.425 | 23.9 | 2.186 | 99.790 | 0.210 |
| 0.300 | 1.9 | 0.174 | 99.963 | 0.037 |
| 0.125 | 0.2 | 0.018 | 99.982 | 0.018 |
| 0.075 | 0.0 | 0.000 | 99.982 | 0.018 |
| pan | 0.0 | 0.000 | 99.982 | 0.018 |

Calculations

R=(N/Mf)*100
P=100-S

# SOIL MOISTURE CHARACTERISTICS

## SAND C

1. Retention curve data

| matric suction (cm) | effective saturation Se |
|---|---|
| 17.0 | 0.00 |
| 13.0 | 0.05 |
| 11.5 | 0.18 |
| 9.0 | 0.62 |
| 6.0 | 0.88 |
| 4.0 | 1.00 |
| 0.0 | 1.00 |

air entry suction = 4 cm

Se = (Sr-Sro)/(1-Sro)

Sro=.15

2. Saturated coefficient of permeability

ksat=4.44*(e^3/1+e)-.04 cm/s

3. Relative permeability curve data

kr = (Se)^3

4. Specific gravity / relative density

Sg=2.64

# APPENDIX C

## EQUATIONS AND ELEMENT MATRICES USED IN THE FORMULATION OF THE FLOW EQUATION

## 1. THE COMBINED SATURATED-UNSATURATED FLOW EQUATION FOR ISOTHERMAL FLOW IN HOMOGENEOUS SOILS

### i. 1-D vertical

$$\frac{\partial}{\partial z}\left[ k_{sat}\, kr\, \left(\frac{\partial \Psi}{\partial z} + 1\right)\right] = \eta \frac{\partial \Psi}{\partial t}$$

### ii. 2-D plane and axisymmetric

$$\frac{1}{r}\frac{\partial}{\partial x}\left[ r\, k_{sat}\, kr \frac{\partial \Psi}{\partial x}\right] + \frac{\partial}{\partial z}\left[ k_{sat}\, kr\, \left(\frac{\partial \Psi}{\partial z} + 1\right)\right] = \eta \frac{\partial \Psi}{\partial t}$$

where $r = 1$ for 2-D plane
$r = x$ for axisymmetric

## 2. ISOPARAMETRIC INTERPOLATION FUNCTIONS

### i. 1-D (two noded linear elements)

$$N_1 = \frac{1}{2}(1 - \xi)$$
$$N_2 = \frac{1}{2}(1 + \xi)$$

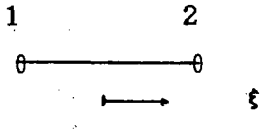


### ii. 2-D plane and axisymmetric (four noded rectangular elements)

$$N_1 = \frac{1}{4}(1 - \xi)(1 - \varsigma)$$
$$N_2 = \frac{1}{4}(1 + \xi)(1 - \varsigma)$$
$$N_3 = \frac{1}{4}(1 + \xi)(1 + \varsigma)$$
$$N_4 = \frac{1}{4}(1 - \xi)(1 + \varsigma)$$

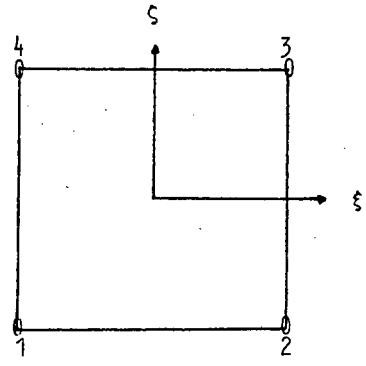

## 3. EQUATIONS FOR THE ELEMENT MATRICES

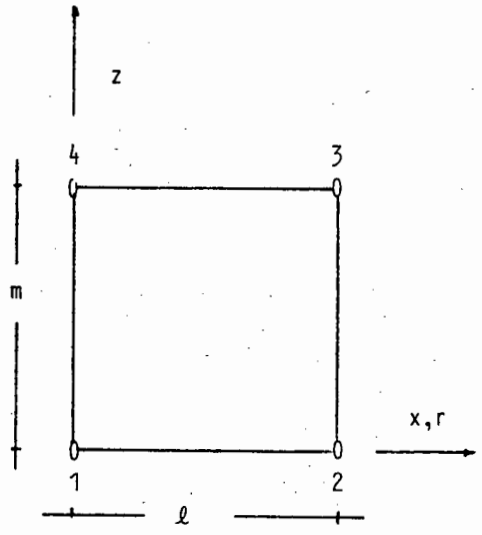


i. 1-D

$$[A]^e = \langle k_{sat}\, kr \rangle \frac{1}{\ell} [A^z]^e$$

$$[B]^e = \langle \eta \rangle \frac{\ell}{6} [B^z]^e$$

$$\{F\}^e = -\langle k_{sat}\, kr \rangle \{F^z\}^e$$

where $[A^z]^e$, $[B^z]^e$ and $\{F^z\}^e$ are the influence coefficient matrices and vector.

ii. 2-D plane and axisymmetric

$$[A]^e = \left(\frac{m}{\ell}\right) \langle r\, k_{sat}\, kr \rangle [A^{xx}]^e + \frac{\ell}{m} \langle r\, k_{sat}\, kr \rangle [A^{zz}]^e$$

$$[B]^e = \frac{m\ell}{4} \langle r\, \eta \rangle [M]^e$$

$$\{F\}^e = -\frac{\ell}{2} \langle k_{sat}\, kr \rangle \{F^z\}^e$$

where $\langle\ \rangle$ indicates the centroidal value

$r = 1$ for 2-D plane (unit thickness)

$r \equiv x$ for axisymmetric (unit radian)

$[A^{xx}]^e$, $[A^{zz}]^e$, $[M]^e$, $\{F^z\}^e$ are the influence coefficient matrices and vector.

## 4. THE INFLUENCE COEFFICIENT MATRICES

i. 1-D

$$[A^z]^e = \begin{bmatrix} 1 & -1 \\ -1 & 1 \end{bmatrix}$$

$$[B^z]^e = \begin{bmatrix} 2 & 1 \\ 1 & 2 \end{bmatrix}$$

$$\{F^z\}^e = \begin{Bmatrix} -1 \\ 1 \end{Bmatrix}$$

3. 2-D plane and axisymmetric

$$[A^{xx}]^e = \frac{1}{6} \begin{bmatrix} 2 & -2 & -1 & 1 \\ -2 & 2 & 1 & -1 \\ -1 & 1 & 2 & -2 \\ 1 & -1 & -2 & 2 \end{bmatrix}$$

$$[A^{zz}]^e = \frac{1}{6} \begin{bmatrix} 2 & 1 & -1 & 2 \\ 1 & 2 & -2 & -1 \\ -1 & 2 & 2 & 1 \\ -2 & -1 & 1 & 2 \end{bmatrix}$$

$$[M]^e = \frac{1}{9} \begin{bmatrix} 4 & 2 & 1 & 2 \\ 2 & 4 & 2 & 1 \\ 1 & 2 & 4 & 2 \\ 2 & 1 & 2 & 4 \end{bmatrix}$$

$$\{F^{zz}\}^e = \begin{Bmatrix} -1 \\ -1 \\ 1 \\ 1 \end{Bmatrix}$$

## 5. THE BOUNDARY FLUX TERM CORRESPONDING TO A SEEPAGE FACE ON SEGMENT 2-3

### i. 2-D plane and axisymmetric

$$-\frac{m}{2} \langle r \rangle \begin{Bmatrix} 0 \\ V_2 \\ V_3 \\ 0 \end{Bmatrix}$$

where $r = 1$ for 2-D plane
(for unit thickness or unit radian).

# APPENDIX D

## RESULTS FROM THE ONE-DIMENSIONAL COLUMN DRAINAGE PROBLEM

## DRAINAGE EXPERIMENT: SAND A (n=.399)

Dry mass of sand = 1577.7 g
Sg of sand = 2.68

Length of sand column = 184.5 cm
Diameter of column = 2.6 cm

| Time (min) | Mass of system (g) | Vol. water drained (cm^3) | Outflow velocity (cm/min) | Cumulated outflow (cm^3) |
|---|---|---|---|---|
| 0.0 | 1944.5 | | | 0.0 |
| 1.0 | 1934.4 | 10.1 | 1.902 | 10.1 |
| 2.0 | 1924.8 | 9.6 | 1.808 | 19.7 |
| 3.0 | 1915.5 | 9.3 | 1.752 | 29.0 |
| 4.0 | 1906.4 | 9.1 | 1.714 | 38.1 |
| 5.0 | 1897.5 | 8.9 | 1.676 | 47.0 |
| 6.0 | 1888.9 | 8.6 | 1.620 | 55.6 |
| 7.0 | 1880.6 | 8.3 | 1.563 | 63.9 |
| 8.0 | 1872.7 | 7.9 | 1.488 | 71.8 |
| 9.0 | 1865.2 | 7.5 | 1.413 | 79.3 |
| 10.0 | 1857.8 | 7.4 | 1.394 | 86.7 |
| 11.0 | 1850.7 | 7.1 | 1.337 | 93.8 |
| 12.0 | 1844.0 | 6.7 | 1.262 | 100.5 |
| 13.0 | 1837.5 | 6.5 | 1.224 | 107.0 |
| 14.0 | 1831.4 | 6.1 | 1.149 | 113.1 |
| 15.0 | 1825.5 | 5.9 | 1.111 | 119.0 |
| 16.0 | 1820.2 | 5.3 | 0.998 | 124.3 |
| 17.0 | 1815.2 | 5.0 | 0.942 | 129.3 |
| 18.0 | 1810.7 | 4.5 | 0.848 | 133.8 |
| 19.0 | 1806.5 | 4.2 | 0.791 | 138.0 |
| 20.0 | 1802.7 | 3.8 | 0.716 | 141.8 |
| 21.0 | 1799.1 | 3.6 | 0.678 | 145.4 |
| 22.0 | 1795.8 | 3.3 | 0.622 | 148.7 |
| 23.0 | 1792.8 | 3.0 | 0.565 | 151.7 |
| 24.0 | 1789.9 | 2.9 | 0.546 | 154.6 |
| 25.0 | 1787.1 | 2.8 | 0.527 | 157.4 |
| 26.0 | 1784.5 | 2.6 | 0.490 | 160.0 |
| 27.0 | 1782.1 | 2.4 | 0.452 | 162.4 |
| 28.0 | 1779.8 | 2.3 | 0.433 | 164.7 |
| 29.0 | 1777.7 | 2.1 | 0.396 | 166.8 |
| 30.0 | 1775.7 | 2.0 | 0.377 | 168.8 |
| 32.0 | 1772.1 | 3.6 | 0.339 | 172.4 |
| 34.0 | 1768.8 | 3.3 | 0.311 | 175.7 |
| 36.0 | 1765.9 | 2.9 | 0.273 | 178.6 |
| 38.0 | 1763.3 | 2.6 | 0.245 | 181.2 |
| 40.0 | 1761.0 | 2.3 | 0.217 | 183.5 |
| 42.0 | 1758.8 | 2.2 | 0.207 | 185.7 |
| 44.0 | 1756.9 | 1.9 | 0.179 | 187.6 |
| 46.0 | 1755.1 | 1.8 | 0.170 | 189.4 |
| 48.0 | 1753.4 | 1.7 | 0.160 | 191.1 |
| 50.0 | 1751.9 | 1.5 | 0.141 | 192.6 |
| 55.0 | 1748.4 | 3.5 | 0.132 | 196.1 |
| 60.0 | 1745.5 | 2.9 | 0.109 | 199.0 |

## DRAINAGE EXPERIMENT: SAND B (n=.361)

Dry mass of sand = 1679.2 g
Sg of sand = 2.67

Length of sand column = 185.4 cm
Diameter of column = 2.6 cm

| Time (min) | Mass of column (g) | Vol. water drained (cm^3) | Outflow velocity (cm/min) | Cumulated outflow (cm^3) |
|---|---|---|---|---|
| 0.0 | 2034.4 | | | 0.0 |
| 0.3 | 2016.5 | 17.9 | 10.116 | 17.9 |
| 0.7 | 1999.7 | 16.8 | 9.494 | 34.7 |
| 1.0 | 1985.5 | 14.2 | 8.023 | 48.9 |
| 1.5 | 1965.0 | 20.5 | 7.723 | 69.4 |
| 2.0 | 1945.8 | 19.2 | 7.233 | 88.6 |
| 2.5 | 1926.6 | 19.2 | 7.233 | 107.8 |
| 3.0 | 1910.8 | 15.8 | 5.952 | 123.6 |
| 3.5 | 1895.6 | 15.2 | 5.726 | 138.8 |
| 4.0 | 1882.6 | 13.0 | 4.897 | 151.8 |
| 4.5 | 1871.4 | 11.2 | 4.219 | 163.0 |
| 5.0 | 1862.4 | 9.0 | 3.390 | 172.0 |
| 5.5 | 1855.5 | 6.9 | 2.599 | 178.9 |
| 6.0 | 1850.2 | 5.3 | 1.997 | 184.2 |
| 6.5 | 1846.0 | 4.2 | 1.582 | 188.4 |
| 7.0 | 1842.6 | 3.4 | 1.281 | 191.8 |
| 8.0 | 1837.0 | 5.6 | 1.055 | 197.4 |
| 9.0 | 1832.5 | 4.5 | 0.848 | 201.9 |
| 10.0 | 1828.6 | 3.9 | 0.735 | 205.8 |
| 11.0 | 1825.3 | 3.3 | 0.622 | 209.1 |
| 12.0 | 1822.4 | 2.9 | 0.546 | 212.0 |
| 13.0 | 1819.5 | 2.9 | 0.546 | 214.9 |
| 14.0 | 1817.2 | 2.3 | 0.433 | 217.2 |
| 15.0 | 1815.0 | 2.2 | 0.414 | 219.4 |
| 16.0 | 1812.8 | 2.2 | 0.414 | 221.6 |
| 17.0 | 1810.9 | 1.9 | 0.358 | 223.5 |
| 18.0 | 1809.3 | 1.6 | 0.301 | 225.1 |
| 19.0 | 1807.7 | 1.6 | 0.301 | 226.7 |
| 20.0 | 1806.1 | 1.6 | 0.301 | 228.3 |
| 22.0 | 1803.5 | 2.6 | 0.245 | 230.9 |
| 24.0 | 1801.0 | 2.5 | 0.235 | 233.4 |
| 26.0 | 1798.8 | 2.2 | 0.207 | 235.6 |
| 28.0 | 1796.9 | 1.9 | 0.179 | 237.5 |
| 30.0 | 1795.0 | 1.9 | 0.179 | 239.4 |
| 32.5 | 1793.1 | 1.9 | 0.143 | 241.3 |
| 35.0 | 1791.3 | 1.8 | 0.136 | 243.1 |
| 40.0 | 1787.8 | 3.5 | 0.132 | 246.6 |
| 45.0 | 1785.0 | 2.8 | 0.105 | 249.4 |
| 50.0 | 1782.8 | 2.2 | 0.083 | 251.6 |
| 55.0 | 1780.6 | 2.2 | 0.083 | 253.8 |
| 60.0 | 1778.5 | 2.1 | 0.079 | 255.9 |

THE INCLINED TUBE PROCEDURE

The rough iterative method of analysis (mentioned in Chapter 6) used to determine the soil-moisture, pressure head and velocity profiles of the sand column, using the "inclined tube" procedure, will now be explained using a column divided into two segments.

1. The first step is to approximate the pressure heads at the nodes of the segments. The centroidal pressure head value is then approximated by :

$$\bar{\psi} = \frac{\psi_i + \psi_{i+1}}{2}$$

2. The centroidal pressure heads, determined using the above equation, are then used to determine the degree of saturation of the segments from the retention curve. The degree of saturation is, in turn, used to determine the relative permeability of the segment from the relative permeability curve. The velocity profile, for the column, may now be determined from the above information.

3. The validity of the approximated nodal pressure heads are now checked.

   3.1 The first check is to determine if the sum of the masses of water per segment (determined from the degrees of saturation) equals the total remaining mass of the water in the column (determined when the tube is in the vertical position).

   3.2 The distribution of the above masses of water are now checked by taking moments about one end of the tube. By taking moments we check that :

$$\frac{M_{w1} \times \ell_1 + M_{w2} \times \ell_2 + M_s \times \ell_s}{\ell_t} = R_1$$

   where $R_1$ is determined when the tube is in the inclined position.

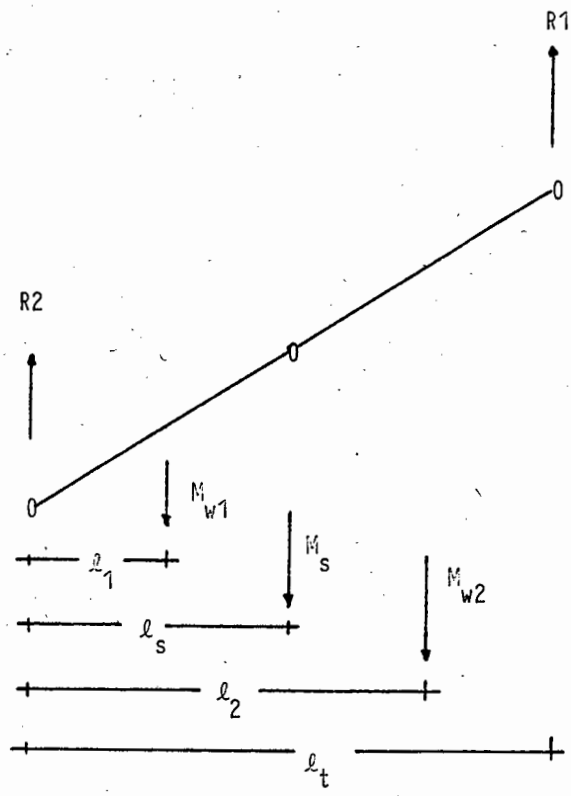


3.3 The velocity at the outlet of the column is the final means by which the nodal pressure heads are checked.

4. An iterative (trial and error) procedure is used (varying the pressure heads) until the above three constraints are met. Once the constraints are met the final soil-moisture, pressure head and velocity profiles can be determined.

It should be noted that more accurate results are obtained by dividing the column into a larger number of segments. The analysis does, however, then tend to become more clumsy.

# APPENDIX E

## RESULTS FROM THE TWO-DIMENSIONAL PLANE DRAINAGE PROBLEM

INPUT DATA FOR THE 2-D PLANE DRAINAGE EXPERIMENT PERFORMED BY WARDLE

1. Dimensions of the flow domain :

   Length = 271,78 cm
   Depth = 40,13 cm
   Width = 31,24 cm

2. The sand had a void ratio of e = 0,574 which gave the flow domain a saturated coefficient of permeability of 28,2 cm/min.

3. The initial height of the water table was 38,1 above the base of the seepage tank. (Initial conditions were determined accordingly).

4. The drainage problem was modelled using a 40 x 15 equi-sized finite element mesh and a time increment of 0,1 min.

## Phreatic surface at 5min

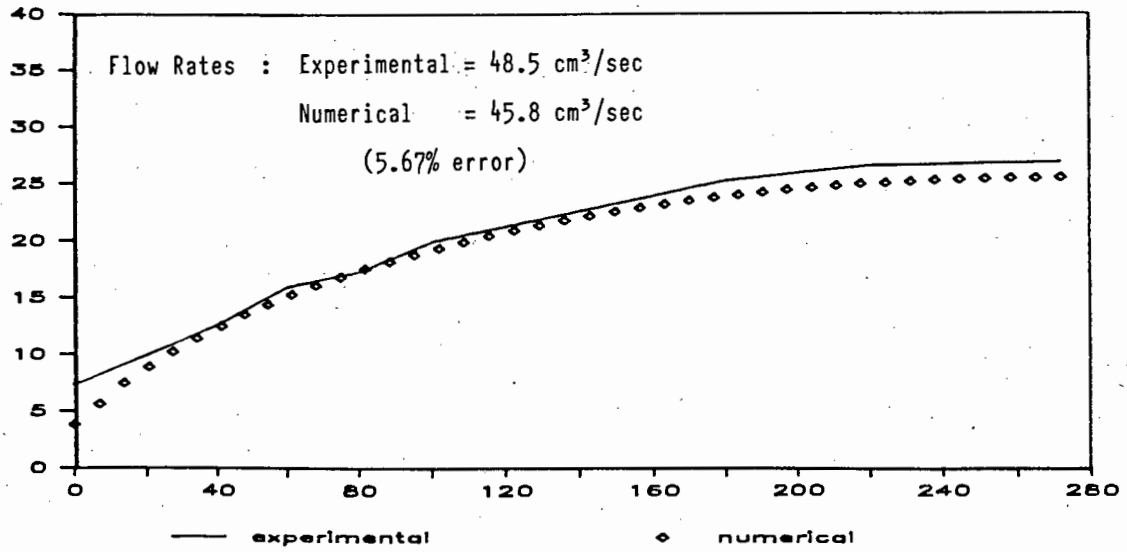


## Phreatic surface at 15 min

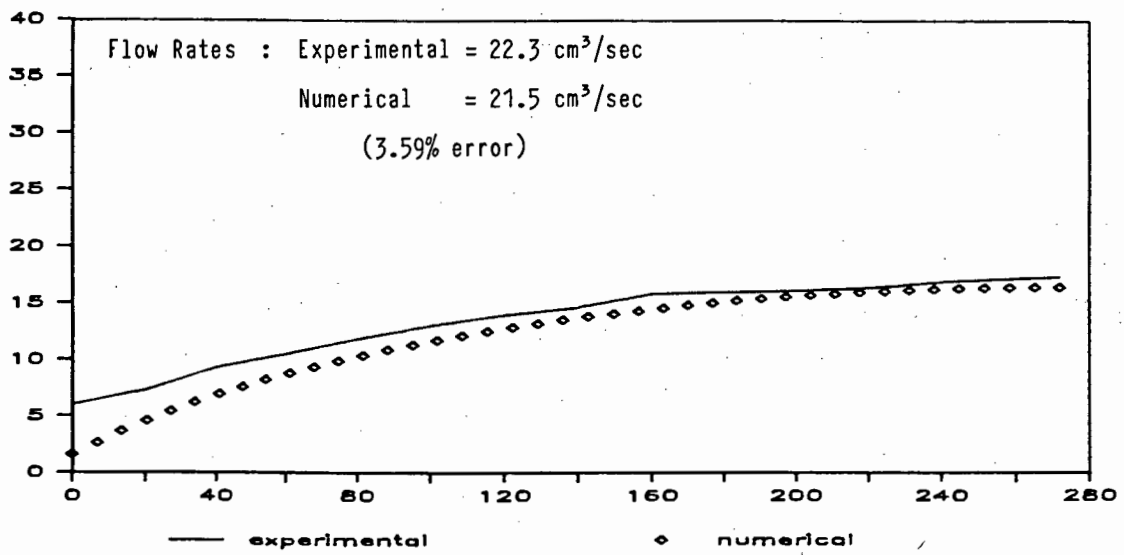


## Phreatic surface at 30 min

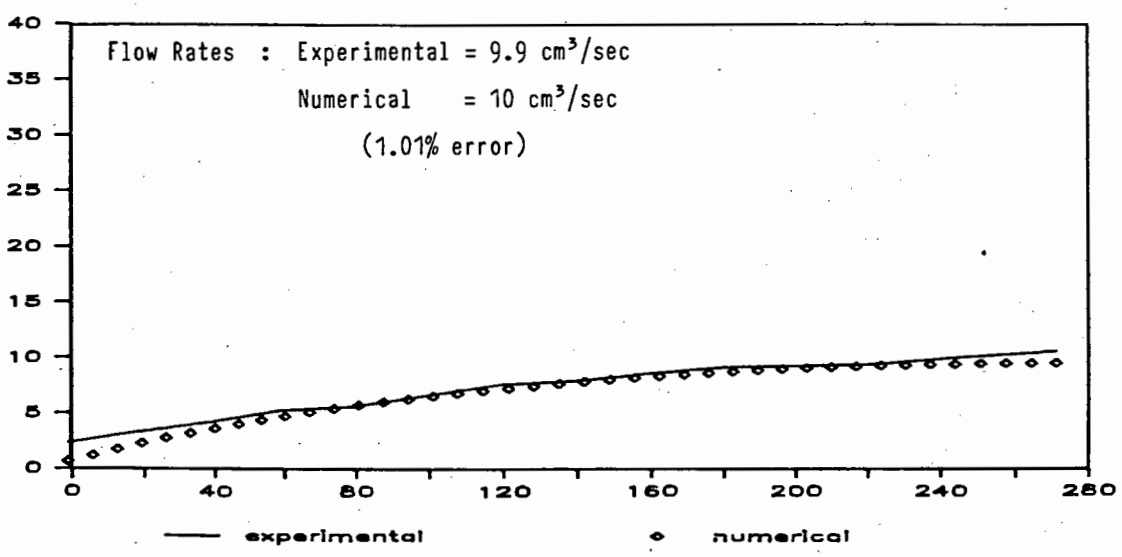

# APPENDIX F

## RESULTS FROM THE TWO-DIMENSIONAL (AXISYMMETRICAL) DRAINAGE PROBLEM

EXPERIMENTAL RESULTS OF THE AXISYMMETRICAL DRAINAGE PROBLEM

SAND C n=.395

| time start (sec) | time end (sec) | mass of container + water (g) | mass of empty container (g) | mass of water (g) | cumulative outflow (cm^3) | outflow rate (cm^3/sec) |
|---|---|---|---|---|---|---|
| 0 | 13 | 3730.6 | 188.8 | 3541.8 | 3548.2 | 272.94 |
| 13 | 40 | 1842.8 | 212.2 | 1630.6 | 5181.7 | 60.50 |
| 40 | 60 | 1166.7 | 185.4 | 981.3 | 6164.8 | 49.15 |
| 60 | 80 | 1134.2 | 231.9 | 902.3 | 7068.7 | 45.20 |
| 80 | 100 | 1068.5 | 221.6 | 846.9 | 7917.2 | 42.42 |
| 100 | 120 | 1011.5 | 206.9 | 804.6 | 8723.2 | 40.30 |
| 120 | 140 | 977.9 | 207.8 | 770.1 | 9494.7 | 38.57 |
| 140 | 165 | 1094.4 | 192.1 | 902.3 | 10398.6 | 36.16 |
| 165 | 180 | 725.1 | 209.1 | 516.0 | 10915.5 | 34.46 |
| 180 | 200 | 886.2 | 191.7 | 694.5 | 11611.3 | 34.79 |
| 200 | 220 | 852.4 | 188.8 | 663.6 | 12276.1 | 33.24 |
| 220 | 240 | 828.8 | 187.9 | 640.9 | 12918.2 | 32.10 |
| 240 | 260 | 801.9 | 206.9 | 595.0 | 13514.2 | 29.80 |
| 260 | 280 | 851.2 | 251.7 | 599.5 | 14114.8 | 30.03 |
| 280 | 300 | 825.5 | 251.7 | 573.8 | 14689.6 | 28.74 |
| 300 | 320 | 854.6 | 261.9 | 592.7 | 15283.4 | 29.69 |
| 320 | 340 | 683.6 | 126.2 | 557.4 | 15841.8 | 27.92 |
| 340 | 360 | 693.7 | 139.1 | 554.6 | 16397.4 | 27.78 |
| 360 | 380 | 699.7 | 154.2 | 545.5 | 16943.9 | 27.32 |
| 380 | 400 | 674.2 | 153.8 | 520.4 | 17465.2 | 26.07 |
| 400 | 420 | 701.9 | 175.0 | 526.9 | 17993.1 | 26.39 |
| 420 | 440 | 618.0 | 107.2 | 510.8 | 18504.8 | 25.59 |
| 440 | 450 | 347.7 | 101.1 | 246.6 | 18751.9 | 24.70 |
| 450 | 460 | 356.3 | 97.4 | 258.9 | 19011.2 | 25.94 |
| 460 | 480 | 688.6 | 206.9 | 481.7 | 19493.8 | 24.13 |
| 480 | 500 | 725.0 | 251.7 | 473.3 | 19967.9 | 23.71 |
| 500 | 520 | 735.8 | 251.7 | 484.1 | 20452.9 | 24.25 |
| 520 | 540 | 723.8 | 261.9 | 461.9 | 20915.6 | 23.14 |
| 540 | 560 | 596.4 | 126.2 | 470.2 | 21386.7 | 23.55 |
| 560 | 580 | 583.1 | 139.1 | 444.0 | 21831.5 | 22.24 |
| 580 | 600 | 599.7 | 154.2 | 445.5 | 22277.8 | 22.32 |
| 600 | 620 | 597.1 | 153.8 | 443.3 | 22721.9 | 22.20 |
| 620 | 640 | 619.7 | 175.0 | 444.7 | 23167.4 | 22.28 |
| 640 | 660 | 521.0 | 107.2 | 413.8 | 23581.9 | 20.73 |
| 660 | 670 | 308.8 | 101.1 | 207.7 | 23790.0 | 20.81 |
| 670 | 680 | 310.9 | 97.4 | 213.5 | 24003.9 | 21.39 |
| 680 | 700 | 615.5 | 206.9 | 408.6 | 24413.2 | 20.47 |
| 700 | 720 | 651.4 | 251.7 | 399.7 | 24813.7 | 20.02 |
| 720 | 740 | 649.4 | 251.7 | 397.7 | 25212.1 | 19.92 |
| 740 | 760 | 643.5 | 261.9 | 381.6 | 25594.4 | 19.11 |
| 760 | 780 | 513.7 | 126.2 | 387.5 | 25982.6 | 19.41 |
| 780 | 800 | 522.9 | 139.1 | 383.8 | 26367.1 | 19.22 |
| 800 | 820 | 512.1 | 154.2 | 357.9 | 26725.6 | 17.93 |
| 820 | 840 | 515.3 | 153.8 | 361.5 | 27087.8 | 18.11 |
| 840 | 860 | 533.8 | 175.0 | 358.8 | 27447.2 | 17.97 |
| 860 | 880 | 449.7 | 107.2 | 342.5 | 27790.3 | 17.16 |
| 880 | 890 | 277.0 | 101.1 | 175.9 | 27966.5 | 17.62 |
| 890 | 900 | 267.1 | 97.4 | 169.7 | 28136.5 | 17.00 |

EXPERIMENTAL RESULTS CONTINUED

| time start (sec) | time end (sec) | mass of container + water (g) | mass of empty container (g) | mass of water (g) | cumulative outflow (cm^3) | outflow rate (cm^3/sec) |
|---|---|---|---|---|---|---|
| 900 | 930 | 717.1 | 206.9 | 510.2 | 28647.7 | 17.04 |
| 930 | 960 | 742.3 | 251.7 | 490.6 | 29139.2 | 16.38 |
| 960 | 980 | 587.5 | 251.7 | 335.8 | 29475.6 | 16.82 |
| 980 | 1000 | 577.0 | 261.9 | 315.1 | 29791.2 | 15.78 |
| 1000 | 1020 | 443.7 | 126.2 | 317.5 | 30109.3 | 15.90 |
| 1020 | 1040 | 445.7 | 139.1 | 306.6 | 30416.4 | 15.36 |
| 1040 | 1060 | 457.8 | 154.2 | 303.6 | 30720.6 | 15.21 |
| 1060 | 1080 | 458.3 | 153.8 | 304.5 | 31025.6 | 15.25 |
| 1080 | 1105 | 546.2 | 175.0 | 371.2 | 31397.5 | 14.87 |
| 1105 | 1120 | 324.4 | 107.2 | 217.2 | 31615.1 | 14.51 |
| 1120 | 1135 | 319.2 | 101.1 | 218.1 | 31833.6 | 14.57 |
| 1135 | 1150 | 317.7 | 97.4 | 220.3 | 32054.3 | 14.71 |
| 1150 | 1170 | 493.9 | 206.9 | 287.0 | 32341.8 | 14.38 |
| 1170 | 1200 | 675.3 | 251.7 | 423.6 | 32766.2 | 14.15 |
| 1200 | 1230 | 660.2 | 251.7 | 408.5 | 33175.4 | 13.64 |
| 1230 | 1260 | 662.2 | 261.9 | 400.3 | 33576.4 | 13.37 |
| 1260 | 1290 | 521.6 | 126.2 | 395.4 | 33972.6 | 13.20 |
| 1290 | 1320 | 523.1 | 139.1 | 384.0 | 34357.2 | 12.82 |
| 1320 | 1350 | 528.5 | 154.2 | 374.3 | 34732.2 | 12.50 |
| 1350 | 1380 | 527.1 | 153.8 | 373.3 | 35106.2 | 12.47 |
| 1380 | 1410 | 538.0 | 175.0 | 363.0 | 35469.8 | 12.12 |
| 1410 | 1440 | 463.7 | 107.2 | 356.5 | 35827.0 | 11.90 |
| 1440 | 1455 | 277.5 | 101.1 | 176.4 | 36003.7 | 11.78 |
| 1455 | 1470 | 272.7 | 97.4 | 175.3 | 36179.3 | 11.71 |
| 1470 | 1500 | 549.5 | 206.9 | 342.6 | 36522.5 | 11.44 |
| 1500 | 1530 | 585.4 | 251.7 | 333.7 | 36856.8 | 11.14 |
| 1530 | 1560 | 584.2 | 251.7 | 332.5 | 37189.9 | 11.10 |
| 1560 | 1590 | 584.8 | 261.9 | 322.9 | 37513.4 | 10.78 |
| 1590 | 1620 | 440.2 | 126.2 | 314.0 | 37828.0 | 10.49 |
| 1620 | 1650 | 448.8 | 139.1 | 309.7 | 38138.2 | 10.34 |
| 1650 | 1680 | 465.6 | 154.2 | 311.4 | 38450.2 | 10.40 |
| 1680 | 1710 | 451.9 | 153.8 | 298.1 | 38748.8 | 9.95 |
| 1710 | 1740 | 469.7 | 175.0 | 294.7 | 39044.1 | 9.84 |
| 1740 | 1770 | 401.5 | 107.2 | 294.3 | 39338.9 | 9.83 |
| 1770 | 1785 | 242.6 | 101.1 | 141.5 | 39480.7 | 9.45 |
| 1785 | 1800 | 243.7 | 97.4 | 146.3 | 39627.2 | 9.77 |
| 1800 | 1830 | 484.6 | 206.9 | 277.7 | 39905.4 | 9.27 |
| 1830 | 1860 | 533.5 | 251.7 | 281.8 | 40187.7 | 9.41 |
| 1860 | 1890 | 524.3 | 251.7 | 272.6 | 40460.8 | 9.10 |
| 1890 | 1920 | 518.0 | 261.9 | 256.1 | 40717.4 | 8.55 |
| 1920 | 1950 | 392.7 | 126.2 | 266.5 | 40984.4 | 8.90 |
| 1950 | 1980 | 386.6 | 139.1 | 247.5 | 41232.3 | 8.26 |
| 1980 | 2010 | 392.7 | 154.2 | 238.5 | 41471.2 | 7.96 |
| 2010 | 2040 | 392.7 | 153.8 | 238.9 | 41710.6 | 7.98 |
| 2040 | 2070 | 413.6 | 175.0 | 238.6 | 41949.6 | 7.97 |
| 2070 | 2100 | 341.3 | 107.2 | 234.1 | 42184.1 | 7.82 |
| 2100 | 2115 | 212.5 | 101.1 | 111.4 | 42295.7 | 7.44 |
| 2115 | 2130 | 214.6 | 97.4 | 117.2 | 42413.1 | 7.83 |
| 2130 | 2160 | 428.9 | 206.9 | 222.0 | 42635.5 | 7.41 |
| 2160 | 2190 | 473.0 | 251.7 | 221.3 | 42857.2 | 7.39 |
| 2190 | 2220 | 463.1 | 251.7 | 211.4 | 43069.0 | 7.06 |
| 2220 | 2250 | 467.7 | 261.9 | 205.8 | 43275.2 | 6.87 |

EXPERIMENTAL RESULTS CONTINUED

| time start (sec) | time end (sec) | mass of container + water (g) | mass of empty container (g) | mass of water (g) | cumulative outflow (cm^3) | outflow rate (cm^3/sec) |
|---|---|---|---|---|---|---|
| 2250 | 2280 | 333.7 | 126.2 | 207.5 | 43483.1 | 6.93 |
| 2280 | 2310 | 341.2 | 139.1 | 202.1 | 43685.5 | 6.75 |
| 2310 | 2340 | 357.4 | 154.2 | 203.2 | 43889.1 | 6.79 |
| 2340 | 2370 | 355.9 | 153.8 | 202.1 | 44091.6 | 6.75 |
| 2370 | 2400 | 368.2 | 175.0 | 193.2 | 44285.1 | 6.45 |
| 2400 | 2430 | 300.1 | 107.2 | 192.9 | 44478.4 | 6.44 |
| 2430 | 2445 | 194.8 | 101.1 | 93.7 | 44572.2 | 6.26 |
| 2445 | 2460 | 192.3 | 97.4 | 94.9 | 44667.3 | 6.34 |
| 2460 | 2490 | 395.9 | 206.9 | 189.0 | 44856.6 | 6.31 |
| 2490 | 2520 | 432.4 | 251.7 | 180.7 | 45037.7 | 6.03 |
| 2520 | 2550 | 435.0 | 251.7 | 183.3 | 45221.3 | 6.12 |
| 2550 | 2580 | 441.6 | 261.9 | 179.7 | 45401.3 | 6.00 |
| 2580 | 2610 | 300.4 | 126.2 | 174.2 | 45575.8 | 5.82 |
| 2610 | 2640 | 312.7 | 139.1 | 173.6 | 45749.7 | 5.80 |
| 2640 | 2670 | 324.0 | 154.2 | 169.8 | 45919.9 | 5.67 |
| 2670 | 2700 | 320.0 | 153.8 | 166.2 | 46086.4 | 5.55 |
| 2700 | 2730 | 340.6 | 175.0 | 165.6 | 46252.3 | 5.53 |
| 2730 | 2760 | 271.6 | 107.2 | 164.4 | 46417.0 | 5.49 |
| 2760 | 2775 | 181.3 | 101.1 | 80.2 | 46497.3 | 5.36 |
| 2775 | 2790 | 175.2 | 97.4 | 77.8 | 46575.2 | 5.20 |
| 2790 | 2820 | 364.3 | 206.9 | 157.4 | 46732.9 | 5.26 |
| 2880 | 2910 | 412.3 | 261.9 | 150.4 | 46883.6 | 5.02 |
| 2910 | 2940 | 275.9 | 126.2 | 149.7 | 47033.6 | 5.00 |
| 2940 | 2970 | 284.2 | 139.1 | 145.1 | 47178.9 | 4.85 |
| 2970 | 3000 | 297.5 | 154.2 | 143.3 | 47322.5 | 4.79 |
| 3000 | 3030 | 295.9 | 153.8 | 142.1 | 47464.8 | 4.75 |
| 3030 | 3060 | 312.0 | 175.0 | 137.0 | 47602.1 | 4.57 |
| 3060 | 3090 | 246.8 | 107.2 | 139.6 | 47741.9 | 4.66 |
| 3090 | 3120 | 236.5 | 101.1 | 135.4 | 47877.6 | 4.52 |
| 3120 | 3150 | 230.3 | 97.4 | 132.9 | 48010.7 | 4.44 |
| 3150 | 3180 | 338.9 | 206.9 | 132.0 | 48143.0 | 4.41 |
| 3180 | 3210 | 381.9 | 251.7 | 130.2 | 48273.4 | 4.35 |
| 3210 | 3240 | 381.1 | 251.7 | 129.4 | 48403.0 | 4.32 |
| 3240 | 3300 | 513.8 | 261.9 | 251.9 | 48655.4 | 4.21 |
| 3300 | 3360 | 371.3 | 126.2 | 245.1 | 48900.9 | 4.09 |
| 3360 | 3420 | 378.2 | 139.1 | 239.1 | 49140.5 | 3.99 |
| 3420 | 3480 | 378.3 | 154.2 | 224.1 | 49365.0 | 3.74 |
| 3480 | 3540 | 381.9 | 153.8 | 228.1 | 49593.5 | 3.81 |
| 3540 | 3600 | 392.6 | 175.0 | 217.6 | 49811.5 | 3.63 |
| 3600 | 3660 | 322.0 | 107.2 | 214.8 | 50026.6 | 3.59 |
| 3660 | 3720 | 308.4 | 101.1 | 207.3 | 50234.3 | 3.46 |
| 3720 | 3780 | 298.5 | 97.4 | 201.1 | 50435.8 | 3.36 |
| 3780 | 3840 | 405.5 | 206.9 | 198.6 | 50634.7 | 3.32 |
| 3840 | 3900 | 443.3 | 251.7 | 191.6 | 50826.7 | 3.20 |
| 3900 | 3960 | 438.0 | 251.7 | 186.3 | 51013.3 | 3.11 |
| 3960 | 4020 | 445.2 | 261.9 | 183.3 | 51197.0 | 3.06 |
| 4020 | 4080 | 303.5 | 139.1 | 164.4 | 51361.7 | 2.74 |
| 4080 | 4140 | 313.7 | 154.2 | 159.5 | 51521.4 | 2.66 |
| 4140 | 4200 | 327.0 | 153.8 | 173.2 | 51695.0 | 2.89 |
| 4200 | 4500 | 981.2 | 187.9 | 793.3 | 52489.7 | 2.65 |
| 4500 | 4800 | 918.5 | 209.1 | 709.4 | 53200.4 | 2.37 |
| 4800 | 5160 | 936.2 | 187.9 | 748.3 | 53950.0 | 2.08 |

EXPERIMENTAL RESULTS CONTINUED

| time start (sec) | time end (sec) | mass of container + water (g) | mass of empty container (g) | mass of water (g) | cumulative outflow (cm^3) | outflow rate (cm^3/sec) |
|---|---|---|---|---|---|---|
| 5160 | 5580 | 969.1 | 209.1 | 760.0 | 54711.4 | 1.81 |
| 5580 | 6060 | 926.7 | 187.9 | 738.8 | 55451.5 | 1.54 |
| 6060 | 6720 | 1042.0 | 209.1 | 832.9 | 56285.9 | 1.26 |
| 6720 | 7200 | 682.6 | 187.9 | 494.7 | 56781.5 | 1.03 |
| 7200 | 9060 | 1544.6 | 209.1 | 1335.5 | 58119.4 | 0.72 |
| 9060 | 10920 | 1001.2 | 187.9 | 813.3 | 58934.2 | 0.44 |
| 10920 | 13320 | 833.1 | 209.1 | 624.0 | 59559.3 | 0.26 |
| 13320 | 15480 | 528.5 | 187.9 | 340.6 | 59900.5 | 0.16 |

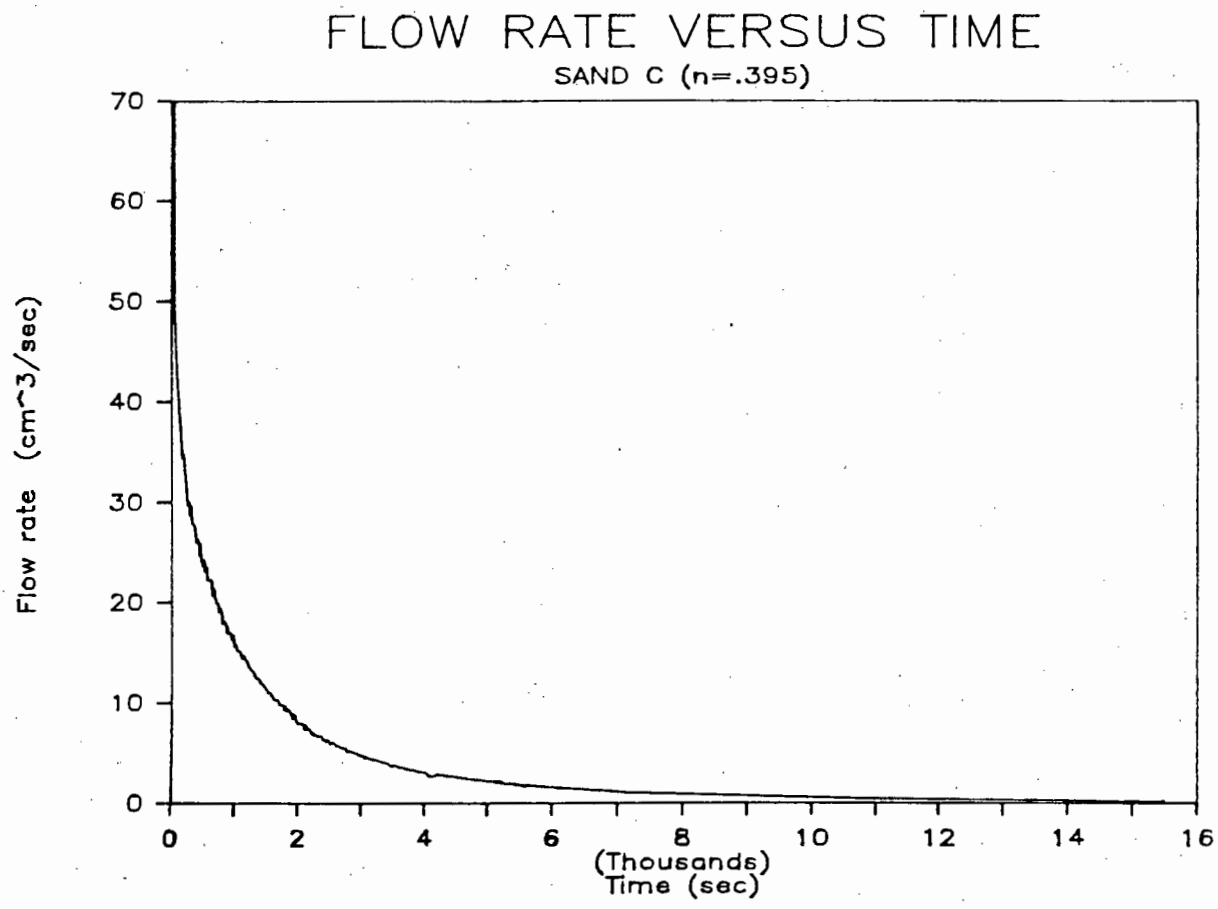
FLOW RATE VERSUS TIME
SAND C (n=.395)
Flow rate (cm^3/sec)
70
60
50
40
30
20
10
0
0
2
4
6
8
10
12
14
16
(Thousands)
Time (sec)

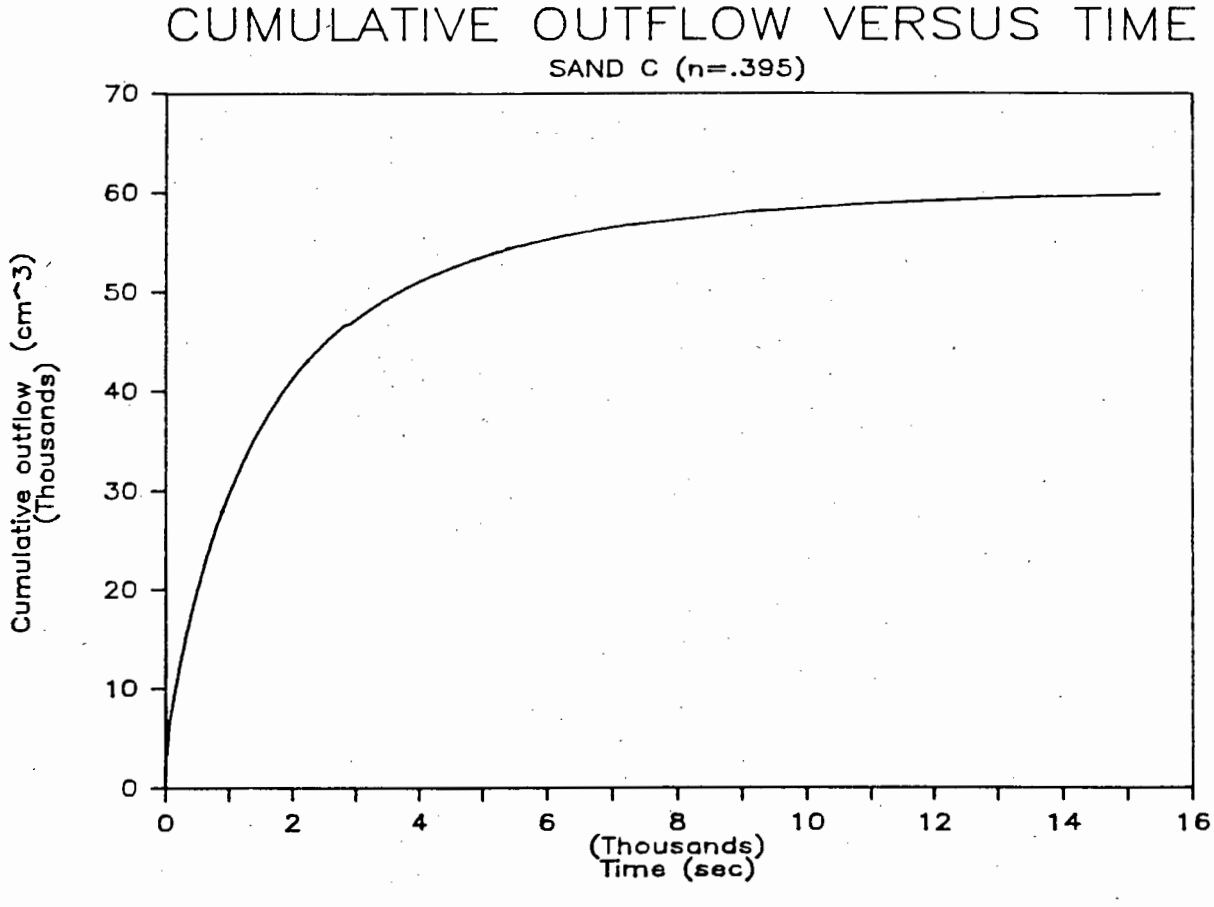
CUMULATIVE OUTFLOW VERSUS TIME
SAND C (n=.395)
Cumulative outflow (cm^3)
(Thousands)
70
60
50
40
30
20
10
0
0
2
4
6
8
10
12
14
16
(Thousands)
Time (sec)

STEADY-STATE FLOW EXPERIMENTAL RESULTS : SAND C (n=.395)

| Radial distance from the axis of symmetry | Height to the phreatic surface | Mass of bucket 1 and water accumulated in one minute | Mass of bucket 2 and water accumulated in one minute | |
|---|---|---|---|---|
| ( cm ) | ( cm ) | ( g ) | ( g ) | |
| 0 | 1 | 1987.1 | 1945.3 | |
| 8.5 | 6.2 | 2001.3 | 2000.3 | |
| 18.66 | 12.6 | 1992.2 | 2051.9 | |
| 28.82 | 19.1 | 1957.1 | 2027.3 | |
| 38.98 | 21.1 | 2008.1 | 2046.8 | |
| 49.14 | 22.8 | 1953.6 | 2032.2 | |
| 59.3 | 24.4 | 2009.2 | 1989.5 | |
| 69.46 | 26 | 2037.5 | 1998.6 | |
| 79.62 | 27.5 | 1992.1 | 2013.6 | |
| 89.78 | 29.6 | 2003.7 | 2017.2 | |
| 99.94 | 29.8 | --- | --- | |
| 110.1 | 30.9 | 1994.19 | 2012.27 | average mass |
| 120.26 | 31.2 | 191.9 | 196.5 | mass of dry bucket |
| 130.42 | 32.1 | --- | --- | |
| 140.58 | 33.3 | | | mass of water |
| 150.74 | 34.3 | 1802.29 | 1815.77 | accumulated in |
| 160.9 | 34.5 | | | one minute |
| 171.06 | 34.9 | | | |
| 181.22 | 35.9 | | | |
| 191.38 | 36.8 | Average flow rate from the wedge :- | | |
| 201.54 | 37.1 | | | |
| 211.7 | 37.8 | 1812.29 cm^3/min | | |
| 221.86 | 38.1 | ========== | | |
| 232.02 | 38.3 | | | |
| 242.18 | 38.5 | | | |
| 252.34 | 39.1 | | | |

# APPENDIX G

A LISTING OF THE PROGRAMME,
WITH AN EXPLANATION OF THE VARIABLES,
USED TO SIMULATE THE AXISYMMETRICAL DRAINAGE PROBLEM

# A DESCRIPTION OF THE VARIABLES

## 1. NUMERICAL AND DOMAIN VARIABLES

XTLEN = length of the flow domain
ZTLEN = depth of the flow domain
XELEM = number of elements comprising the length of the flow domain
ZELEM = number of elements comprising the depth of the flow domain
XLEN = length of a finite element
ZLEN = depth of a finite element
XNODE = number of nodes comprising the length of the flow domain
ZNODE = number of nodes comprising the depth of the flow domain
TNODE = total number of nodes in the finite element mesh
TELEM = total number of elements in the finite element mesh
TWF = time weighting factor
DTIM = time increment
MAXDTIM = maximum recommended value for DTIM
MINDTIM = minimum recommended value for DTIM
LTIM = length of time for programme to run
ALTIM = total number of time levels for the run
TSTEP = time levels for the run
DUMMY = iterations per time level

## 2. SOIL PROPERTY VARIABLES

POROS = porosity of the sand
KSAT = saturated coefficient of permeability
KREL = relative permeability
DSRC = specific moisture capacity
NSR = current degree of saturation
OSR = previous degree of saturation

## 3. INITIAL CONDITION VARIABLES

HWTT = initial height of the water table at the top end of the flow domain

HWTB = initial height of the water table at the outflow end of the flow domain

WTG = gradient of the water table

DSFL = length of unsaturated zone on the outflow face

NDN = number of nodes in the above length

NSFL = number of nodes in the saturated zone on the outflow face.

## 4. PRESSURE HEAD VARIABLES

TCHI = nodal pressure head from previous time level

NCHI = nodal pressure head from future time level

CHI = nodal pressure head from current iteration

OCHI = nodal pressure head from previous iteration

MCHI = nodal pressure head at the mid-time level

NCCHI = current pressure head at the centroid of the element

OCCHI = previous pressure head at the centroid of the element

CHIMIN = value of the pressure head increment used when determining the specific moisture capacity term for the first iteration in a time level.

## 5. UNDER-RELAXATION FORMULA VARIABLES

ERR = current largest absolute head error between iterations

OERR = previous largest absolute head error between iterations

GPAC = under-relaxation parameter

PFAC = under-relaxation parameter

## 6. MATRIX VARIABLES

ASMX =
ASMZ =
BSM =
FSM =
} element matrices

COAMX =
COAMZ =
COBM =
COFM =
} element matrix coefficients

AMATZ =
AMATX =
BMAT =
FMAT =
} global matrices

TAFM =
TFFM =
} portions of the global matrices deleted when imposing the boundary conditions but required for back substitution (determination of seepage face fluxes)

AFLUX = normal nodal seepage face flux on the outflow face.

## FLOPPY DISK INFORMATION

The floppy disk attached to the cover of this thesis is self bootable and contains uncompiled versions of the three programmes used to simulate the three drainage problems. The disk also contains the executable TRUE BASIC file which allows the programmes to be run. The disk does, however, not contain any other TRUE BASIC files.

The programmes are stored under the file names.

1. COLUMN (column drainage problem)
2. 2DPLANE (2-D plane drainage problem)
3. AXI (axisymmetrical drainage problem)

These programmes may be loaded by typing

OLD < FILE NAME >

and run by pressing F9.

```
!KETTERS
!-------

!  A programme to simulate saturated/unsaturated ground water flow using
!     finite elements and a Pichard iterative scheme for time marching.

! DRIVER
! ELEMENT MATRIX DATA
! DETERMINATION OF THE DEGREE OF SATURATION   (Sr)
! DETERMINATION OF THE RELATIVE PERMEABILITY  (kr)
! DETERMINATION OF THE MATRIX COEFFICIENTS
! ASSEMBLY OF THE GLOBAL MATRACES IN BANDED FORM
! ASSEMBLY OF THE FINAL MATRACES ACCORDING TO THE FLOW EQUATION
! MATRIX SOLVER
! DETERMINATION OF SEEPAGE FACE FLUXES BY BACKSUBSITTUTION
! DATA OUTPUT


!DRIVER PROGRAMME
!----------------

CLEAR

INPUT PROMPT " Length of soil sample (cm)         =  ": XTLEN
INPUT PROMPT " Depth  of soil sample (cm)         =  ": ZTLEN
INPUT PROMPT " Porosity of soil                   =  ": POROS
INPUT PROMPT " Saturated permeability (cm/min)    =  ": KSAT
print   ""
INPUT PROMPT " Number of elements in x-direction =  ": XELEM
INPUT PROMPT " Number of elements in z-direction =  ": ZELEM
print   ""
INPUT PROMPT "Time weighting factor (0 < w < 1)   =  ": TWF
print   ""

DIM ASMX(4),ASMZ(4),BSM(4),FSM(2)
DIM COAMX(500),COAMZ(500),COBM(500),COFM(500)
DIM TAFM(15,15),TFFM(15),AFLUX(15)
DIM AMATX(500,15),AMATZ(500,15),BMAT(500,15),FMAT(500)
DIM TCHI(500),OCHI(500),CHI(500)
DIM MCHI(500),NCCHI(500),OCCHI(500)
DIM NSR(500),OSR(500),KREL(500),DSRC(500)

open #2: name"g2moist.prn",create new

       LET xlen=xtlen/xelem
       LET zlen=ztlen/zelem
       LET xnode=xelem+1
       LET znode=zelem+1
       LET telem=zelem*xelem
       LET tnode=znode*xnode

 LET mindtim=(.01*poros*(zlen^2))/ksat
 LET maxdtim=(.1*poros*(zlen^2))/ksat

 print   ""
 print   "Max value of time increment (min) =",maxdtim
 print   "Min value of time increment (min) =",mindtim
 print   ""
 INPUT PROMPT "Value of time increment to be used (min) = ": dtim
 INPUT PROMPT "Time for programme to run          (min) = ": ltim
 print   ""
 INPUT PROMPT "Height of water table at top end     (cm) = ": hwtt
```

```
INPUT PROMPT "Height of water table at bottom end  (cm) = ": hwtb

! DETERMINATION OF THE INITIAL CONDITIONS

      LET wtg=(hwtt-hwtb)/xtlen
      LET dsfl=ztlen-hwtb
      LET ndn=IP(dsfl/zlen)+1
      LET nsfl=znode-ndn

         FOR j=1 to ndn
             LET tchi(znode+1-j)=(j-1)*zlen-dsfl
         NEXT j

         FOR j=1 to nsfl
             LET tchi(j)=0
         NEXT j

       FOR l=2 to xnode
         LET hwt=hwtb+wtg*(l-1)*xlen
           FOR j=1 to znode
             LET tchi((l-1)*znode+j)=hwt-(j-1)*zlen
           NEXT j
       NEXT l

      LET altim=ltim/dtim

CALL Matdat ( asmx(),asmz(),bsm(),fsm() )

FOR tstep= 1 to altim

! THE FIRST PREDICTION OF THE PRESSURE HEADS

     IF tstep=1 then
         FOR i=1 to tnode
             LET chi(i)=tchi(i)
         NEXT i
     END IF

! THE FIRST ITERATION PER TIME LEVEL
! ----------------------------------

          LET dummy=1
          LET chimin=-.75

! DETERMINATION OF THE PRESSURE HEADS AT THE MID-TIME INTERVAL

          FOR i=1 to tnode
              LET mchi(i)=((1-twf)*tchi(i))+twf*chi(i)
              LET ochi(i)=chi(i)
          NEXT i

! DETERMINATION OF THE PRESSURE HEADS AT THE CENTRIOD OF THE ELEMENT

          FOR l=1 to xelem
           FOR k=1 to zelem
               LET ncchi((l-1)*zelem+k)=(mchi((l-1)*znode+k)+
                  mchi((l-1)*znode+k+1)+mchi((l-1)*znode+znode+k+1)+
                  mchi((l-1)*znode+znode+k+1)+mchi((l-1)*znode+znode+k))
           NEXT k
          NEXT l

! DETERMINATION OF THE DEGREE OF SATURATION AND RELATIVE PERMEABILITY
```

```
        FOR i=1 to telem
               CALL Moist ( i,ncchi(),nsr() )
               CALL Perm ( i,nsr(),krel()  )
                 LET osr(i)=nsr(i)
                 LET occhi(i)=ncchi(i)
        NEXT i

! APPROXIMATING THE CENTROIDAL PRESSURE HEADS FOR THE FIRST ITERATION
! IN THE TIME LEVEL

          FOR l=1 to xelem
           FOR k=1 to zelem
               LET ncchi((l-1)*zelem+k)=((mchi((l-1)*znode+k)+
                  mchi((l-1)*znode+k+1)+mchi((l-1)*znode+znode+k+1)+
                  mchi((l-1)*znode+znode+k))/4)+chimin
           NEXT k
          NEXT l

! DETERMINATION OF THE DEGREE OF SATURATION AND RELATIVE PERMEABILITY

        FOR i=1 to telem
               CALL Moist ( i,ncchi(),nsr() )
               CALL Perm ( i,nsr(),krel()  )
        NEXT i

! DETERMINATION OF THE FINAL MATRICES ACCORDING TO THE FLOW EQUATION

CALL Elemmat ( chimin,telem,xelem,zelem,xlen,zlen,poros,ksat,dsrc(),
               ncchi(),occhi(),nsr(),osr(),krel(),coamx(),coamz(),cobm()
CALL Globalmat (znode,xnode,tnode,xelem,zelem,coamx(),coamz(),cobm(),
                cofm(),asmx(),asmz(),bsm(),fsm(),amatx(,),amatz(,),
                bmat(,),fmat() )
CALL Equatmat  ( znode,xnode,tnode,zelem,twf,dtim,tchi(),amatx(,),
                 amatz(,),bmat(,),fmat() )

! IMPOSING THE BOUNDARY CONDITIONS

    FOR j=1 to nsfl
        FOR k=1 to znode+2
            LET tafm(j,k)=amatx(j,k)
            LET amatx(j,k)=0
         NEXT k
            LET tffm(j)=fmat(j)
            LET fmat(j)=0
     NEXT j

! SOLVING THE FLOW EQUATION FOR THE NEW PRESSURE HEADS

 CALL Matsolve ( nsfl,znode,tnode,xelem,telem,dtim,
                 amatx(,),fmat(),chi() )

! UPDATING THE SEEPAGE FACE LENGTH AND DETERMINATION OF THE NORMAL
! NODAL FLUXES

 CALL Backsub ( dummy,tstep,nsfl,znode,xlen,zlen,chi(),
                ,aflux(),tffm(),tafm(,)  )

! DETERMINATION OF THE LARGEST ABSOLUTE ERROR IN THE PRESSURE HEADS FOR
! THE APPLICATION OF THE UNDER-RELAXATION FORMULA

    LET err=chi(1)-ochi(1)
```

```
        FOR i= 1 to tnode-1
           IF abs(chi(i+1)-ochi(i+1)) > abs(err) then
           LET err=chi(i+1)-ochi(i+1)
        NEXT i

    LET gfac=1
    LET oerr=err

! UPDATING THE CENTROIDAL PRESSURE HEADS AND THE DEGREES OF SATURATIONS

      FOR i=1 to telem
        LET occhi(i)=ncchi(i)
        LET osr(i)=nsr(i)
     NEXT i

! NEW APPROXIMATION OF THE PRESSURE HEADS AT THE MID-TIME INTERVAL

      FOR i=1 to tnode
        LET mchi(i)=(chi(i)*twf)+(tchi(i)*(1-twf))
        LET ochi(i)=chi(i)
     NEXT i

! THE REMAINING ITERATIONS PER TIME LEVEL
! ---------------------------------------

LET dummy=2

! SPECIFICATION OF THE TOLERANCE

 DO WHILE abs(err) > .1

! EVALUATING THE PRESSURE HEADS AT THE CENTROID OF THE ELEMENT

          FOR l=1 to xelem
           FOR k=1 to zelem
               LET ncchi((l-1)*zelem+k)=(mchi((l-1)*znode+k)+
                  mchi((l-1)*znode+k+1)+mchi((l-1)*znode+znode+k+1)+
                  mchi((l-1)*znode+znode+k+1)+mchi((l-1)*znode+znode+k))
           NEXT k
          NEXT l

! DETERMINATION OF THE DEGREE OF SATURATION AND RELATIVE PERMEABILITY

         FOR i=1 to telem
             CALL Moist ( i,ncchi(),nsr() )
             CALL Perm ( i,nsr(),krel()  )
         NEXT i

! DETERMINATION OF THE FINAL MATRICES ACCORDING TO THE FLOW EQUATION

CALL Elemmat ( chimin,telem,xelem,zelem,xlen,zlen,poros,ksat,dsrc(),
               ncchi(),occhi(),nsr(),osr(),krel(),coamx(),coamz(),cobm()
CALL Globalmat (znode,xnode,tnode,xelem,zelem,coamx(),coamz(),cobm(),
                cofm(),asmx(),asmz(),bsm(),fsm(),amatx(,),amatz(,),
                bmat(,),fmat() )
CALL Equatmat  ( znode,xnode,tnode,zelem,twf,dtim,tchi(),amatx(,),
                 amatz(,),bmat(,),fmat() )

! IMPOSING THE BOUNDARY CONDITIONS

    FOR j=1 to nsfl
        FOR k=1 to znode+2
```

```
            LET tafm(j,k)=amatx(j,k)
            LET amatx(j,k)=0
          NEXT k
              LET tffm(j)=fmat(j)
              LET fmat(j)=0
      NEXT j

! SOLVING THE FLOW EQUATION FOR THE NEW PRESSURE HEADS

 CALL Matsolve ( nsfl,znode,tnode,xelem,telem,dtim,
                 amatx(,),fmat(),chi() )

! DETERMINATION OF THE LARGEST ABSOLUTE ERROR IN THE PRESSURE HEADS FOR
! APPLICATION OF THE UNDER-RELAXATION FORMULA

    LET err=chi(1)-ochi(1)
        FOR i= 1 to tnode-1
           IF abs(chi(i+1)-ochi(i+1)) > abs(err) then LET err=chi(i+1)-o
        NEXT i

   LET pfac=err/(gfac*oerr)
          LET gfac=((3+pfac)/(3+abs(pfac)))
      IF gfac<.5 then let gfac=.5
          LET oerr=err

       FOR i=1 to telem
              LET occhi(i)=ncchi(i)
              LET osr(i)=nsr(i)
        NEXT i

! APPLICATION OF THE UNDER-RELAXATION FORMULA AND
! DETERMINATION OF THE NEW PRESSURE HEADS AT THE MID-TIME INTRVAL

       FOR i=1 to tnode
              LET chi(i)=(1-gfac)*ochi(i)+gfac*chi(i)
              LET mchi(i)=(chi(i)*twf)+(tchi(i)*(1-twf))
              LET ochi(i)=chi(i)
        NEXT i

! UPDATING THE SEEPAGE FACE LENGTH AND DETERMINATION OF THE NORMAL
! NODAL FLUXES

 CALL Backsub ( dummy,tstep,nsfl,znode,xlen,zlen,chi(),
                ,aflux(),tffm(),tafm(,)  )

! LIMITING THE NUMBER OF ITERATIONS PER TIME LEVEL

  LET dummy=dummy+1
  IF dummy >= 10 then print "no convergence after 10 iterations",err
  IF dummy >= 10 then let err=.09

 LOOP

! DETERMINATION OF THE PRESSURE HEADS, AT THE CENTROID OF THE ELEMENT,
! FOR THE DETERMINATION OF THE DEGREE OF SATURATION FOR OUTPUT

          FOR l=1 to xelem
           FOR k=1 to zelem
               LET ncchi((l-1)*zelem+k)=(mchi((l-1)*znode+k)+
                  mchi((l-1)*znode+k+1)+mchi((l-1)*znode+znode+k+1)+
                  mchi((l-1)*znode+znode+k+1)+mchi((l-1)*znode+znode+k))
           NEXT k
```

```
          NEXT 1

! DETERMINATION OF THE DEGREE OF SATURATION

    FOR i=1 to nelem
             CALL Moist ( i,ncchi(),nsr() )
             CALL Perm ( i,nsr(),krel()  )
     NEXT i

CALL Output ( aflux(),nsfl,xlen,zlen,telem,zelem,xelem,xnode,znode,
              tstep,dtim,ksat,krel(),nsr(),chi(),ncchi()  )

! PREDICTING THE PRESSURE HEADS FOR THE NEXT TIME LEVEL

     FOR  i=1 to tnode
       LET tph=chi(i)
       LET chi(i)=1.5*chi(i)-.5*tchi(i)
       LET tchi(i)=tph
    NEXT i

NEXT tstep

print  ""
print  "END OF RUN"

END


SUB Matdat ( asmx(),asmz(),bsm(),fsm() )

! ELEMENT MATRIX DATA
! -------------------

 LET  asmx(1)=2
 LET  asmx(2)=-2
 LET  asmx(3)=-1
 LET  asmx(4)=1

 LET  asmz(1)=2
 LET  asmz(2)=1
 LET  asmz(3)=-1
 LET  asmz(4)=-2

 LET  bsm(1)=4
 LET  bsm(2)=2
 LET  bsm(3)=1
 LET  bsm(4)=2

 LET fsm(1)=-1
 LET fsm(2)=1

END SUB


SUB Moist ( i,ncchi(),nsr() )

!DETERMINATION OF Sr, GIVEN MATRIC SUCTION, AT CENTRIOD OF ELEMENT
!-----------------------------------------------------------------

LET temp=ncchi(i)*(-1)

 IF temp<4 then let nsr(i)=1
```

```
 IF temp>=4 and temp<=11.5 then let
    nsr(i)=-1.23636e-3*(temp^3)+1.89576e-2*(temp^2)-.146612*(temp)+1.362
 IF temp>=11.5 and temp<=13.925 then let
    nsr(i)=1.146e-2*(temp^2)-.355*(temp)+2.864
 IF temp>13.925 then let nsr(i)=.15

END SUB


SUB Perm ( i,nsr(),krel()  )

!DETERMINATION OF kr ,GIVEN Sr, AT CENTRIOD OF ELEMENT
!-----------------------------------------------------

LET krel(i)=((nsr(i)-.15)/(1-.15))^3

END SUB


 SUB Elemmat ( chimin,telem,xelem,zelem,xlen,zlen,poros,ksat,dsrc(),
               ncchi(),occhi(),nsr(),osr(),krel(),coamx(),coamz(),
               cobm(),cofm() )

!DERIVATION OF THE ELEMNT MATRIX COEFFICIENTS
!-------------------------------------------

LET crad=66.1+xlen/2

  FOR i=1 to xelem
   FOR j=1 to zelem
    LET denom=ncchi(j+(i-1)*zelem)-occhi(j+(i-1)*zelen)
    IF denom=<chimin then let denom=chimin
    LET dsrc(j+(i-1)*zelen)=(nsr(j+(i-1)*zelen)-osr(j(i-1)*zelen))/denom

    LET coamx(j+(i-1)*zelem)=(zlen/xlen)*ksat*krel(j+(i-1)*zelem)*(1/6)*
         (crad+(i-1)*xlen)
    LET coamz(j+(i-1)*zelem)=(xlen/zlen)*ksat*krel(j+(i-1)*zelem)*(1/6)*
        (crad+(i-1)*xlen)
    LET cobm(j+(i-1)*zelem)=(xlen*zlen)*
        (nsr(j+(i-1)*zelem)*1e-6+poros*dsrc(j+(i-1)*zelem)*(1/36)*
        (crad+(i-1)*xlen)
     LET cofm(j+(i-1)*zelem)=(-xlen/2)*ksat*krel(j+(i-1)*zelem)*
        (crad+(i-1)*xlen)
     NEXT j
    NEXT i

END SUB


SUB Globalmat (znode,xnode,tnode,xelem,zelem,coamx(),coamz(),cobm(),
    cofm(),asmx(),asmz(),bsm(),fsm(),amatx(,),amatz(,),bmat(,),fmat() )

!ASSEMBLING THE GLOBAL MATRICES IN BANDED FORM
!--------------------------------------------
```

This subroutine containes a number of IF statements which occupy a large amount space. Since these statements are not essential to the understanding of the programme they are not included here. They may, however, be found from the programme "axi.tru" on the floppy disk.

```
SUB  Equatmat    ( znode,xnode,tnode,zelem,twf,dtim,tchi(),amatx(,),
                   amatz(,),bmat(,),fmat() )

!FORMING THE FINAL MATARCES IN BANDED FORM ACCORDING TO
!         THE FLOW EQUATION
!-------------------------------------------------------

FOR k=1 to tnode
  FOR j=1 to znode+2
     LET amatx(k,j)=twf*amatx(k,j)+twf*amatz(k,j)+bmat(k,j)/dtim
  NEXT j
NEXT k

FOR l=1 to xnode
 FOR k=1 to znode
  LET ftp=0
  LET ctp=0
   FOR j=1 to znode+2
     LET ftp=(amatx((l-1)*znode+k,j)*tchi((l-1)*znode+j+k-1)+amatz((l-1)
     LET ftp=ftp+(bmat((l-1)*znode+k,j)*tchi((l-1)*znode+k+j-1))/dtim
     LET ctp=ftp+ctp
   NEXT j

 IF ((l-1)*znode+k)>1 then
  LET cft=0
  LET nft=0
  LET kct=((l-1)*znode+k-1)
   IF kct>=znode+1 then LET kct=znode+1

   FOR j=1 to kct
     LET nft=(amatx((l-1)*znode+k-j,j+1)*tchi((l-1)*znode-j+k)+
          amatz((l-1)*znode+k-j,j+1)*tchi((l-1)*znode-j+k))*(twf-1)
     LET nft=nft+(bmat((l-1)*znode+k-j,j+1)*tchi((l-1)*znode+k-j))/dtim
     LET cft=nft+cft
   NEXT j

   END IF

  LET fmat(k+(l-1)*znode)=ctp+cft+fmat(k+(l-1)*znode)

 NEXT k
NEXT l

END SUB


SUB Matsolve ( nsfl,znode,tnode,xelem,telem,dtim,amatx(,),fmat(),chi() )

!BANDED MATRIX SOLVER
!--------------------

LET band=znode+2
LET count=tnode-1

FOR piv=(nsfl+1) to count
       LET pivot=piv+1
       LET lim=piv+band-1
IF lim>=tnode then let lim=tnode
IF amatx(piv,1)<>0 then
     FOR row=pivot to lim
            LET col=row-piv+1
            LET fac=amatx(piv,col)/amatx(piv,1)
```

```
          FOR col=row to lim
                LET icol=col-row+1
                LET jcol=col-piv+1
                LET amatx(row,icol)=amatx(row,icol)-fac*amatx(piv,jcol)
          NEXT col
                LET fmat(row)=fmat(row)-fac*fmat(piv)
      NEXT row
   END IF
NEXT piv

FOR k=(nsfl+2) to tnode
       LET piv=tnode-k+(nsfl+2)
    IF amatx(piv,1)<>0 then
       LET fmat(piv)=fmat(piv)/amatx(piv,1)
       LET lim=piv-band+1
     IF lim<=(nsfl+1) then LET lim=(nsfl+1)
       LET pivot=piv-1
    FOR l=lim to pivot
         LET row=pivot-l+lim
         LET col=piv-row+1
         LET fac=amatx(row,col)
         LET fmat(row)=fmat(row)-fac*fmat(piv)
    NEXT l
 END IF
NEXT k

        LET fmat(nsfl+1)=fmat(nsfl+1)/amatx(nsfl+1,1)

FOR k=1 to tnode
  LET chi(k)=fmat(k)
NEXT K

END SUB


SUB Backsub ( dummy,tstep,nsfl,znode,xlen,zlen,chi(),aflux(),
              aflux(),tffm(),tafm(,)  )

!BACK SUBSITUTION TO DETERMINE THE FLUXES ON THE OUTFLOW FACE
!-------------------------------------------------------------

 FOR j=1 to nsfl

LET tcafm=0
LET tdafm=0

    FOR k=1 to znode+2
      LET cafm=tafm(j,k)*chi((j-1)+k)
      LET tcafm=tcafm+cafm
    NEXT k

       LET aflux(j)=(tcafm-tffm(j))*(2/zlen)*(1/66.1)

   IF j>1 then
       LET dc=j-1
     FOR k=1 to dc
       LET dafm=tafm(j-k,k+1)*chi(j-k)
       LET tdafm=tdafm+dafm
     NEXT k
       LET aflux(j)=(tcafm+tdafm-tffm(j))/zlen
  END IF
```

```
NEXT j

! UPDATING THE SEEPAGE FACE LENGTH

  FOR k=nsfl+1 to znode
   IF chi(k)>0 then let chi(k)=0
  NEXT k

  FOR k=1 to nsfl
   IF aflux(k)>0 then
    LET nrsf=k
    LET k=nsfl+1
       if tstep=1 and dummy=1 then
         LET nsfl=nsfl-(nsfl+1-nrsf)+2
        if nsfl>=znode then let nsfl=znode-1
       else
         LET nsfl=nsfl-(nsfl+1-nrsf)
        if nsfl>=znode then let nsfl=znode-1
       end if
   END IF
  NEXT k

END SUB


SUB Output ( aflux(),nsfl,xlen,zlen,telem,zelem,xelem,xnode,znode,
            tstep,dtim,ksat,krel(),nsr(),chi(),ncchi() )

! OUTPUT FROM THE MAIN PROGRAMME FOR A FLOW DOMAIN WITH TEN ELEMENTS
!                    IN THE VERTICAL DIRECTION
!-----------------------------------------------------------------------

open #2:name "g2moist.prn"

if tstep*dtim=5 or tstep*dtim=15 or tstep*dtim=30 then
   if tstep*dtim=5 then
     set #2: pointer begin
   else
     set #2: pointer end
   end if

  FOR k=1 to xnode
    print #2,using "###.##": chi(znode*xnode+1-(k-1)*znode-1)+zlen*10;
    print #2,using "###.##": chi(znode*xnode+1-(k-1)*znode-2)+zlen*9;
    print #2,using "###.##": chi(znode*xnode+1-(k-1)*znode-3)+zlen*8;
    print #2,using "###.##": chi(znode*xnode+1-(k-1)*znode-4)+zlen*7;
    print #2,using "###.##": chi(znode*xnode+1-(k-1)*znode-5)+zlen*6;
    print #2,using "###.##": chi(znode*xnode+1-(k-1)*znode-6)+zlen*5;
    print #2,using " ###.##": chi(znode*xnode+1-(k-1)*znode-7)+zlen*4;
    print #2,using " ###.##": chi(znode*xnode+1-(k-1)*znode-8)+zlen*3;
    print #2,using " ###.##": chi(znode*xnode+1-(k-1)*znode-9)+zlen*2;
    print #2,using " ###.##": chi(znode*xnode+1-(k-1)*znode-10)+zlen*1;
    print #2,using " ###.##": chi(znode*xnode+1-(k-1)*znode-11)+zlen
  NEXT k
    print #2:""
  FOR k=1 to xelem
   print #2,using " #.###": nsr(zelem*xelem+1-(k-1)*zelem-1);
   print #2,using " #.###": nsr(zelem*xelem+1-(k-1)*zelem-2);
   print #2,using " #.###": nsr(zelem*xelem+1-(k-1)*zelem-3);
   print #2,using " #.###": nsr(zelem*xelem+1-(k-1)*zelem-4);
   print #2,using " #.###": nsr(zelem*xelem+1-(k-1)*zelem-5);
   print #2,using " #.###": nsr(zelem*xelem+1-(k-1)*zelem-6);
```

```
    print #2,using " #.###": nsr(zelem*xelem+1-(k-1)*zelem-7);
    print #2,using " #.###": nsr(zelem*xelem+1-(k-1)*zelem-8);
    print #2,using " #.###": nsr(zelem*xelem+1-(k-1)*zelem-9);
    print #2,using " #.###": nsr(zelem*xelem+1-(k-1)*zelem-10)
   NEXT k
   print #2:""
    FOR k=1 to nsfl
      print #2:aflux(k)
    NEXT k

 END IF

END SUB
```